Segmented Rotor Switched Reluctance Motors

Eyhab Aly Kamel El-Kharashi

A thesis submitted for degree of Doctor of Philosophy in Electrical Engineering

School of Electrical, Electronic and Computer Engineering

University of Newcastle upon Tyne

2003

Abstract

Segmented Rotor Switched Reluctance Motors

This thesis introduces and researches the concept of a new form of switched reluctance motor, in which the rotor is made from a series of discrete segments. Single phase machines are initially examined and design rules established. Predictions of air-gap force density are compared with toothed rotor equivalents and it is shown that much greater force densities are theoretically possible with the segmental design.

The thesis then proceeds to apply the concepts developed to two different three phase configurations, which show particular advantages. Two demonstrator machines are designed and built, and their method of construction described. Measured static test results are initially presented for each machine and compared with a conventional switched reluctance motor of the same dimensions, revealing both the advantages and disadvantages of the two segmental rotor configurations.

Both demonstrator machines are then run as SRM drives, with the current to each phase supplied from an asymmetric half bridge converter. The current and voltage waveforms are monitored, along with measurements of mean torque output. Waveforms are compared with those predicted by simulations and conclusions are drawn regarding the performance of the drive systems.

The results of this work clearly demonstrate that segmental rotor SRMs have much greater torque capability than conventional toothed geometries. Of the two demonstrator machines constructed, one has a very high torque per unit loading, but has relatively long end-windings; the other has slightly reduced torque per unit loading but overcomes the problem of long end-windings. Both machines appear to outperform other forms of reluctance motor.

Acknowledgement

I would like to express my deepest gratitude to both my supervisors Prof. Barrie C. Mecrow and Prof. J. W. Finch, for their patience, guidance, and encouragement during the development and completion of this research.

Special thanks to Dr. Christian Weiner for helping in MATLAB.

Thanks also to P. Dickinson, S.Turner, R. Hall, M. Armstrong, M. Leaver and all the RA's, and the postgraduate students in the UG lab.

My thanks also to all the technicians in the department.

List of Contents

List of Figures

Notes about some figures:

Flux Density Plot: red shading indicates regions of high flux density and the blue shading indicates regions of low flux density.

Saturation Plot: red shading indicates regions of high saturation and the blue shading indicates regions of low saturation.

Chapter 1

Chapter 2

PAGE MISSING IN ORIGINAL

Chapter 3

Chapter 4

Chapter 5

Chapter 6

Chapter 7

Chapter 8

Chapter 9

Chapter 10

List of Symbols

12/8 Denotes a machine configuration of 12 stator teeth and 8 rotor poles.

12/10 Denotes a machine configuration of 12 stator teeth and 10 rotor poles.

A Electric Loading in terms of r.m.s. MMF per unit length of periphery.

F Force

W' Co-energy

I current (Amperes)

T Torque

l Axial Length (Unit length)

t Width of air-gap which actively carries magnetic flux in the aligned position

x Distance between adjacent rotor segments.

y Width of triangular stator slot closure at the air-gap

ϕ Magnetic flux

ψ Flux-Linkage

L Phase coil inductance

λ pole pitch

SRM Switched Reluctance Motor

dc Direct Current

ac Alternating Current

IGBT Insulated Gate Bipolar Transistor.

θ Rotor Position

Subscripts

r referred to rotor, **s** referred to stator

Convention SRM: Switched Reluctance Motor with Toothed-Rotor.

Segmented-Rotor SRM: Switched Reluctance Motor with Isolated Iron Segments. Each Segment Represents one Rotor Pole.

Short Pitched SRM: Switched Reluctance Motor in which Each Coil Links One Stator Tooth.

Fully Pitched SRM: Switched Reluctance Motor in which Each Coil Links One Stator Pole Arc.

MMF: units in Amperes.Turns.

1 Introduction

1.1 General

Switched reluctance motors (SRMs) have generally been developed with the intention of producing a low cost variable speed drive with a high mean torque output. Extensive research has refined the design concept so that it is now well understood, with dimensions established for optimisation of the maximum specific output torque, maximum speed and the maximum efficiency of any conventional SRM. This research accepts that further significant gains can not be made within the existing SRM structure of a toothed stator and rotor then attempts to find more radical changes to SRM design instead. New magnetic concepts are introduced, analysed and developed into working prototypes, which seem to offer very significant advantages over existing topologies.

1.2 Overview of Switched Reluctance Motors

The Switched Reluctance Motor (SRM) is a variable reluctance stepping motor that is designed to convert electrical energy to mechanical energy efficiently. It belongs to the class of machines that depend upon magnetic reluctance variation to produce torque.

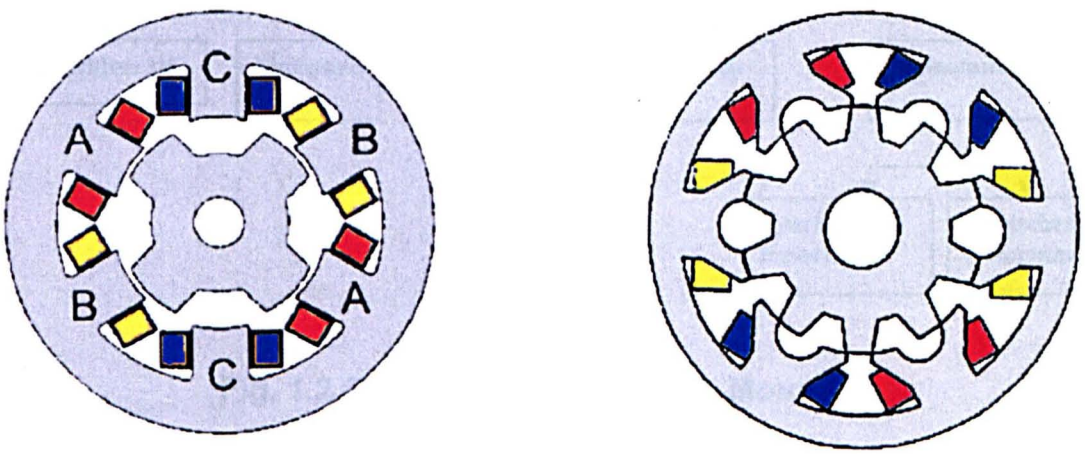

(a) One Tooth per Pole (b) Two Teeth per Pole

Fig. 1.1 Conventional SRM

The SRM has a very simple, robust and rugged structure, as shown by the two examples in Fig. 1.1. The stator and rotor are made of laminated iron. The rotor is a brushless toothed structure with no windings or magnets; all windings are in the stator. Consequently the rotor losses can be extremely low and the rotor can be very strong, allowing high speed operation [1]. Moreover, the motor can work between –100°C and +250°C because of the absence of windings or magnets on the rotor. It is argued that the simplicity of construction makes the cost of this motor low [2-20].

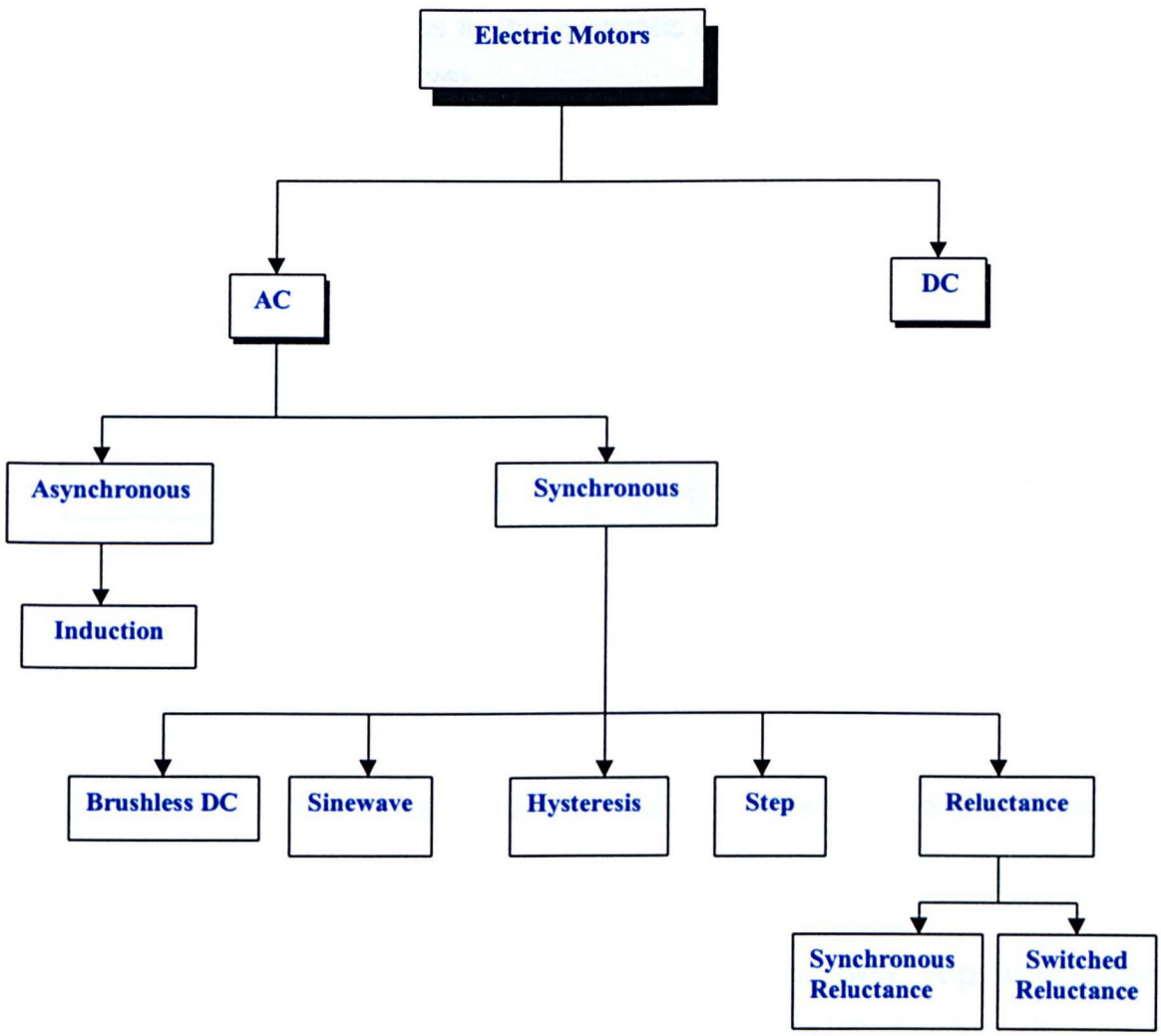

Fig. 1.2 Classification of Electric Motors

As shown in Fig. 1.2, there are two types of reluctance motors: the synchronous reluctance and switched reluctance. Synchronous motors are classed as singly salient (only the rotor is salient) and are generally excited with sinusoidal current.

Switched reluctance motors have both salient rotors and stators and are hence classed as doubly salient. The phase windings are generally excited with pulses of unidirectional current, with the timing of the pulses controlled as a function of the rotor position.

The switched reluctance motor has many advantages over other electric motors used in drive applications Fig. 1.3. The principal advantage is one of simple, low cost construction. However the SRM has two main drawbacks: it has large ripples in the torque characteristic and can suffer from high levels of acoustic noise. These effects can be reduced by modifications to the magnetic circuit [21-32] and through the use of novel control techniques [33-38].

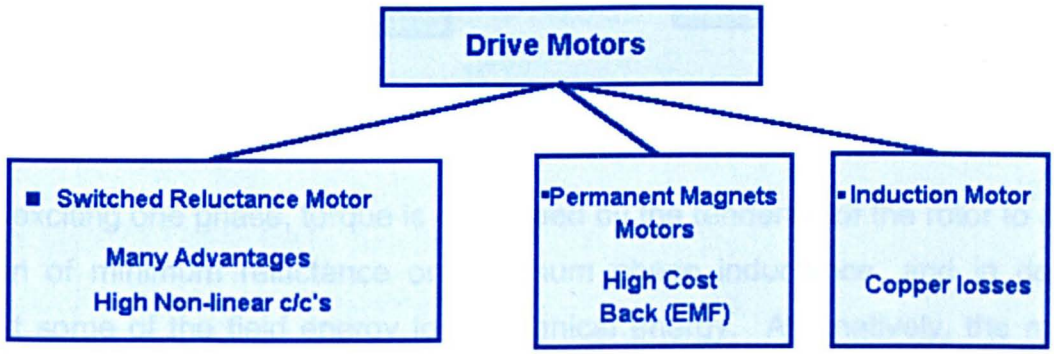

Fig. 1.3 Motors used in Drive Applications

The block diagram of a typical switched reluctance drive is shown in Fig. 1.4. Unlike induction motors or DC motors the switched reluctance motor can not run directly from a simple DC supply or sinusoidal AC supply. It requires a power electronic converter fed from a DC supply, so as to energise each phase with a current pulse at the appropriate instants of time. The flux in the switched reluctance motor is not constant, but must be established from zero every working step. A power converter circuit must supply unipolar current pulses, timed accurately to coincide with the rising inductance period of each phase winding. SRMs are electronically commutated, therefore, some means of rotor position detection must be provided. It is therefore advantageous to feed rotor position information from a shaft mounted-sensor back to the control board. The power converter must also regulate the magnitude of the current, to meet the (torque and speed) demand placed on the drive

by the load. A phase current measuring device and current regulator should therefore be present.

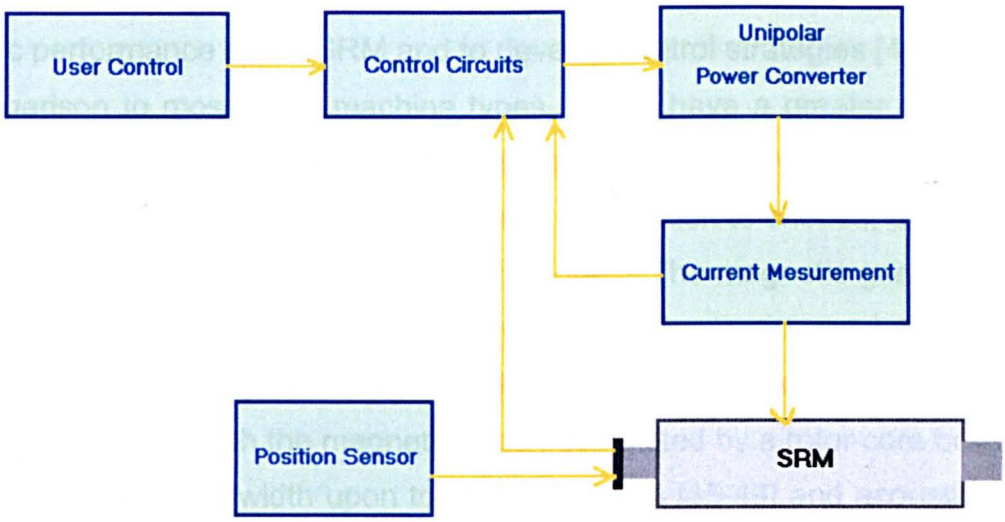

Fig. 1.4 SRM Circuit

When exciting one phase, torque is developed by the tendency of the rotor to adopt a position of minimum reluctance or maximum phase inductance, and in doing so convert some of the field energy to mechanical energy. Alternatively, the machine may be viewed as being in a state where, when exciting one stator pole, all positions are unstable, except the position of minimum reluctance: the rotor poles consequently move to this stable position, known as the aligned position. The instantaneous torque developed is time varying in magnitude and its average depends on the excitation current waveform and its timing relative to the rotor position. The control circuit controls the excitation level and sequence to adjust the speed and torque of the switched reluctance motor [39-41].

1.3 SRM Design

Two US patents filed by Bedford and Hoft in 1971 and 1972 describe many of the essential features of the modern switched reluctance motor [42]. In 1974 Lawrenson et al [43] wrote one of the fundamental papers of switched reluctance motor design. In this paper it was shown that the reluctance torque produced by an SRM is fundamentally limited to a certain value when the diameter and the axial length are kept constant. This will be discussed in detail in chapter (2).

The electromagnetic analysis of doubly salient motors has progressed to the point where the geometry of laminations can be optimised for particular applications. There is software to predict the static characteristic of the SRM, to predict the dynamic performance of the SRM and to develop control strategies [44].

In comparison to most other machine types, SRMs have a greater range of design options. There are the apparent complications of different pole combinations, different phase numbers, ranges of pole arcs from which to choose, etc. These pose a completely new set of problems to the designer. The magnetic geometry of SRMs has been effectively fixed for over twenty years. The basic structure consists of a series of stator teeth or poles, magnetically connected together by a core back, and a series of rotor teeth, with the magnetic circuit completed by a rotor core back.

The effect of the tooth width upon torque production [45-49] and acoustic noise [50-52] is well established: the influence of pole number upon mean torque ascertained [53], and designs which reduce torque ripple determined [54-56]. There has been examination of the optimum shape of tooth tip and whether the tooth should be tapered [49,57]. Multi-tooth per pole designs have been studied [58-59], but not generally developed, so the geometry effectively remains fixed. Rotor and stator teeth are generally straight or only slightly tapered: the tooth width of both rotor and stator is typically 33-50% of the pole pitch and the tooth tips do not have substantial pole shoes.

There has been greater diversity in the electrical design of SRMs. The majority continue to use simple concentrated windings, wrapped around a single tooth, because of their simplicity and short end-windings. However, there have been developments using fully pitched windings to increase the electrical utilisation of the machine, thus improving torque capability at the expense of increased end-winding length.

SRM design depends upon accurate determination of the machine's relationship between the excitation current and magnetic flux linking the windings. Whilst there have been many design programmes developed using analytical approximations, these are not general enough to encompass more radical design variations. For this reason the finite element method has been chosen in this work to predict machine characteristics. Complex geometries can be modelled, including magnetic saturation, giving a highly flexible design tool. Because the structures studied give rise to an

essentially two dimensional magnetic field only 2D finite element methods have been employed throughout.

1.4 The Characteristic of the Switched Reluctance Motor

The Flux–Linkage versus Current characteristic of the SRM is very important in its operation and performance. There are two extreme positions, which characterise this motor, the aligned position where the inductance is maximised and the unaligned position where the inductance is minimised. The area between them is proportional to the torque. For comparison between the average torque capabilities of different designs of SRM having (the same length and diameter) it is enough to look to the area enclosed between the aligned and the unaligned position.

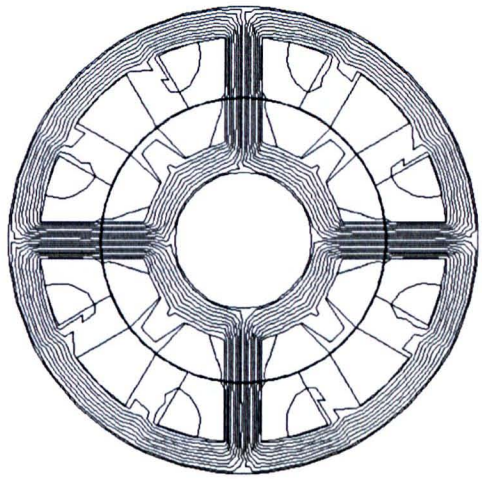

Fig. 1.5 Magnetic Flux Plot 12/8 Short Pitched SRM at the Aligned Position

In the aligned position the phase inductance is at its maximum value. At low current levels most of the reluctance is in the air gap, but the long path through the stator yoke can also absorb a significant MMF and reduce the aligned inductance appreciably, even at low currents. So shortening the flux path increases the inductance in the aligned position.

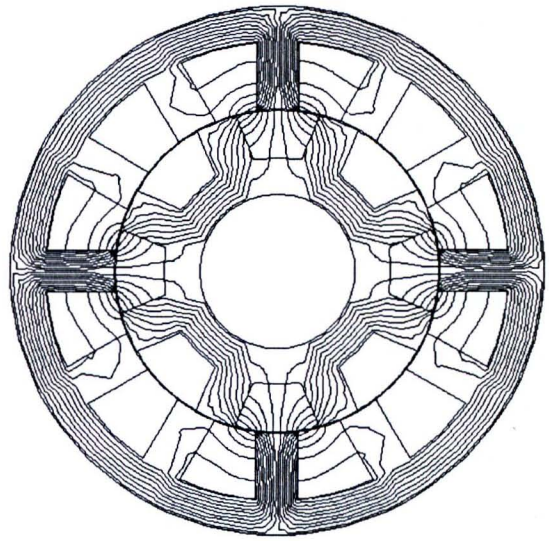

Fig. 1.6 Magnetic Flux Plot of 12/8 Short Pitched SRM at the Unaligned Position

In the unaligned position the phase inductance is at its minimum, because the magnetic reluctance of the flux path is at its highest as a result of the large air gap between the stator and the rotor. The air gap reluctance is much greater than that of the iron sections [60].

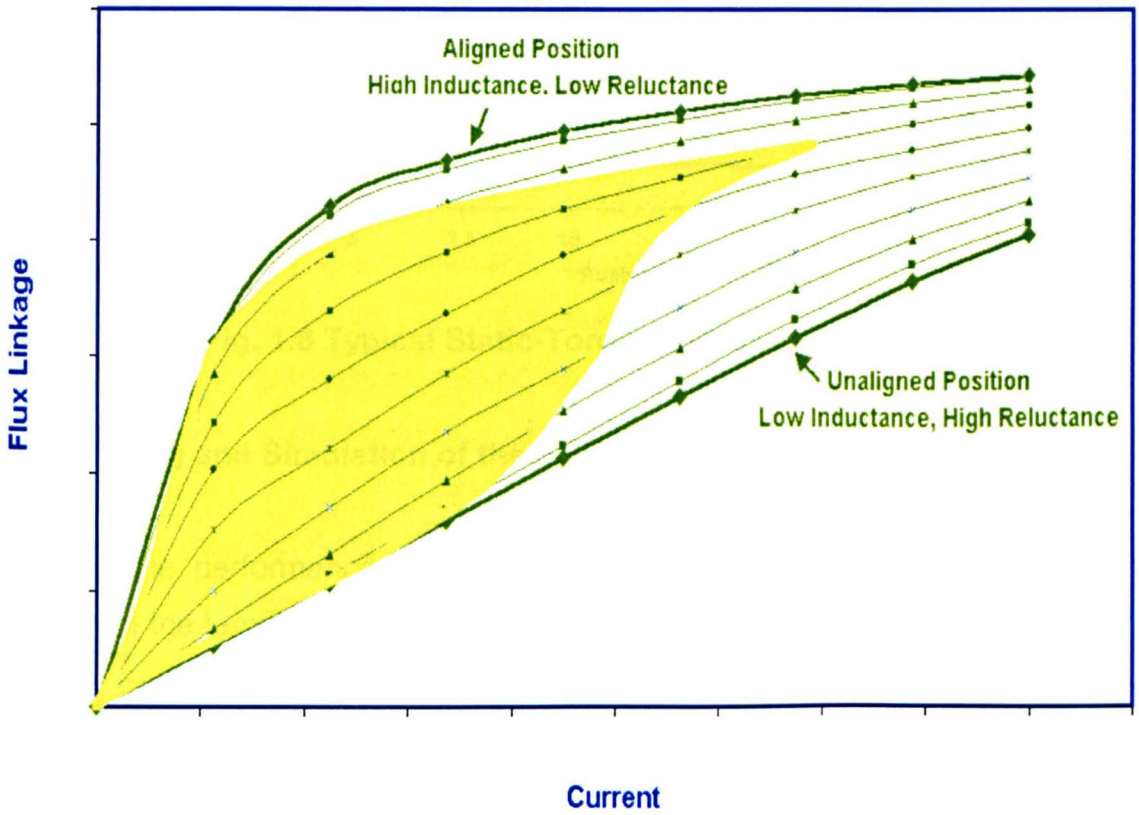

Fig. 1.7 Typical C/C's of a SRM

Fig. 1.7 shows the characteristic of the SRM and a typical flux linkage trajectory. The characteristics are fixed for a given machine design, but the flux linkage trajectory depends on the operation of the SRM. In the unaligned position the length of the air gap is a maximum and the flux path is long. That means the flux density is low, so there is no saturation or low saturation (the relation between the flux linkage and the current at the unaligned position is linear or approximately linear). In case of the aligned position the air gap is small, the flux path is short and flux density is high so there is saturation; the highest saturation in the machine is at this position.
Fig. 1.8 shows a typical variation of torque with respect to position for a series of different current levels, illustrating the nonlinear nature of torque variation.

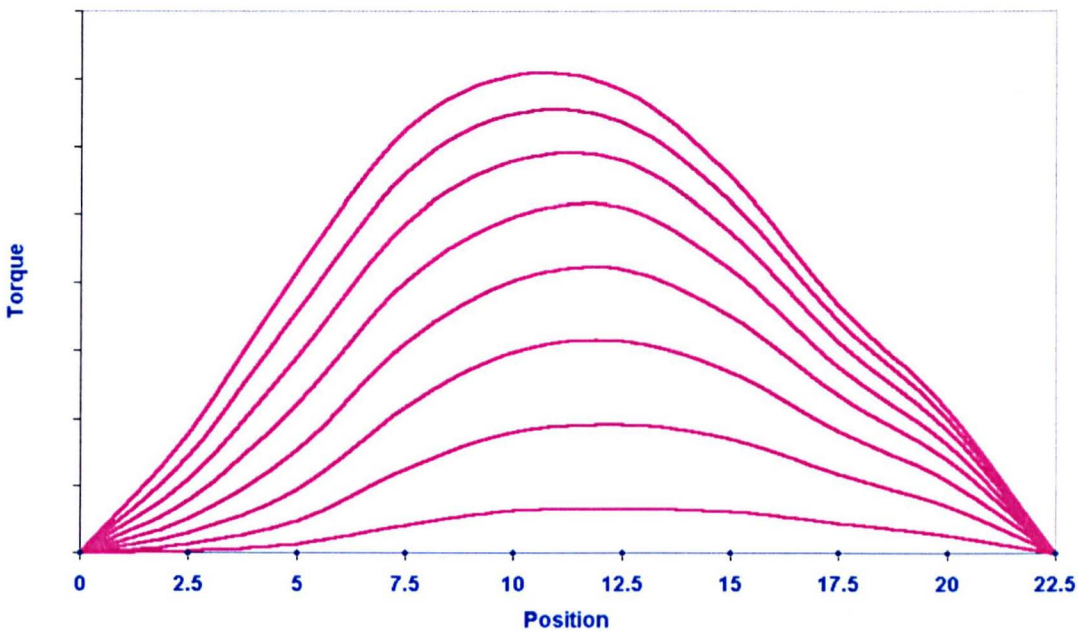

Fig. 1.8 Typical Static-Torque C/C's (e.g. 12/8 SRM)

1.5 Modelling and Simulation of the SRM Drive System

The machine performance has been predicted analytically from the fundamental equation of the terminal voltage of any machine

$$v = R.i + \frac{\partial \psi}{\partial t}$$

Then by solving one of the following 1 st order differential equations [61-62]:

$$v = R \cdot i + \frac{di}{dt} \cdot \frac{\partial \psi}{\partial i}(\theta, i) + \omega \cdot \frac{\partial \psi}{\partial \theta}(\theta, i)$$

$$v = R \cdot i + \frac{di}{dt} \cdot \frac{\partial \psi(\theta, i)}{\partial i} + \omega \cdot \frac{\partial \psi(\theta, i)}{\partial \theta}$$

$$v = R \cdot i + \frac{di}{dt} \cdot L(\theta, i) + \omega \cdot i \cdot \frac{\partial L}{\partial \theta}(\theta, i)$$

$$v = R \cdot i + \frac{di}{dt} \cdot L(\theta, i) + \omega \cdot i \cdot \frac{dL(\theta, i)}{d\theta}$$

A numerical approach to the simulation of SRMs has been introduced in [61]. The flux-linkage can be determined from this equation

$$\psi = \int \left(v - R \cdot i(\theta, \psi) \right) \delta t$$

The torque can be obtained indirectly from the co-energy

$$W'(\theta, i) = \int_0^i \psi(\theta, i)\, di \Big|_{\theta = const}$$

$$T(\theta, i) = \frac{dW'(\theta, i)}{d\theta} \Big|_{i = const}$$

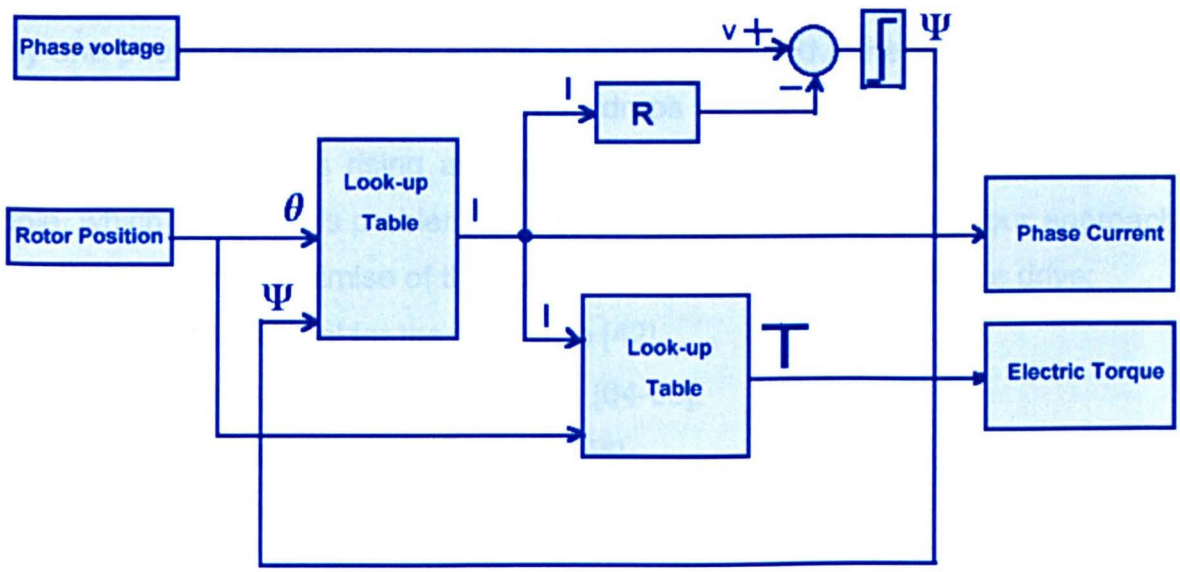

Fig. 1.9 The Block Diagram of SRM Simulation

Fig. 1.9 is the block diagram of the SRM simulation package. The flux linkage characteristic data is taken from an adaptive finite element solution of the magnetic characteristics; it is stored in tables (one for the flux-linkage characteristic and one for the torque), then loaded in to a simulation of the SRM using Matlab/Simulink [62].

1.6 Torque Ripple

Torque ripple is the primary disadvantage of SRMs and limits their applications. Reluctance torque is developed when energising a pair of stator poles with a pair of rotor poles at any unaligned position. As the rotor poles approach the aligned position, inductance increases until the rotor poles align with the excited pair of stator poles. While the inductance is increasing, torque is positive, since $dL/d\theta$ is positive. As the rotor poles rotate past the excited stator poles, inductance begins to decrease, making $dL/d\theta$ negative, which means that a negative, or braking torque is produced. To prevent this braking effect on the rotor the current is removed from the phase before the aligned position is reached, de-energising the stator poles. Subsequently, or simultaneously, a second phase is energised. If the second phase is energised when the inductance between the second pair of stator poles and the rotor poles is increasing, positive torque is maintained and the rotation continues. Continuous rotation is developed by energising and de-energising the stator poles in this fashion. The total torque is the sum of individual torques described above. Since only one phase is energised at a time in a traditional SRM, the torque developed by the machine is not smooth [63]. Torque drops off steeply near the unaligned and aligned positions. This rising and falling torque phenomenon is known as torque ripple, which is a serious problem for some applications. There are four approaches that can be used to minimise of the torque ripple of switched reluctance drive:

- Selecting the material for the rotor core [42].
- Shaping the magnetic circuit geometry [64-65].
- Shaping the phase current waveform [66].
- Applying appropriate control [67].

The optimum minimisation of torque ripple is achieved by the combined action of all four approaches [68].

1.7 Aims and Objectives of the this Thesis

This research aims to increase the torque density of switched reluctance motors through the adoption of new magnetic topologies. A constraint upon any new topology is that it should remain simple to construct and be suitable for mass production.

The research has contributed the following developments:

(a) Introduction of the idea of using isolated segmental rotor poles in an SRM.

(b) Evaluation of the concept on simple single phase machines with linear motion.

(c) Development of a multi-phase rotating SRM with a segmental rotor and fully pitched windings.

(d) Development of a multi-phase rotating SRM with a segmental rotor and single tooth windings.

(e) Production of two three phase demonstrator machines.

(f) Presentation of static and running results and detailed comparison with predictions.

(g) Demonstration that the new concepts significantly increase the torque capability of SRMs.

(h) Comparison with conventional SRMs.

(i) Estimating the losses (iron and copper).

(j) Testing the new design when two phases are excited simultaneously.

1.8 Thesis Layout

Chapters 2-11 are laid out as follows:

Chapter 2: General development of the segmental rotor concept. This chapter reviews methods for increasing the torque capability of SRMs then introduces the concept of a segmented-rotor SRM. A basic evaluation of the concept reveals its advantages and establishes some simple design rules.

Chapter 3: This chapter presents in detail the analysis, design and optimisation of a three phase segmental-rotor SRM with fully pitched windings. A detailed design is produced and compared to conventional SRM geometries.

Chapter 4: The fully pitched segmented-rotor SRM has relatively long end-windings, thus increasing the end-windings copper loss. This chapter introduces an alternative design in which the windings are placed round a single tooth to reduce the end-winding length. Once more, design rules are established and a demonstrator design finalised.

Chapter 5: Comparisons between predictions for the new designs and a conventional SRM are presented.

Chapter 6: This chapter details the construction and static testing of the machine developed in chapter 3. Comparisons between predicted and measured results are presented.

Chapter 7: This chapter deals with the construction and static testing of the machine design developed in Chapter 4. Once more, measured results are compared with predicted values.

Chapter 8: Discusses the mutual Interaction between phases.

Chapter 9: The magnetic flux distribution in different parts of the machine is evaluated and used to estimate iron loss. These estimations of iron loss are compared with those occurring in a conventional SRM.

Chapter 10: Running tests are presented for the two new machines.

Chapter 11: Conclusions.

2 General Development of the Segmental Concept

2.1 Introduction

Chapter one has discussed the general merits of the SRM compared to other types of electric motor. Machine designers have attempted to improve the performance of SRMs, including ways to increase their output torque, decrease the losses, decrease torque ripple and decrease acoustic noise. This chapter introduces a fundamentally new design of SRM, which shows superior average torque capability compared to the conventional design of SRMs. The new design introduces a new magnetic circuit geometry, particularly in the rotor of the machine. The new rotor consists of isolated iron segments, with each segment representing a separate rotor pole. The chapter explains in detail the development of the segmental concept, including both magnetic and electric aspects of the design. For clarity the concept is initially applied to a geometrically linear, single phase, segmented-rotor SRM [69-70].

2.2 The Relation between the Flux-Linkage Characteristic and the SRM Output

The torque delivered by an SRM is given instantaneously by the rate of change of co-energy in the machine. In moving from a rotor position, θ, through an angle $\delta\theta$ the co-energy converted to torque is usually represented by the area between the flux-linkage-current curves at angles θ and $\theta+\delta\theta$.

If current is applied at the unaligned position and removed at the aligned position then the mean torque developed is given by the area between the two flux-linkage characteristics at these extreme positions, divided by the angle traversed. Any SRM designer can therefore attempt to increase the output torque of the SRM by increasing this area. It should be noted that the inductance at the aligned position can not be infinity because of many reasons, such as the permeance of the iron, and the inductance at the unaligned position can not be zero because of cross slot leakage flux. So one of the SRM designer's considerations will be to increase the area between these two lines as much as possible.

2.3 The Limit of the Torque in a Conventional SRM

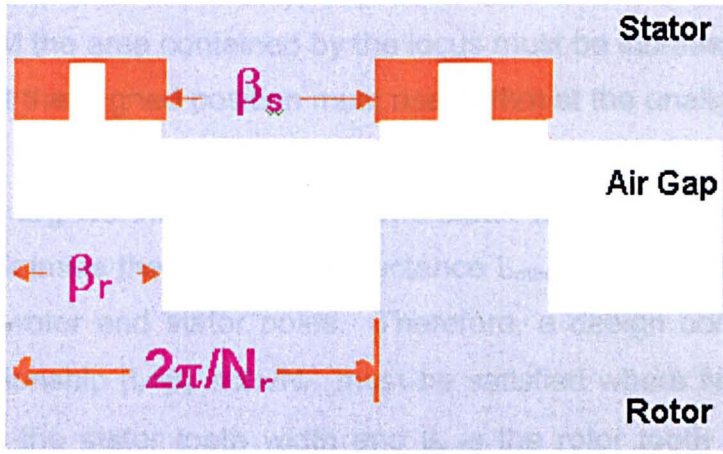

Fig. 2.1.a Simple Linear Case of Doubly Salient Reluctance Motor

Fig. 2.1.a shows a simple rectilinear example of a conventional doubly salient construction. The figure is used here to explain the torque limitations of conventional designs of switched reluctance motor.

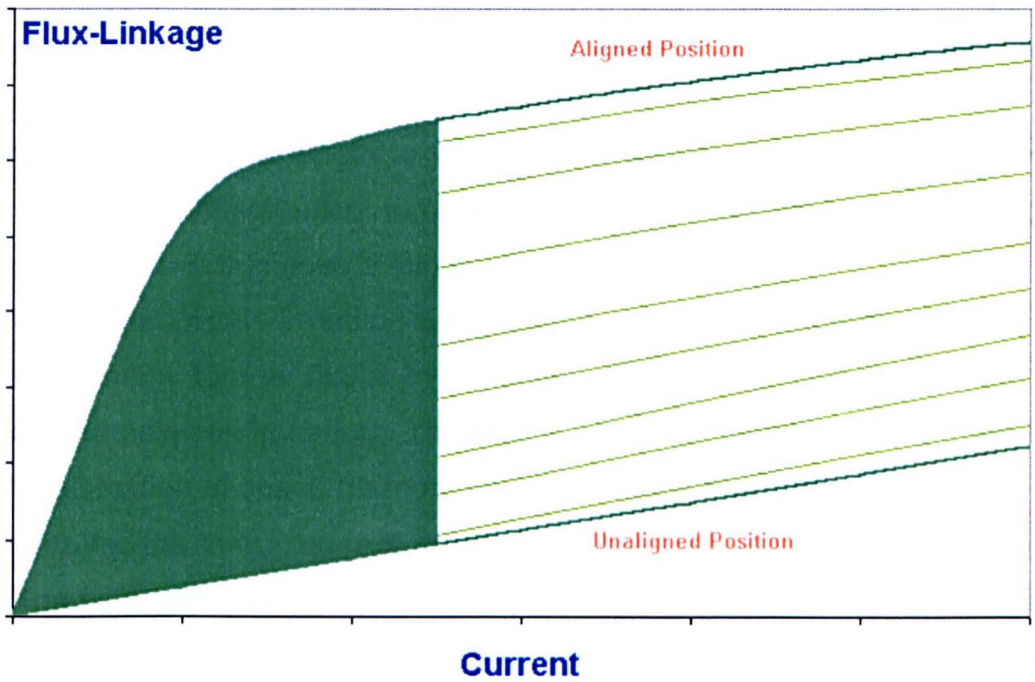

Fig. 2.1.b The Non Linear Characteristic of the Switched Reluctance Motor (The Flux-Linkage Trajectory under Current Control)

Fig. 2.1.b shows typical flux-linkage/current curves for a range of positions and also a typical flux-linkage locus traversed under current control. To increase the output torque of the SRM the area contained by the locus must be increased. Clearly, either the flux-linkage at the aligned position must rise or that at the unaligned position must fall.

To maximise the aligned inductance L_{max} one stator tooth must be aligned with one rotor tooth. To minimise the unaligned inductance L_{min} it is essential that there is no overlap between rotor and stator poles. Therefore, a design constraint exists [71] wherein the relationship $\beta_r+\beta_s \leq 2\pi/N_r$ must be satisfied where N_r is the number of rotor poles, β_s is the stator tooth width and β_r is the rotor tooth width. Under the above constraint L_{min} is limited by the leakage fields. The cross-sectional area of the flux path in the aligned position is maximised when $\beta_s=\beta_r=\pi/N_r$. The aligned inductance, L_{max}, is then limited by the permeance of the main flux path. At low values of excitation this is dominated by the air gap length, whilst at high excitation levels it is dominated by magnetic saturation of the laminations [71].

2.4 Summary of Previous Attempts to increase the Torque Capability of SRM

1-Decreasing the air gap length to increase the aligned flux-linkage. This will only have a significant effect upon torque production during low levels of excitation. Mechanical constraints impose a minimum air-gap length [72].

2-In [73-74] a complicated method was used to achieve both the maximum T/I^2 ratio and the minimum torque ripple by selecting the optimal combination of current waveform and pole configuration. The idea is based on a principle that there exists a special combination of space harmonics of inductance and time harmonics of current which improves the torque/current ratio and, at the same time, eliminates the torque ripple. The pole configuration is designed to have a predominant 3^{rd} space harmonic of inductance and the current is regulated to have a predominant 3^{rd} time harmonic. The method was very complicated and ignored some sources of the ripples such as the effect of the converters [75-78].

3- Using multi-teeth per stator pole. An increase in the torque developed by a multi-teeth stator pole configuration has been reported by Finch [79] (see Fig. 2.2).

However, the machine proved difficult to wind and was acoustically noisy. For this reason it has not been adopted by industry.

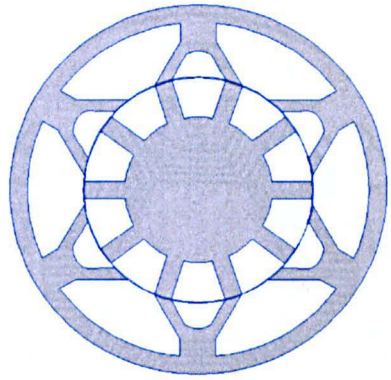

Fig. 2.2 Multi-Tooth per Stator Pole

4-By using two stators to drive one rotor [80] as shown in Fig. 2.3. This enables the electric loading to be increased, but is very difficult to construct in a rotating machine.

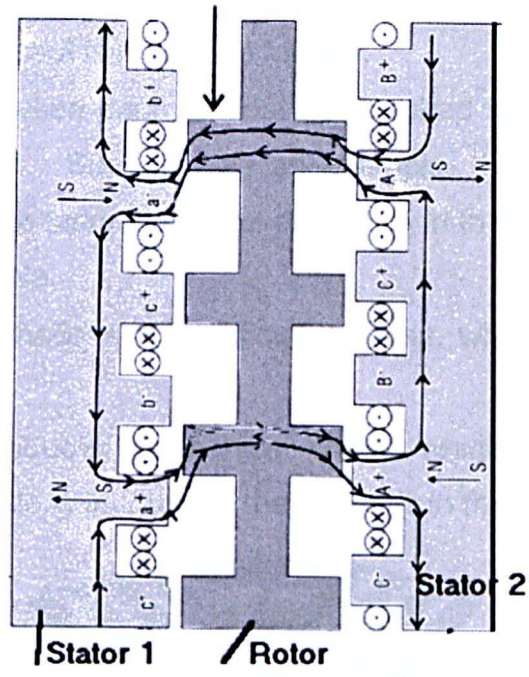

Fig. 2.3 Two Stators Driving one Rotor

5-Using a fully pitched windings, which enables an increase in the MMF per pole. Because this machine has longer end-windings it is only suitable for applications where the axial length is greater than the length of a pole pitch [81-83].

6-The use of axially laminated rotors. Lipo [84-87] and Xu [88-89] made prototype machines of this type, borrowing a technology developed for synchronous reluctance

machines. The laminations were folded to form flux guides, providing maximum inductance when a flux guide of the rotor is aligned with a slot.

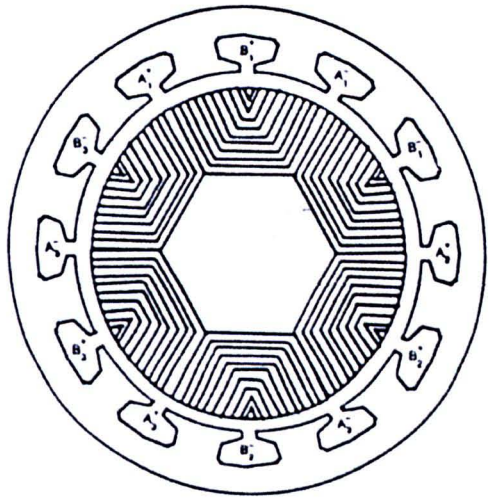

Fig. 2.4 SRM with Axial Laminated Rotor

The axially laminated concept is limited as follows:

- There is isolation between each lamination, required to provide a flux barrier in the unaligned position. Suppose, as an example, the ratio of the iron to the isolation is 2:1, then the saturation level of the flux in the aligned position is limited to 2/3 that of a solid pole.
- Bending the iron laminations is a difficult process, which is not suited to mass production.
- Bending the iron introduces mechanical stress, which influences the magnetic characteristics, particularly increasing the iron loss in the laminations.

Fig. 2.5 Cross Section of one Segment of an Axially Laminated SRM

7-Short Flux Loops by selecting the windings configuration: If the length of the magnetic circuit is reduced then so is its reluctance, therefore any reduction in path length should increase the flux-linkage for a given source MMF. This philosophy was adopted by Hendershot [90] and Michaelides and Pollock [91]. The technique

adopted by Michaelides and Pollock will be explained with reference to figures 2.6 and 2.7.

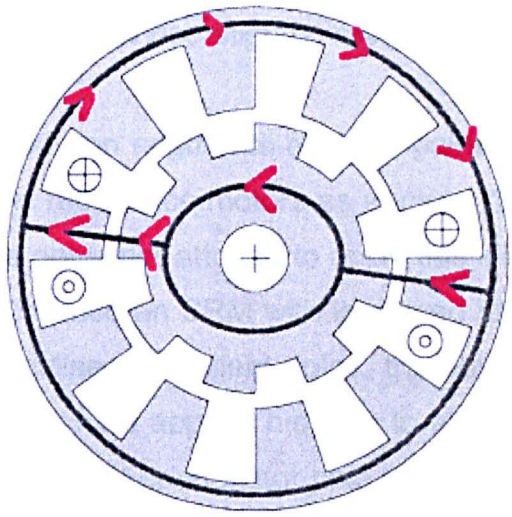

Fig. 2.6 5-Phase Short Pitched SRM (Only one Phase Excited)

Fig. 2.6 shows a 5-phase SRM with a short pitched windings and only one phase excited. Magnetic flux exits from the stator pole, through the air-gap to the rotor pole, through the rotor core back, out another rotor pole which is diametrically opposite, back across the air gap and returns round one half the stator core back. Because the core back paths are long this is referred to as a long flux loop.

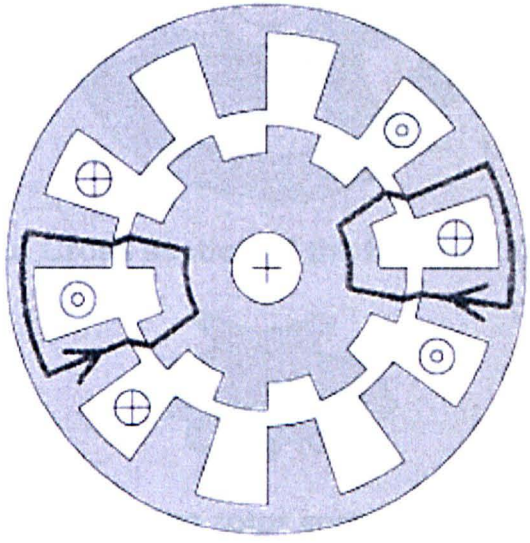

Fig. 2.7 Five Phases Short Pitched SRM (Two Phases Excited Simultaneously)

Fig. 2.7 shows the same machine, with adjacent coils excited by opposite polarities. When two phases are excited simultaneously the flux loops became much shorter than the previous case and the magnetic reluctance is decreased. For a fixed MMF the magnetic flux should therefore rise slightly, resulting in an increase in the torque capability.

8-The idea of using isolated iron segments as rotor poles in reluctance motors was established in synchronous reluctance motors as early as 1960 [92-96]. A patent by Horst [97] seems to be the only prior attempt to apply this idea to switched reluctance motors. His idea was to produce an SRM with improved rotor design which reduces the flux path lengths and utilises all salient poles, thereby increasing power density and reducing motor losses. Horst applied his idea to a 2-phase machine only. The windings were disposed such that each stator pole is adjacent to two phase windings of opposite polarity with the magnetic flux through each stator varying in direction with the energisation of the various phases. Note how the air-gap length is distorted to one end of a segment. This gives a preferred direction of rotation and may help overcome the problem of rotor positions where zero torque occurs.

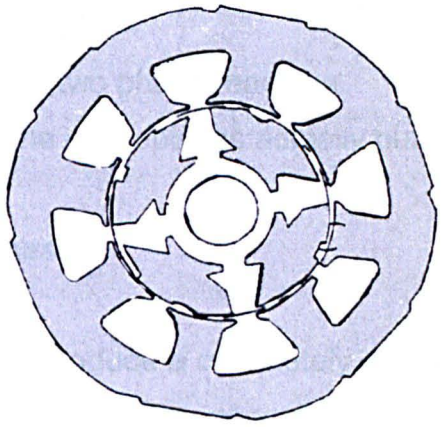

a) Cross section of the Horst SRM

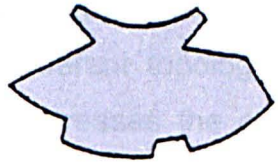

b) One rotor segment

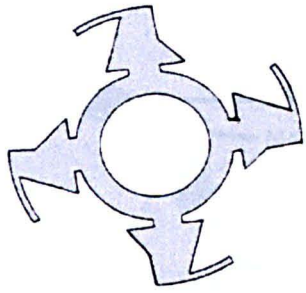

c) Non magnetic material to fit between the segments

Fig. 2.8 Horst Design of SRM

Fig. 2.8.c shows the non-magnetic material provides structural integrity to the rotor and holds the rotor segments firmly in place.

The limitations of Horst's invention are as follows:

1-He did not present any information on how to determine the proper values of the magnetic circuit parameters.

2-The shape of the segment was complex.

3-There was no discussion of the impact of the centrifugal forces at different speeds on the segments and the fittings.

4-The concept was limited to a two phase machine.

5-There is no evidence that the concept was actually built.

2.5 The New Idea in this Thesis

The aim of this research is to produce a completely new topology whilst retaining the simplicity of existing switched reluctance geometries. Complicated design will make the analysis, the performance prediction and, most importantly, motor construction both difficult and prohibitively expensive. The rotor of the conventional SRM will be replaced by another rotor of a different topology; this will be shown to create a greater reluctance variation that increases the output torque. Changing the rotor topology randomly is a waste of time as the changes may not have a significant impact. The new rotor must satisfy two points: to increase the saliency and to shorten the flux loops.

2.5.1 Describing the New Rotor

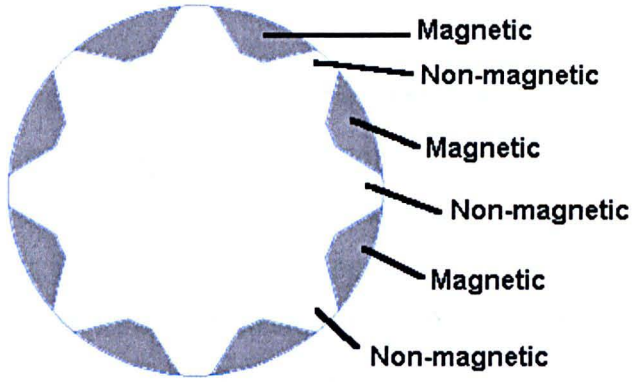

Fig. 2.9 Variable Reluctance Rotor

Fig. 2.9 shows the proposed new rotor of the single phase segmented-rotor SRM. The new rotor magnetic structure will be made from a series of isolated segments of laminations in an attempt to increase the saliency ratio and thus increase the torque capability. The segments collect the flux coming from the stator to close the magnetic circuit. In the conventional design when the stator tooth is energised the magnetic force pulls the rotor pole to the aligned position; magnetic flux enters the rotor via one rotor tooth, crosses the rotor core back and then exits from another rotor tooth. In the new design the flux enters the segment at one circumferential end and exits from the other end, returning via an adjacent stator tooth. Consequently the flux path is short, passing through a stator core back of arc equal to one tooth pitch [98].

In a conventional SRM the peak magnetic flux linking any one conductor is never more than one half the magnetic flux flowing down an excited stator tooth. In the new machine concept it is possible for the entire magnetic flux of a single stator tooth to link each conductor, thereby increasing the flux-linkage of a winding. Consequently the probability of the new design being able to deliver more torque than the equivalent conventional SRM is high, assuming the motor is designed and optimised properly.

The constraints and limitations of the new machine are fundamentally differ from those of a conventional SRM design; hence this thesis will attempt to provide an insight into the performance and limitations of this new machine.

2.5.2 New and Conventional Topologies from the View Point of Design and Optimisation

Design methods for conventional SRMs are well documented by several authors [99], with many successful prototypes having been built and used in industry, but in the case of the new SRM the basics of operation must be established first. To maximise generality, the concept will first be developed for simple, single phase, rectilinear examples and then applied to a multi-phase, segmented-rotor SRM.
The mechanical design of a segmental rotor is extremely important: a suitable means of fitting the segments onto the rotor must not affect the magnetic operation of the machine or introduce undue complexity, but the segments must be able to rotate at high speeds without flying off or moving from their place of fitting. The rotor design must not sacrifice the well-known advantages and features of the SRM (e.g. low cost, robustness, wide temperature and speed capability).

Like all motors the design of the new segmented-rotor SRM can be considered in three main parts [100-102]:

a) The magnetic circuit.
b) The electric circuit.
c) The mechanical design.

2.6 Simple Rectilinear Case of the New Design

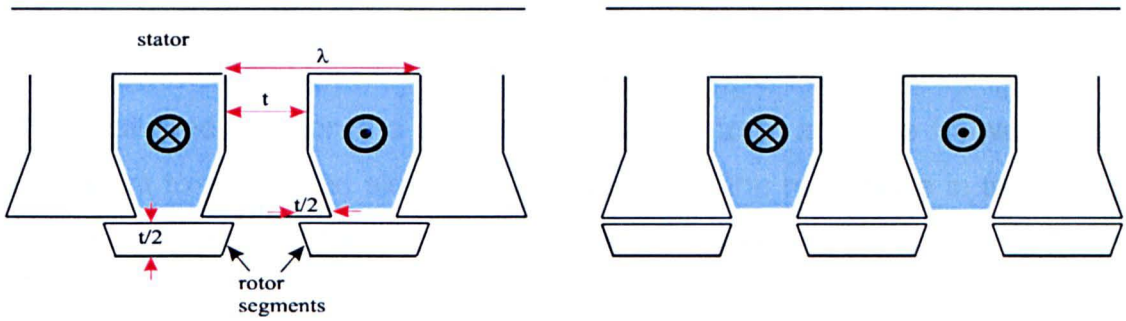

Fig. 2.10.a Rectilinear Representation of a Single Phase Segmental Rotor SRM, Showing first the Aligned Position and then the Unaligned Position

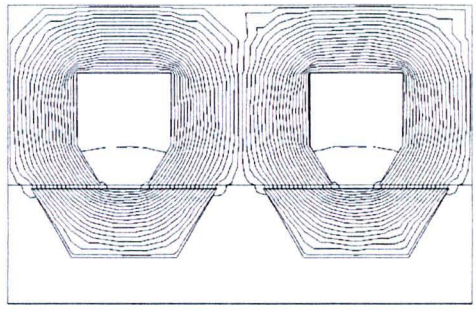

Fig. 2.10.b Magnetic Flux Plot, Showing the Single Phase Representation of Fig. 2.10.a in the Aligned Position

Fig. 2.10.a shows a rectilinear, single phase, segmental machine in which each stator coil encloses a single tooth. Fig. 2.10.b shows the magnetic flux distribution in the aligned position. The magnetic flux flows down one tooth, through a rotor segment and returns via the adjacent stator tooth. All the conductors in each slot only couple with flux driven by their own magneto-motive force, with very little mutual coupling between one slot and another. Torque production can therefore be envisaged on a per slot basis in which the slot MMF drives flux round the slot and the slot permeance is modulated by the rotor segments [69-70].

2.7 Design Rules for a Segmented Rotor SRM

The design concept has been progressed with the following rules:

1-In the aligned position the cross sectional area of the flux path should be equal at all locations to make the flux density uniform. This prevents regions of increased magnetic saturation and maximises the inductance in the aligned position.
2-In the unaligned position the segments must not form a bridge between the two teeth adjacent to an excited slot. This will maximise the reluctance in the unaligned position and ensure that the unaligned permeance depends principally upon cross-slot leakage flux.
3-The rotor segments should be shaped so as not to compromise rule 1 above whilst simultaneously ensuring that the shape does not unduly increase the unaligned permeance.

4-Overall optimisation of the parameters of the machine such as stator tooth width, the outside diameter of the rotor, the height of the pole shoe the angle of tapering of the pole shoe and the segment etc. must be considered simultaneously with the electric circuit, whilst not neglecting mechanical considerations.

The overall performance of the design concept will be judged by comparing it with the equivalent conventional one. The comparison must be comprehensive, including where possible the cost of construction, all sources of loss, mean torque and torque ripple and converter requirements.

2.8 Maximising the Area between the Aligned and the Unaligned Position

2.8.1 Maximising the Inductance in the Aligned Position

In a conventional SRM when one rotor tooth aligns itself with the energised stator pole this is called the aligned position. In the new segmented-rotor SRM the aligned position is the position when one rotor segment magnetically shorts two stator teeth and the permeance of an excited slot is at its maximum. This position occurs when the segment is centrally placed under the excited slot.

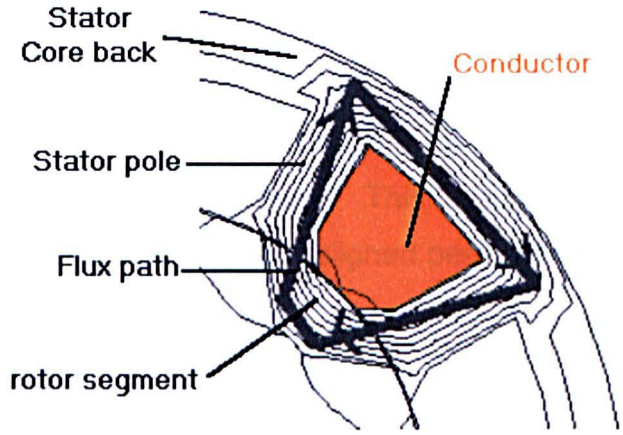

Fig. 2.11 One Segment links two Teeth in the Aligned Position

As shown in Fig. 2.11 the segment closes the flux path, making the flux path short. Two stator teeth link the segment.

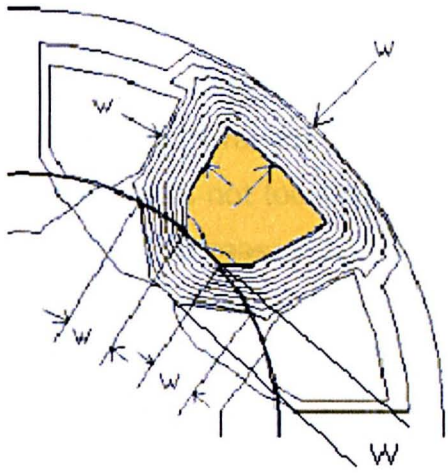

Fig. 2.12 How to Minimise the Flux Path Reluctance in the Aligned Position

Fig. 2.12 shows an attempt to meet the design rules of section 2.8. The core back width, the stator tooth width, the overlap arc between rotor segment and stator tooth and the radial height of the rotor segment have all been made equal. Note to meet these requirements the stator teeth have slot closure segments; without these it is not possible to maintain a large enough overlap angle between the rotor segments and the stator tooth tips.

2.8.2 Minimising the Reluctance in the Unaligned Position

In the unaligned position the segment must not close any flux path or part of it. As an example see Fig. 2.13 where the gap between rotor segments has been chosen to be equal to that of the stator slot opening. This ensures that neither the rotor or stator geometry contribute unduly to the unaligned permeance.

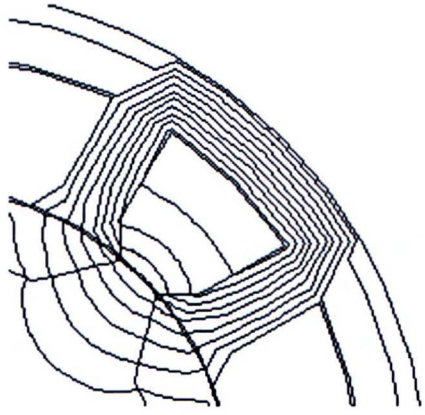

Fig. 2.13 the Magnetic Flux Path is open in the Unaligned Position

2.9 Optimum Value of the Tooth Width "t"

As the stator tooth width and rotor segment size is increased then the magnitude of the magnetic flux path permeance is increased and the torque per unit MMF will rise, providing the unaligned permeance is not too large. However, as the magnetic flux path increases in size the slot area decreases, so there is progressively less room for a winding. A global optimum of all dimensions is difficult to define, since it requires knowledge of the thermal performance of the machine. However, it is useful to explore the influence of tooth width upon the magnetic characteristics. The next section is dedicated to understanding the influence of tooth width in a rectilinear, single phase, segmented-rotor SRM.

2.9.1 Influence of Tooth Width in a Rectilinear Segmented Rotor SRM

In this section the tooth width will be varied and the Flux/MMF characteristics determined for a specific geometry. The area enclosed between the aligned and unaligned characteristics will be compared for both conventional and segmental topologies in order to give a measure of air-gap force density.

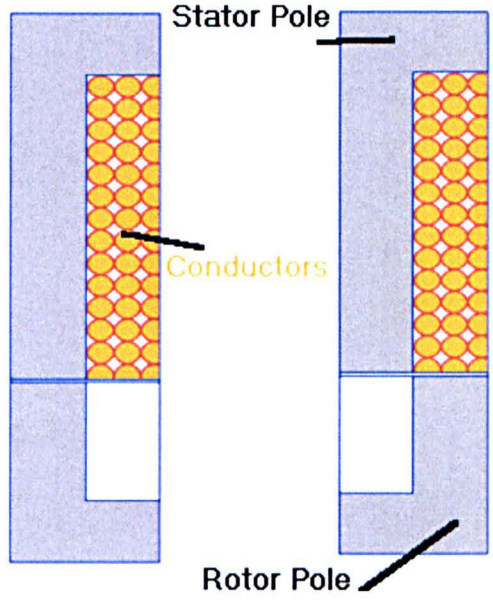

A- Aligned position B- Unaligned position

Fig. 2.14.a Conventional Design

Fig. 2.14.a shows the simple rectilinear model for the conventional topology. The design of this topology is taken as the standard design of the SRM (the core back width is equal to half the tooth width). The figure shows one half tooth, one half slot and the rotor and stator core backs. The boundaries of the figure form lines of symmetry, so that finite element modelling of this region is enough to define a fuller system with many teeth and slots. The MMF of the conductor in the slot can be varied and a graph of the aligned and unaligned Flux/MMF characteristics plotted. From the area enclosed between these characteristics a calculation of the mean air-gap force density can then be made. The procedure is repeated for a range of tooth widths and the various results compared.

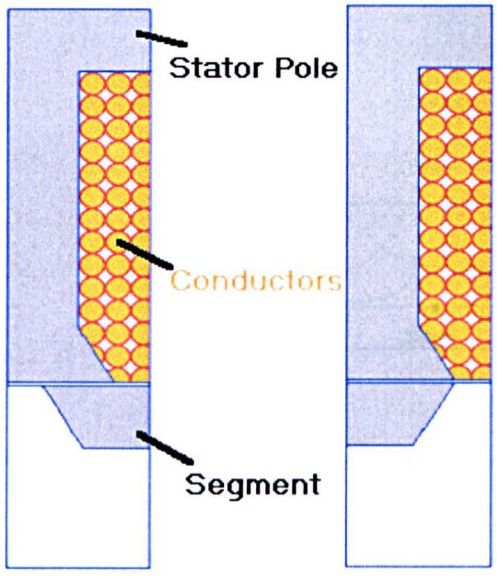

a- Aligned position b-Unaligned position

Fig. 2.14.b New Segmental Design

Fig. 2.14.b shows the equivalent new rectilinear model. The figure shows half of one stator pole and half of one rotor pole in both the aligned and the unaligned positions. The stator core-back, the overlap and the height of the segment are equal to one half the stator tooth width.

This has given two equivalent groups, one for the conventional design and one for the new design. The value of the air-gap tangential force produced by each group depends on many parameters, including the height of the poles, width of the tooth, air

gap length and the shape of the segment. For each group a slot pitch, λ, of 20.0 mm is used, along with an air-gap length of 0.3 mm. A standard silicon steel magnetisation curve is assumed for the magnetic components. The width of the teeth, t, is varied, whilst other dimensions are held fixed. Rotor teeth are chosen to be deep enough so that the rotor core back does not play a major part in the unaligned inductance, but stator cross-slot leakage flux is significant. The aligned position and the unaligned position will be inspected for both designs for different tooth widths.

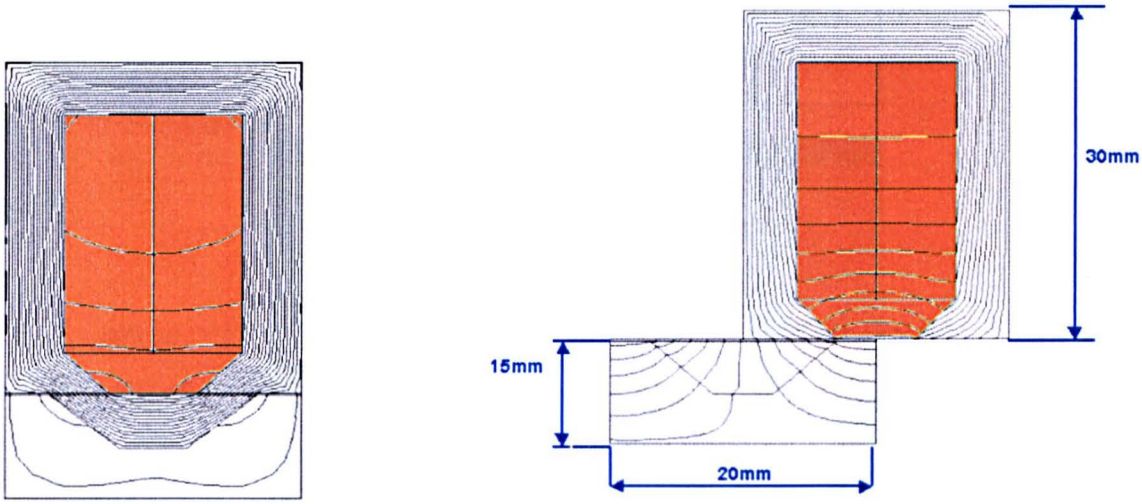

A- aligned position **B- unaligned position**

Fig. 2.15 Two Half Poles of the Stator and One Segment of the Rotor

Fig. 2.15 illustrates the magnetic flux distribution in the segmental machine in both the aligned and unaligned positions. The unaligned position is a position of unstable equilibrium. Once the rotor is displaced from this position it experiences a force seeking to move the segment from the unaligned position (maximum reluctance position) to the aligned position (minimum reluctance position). The reluctance force produced due to moving the segment from the position of minimum inductance to the position of maximum inductance is proportional to the area between the aligned and unaligned flux characteristics positions in both cases.

Fig. 2.16 shows the aligned and the unaligned positions for five different values of the ratio of the tooth width to the pole pitch, t/λ, varying from 0.3 to 0.7. In each case the horizontal axis corresponds to the MMF per half slot and the vertical axis is the

average magnetic vector potential of the conductors in the half slot. This corresponds to the average flux linkage per unit axial length.

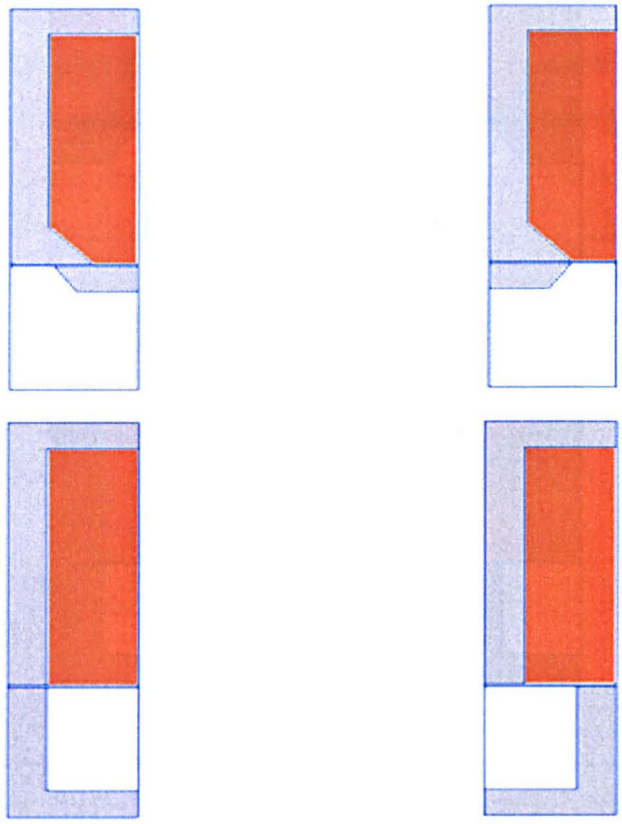

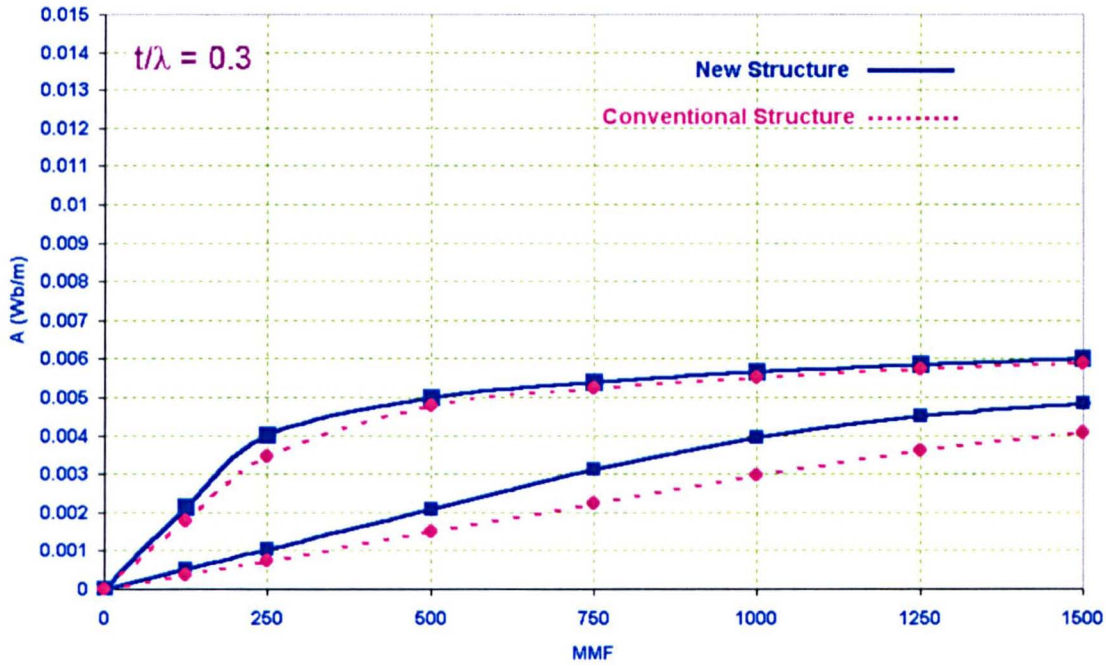

Fig. 2.16.a Flux versus MMF Characteristic (t/λ=0.3)

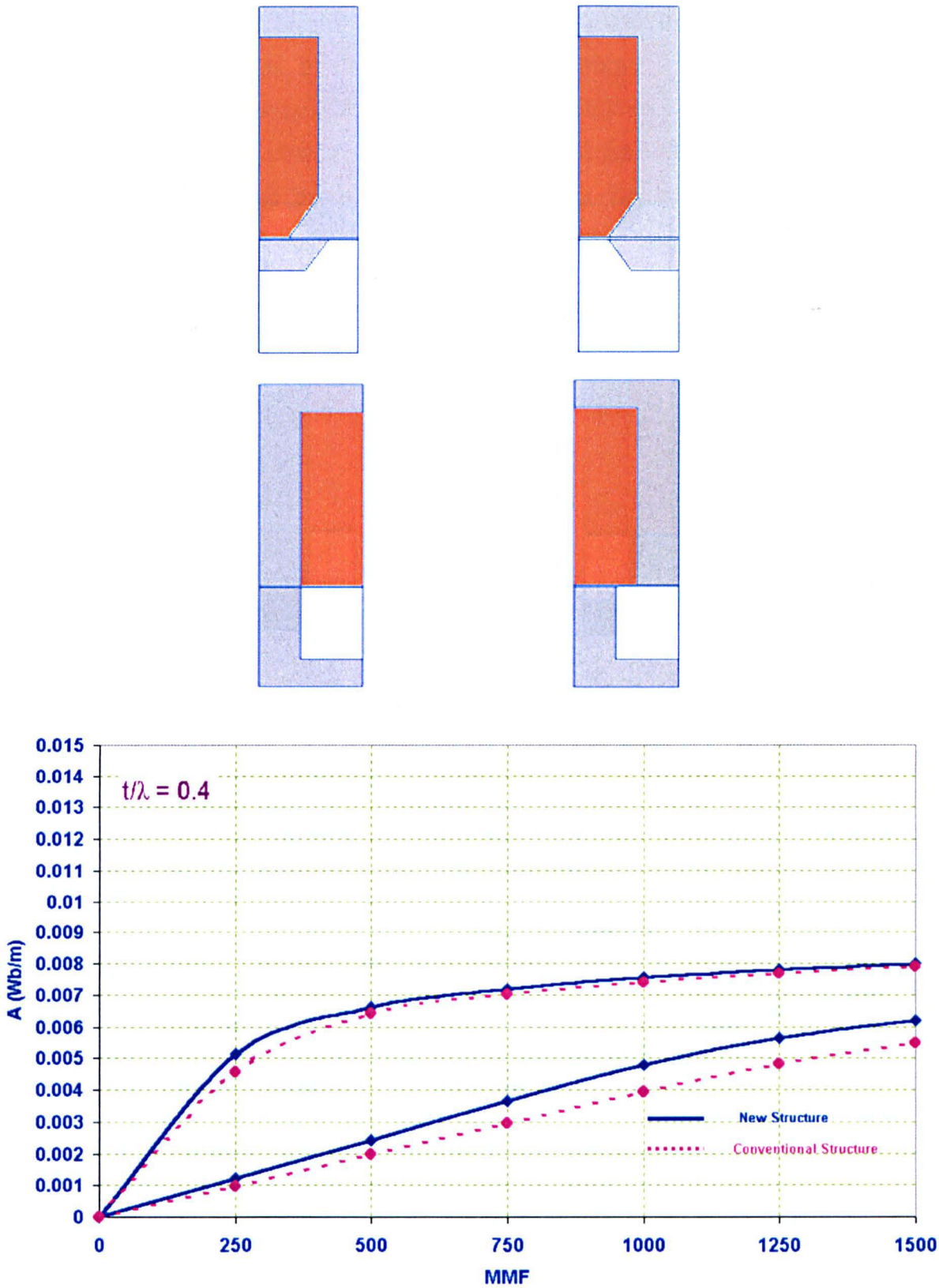

Fig. 2.16.b Flux versus MMF Characteristic (t/λ=0.4)

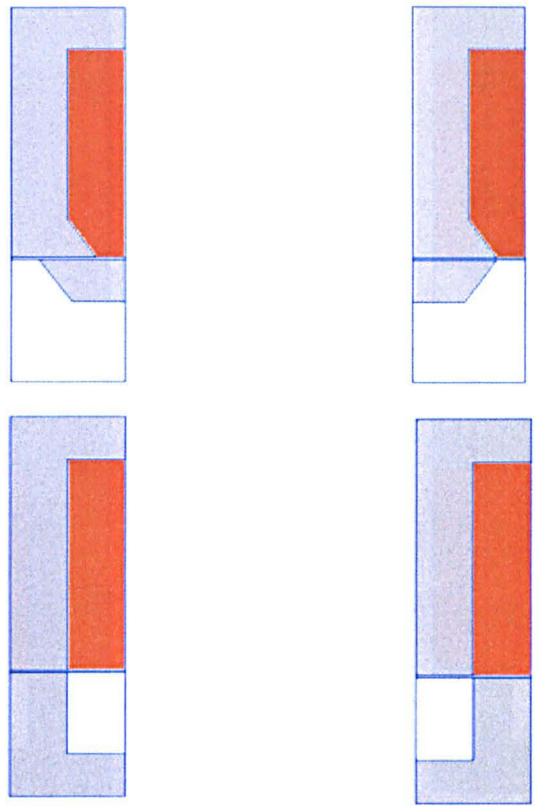

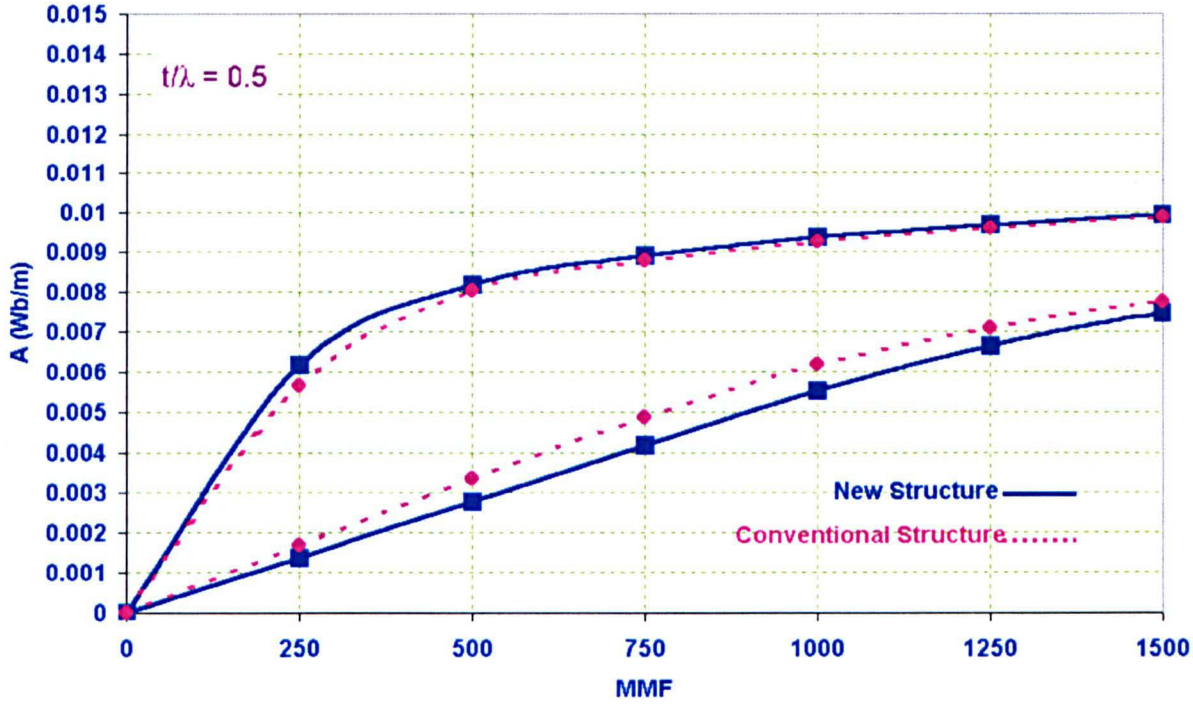

Fig. 2.16.c Flux versus MMF Characteristic (t/λ=0.5)

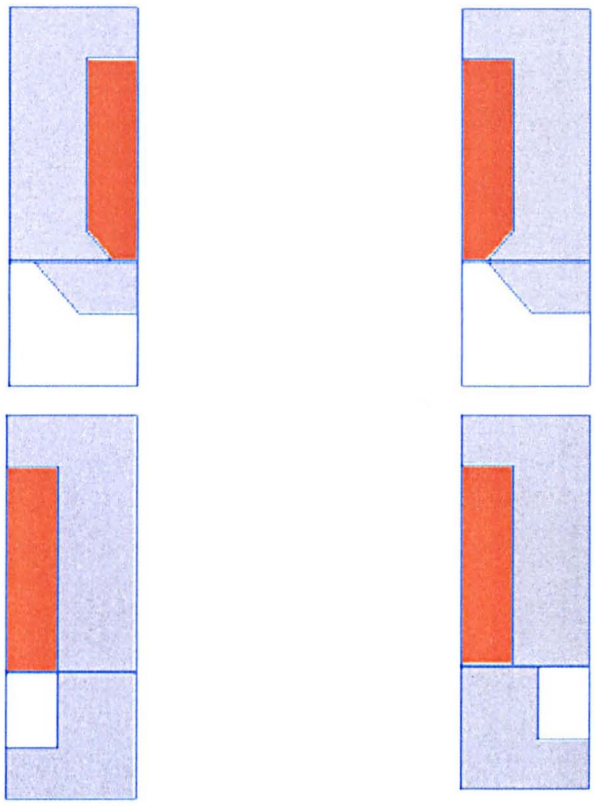

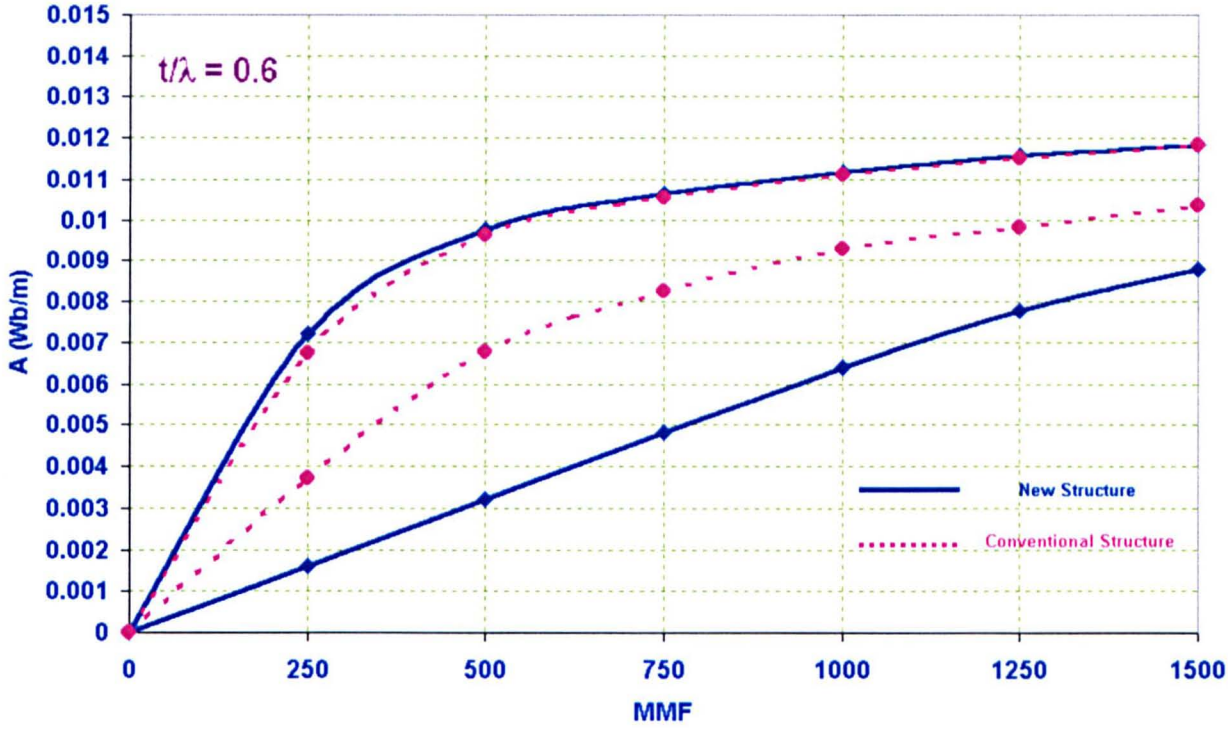

Fig. 2.16.d Flux versus MMF Characteristic (t/λ=0.6)

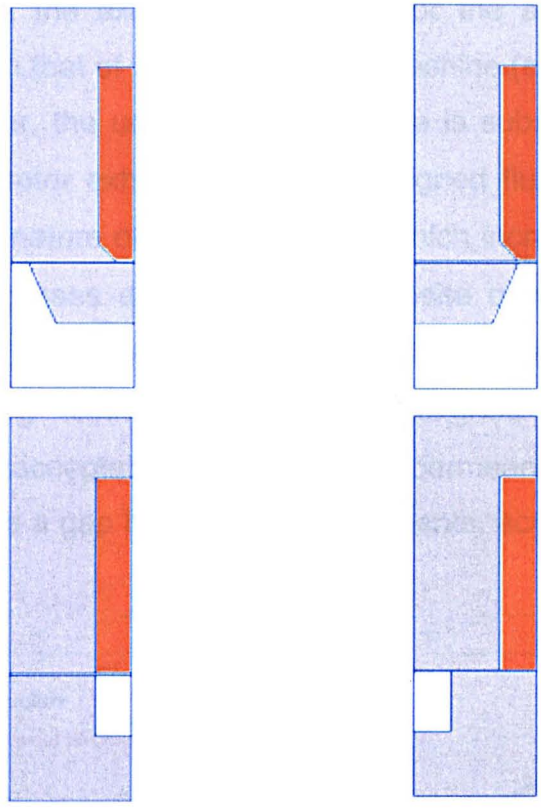

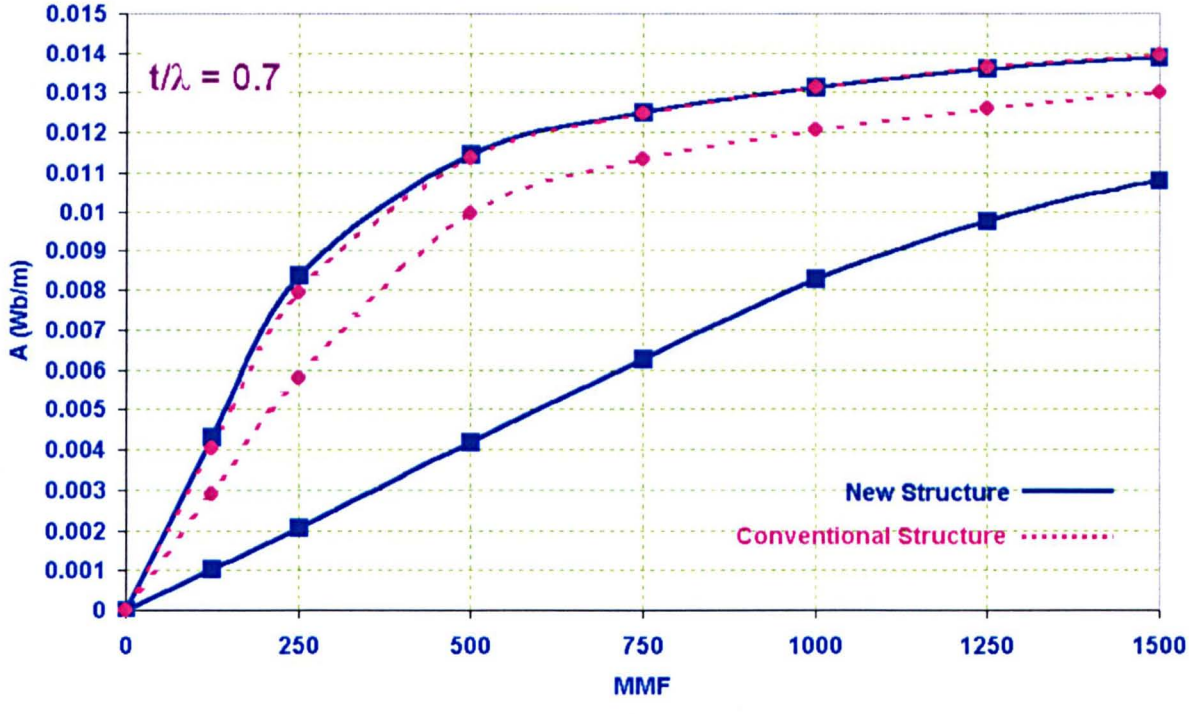

Fig. 2.16.e Flux versus MMF Characteristic (t/λ=0.7)

As might be expected, the aligned flux-linkage for the segmental rotor machine corresponds closely with that of the conventional machine (shown as a dashed line in the Fig. 2.16). However, the unaligned flux-linkage is substantially different. When $t/\lambda<0.5$ the segmental rotor exhibits a higher unaligned flux linkage, predominantly due to the semi-closed nature of the stator slots, which increases the cross slot flux. However, once t/λ increases above 0.5 the opposite occurs, with the segmental design having a lower unaligned flux-linkage. This is because the conventional design has overlapping teeth, even in the unaligned position when $t/\lambda>0.5$, corresponding to an unacceptably high unaligned permeance, whilst the segmental design always maintains a gap between rotor segments, across which unaligned flux must pass [69-70].

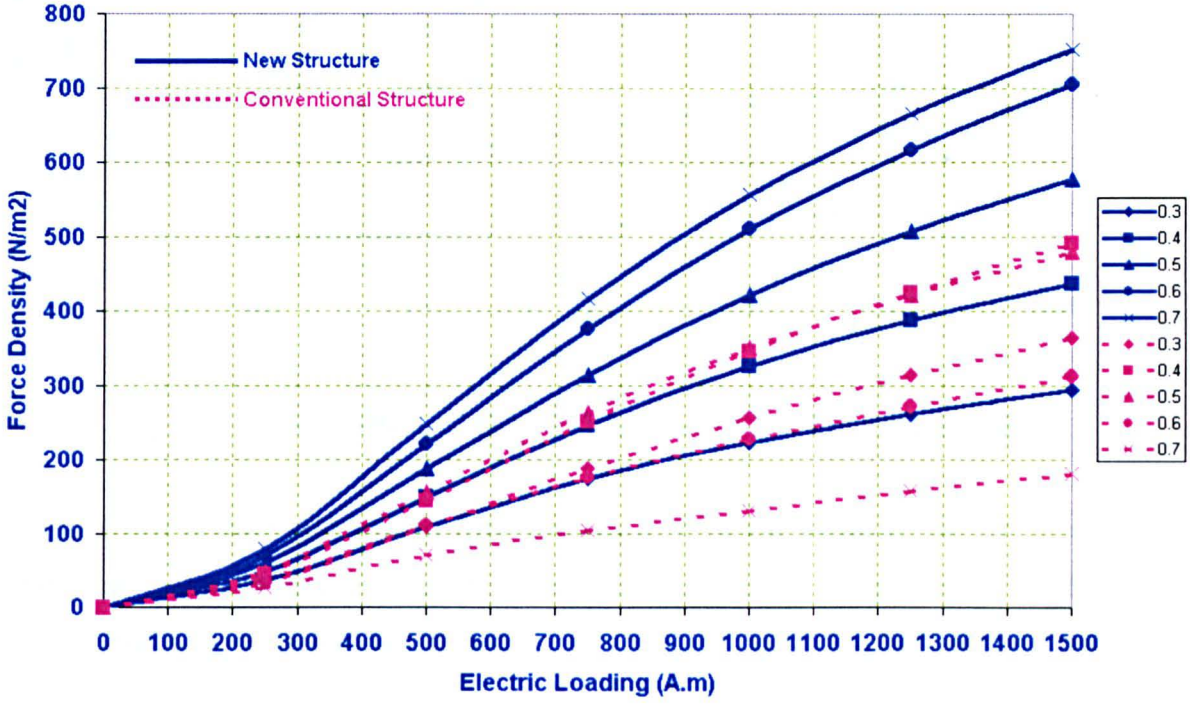

Fig. 2.17.a Average Air-Gap Force Density versus the Electric Loading, Showing the Variation with t/λ

Fig. 2.17.a shows the effect upon the mean force density. The conventional machine can be seen to have a greater force density when $t/\lambda<0.4$ but when $t/\lambda>0.5$ the segmental design offers greatly superior performance. As t/λ rises beyond 0.5 in the segmental design the force density continues to rise, even when t/λ approaches 0.7. By this time the force density is approximately 40% greater than that which can be

achieved with the best possible conventional toothed design. Of course it is not generally sensible to design a machine with $t/\lambda>0.5$, because it results in a very narrow slot, with insufficient room for the windings. Hence, unless other gains can be found, the segmental design is no more than an academic novelty, with the magnetic capability of increased torque production, but no practical application.

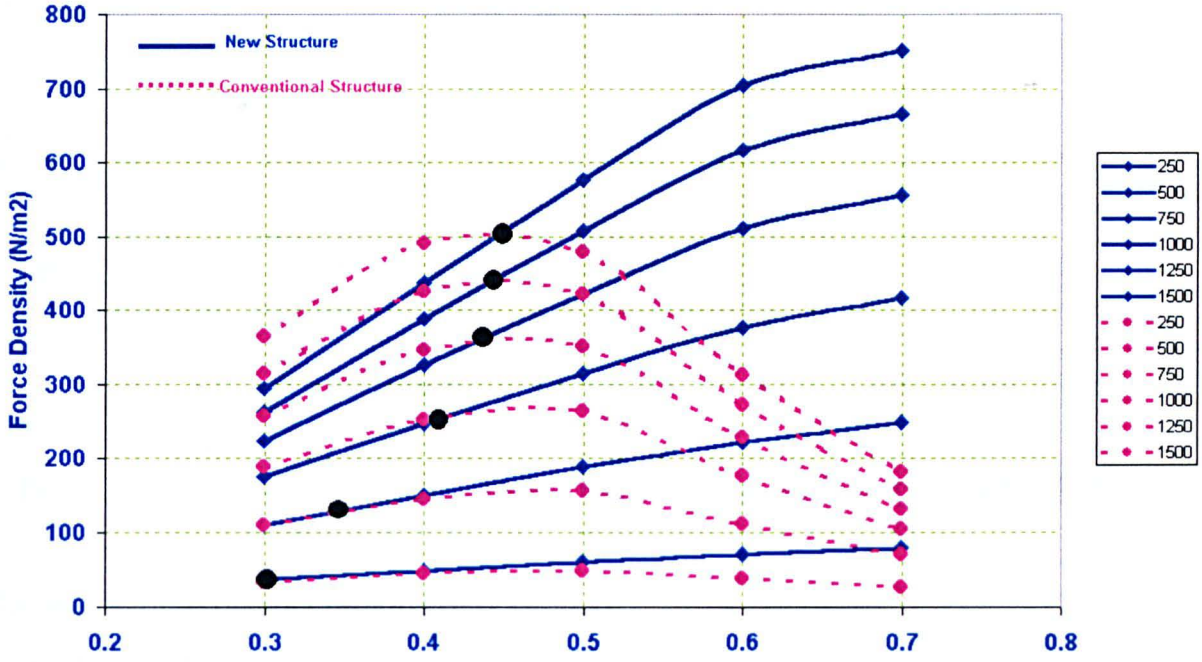

Fig. 2.17.b Variation of the $(t/\lambda)_{critical}$ with the Electric Loading

It is therefore possible to define ratio $(t/\lambda)_{critical}$: it is the value of t/λ for fixed electric loading; at lower values the conventional structure gives more torque and above it the new structure gives higher torque.

Fig. 2.17.b shows the critical value of the ratio t/λ depends on the value of the electric loading. This $(t/\lambda)_{critical}$ increases with the electric loading and becomes fixed at a value between 0.4 and 0.5.

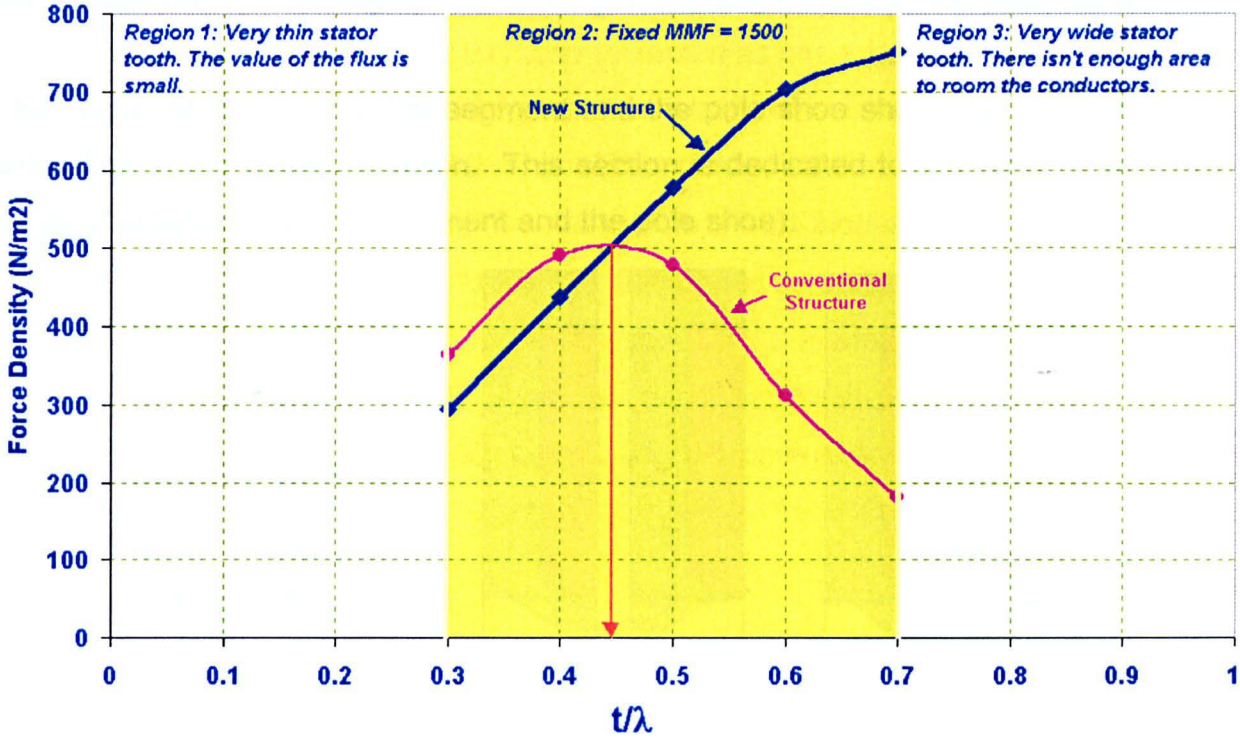

Fig. 2.17.c Effect of Changing t/λ on the Average Torque (Fixed MMF=1500)

There are three distinct regions of operation:

1-The tooth width is narrow when t/λ 0<0.3. Both the conventional topology and the new topology have low values of peak flux and force density.

2-The tooth width is very wide when t/λ>0.7. There is not enough area for the conductors in either topology.

3-Region 0.3<t/λ<0.7 has a critical value of t/λ, below which the conventional topology gives the greater torque and above which the new topology produces the greater torque.

Evaluation of the new topology indicates that it can be used to design a SRM capable of giving much more torque than an equivalent conventional SRM, providing the parameters are optimised properly and there is sufficient room for the windings.

This optimum value of t/λ will depend upon other aspects of the design: so far only a single phase machine has been considered, in multiphase machines other issues influence the space available for the winding and therefore the optimum tooth width.

2.9.2 Selection of the angles of tapering of the segment and the pole shoe

The angles of tapering for the segment and the pole shoe should be equal to avoid saturation in the aligned position. This section is dedicated to a search for the best angle of tapering (both the segment and the pole shoe).

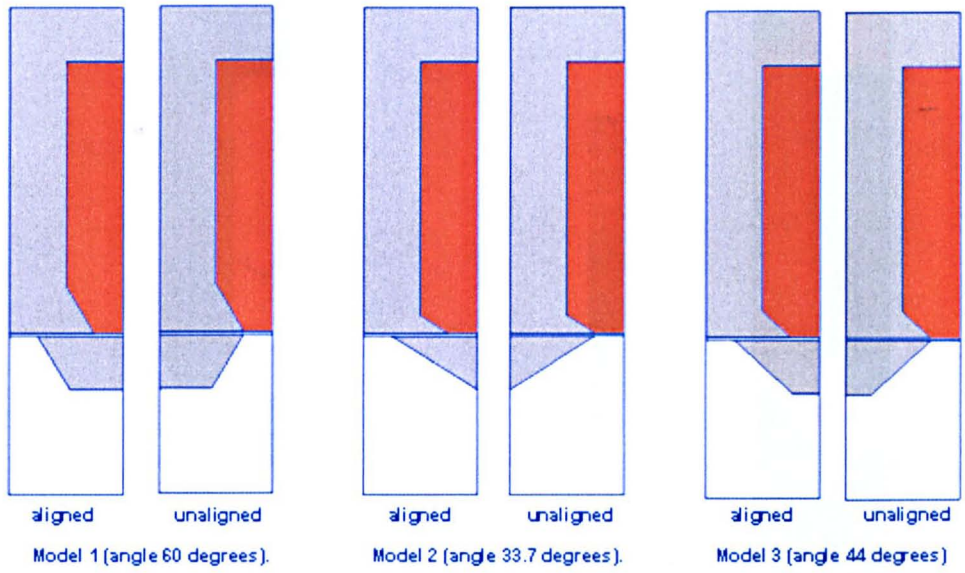

Fig. 2.18.a Three Different Models of the New Design (the same dimensions of Fig 2.15 except the angles of tapering)

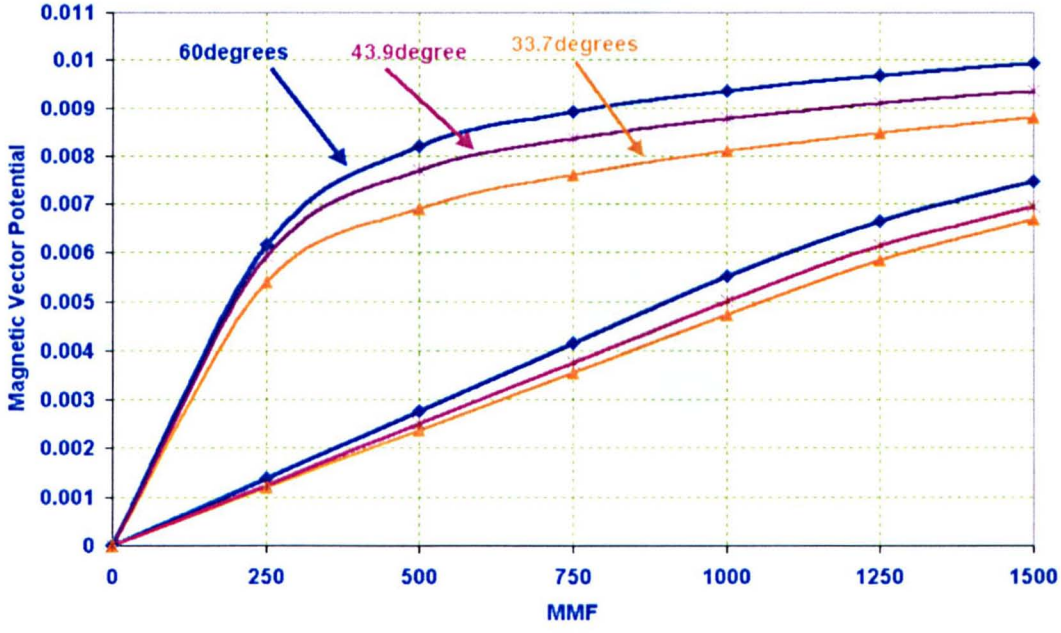

Fig. 2.18.b Aligned and Unaligned Positions for three Models have Different Angles of Tapering

Fig. 2.18.b shows the impact of changing the angle of tapering on the characteristic of the three models. There is not much influence because previous rules of the design minimised the saturation in the aligned position and maximised the reluctance in the unaligned position. An angle of 60 degrees appears best because the area between the aligned and the unaligned is slightly greater than the other two cases.

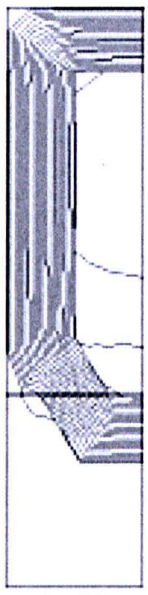

Magnetic Flux Plot

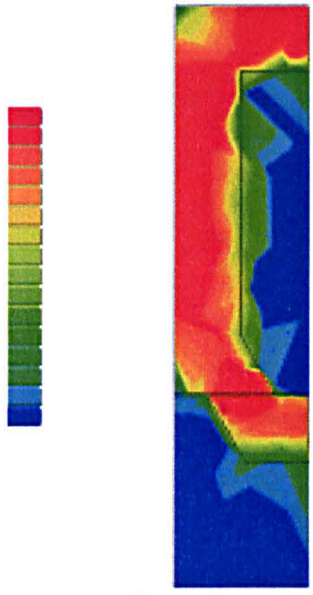

Flux Density

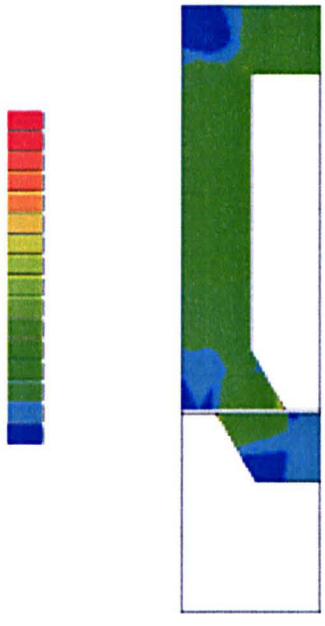

Saturation

Model 1 (tapering angle 60 degrees, t/λ=0.5)

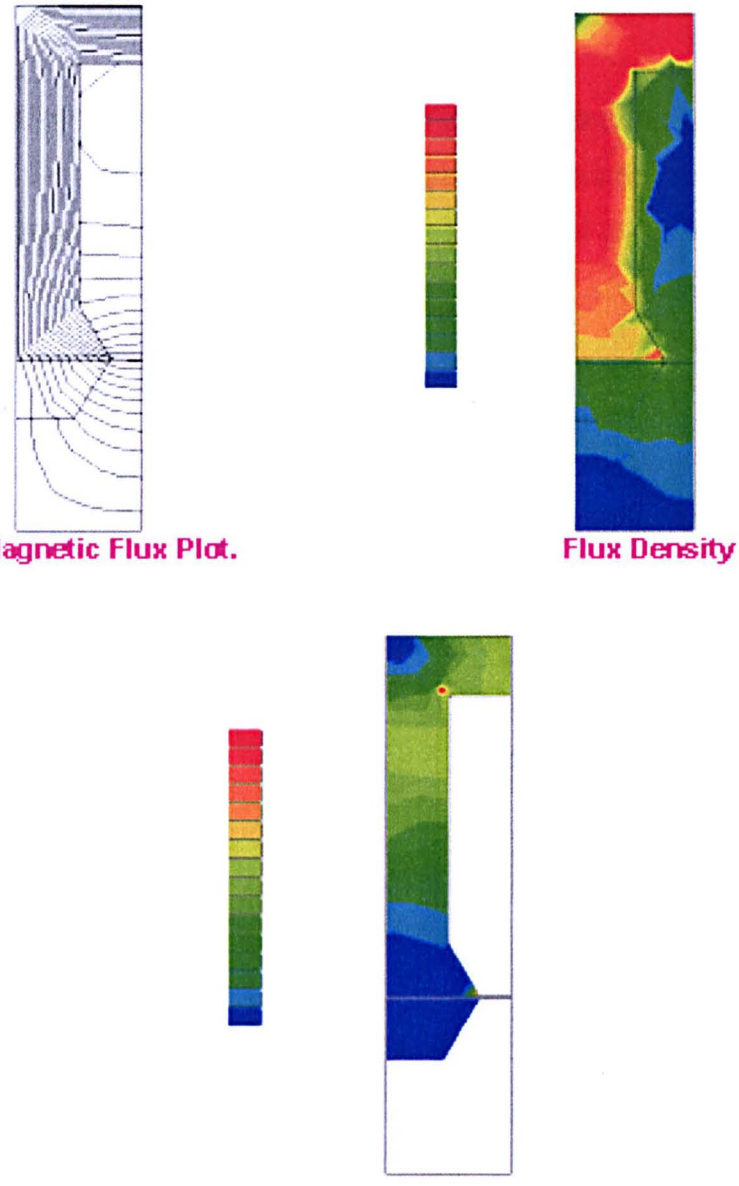

Fig. 2.18.c Magnetic Flux Plot, Flux Density and Saturation

Fig. 2.18 shows the impact of changing the angle of tapering on the aligned and the unaligned positions (the design rules were applied in all three model, only the angle of tapering was changed). The figure shows the flux density is uniform and the saturation is very low.

2.9.3 Different Shapes of the Segments

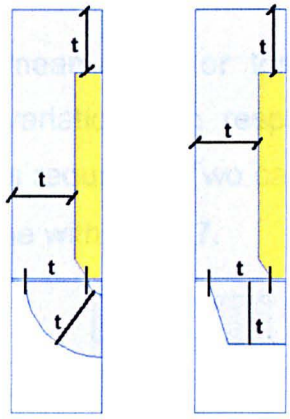

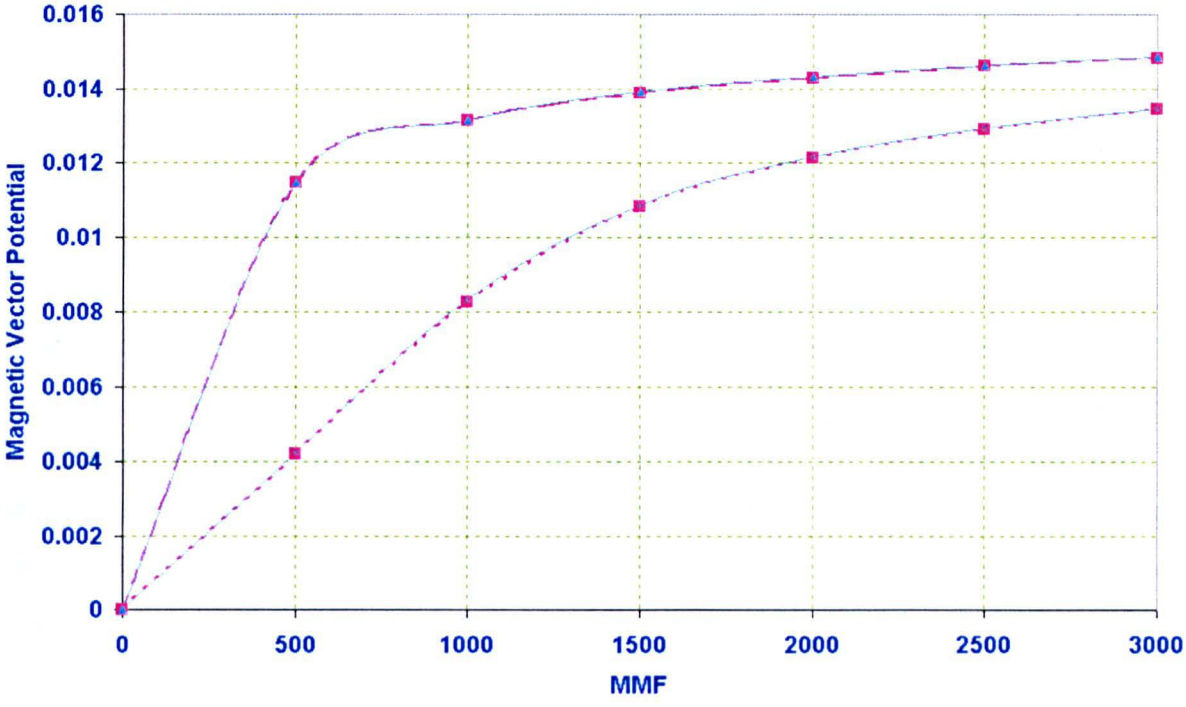

Fig. 2.19 Magnetic Vector Potential for two Different shapes of the Segment and $t/\lambda=0.7$ for both

Fig. 2.19 shows comparison between the trapezoidal segment and another shape, in which a curved rotor segment is employed. Both segment shapes give virtually identical Flux/MMF curves, so that it is impossible to differentiate between them in the figure.

2.9.4 The Instantaneous variation of Force with Position

In addition to evaluating the mean force or torque density it is necessary to understand the instantaneous variation with respect to position, since for some applications a low torque ripple is required. Two cases will be evaluated for the new topology; one with $t/\lambda=0.5$ and one with $t/\lambda=0.7$.

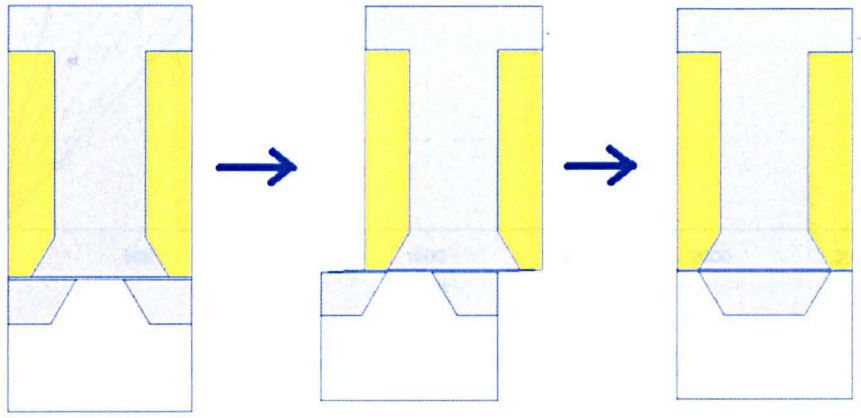

Fig. 2.20 Simple Rectilinear case of the New Design

Fig. 2.20 shows a simple rectilinear case of the new design (the dimensions as Fig. 2.15, the distance between the aligned to the unaligned is 10 mm). Flux/MMF characteristics were determined for a large number of positions, so that the instantaneous variation of co-energy with position can be predicted. Fig 2.21 shows both the flux-linkage curves and the derived force curves for a series of constant currents, based upon a machine with 100 turns per pole.

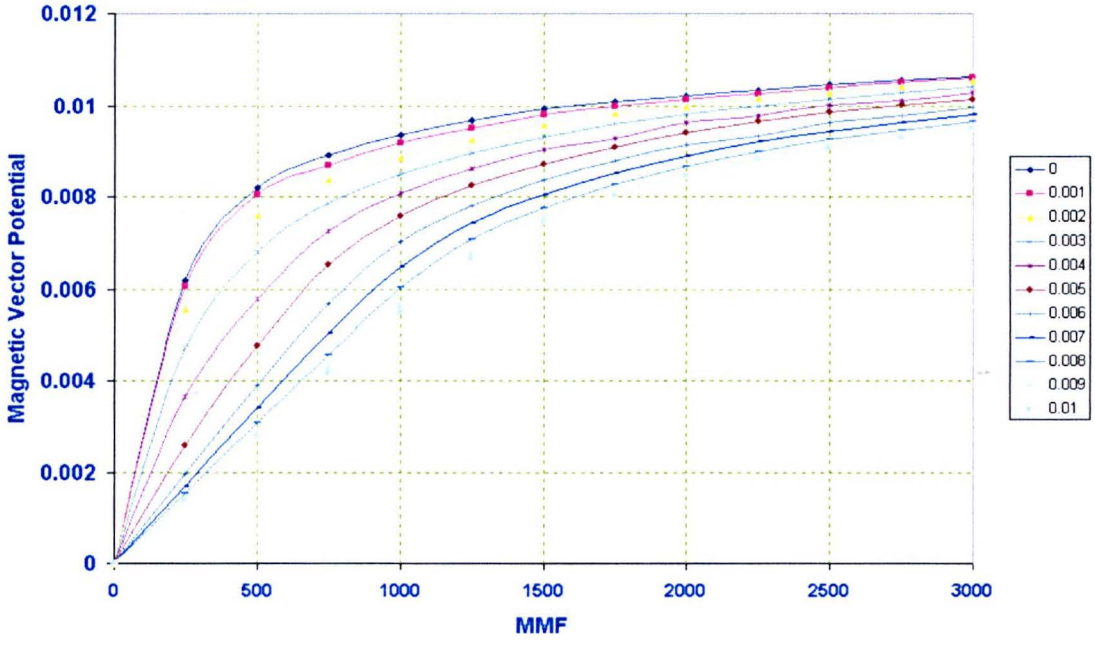

Linear movement (each step) =0.001

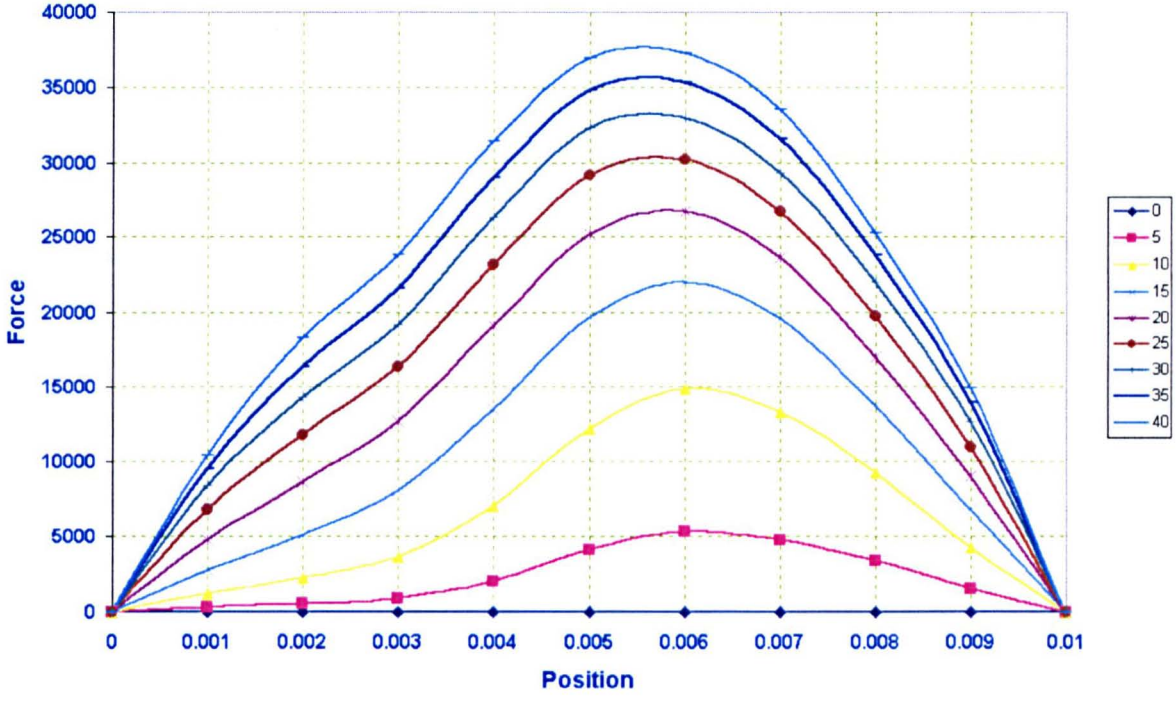

Force characteristic versus the linear distance of movement for different values of the current, t / λ = 0.5, using number of turns = 100

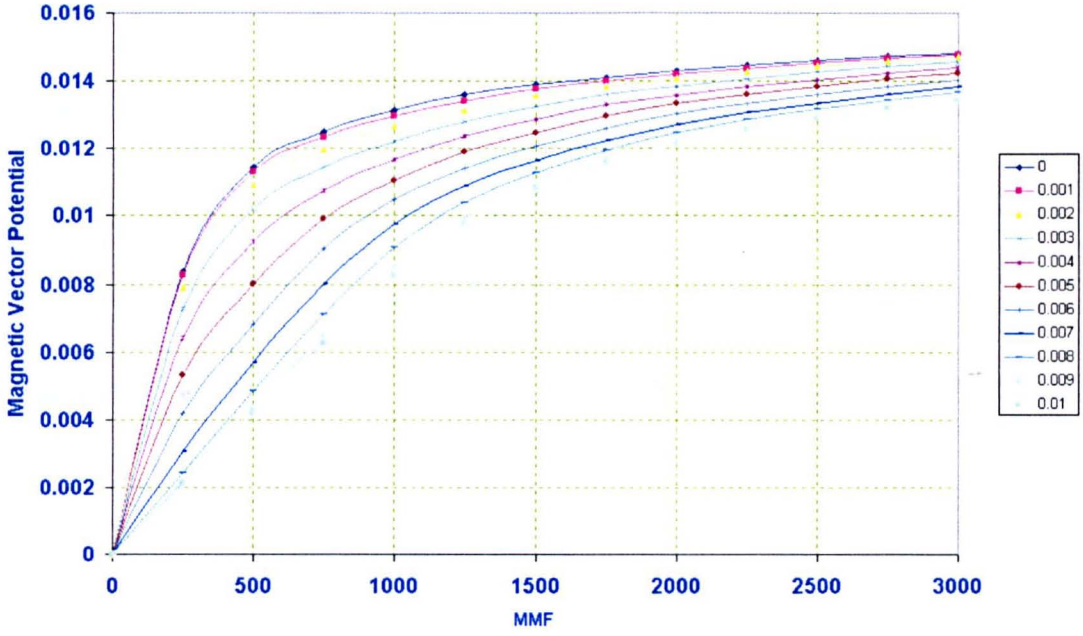

Linear movement (each step) =0.001

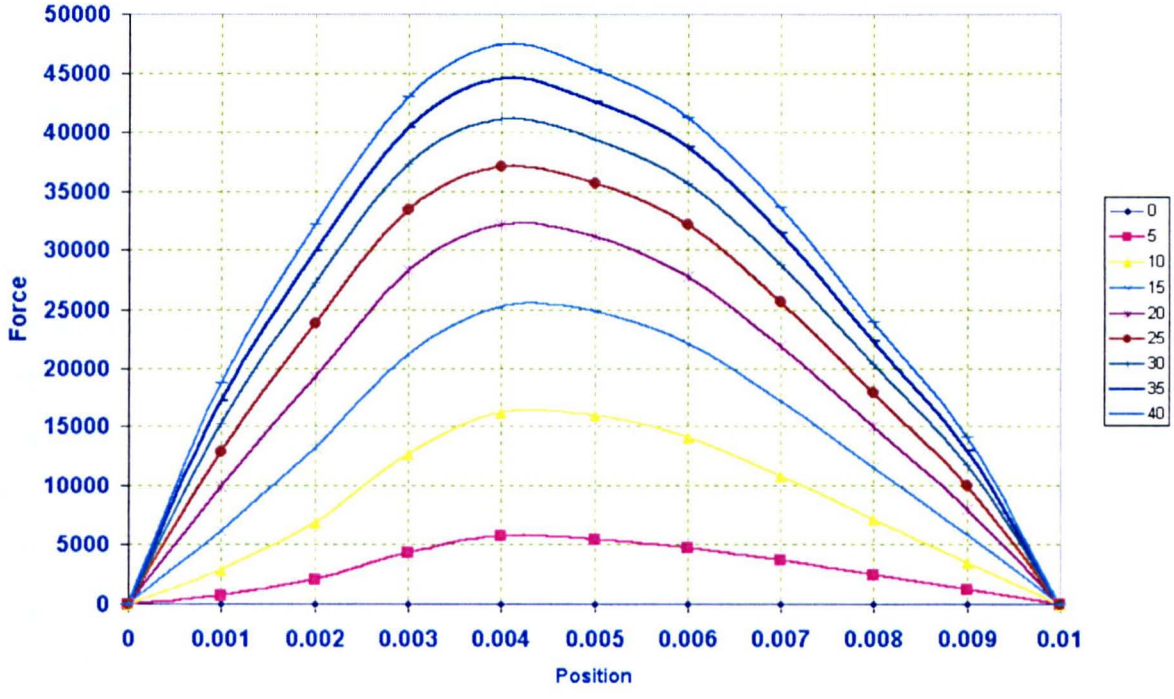

Force C/C's versus the linear distance of movement for different values of the current, t / λ = 0.7, using number of turns = 100

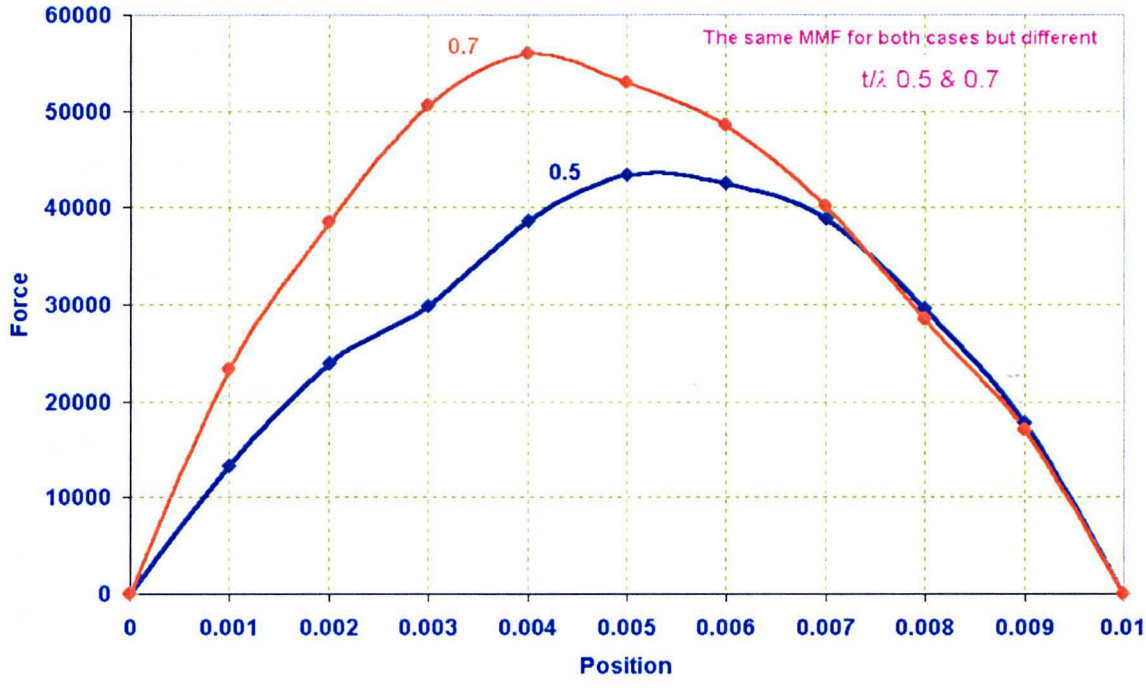

Fig. 2.21 Static Force Variation of the New Topology for two Different Tooth Widths

Fig. 2.21 shows at low current the general shape of the force waveforms is somewhat different to that which is commonly encountered in toothed rotor SRMs: The force continues to rise almost linearly with rotor displacement from the aligned position until approximately midway to the unaligned position. To help understand this, consider the permeance variation at low currents, which is dominated by the air-gap permeance. A simple approximation to the permeance variation can be made by neglecting all fringing flux. This will be used to highlight the difference in torque production between the conventional and segmented machines.

In toothed rotor SRMs the magnetic flux crosses two air-gaps of identical form. At full alignment the permeance is at a maximum, and as the rotor moves away from alignment the permeance falls linearly. Because the rate of change of permeance has this linear (constant) variation over most of the current stroke the torque produced at constant current is predicted to be constant.

With the segmental SRM the variation of air-gap permeance with position is more complex. Magnetic flux flows down one tooth, into a rotor segment and returns via

an adjoining stator tooth. In the aligned position the reluctance of the two air-gaps linking a rotor segment to adjoining stator teeth are equal but, as the rotor moves from the aligned position, the reluctance of one air-gap falls whilst that of the other rises. Hence, the initial rate of change of permeance is zero but, as the asymmetry rises, the rate of change of permeance also rises, until it reaches a maximum at the point where there ceases to be any overlap between the rotor segment and one of the stator teeth.

A consequence of the above effects is that a segmental rotor SRM is likely to have greater torque ripple than a toothed rotor SRM when operating at low excitation levels. At higher excitation levels saturation effects become important and the difference in torque ripple between the two machine types is likely to be much smaller.

2.10 General Conclusions for the Rectilinear, Single Phase Case

A segmental rotor construction can be used to increase the performance of switched reluctance motors, also offering gains over axially laminated rotor designs. In single phase machines the air-gap force density exceeds that of a conventional SRM when the active portion of the air-gap exceeds one half of a pole pitch. However, under such circumstances there may be insufficient room for the windings. The influence of the rotor segment shape has been studied, and it has been found that a trapezoidally shaped segment offers a good compromise between the need for a low unaligned permeance and a high aligned permeance. The angle of the trapezoidal segment has also been shown to be optimal at around 60 degrees to the air-gap. The permeance variation with rotor position is far from linear, leading to static force and torque curves which are substantially different to those of a conventional SRM. For an unsaturated machine the air-gap force rises almost linearly with displacement from the aligned position until the point at which the rotor segment fails to overlap both teeth adjacent to an excited slot. Once this position is exceeded the force falls quite rapidly to zero at the unaligned position.

3 Applying the Segmental Concept to a 3-Phase, Fully Pitched SRM

3.1 Introduction

This chapter develops a design for a multi-phase segmented-rotor SRM. The proposed motor will be 3-phase, with 12 stator teeth and 8 isolated iron segments (each segment represents a rotor pole). In order to provide a good comparison with other SRM prototypes, which have been built during earlier research work, the axial length of the laminations is chosen to be 150mm, with the stator diameter also chosen to be 150mm. The machine will have a radial / circumferential magnetic field, with an inner rotor, in line with the vast majority of electrical machines. In this first prototype the stator coils will span three teeth, making what is in effect a fully pitched winding. The design developed in this chapter will be built and extensively tested. Static tests enable measured parameters to be determined and rotational tests reveal measured performance. The simulated results presented in this chapter will later be compared with these measured results.

3.2 The Multi-Phase Rotating Segmental Rotor Switched Reluctance Motor

The previous chapter established that the use of isolated iron segments as rotor poles will only increase the output torque if there is proper selection of the parameters and windings.

Parameter selection will be undertaken by first establishing some design rules and then comparing a series of different models of the new multi-phase segmented-rotor SRM with an equivalent conventional SRM with the same outside diameter and lamination stack length. A question appears directly - which design of the equivalent conventional SRM should be used in this comparison?

Two designs of conventional SRM were finally chosen: both designs were 12/8 three phase machines with short pitched windings, making the machine operate at the same electrical frequency as the new segmental machine. The first "standard" design has parallel sided teeth with a ratio of t_r/λ_r equal to 0.33 ($t_r=t_s$), a core back width equal to half the stator tooth width and a rotor diameter 60% the stator outside diameter. As in the segmental design the air-gap length was chosen to be 0.3 mm.

The second design has a slightly wider core back and teeth, corresponding to the ratio of $t_r/\lambda_r = 0.4$ ($t_r = t_s$). This design is used for low torque ripples applications [69-70][103-107].

3.2.1 Design of the Multi-Phase, Segmented-Rotor SRM Evolved Using the Following Steps

1-The stator core back, the stator tooth width, the length of rotor segment to tooth overlap in the aligned position and the radial height of the segment were all made equal so that the magnetic flux density was constant throughout the magnetic flux path when in the aligned position. This was to maximise the saturation flux in the aligned position.

2-The ratio of rotor diameter to stator outside diameter was chosen to be 60%. This has been found to be close to the optimum for conventional SRMs and leaves plenty of room for mechanical fitting of the rotor segments onto a non-magnetic shaft.

3-A series of designs were produced for gradually increasing values of stator teeth, starting from the thinnest possible value which produces significant flux up until the widest possible value which still leaves significant slot area for the conductors.

4-The magnetisation curve was obtained for each design using adaptive finite element analysis. This was used to assess the new designs and to compare them with the conventional design models.

5-With the segmental rotor machine there is no magnetic short circuit formed by the rotor structure, so the magnetic flux must always enclose a single stator slot. Thus, in moving to a multiphase design it is natural to split the structure so that a single unit comprises of one stator slot, and that the design should have the capability to excite only those slots of equal phase, as shown in Fig. 3.1

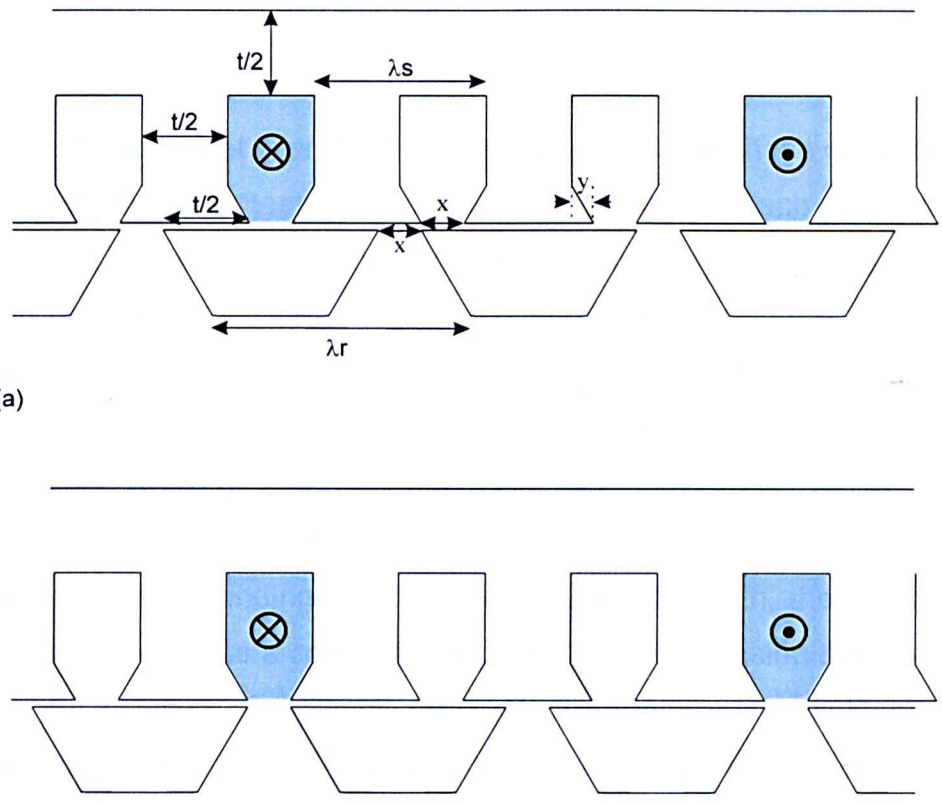

Fig. 3.1 Three Phase Segmental Rotor Design, Showing the Desired MMF Pattern of a Single Phase (fully pitched)
(a) Aligned Position (b) Unaligned Position

The obvious manner in which to do this is to use a winding arrangement where each slot contains only the winding of a single phase. An arrangement which does this is shown in Fig. 3.1, with each coil spanning three slots [69-70].

As in the single phase design, the gap between rotor segments is chosen to be equal to that of the stator slot opening so that neither the rotor or stator contribute excessively to the unaligned inductance. The length of overlap between a rotor segment and the tooth width is also made equal to the main stator tooth width, thus equalising magnetic flux densities throughout the magnetic circuit in the aligned position. From these two design rules the slot opening, x, and the tooth tip closure, y, can be derived using the following equations:

Equating values with the rotor pole arc $$t + 2x = \lambda_r \quad (3.1)$$

From the arc of the stator pole $$\frac{t}{2} + x + 2y = \lambda_s \quad (3.2)$$

The principal difference between the three phase and single phase designs lies in the required width of the stator teeth. In the single phase version each stator tooth had to carry the flux from two rotor segments, and was of width, t. In the three-phase version, with one phase excited, each stator tooth carries only the flux of one rotor segment, so the tooth width can be reduced to t/2. It is this feature which is critical in making a three phase segmental rotor SRM a sensible proposition because it allows a high value of t/λ, whilst retaining enough room for the windings [69-70].

The above reasoning is not entirely complete. Whilst the conventional, toothed rotor SRM has short pitched windings placed around a single tooth, the segmental SRM has windings which enclose a complete magnetic pole, comprising three teeth, so the winding can be classed as fully pitched. Whilst the winding is identical to that employed in conventional SRMs with fully pitched windings, the similarity ends there. In the segmental rotor SRM torque results from changing self inductance, whilst in toothed rotor SRMs with fully pitched windings the torque is produced by changing mutual inductance, and therefore two or more phases need to be simultaneously conducting.

Compared to a conventional short pitched windings SRM there are considerably longer end windings, which produce additional copper mass and windings loss. The importance of this additional loss is dependent upon the machine axial length and pole number.

3.3 Designing New High Torque Three Phase 12/8 Fully Pitch Segmented Rotor SRM

The design will initially be developed using MMFs and flux. In later chapters the number of turns will be estimated according to the optimisation of the electric circuit after considering the copper losses and the current density.

Appendix 1 shows a mathematical derivation of the critical dimensions of the segmented rotor machine for a range of tooth widths, according to the above design rules [108-109]. Four different models were then produced and are illustrated in Fig.

3.2. In addition to showing the geometry, examples of adapted finite element meshes are also given, alongside representative flux distribution plots with one phase excited. Note how there is fine discretisation in the vicinity of the air-gap because it is in this region that most of the magnetic energy is stored [110-111].

Note: W is the stator tooth width

Model 1

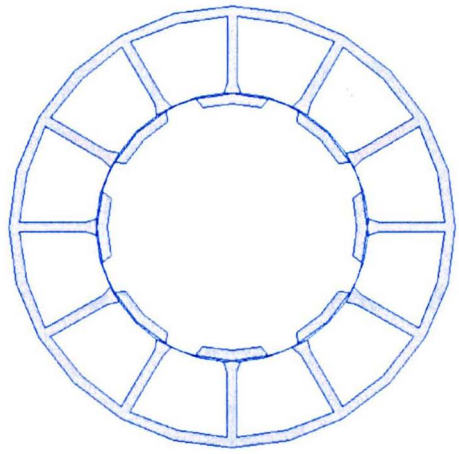

a) 12/8 segmented-rotor fully pitched model W=0.0035, t/λ = 0.196 (aligned position)

Model 2

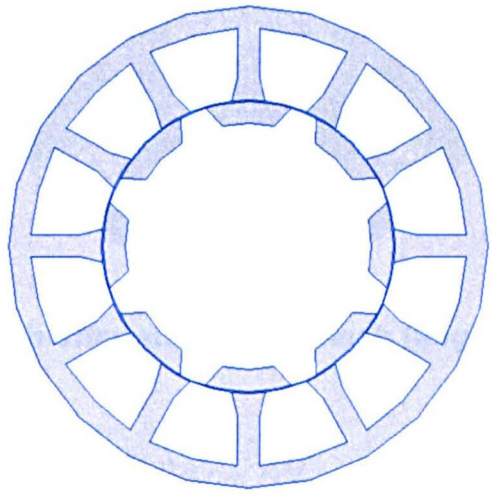

b) 12/8 segmented-rotor fully pitched model W=0.007, t/λ=0.3926 (aligned position)

Model 3

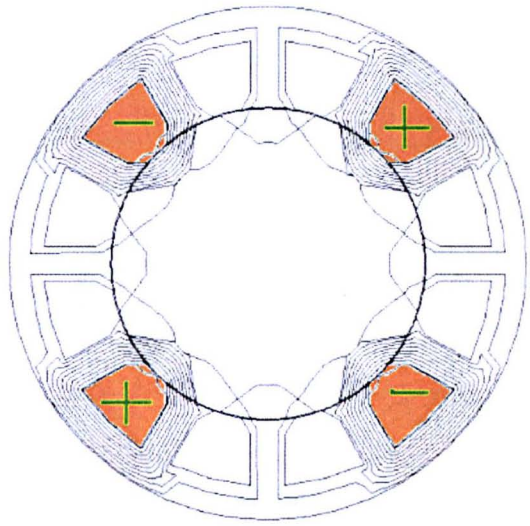

c) 12/8 segmented rotor SRM fully pitched model W=0.01, t/λ=0.56 (aligned position)

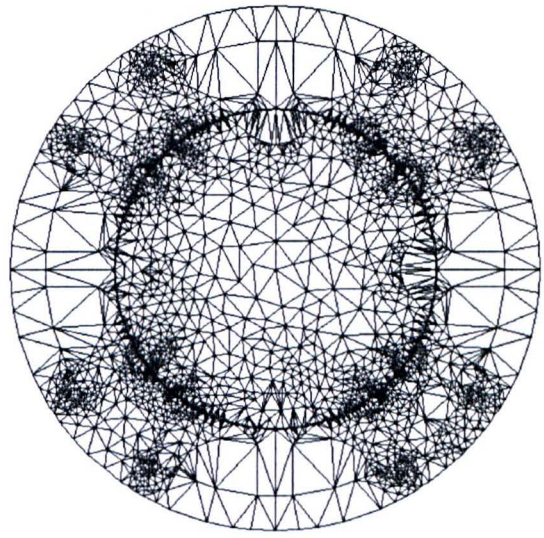

The final mesh after adaptation mesh (aligned position)

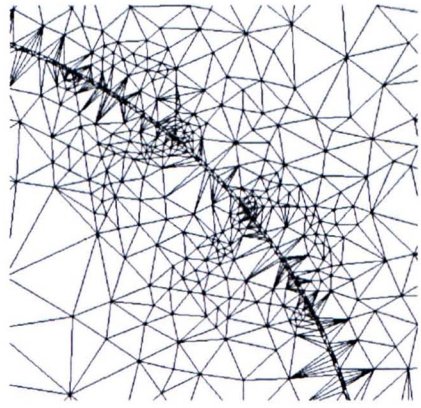

The mesh near the air gap

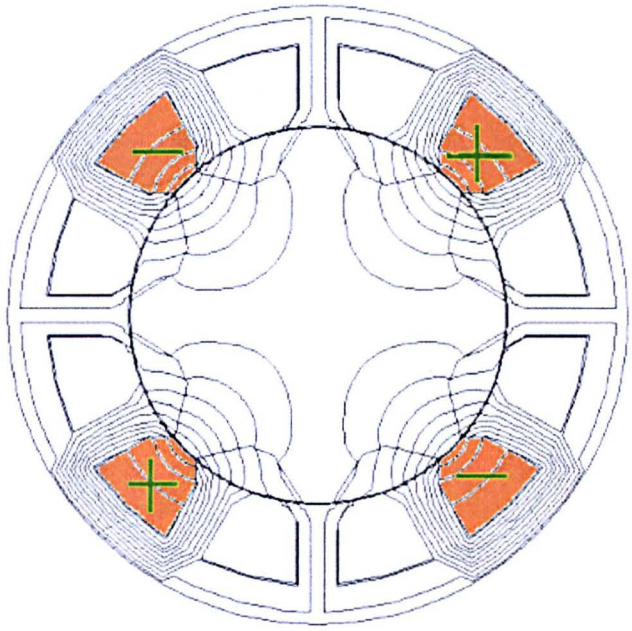

12/8 segmented-rotor SRM fully pitched model W=0.01, t/λ=0.56 (unaligned position)

Model 4

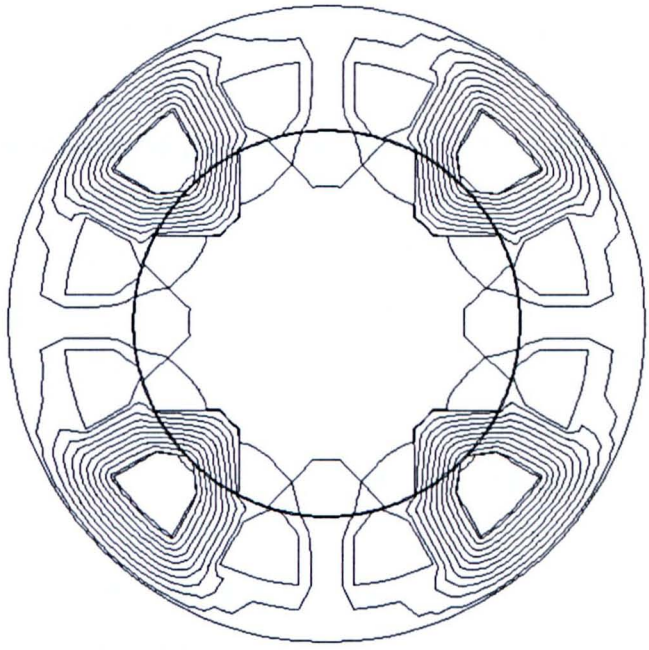

d) 12/8 segmented-rotor SRM fully pitched model W=0.013, t/λ=0.729 (aligned position)

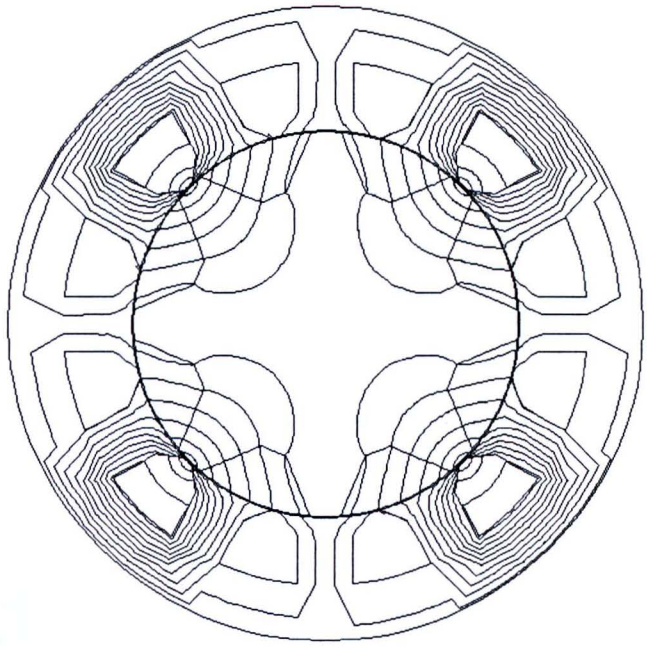

12/8 segmented-rotor SRM, fully pitched model W=0.013, t/λ=0.729 (unaligned position)

Fig. 3.2 Different Models for the 12/8 Fully Pitched Segmented-Rotor for Different Stator Tooth Width (W)

3.4 Finite Element Analysis of the Conventional Short Pitched 12/8 SRM

Figs. 3.3 and Fig.3.4 show magnetic flux plots for the conventional 12/8 SRM in both the aligned and unaligned positions. Note how whilst excitation of one phase in the segmental machine energises eight stator teeth, only four stator teeth are energised in the conventional machine. The conductors of one phase in the conventional SRM fill half of eight slots, with the other halves of these slots filled by the conductor of other phases [112-113].

Note how in both the segmental and conventional machines the rotor diameter is 90.08 mm, resulting in a rotor pole arc as follows:-

$\lambda_r = 2^* \pi ^* r/8=(2^*(22/7)^*0.0454)/8=0.03566.$

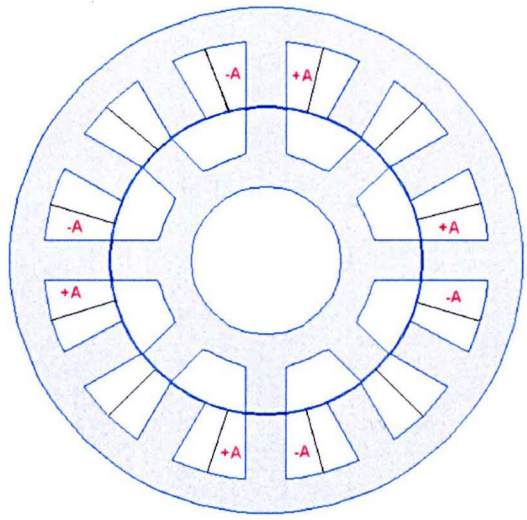

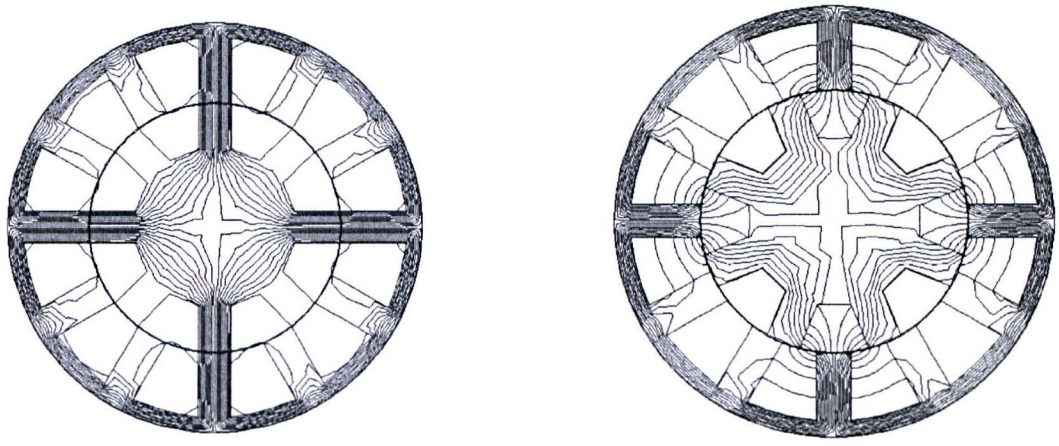

a-aligned position b-unaligned position

Fig. 3.3 Conventional 12/8 Short Pitched SRM

(standard design: $t_r/\lambda_r=0.33$ and $t_r=t_s$)

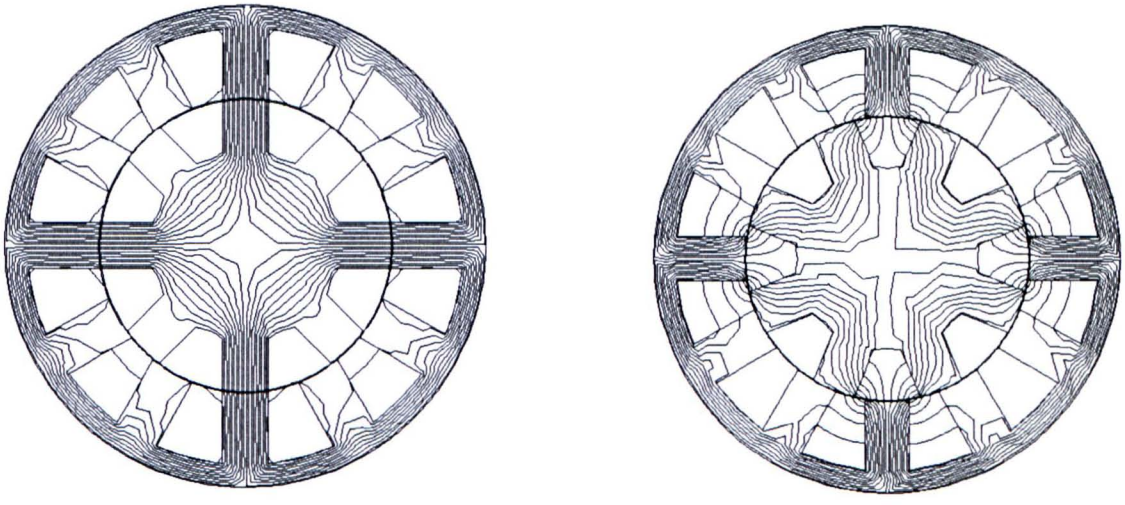

a-aligned Position b-unaligned position

Fig. 3.4 Conventional 12/8 Short Pitched SRM

(wide teeth: $t_r/\lambda_r=0.4$ and $t_r=t_s$)

For simplification the end-windings effect was initially ignored in the analysis.

Stator Outside Diameter	150 mm
Rotor Diameter	90.8 mm
Air Gap Length	0.3 mm
Stator Core-Back	5.88 mm
Rotor Core Back	5.88 mm
Stator Tooth Width	11.76 mm
Rotor Tooth Width	11.76 mm

Table 3.1 Dimensions of Conventional 12/8 Short Pitched SRM

(standard design: t_r/λ_r=0.33 and t_r=t_s)

Stator Outside Diameter	150 mm
Rotor Diameter	90.8 mm
Air Gap Length	0.3 mm
Stator Core-Back	7.046 mm
Rotor Core Back	7.046 mm
Stator Tooth Width	14.092 mm
Rotor Tooth Width	14.092 mm

Table 3.2 Dimensions of Conventional 12/8 Short Pitched SRM

(wide teeth: t_r/λ_r=0.4 and t_r=t_s)

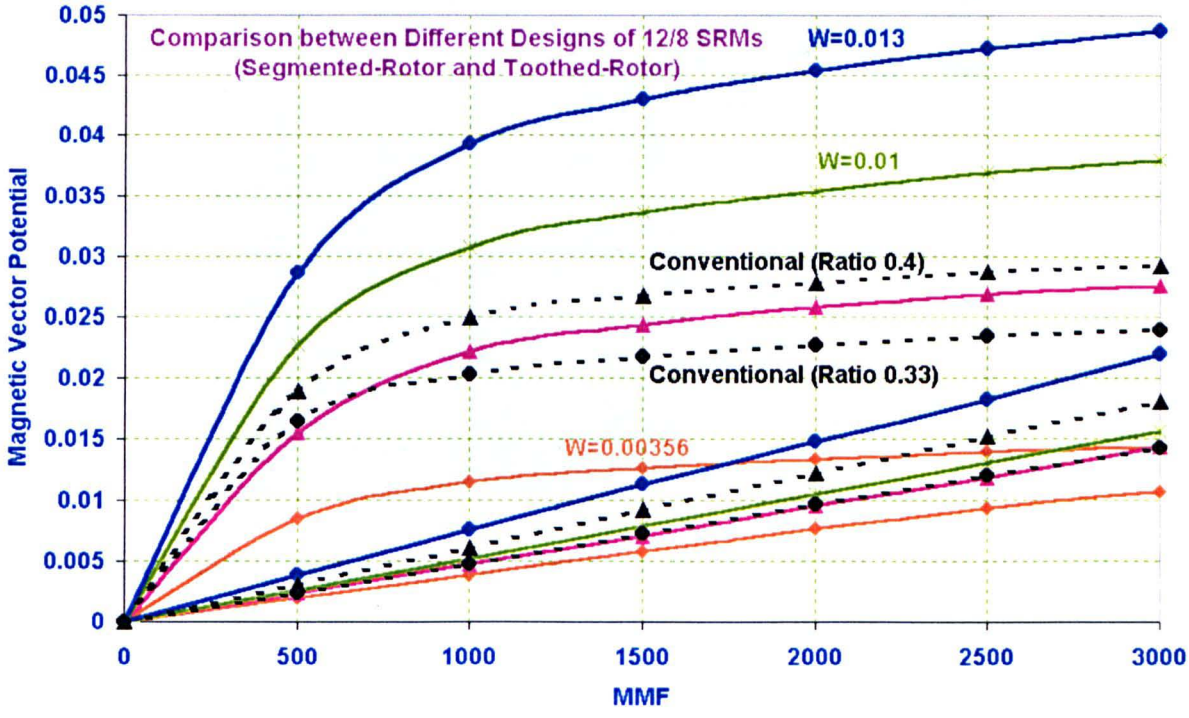

Fig. 3.5 Comparison between the New and Conventional Designs

The vertical axis in Fig. 3.5 represents the average magnetic flux linking any one turn per meter of axial length. The horizontal axis represents the MMF driving the magnetic flux around any one flux path. The area enclosed between the two curves is in effect one half the co-energy per unit length of the entire machine.

Model Number	1	2	3	4
W	0.0035	0.007	0.01	0.013
2*W/Rotor Pole Pitch = t/λ	0.196	0.3926	0.56	0.729
Slot Area (mm^2)	615	403	351	227
Area between aligned and unaligned positions (unit co-energy) MMF=3000	18.5	49.5	76.758	94.06

Table 3.3 Comparison between the Four Models of the New SRM, 2W is equivalent to t here in the Segmented Rotor SRM

Conventional Short Pitch 12/8 SRM		
Model Number	1	2
t/λ	0.33	0.4
Slot Area(mm^2)	430	344
Area between the aligned and the unaligned positions Unit Co-energy MMF = 3000	42.1	50.3

Table 3.4 Comparison between the Two Models of the Conventional SRM

Fig. 3.5 shows the magnetic vector potential of the aligned and the unaligned positions for the four models of the new segmental design and the two models of the conventional design versus the MMF per slot. Needless to say, the results are only

valid for the particular dimensions of the machine models. They will now be compared with respect to torque capability.

Regarding the models of the conventional SRM

1-For the ratio t/λ =0.33, the area of one slot = 430 mm^2 and the area between the aligned and the unaligned position curves give 42.1J per turn per unit length of co-energy for MMF=3000 Amp-turn per slot.

2-For the ratio t/λ =0.4, the area of one slot = 344 mm^2 and the area between the aligned and the unaligned position curves give 50.3J per turn per unit length of co-energy for MMF=3000 Amp-turn per slot.

Consider the segmental designs. As the tooth width is increased the flux linking any one coil rises. Because each coil links the flux of two stator teeth then for a given stator tooth body width there is approximately twice the saturated flux-linkage of a conventional SRM. Hence the two segmental designs with wider teeth can deliver much more torque per unit MMF than the equivalent conventional designs.

A valid comparison between the range of designs must take into account the varying slot area and end-windings length [114-115]. For initial comparison two extremes have been taken as follows:

1. The current density has been fixed. This is valid when there is some form of direct cooling of the conductors. A nominal r.m.s. value of 10 amps per square millimetre has been chosen.
2. The loss per slot has been fixed. This is valid if there is good thermal conduction across the slot and most of the temperature rise occurs between the machine frame and surrounding air. In this initial comparison no account is taken of end-windings losses. The relative effect of these losses is a function of axial length; end-windings will be much longer in the segmental machine and so in neglecting them the results will disproportionately favour the new design.

3.4 Comparison based upon Fixed Current Density

Assume a square wave of excitation in which one phase is conducting at any one instant. Also assume that the entire area between aligned and unaligned flux-linkage curves is enclosed.

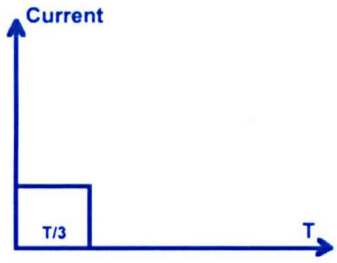

$$I_{rms} = \sqrt{\frac{1}{T}\int_0^{T/3} I_m{}^2 dt} = I_m/\sqrt{3}$$

Assume the winding current density $J_{rms} = 10A/mm^2$

Assume the slot fill factor =0.4

a) New SRM 12/8 Fully Pitched

There are two coils per phase and each coil side fills one slot.

MMF (per phase)= $\sqrt{3}$ (for the maximum value of the current)

*10(current density)*2 (two coils per phase)*Area of one slot * slot fill factor

12/8 segmental model 1: $MMF1 = \sqrt{3}*10*2*615*0.4 = 8521$

12/8 segmental model 2: $MMF2 = \sqrt{3}*10*2*403*0.4 = 5584$

12/8 segmental model 3: $MMF3 = \sqrt{3}*10*2*351*0.4 = 4863$

12/8 segmental model 4: $MMF4 = \sqrt{3}*10*2*227*0.4 = 3145$

b) Conventional Short Pitched 12/8 SRM

There are four coils per phase and each coil side fills one half slot.

MMF (per phase)= $\sqrt{3}$ (for the maximum value of the current)

*10(current density)*4 (two coils per phase)*half area of one slot * slot fill factor

Model $t_r/\lambda = 0.33$, $t_r = t_s$: $MMF5 = \sqrt{3}*10*4*(430/2)*0.4 = 5958$

Model $t_r/\lambda = 0.4$, $t_r = t_s$: $MMF6 = \sqrt{3}*10*4*(340/2)*0.4 = 4766$

Calculation of the torque for comparison:

Average Torque per unit Length = [Number of the phases * the number of the loops per cycle* area between the aligned to the unaligned position]/ 2π

The 12/8 new segmented-rotor SRM: has three phases and there are eight energy loops per cycle. This is the same as the conventional SRM.

The average torque $=\frac{3*8}{2\pi}$ * area enclosed by the aligned and the unaligned positions.

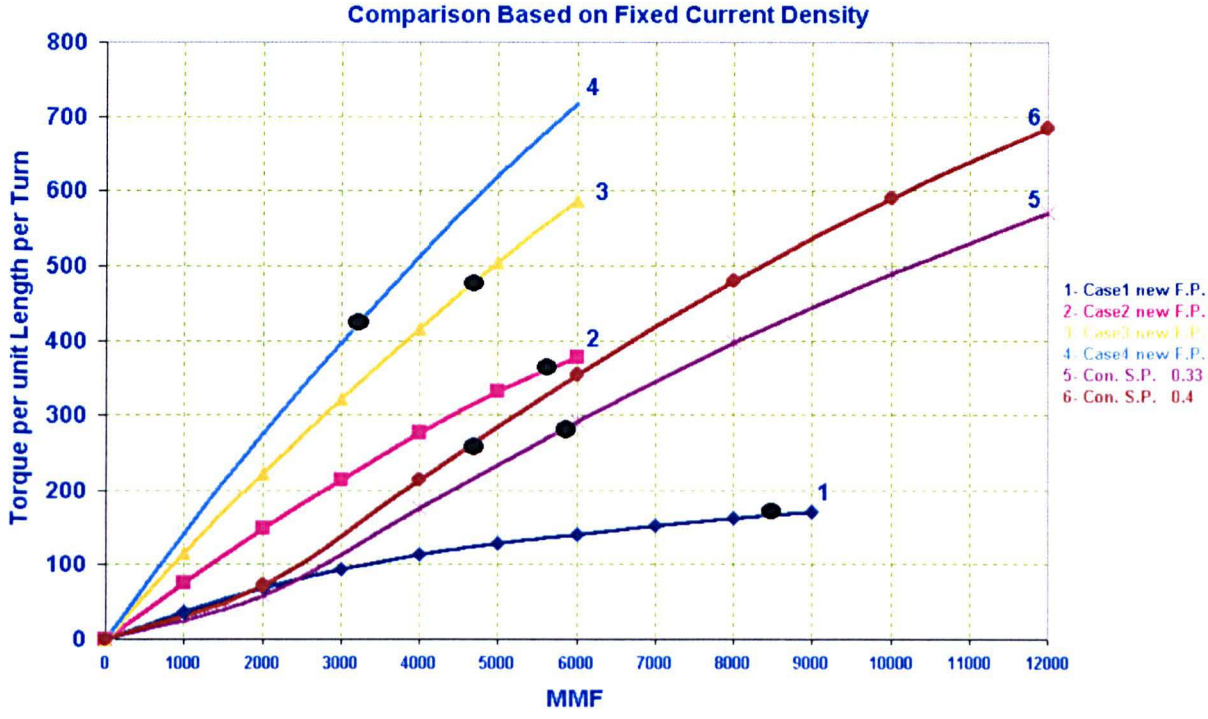

Fig. 3.6.a Comparison Based on Fixed Current Density

Black dots represent the calculated MMF for each machine corresponding to a current density of 10 A/mm^2

The Y-axis in Fig. 3.6.a is the torque per unit length per turn. The MMF on the x-axis is for two slots of the new design because there are two coils per phase in all the new SRMs. So the entire resultant MMF per phase is from two coils; each coil fills two stator slots completely linking one stator pole arc. But in the conventional SRMs the

x-axis is the MMF for four coils because there are four coils per phase, each coil links one stator tooth and fills two halves of two stator slots.

3.5 Comparison Based on Fixed Copper Loss

Copper Losses = $J^2 * \rho * \text{Copper Volume}$.

For constant losses: $J^2 * \text{Copper Volume} = \text{Constant}_1$

$$J^2 * \text{Slot Area} = \text{Constant}_2$$

$$J \alpha \sqrt{\frac{1}{\text{slot area}}}$$

Calculation of the current density.

The current density is inversely proportional to the square root of the slot area if the overall loss is to be held constant.

a)for the new 12/8 full pitch SRM:

$$J_1 \alpha \sqrt{\frac{1}{10^{-3} * 0.615}} \alpha \ 40.32$$

$$J_2 \alpha \sqrt{\frac{1}{10^{-3} * 0.403}} \alpha \ 49.81$$

$$J_3 \alpha \sqrt{\frac{1}{10^{-3} * 0.351}} \alpha 53.37$$

$$J_4 \alpha \sqrt{\frac{1}{10^{-3} * 0.227}} \alpha \quad 66.37$$

b)for the conventional short pitched SRM:

Model 1: $t/\lambda = 0.33$

$$J_5 \alpha \sqrt{\frac{1}{10^{-3} * 0.43}} \alpha \ 48.22$$

Model 2: $t/\lambda = 0.4$

$$J_6 \alpha \sqrt{\frac{1}{10^{-3} * 0.34}} \alpha \ 54.23$$

Taking the conventional machine with t/λ = 0.33 as a reference and using a peak MMF of 3500 AT it is now possible to determine the MMF in the other machines for the same loss, as follows: -

$$MMF_5 \alpha J_5 A_5 \quad \& \quad MMF_1 \alpha J_1 A_1$$

So $$\frac{MMF_5}{MMF_1} = \frac{J_5 A_5}{J_1 A_1}$$

$$MMF_1 = \frac{3500 * 40.3238 * 615}{48.22 * 430} = 4186$$

MMF(s) for the new fully pitched 12/8 models

Model 1	4186
Model 2	3388
Model 3	3161
Model 4	2542

MMF(s) for the conventional 12/8 short pitched models

Model 1: 0.33	3500
Model 2: 0.4	3148

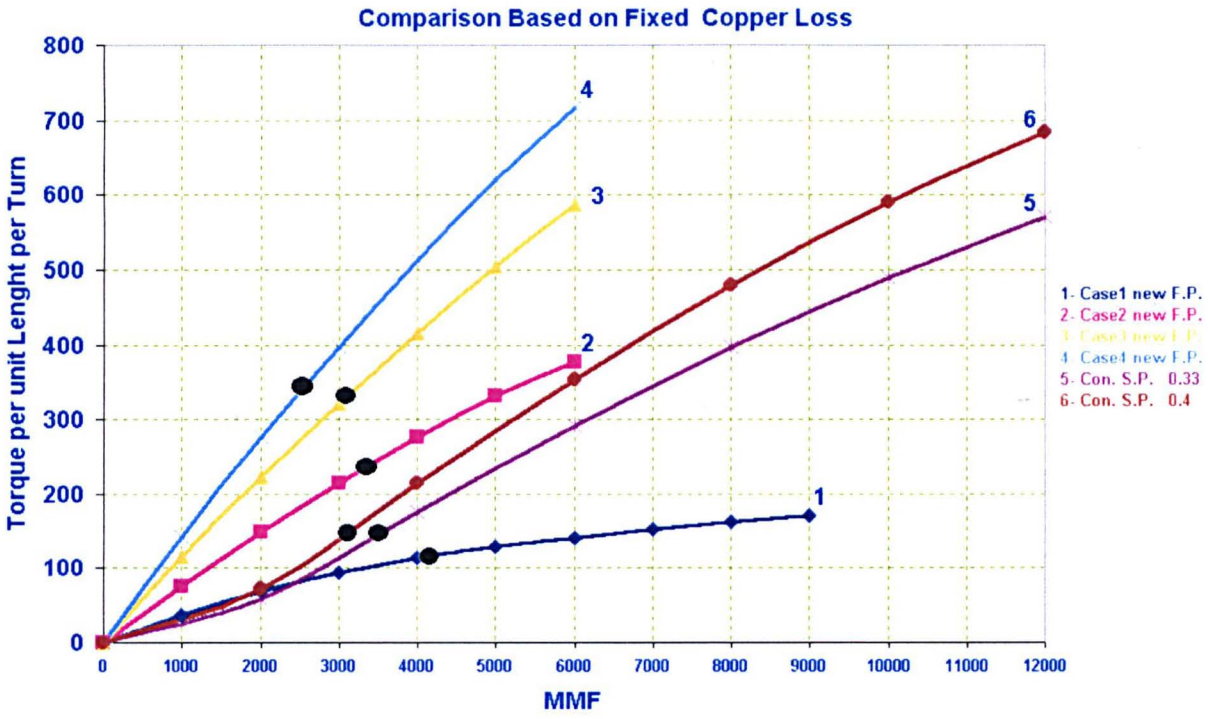

Fig. 3.6.b Comparison between the New SRM and the Conventional One Based on Fixed Copper Losses

Black dots correspond to point of equal winding loss

Fig. 3.6.b shows the comparison between the new designs and the conventional designs based on fixed copper loss.

It can be seen that, irrespective of whether fixed current density or fixed copper loss criteria are applied, the new segmental designs 3 and 4, which are those with wider teeth, give by far the greatest performance. For a fixed current density the maximum performance occurs with design 3, because the loss of MMF with design 4 (wider teeth give a lower slot area) more than compensates for the increase in flux. Note how the torque produced is approximately double that of the conventional designs. For a fixed winding loss design 4 outperforms design 3, as shown in Fig. 3.6b. The conclusion is that the optimum value of tooth width is between that of model 3 and model 4.

From the above table there is a ratio t/λ between the 0.56 and 0.729 of models 3 and 4 which gives the optimum solution. These models were examined in more detail, along with an additional model, employing an intermediate value of $t/\lambda=0.67$. This latter ratio is useful for comparing the two types of SRM. For example one of the conventional design, with the standard ratio ($t/\lambda=0.33$), and the new optimum design,

ratio of stator tooth width / rotor pole pitch = 0.33 (t/λ=0.67), to see the percentage increase in the torque and the performance for the same ratio of the tooth width to the pole arc.

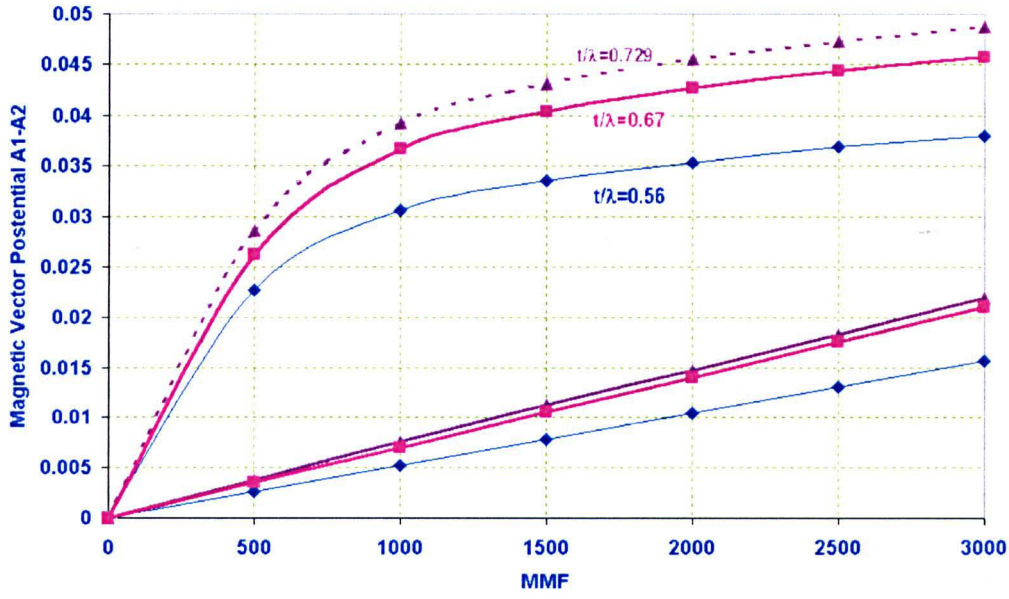

Fig. 3.7 Comparing the Aligned and the Unaligned Positions with the Best Two Models

This comparison is given in Fig. 3.7, which shows the aligned and unaligned flux-linkage curves for the three models of different tooth width (the magnetic vector potential per coil versus the MMF per slot) (Appendix 1).

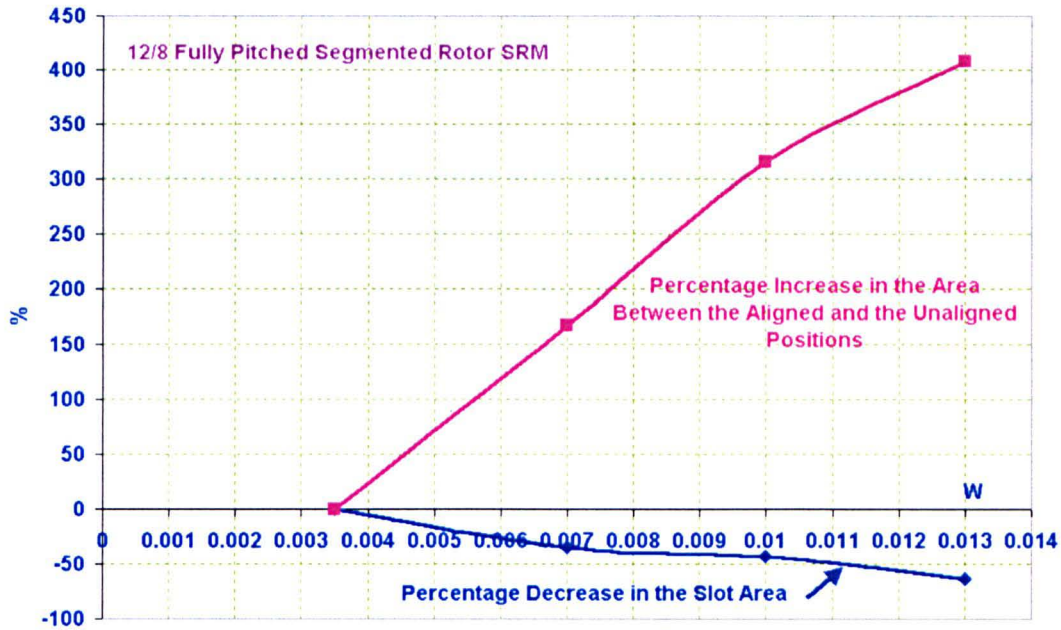

Fig. 3.8 Studying the Gain in the Output when the Slot Area Decreases

Fig. 3.8 shows the impact of changing the tooth width on both the torque and the slot area. The target from these two graphs is to understand the effect of changing the tooth width on both the torque and the slot area to get the highest possible torque and at the same moment to leave enough slot area for the conductors.
When the tooth width is small the output is low. Starting to increase the tooth width causes the torque to increase by a high ratio, because the Flux-Linkage trajectory is in the linear region and has low saturation. But after that widening the tooth width increases the torque only a small amount because the flux-linkage trajectory moves into the deeply saturated region. So widening the tooth width must stop because there is not enough area for conductors and at the same moment the gain in the torque is small.
The choice of $t/\lambda=0.67$ seems to give a good compromise between flux-linkage per unit MMF and slot area and was therefore chosen for the prototype.

3.6 Searching for the Best Way to Fit the Segments to the Shaft

After finishing the design of the magnetic and electric circuit of the new motor the mechanical design has to be considered. The first step in the mechanical design to allow successful building of the new motor is the manner of fitting the segments to the shaft. The fitting must not adversely affect the design of the magnetic circuit.
Fig. 3.9 shows how the segments will be fitted in the shaft. The eight rotor segments will be constructed from stacks of separate laminations, which will be assembled onto a non-magnetic shaft and will be held by a stainless steel wedging system. The wedges fit into dovetails in the segments, and they will then be bolted to the shaft. The segments will be also clamped axially using end-rings.

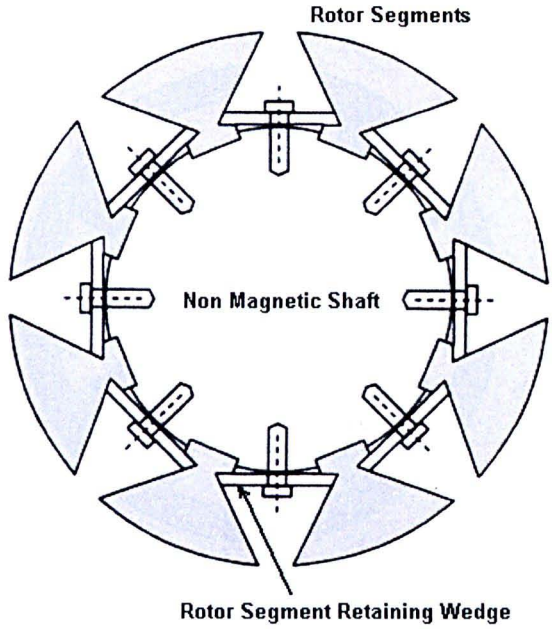

Fig. 3.9 Wedging System Used to Hold the Rotor Segments onto the Rotor Shaft

A brief study of the shape of the dovetail segments was then undertaken. Two examples are shown below; one which uses wide, shallow segments and one which uses deeper, segments, so that the dovetails of adjacent segments may be located further apart.

3.6.1 Wide Fitting

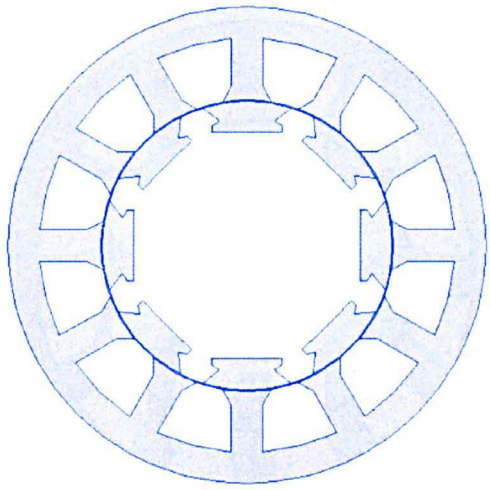

a

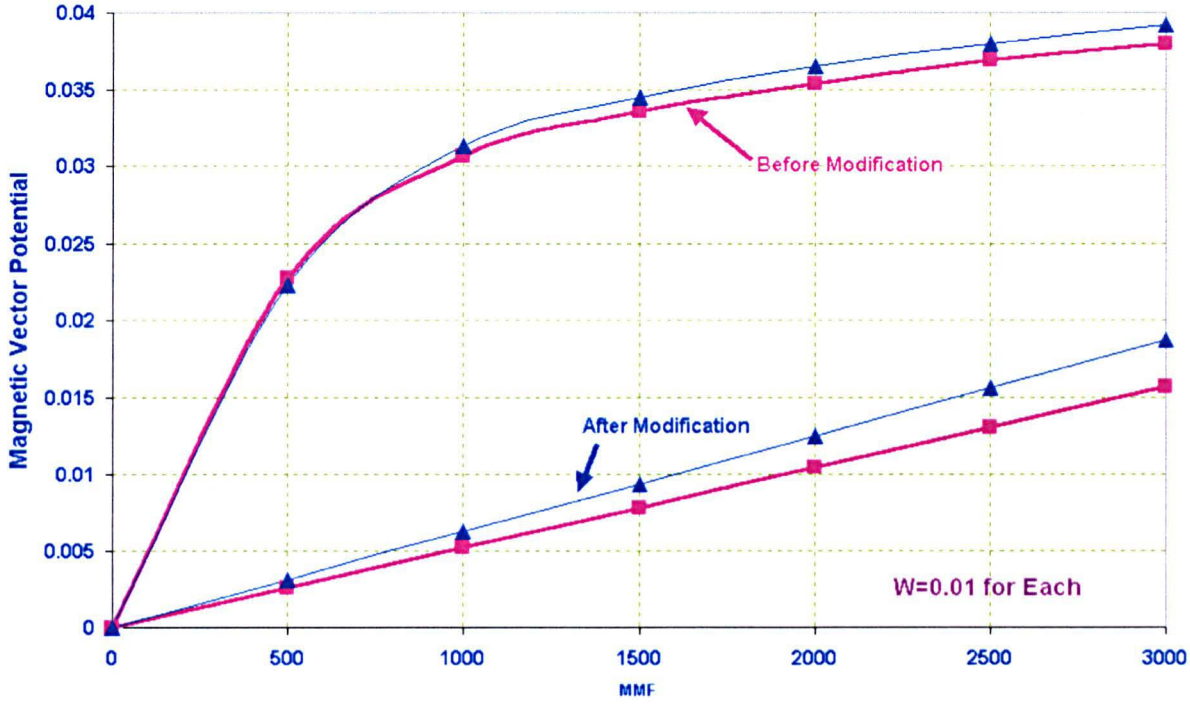

b

Fig. 3.10 Wide Fitting

Fig. 3.10 illustrates how wide fitting of the segments slightly decreases the reluctance in the unaligned position, but the reluctance in the unaligned position is decreased by a larger amount, so the area between the aligned curves is decreased, leading to a reduction in torque capability.

3.6.2 Deep and Tapered Fitting

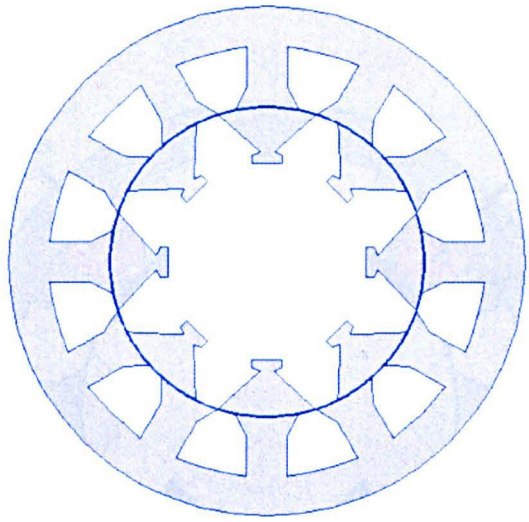

a

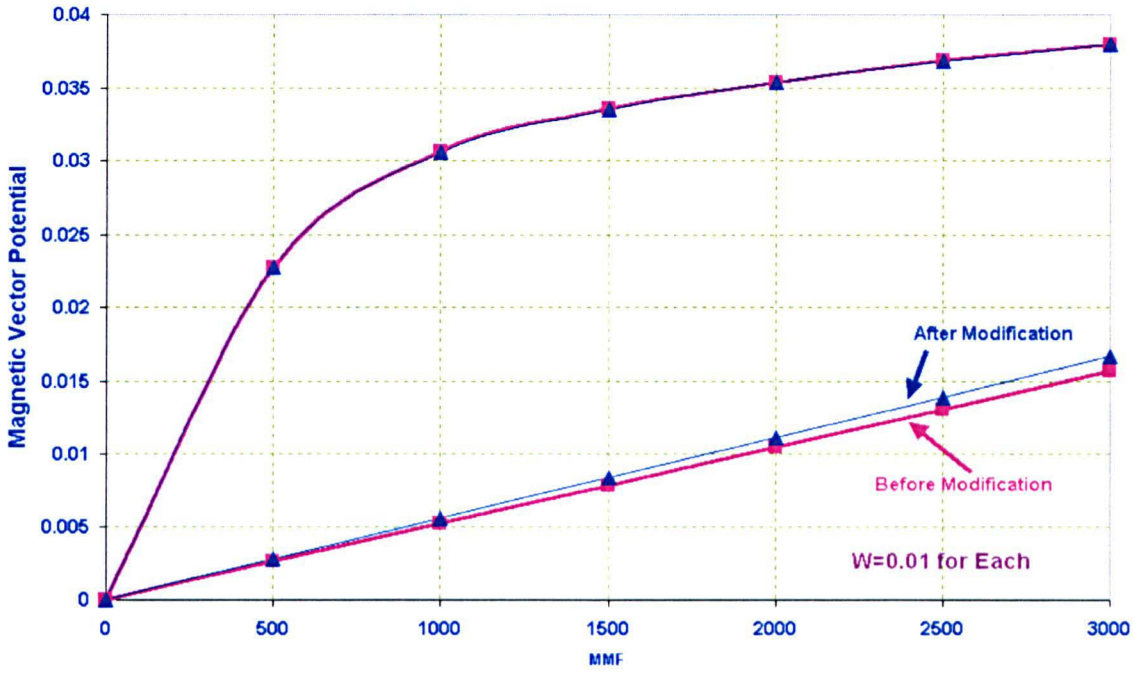

b

Fig. 3.11 New Way of Fitting the Segments to the Shaft

Fig. 3.11 shows how the deep and tapered fitting has very little impact upon the magnetic characteristics. This design was therefore used in construction of the prototype.

3.7 The Characteristic of the New Complete-Optimised Fully Pitched 12/8 Segmented Rotor SRM

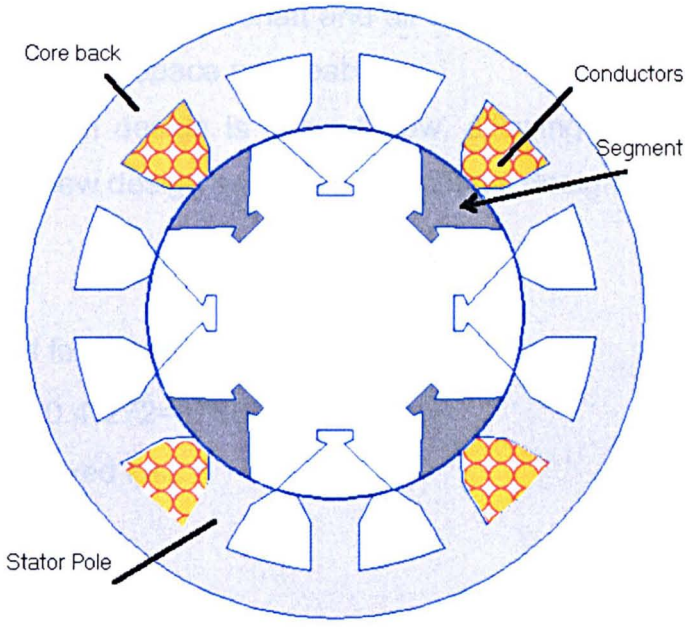

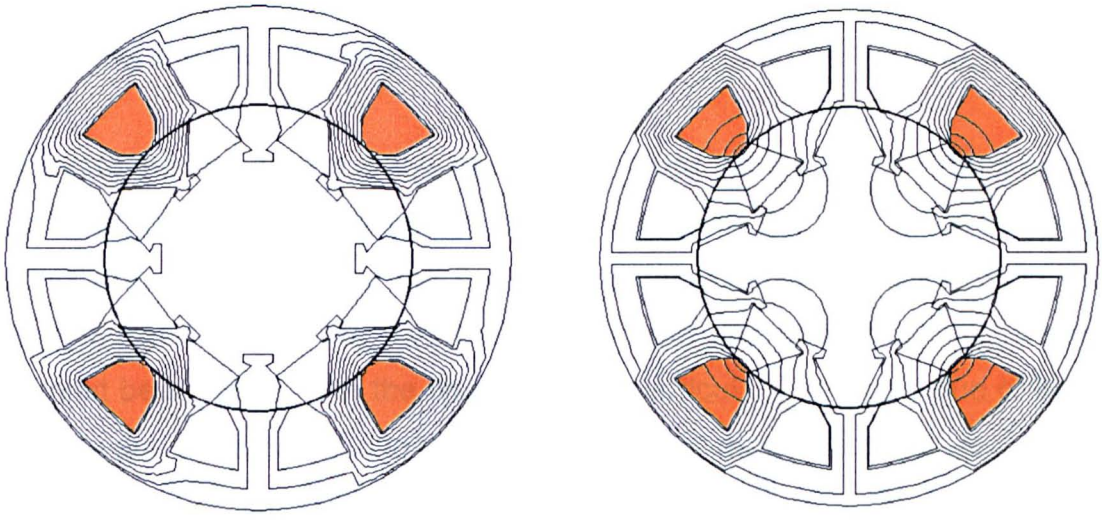

Aligned Position

Unaligned Position

Fig. 3.12 Optimised New 12/8 SRM and the Magnetic Flux Plot

Fig. 3.12 shows the magnetic flux plot of the aligned and the unaligned positions of the new optimised 12/8 segmented-rotor SRM. The rotor segment is shaped to be fitted properly in the shaft without affecting the magnetic circuit design. The flux plot shows the cross leakage flux. The shaft and all the materials between the segments are modelled as having free space permeability.

The data of the optimum design is given below, allowing for comparison with the previous cases of the new design and the conventional design:

Area of slot=272 mm^2

For the comparison of fixed current density

$MMF_{Optimum}=\sqrt{3}*10*2*0.4*272=3768.94$

For the comparison of fixed loss

$$J_{Optimum}\alpha\sqrt{\frac{1}{10^{-3}*0.272}}\alpha\ 60.63$$

$$MMF_{Optimum}=2783.41$$

3.8 Checking the Flux Density in the New SRM

According to the key-design of this new type of SRM the flux density must be uniform through the flux path in the aligned position to maximise the inductance in the aligned position. Also one section of the flux loop in the unaligned position must be non-magnetic so as to maximise the reluctance in the unaligned position. These two things must be checked from the finite element particularly at high value of MMF (the flux density and the saturation in different parts in the magnetic circuit).

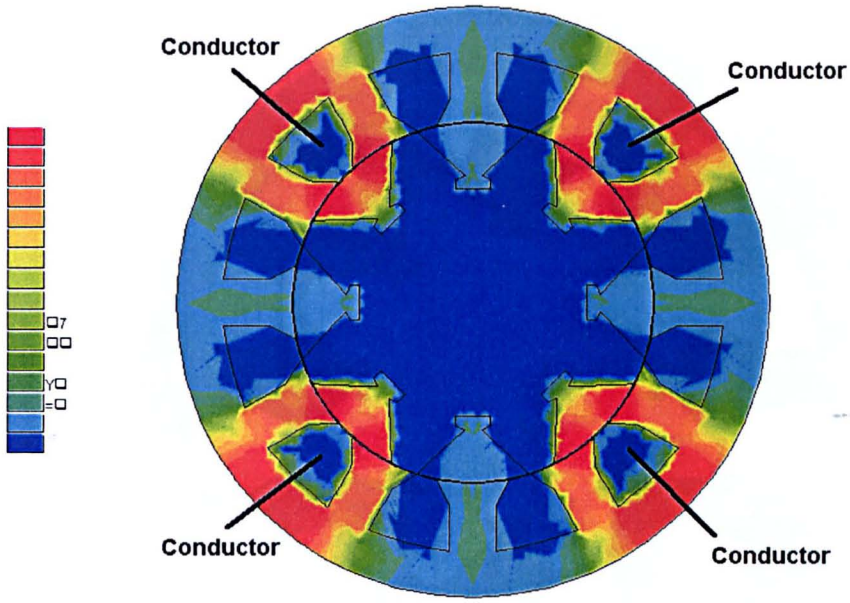

Fig. 3.13.a Aligned Position (MMF/Slot=3000)

Fig. 3.13.a shows the 12/8 new optimised segmented-rotor SRM in the aligned position and the distribution of the flux density in the aligned position. The flux density is approximately the same around the conductors.

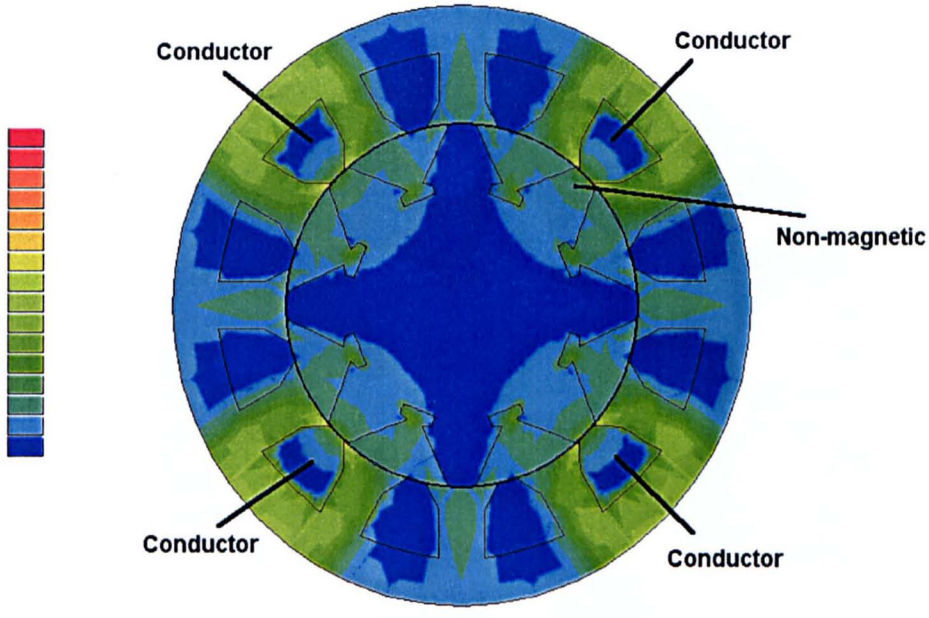

Fig. 3.13.b Unaligned Position (MMF/Slot=3000)

Fig. 3.13.b shows the flux density distribution in the unaligned position of the 12/8 fully pitched segmented-rotor SRM. One section is completely non-magnetic. The flux is the cross leakage flux only.

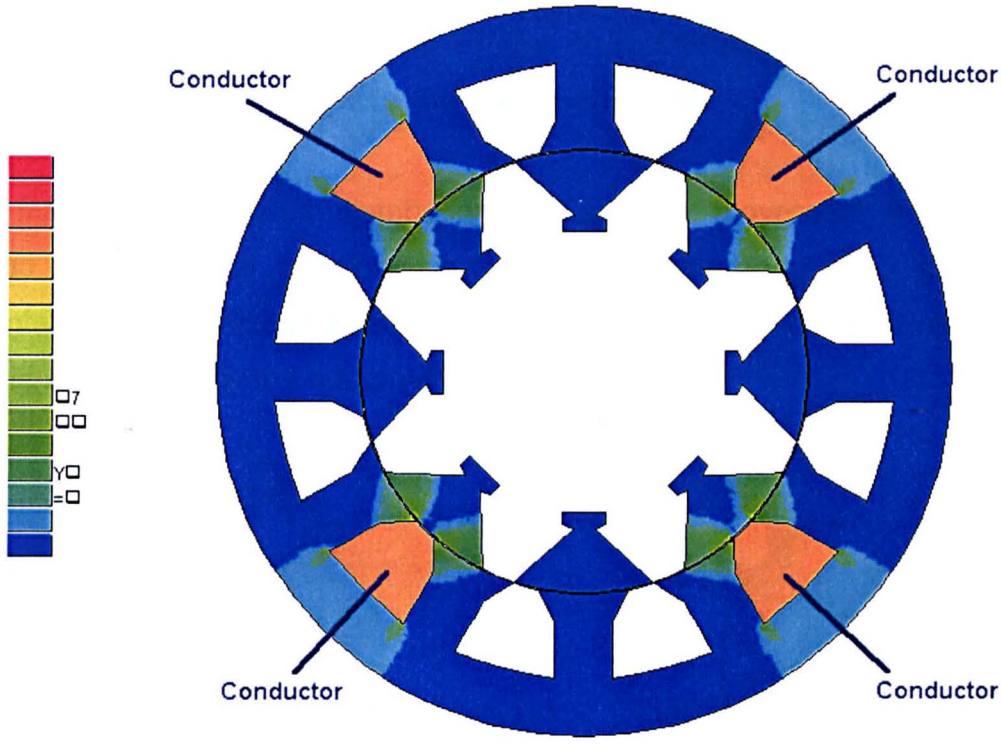

Fig. 3.14.a Saturation in the Aligned Position (MMF/Slot=3000)

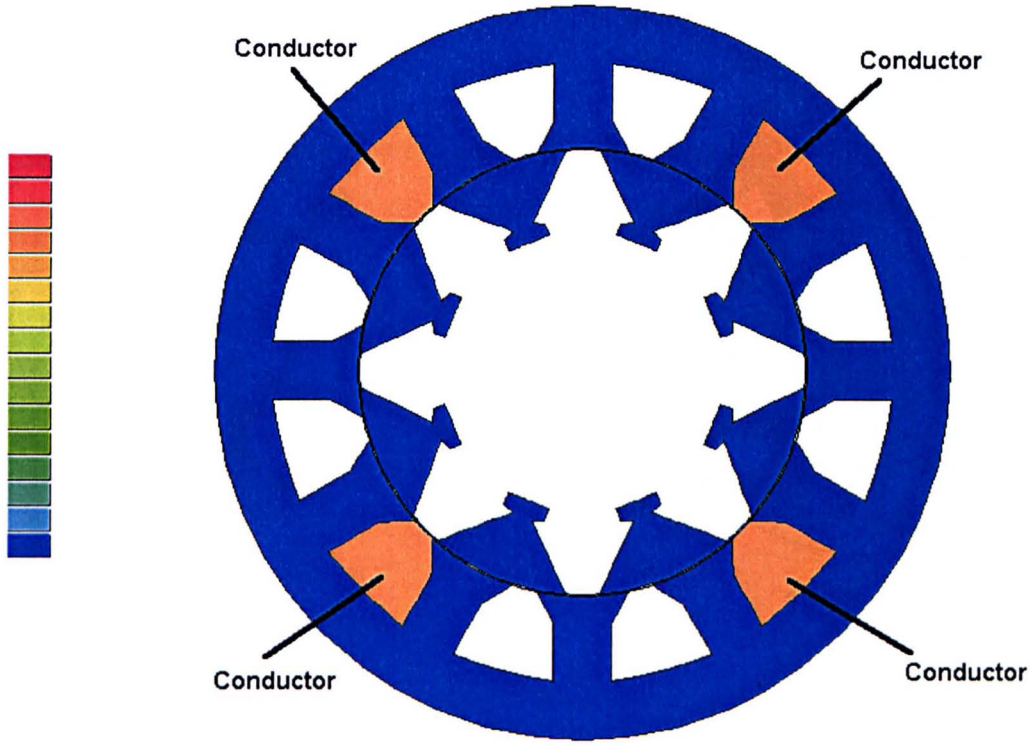

Fig. 3.14.b Saturation in the Unaligned Position (MMF/Slot=3000)

Fig. 3.14 shows little saturation in the aligned and the unaligned positions.

3.9 The Predicted Characteristics of the New Optimised Fully Pitched 12/8 Segmented-Rotor SRM (adaptive finite element model)

Fig. 3.15.a shows the flux distribution through the movement from aligned to unaligned positions (all positions in mechanical degrees). To give accurate representation of the Flux-Linkage characteristic models for different rotor positions were built and solved by the adaptive finite element.

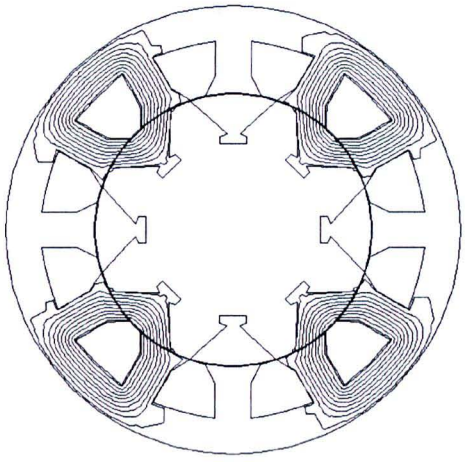

Zero

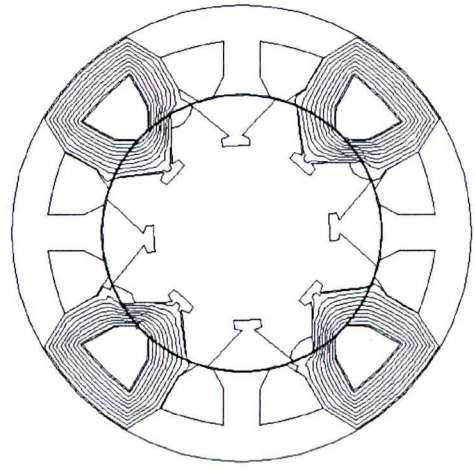

3.75

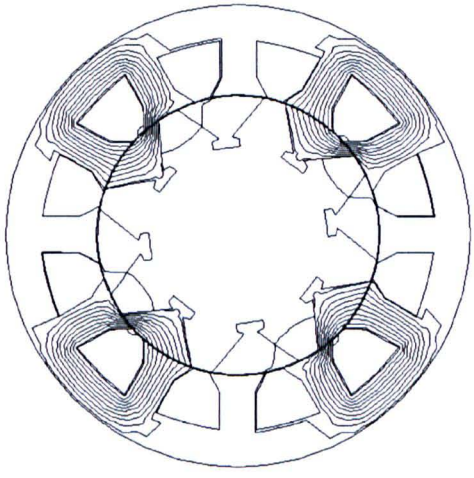

9.5

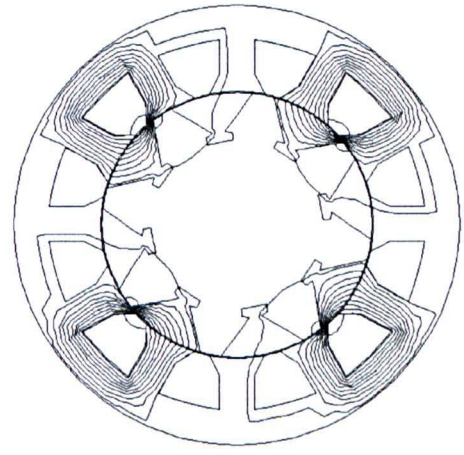

11.25

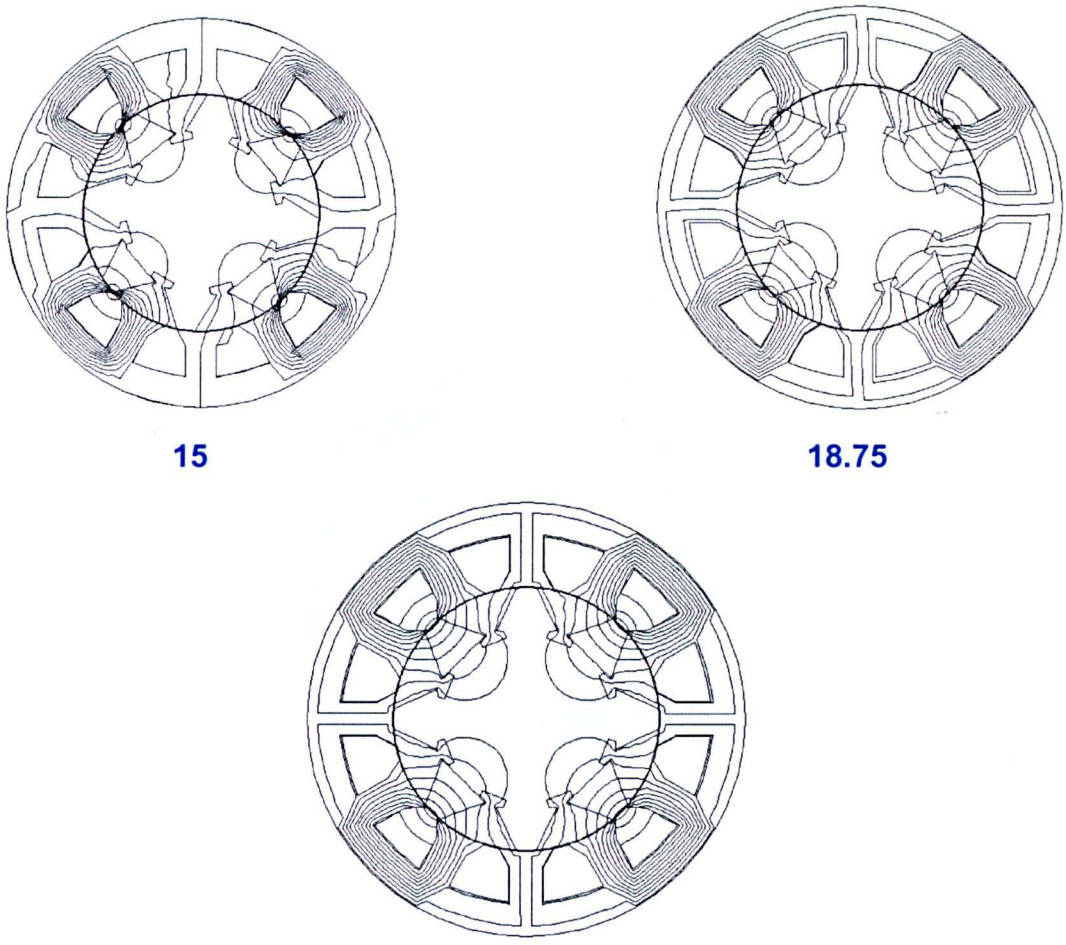

Fig. 3.15.a 12/8 Segmented-Rotor SRM Magnetic Flux Plot for Different Rotor Positions

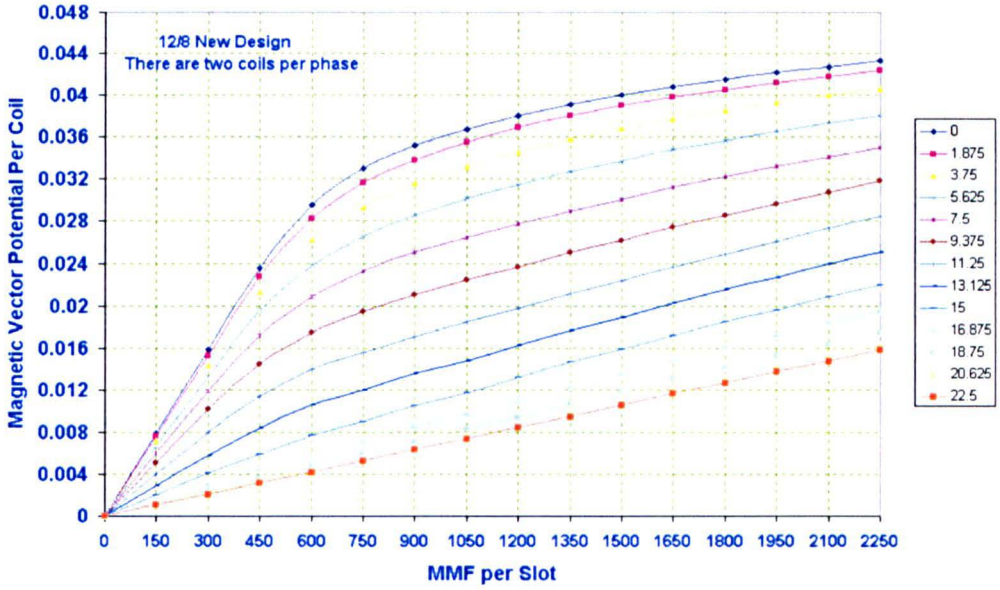

Fig. 3.15.b Magnetic Vector Potential per Coil versus the MMF per Slot of the New 12/8 SRM

Fig. 3.15.b shows the magnetic vector potential of the new SRM. It is assumed there are two coils per phase. The characteristic of the magnetic vector potential per coil versus the MMF per slot is believed accurate. Each point was obtained from modelling using a 2D adaptive finite element model. No account of end-windings and other end effects is included.

3.10 Overview and Comments on the New 12/8 SRM

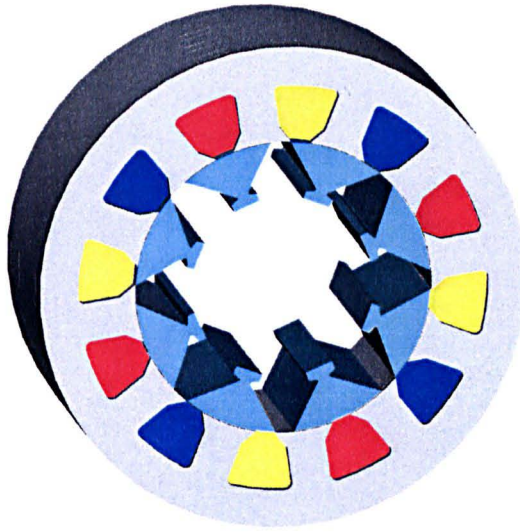

Fig. 3.16 Simple Structure of the New Motor

The simple structure of the newly designed segmented-rotor SRM shown in Fig. 3.16 can be deceiving. The analysis, design and optimisation are indeed complicated because several parameters must be chosen simultaneously.

Classical analytical equations to describe the machine performance are not suitable in this case with high levels of magnetic non-linearity, coupled with non-sinusoidal excitation techniques and non-sinusoidal spatial variation of parameters which require analytical models to be over simplified, so that they no-longer adequately represent the machine. The numerical finite element method presented is both simple to implement and gives accurate results within a short time period.

3.11 The Segmented-Rotor SRM with Inner Stator

The inner rotor of the new segmented-rotor SRM has a draw back. The rotor segments are relatively shallow, leaving a large volume for the shaft. This volume is greater than the required to transmit the torque, but cannot be utilised magnetically.

This means there are large areas inside the motor that are not used to produce torque. This problem no longer occurs if the topology is reversed, with the stator on the inside and the rotor outside. Outer rotor electrical machines are less common that their inner rotor counterparts but are still frequently encountered. If the machine is naturally cooled at its outer surface there is a reduced ability to remove heat from the windings, so the SRM designer must give careful consideration to ventilation.

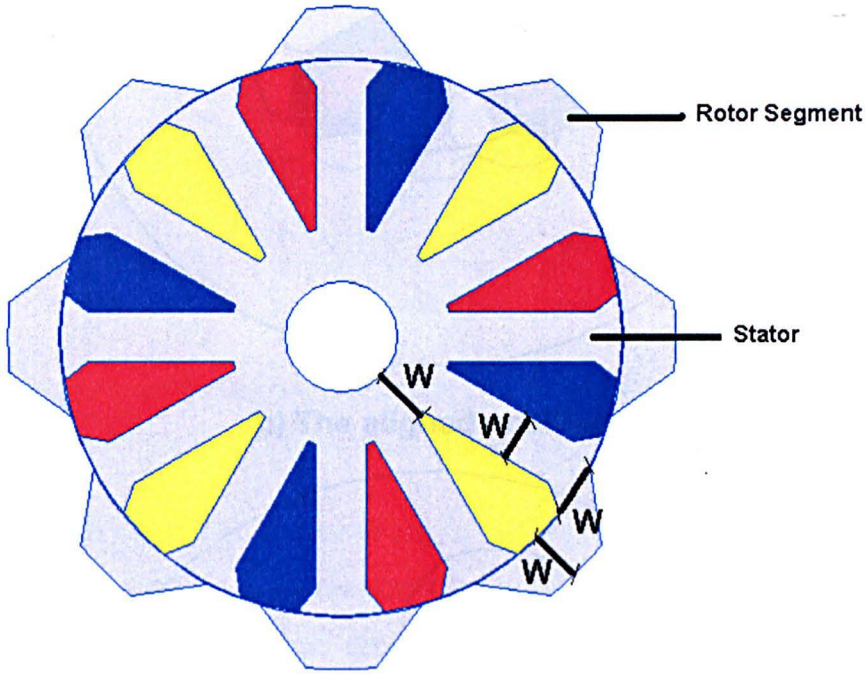

a) Inner Stator Segmented-Rotor SRM, General Rules of Designing Segmented-Rotor SRM is used also here

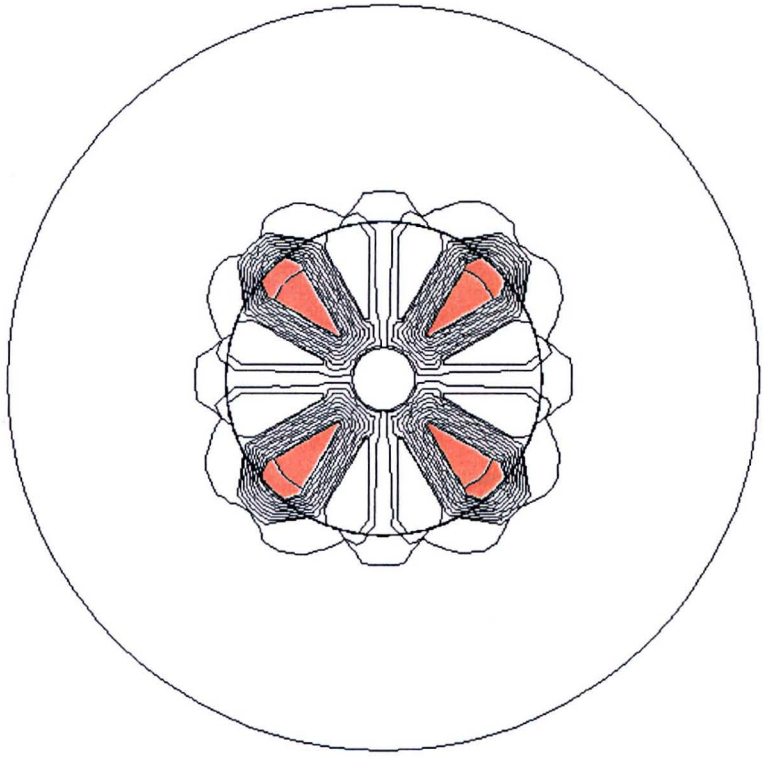

b) The aligned position

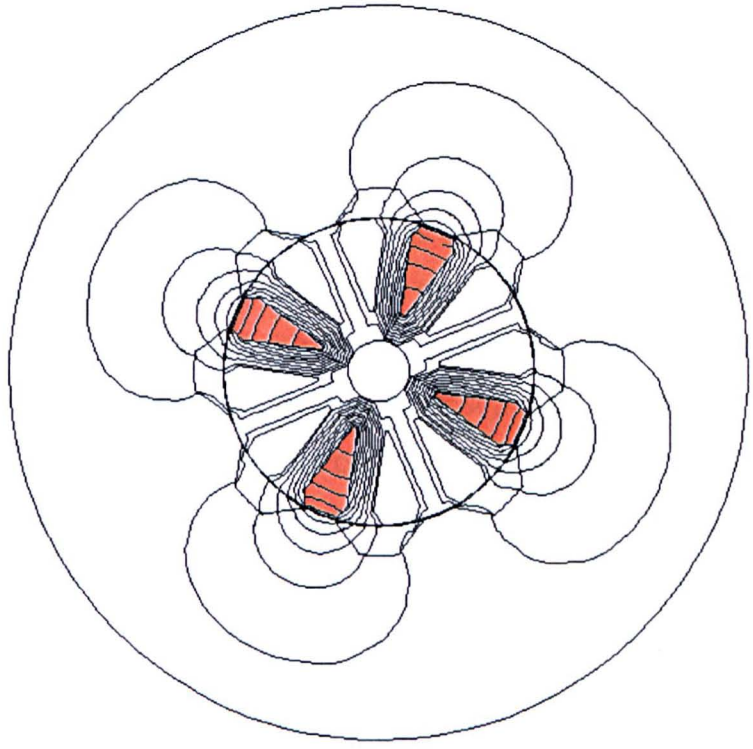

c) The unaligned position

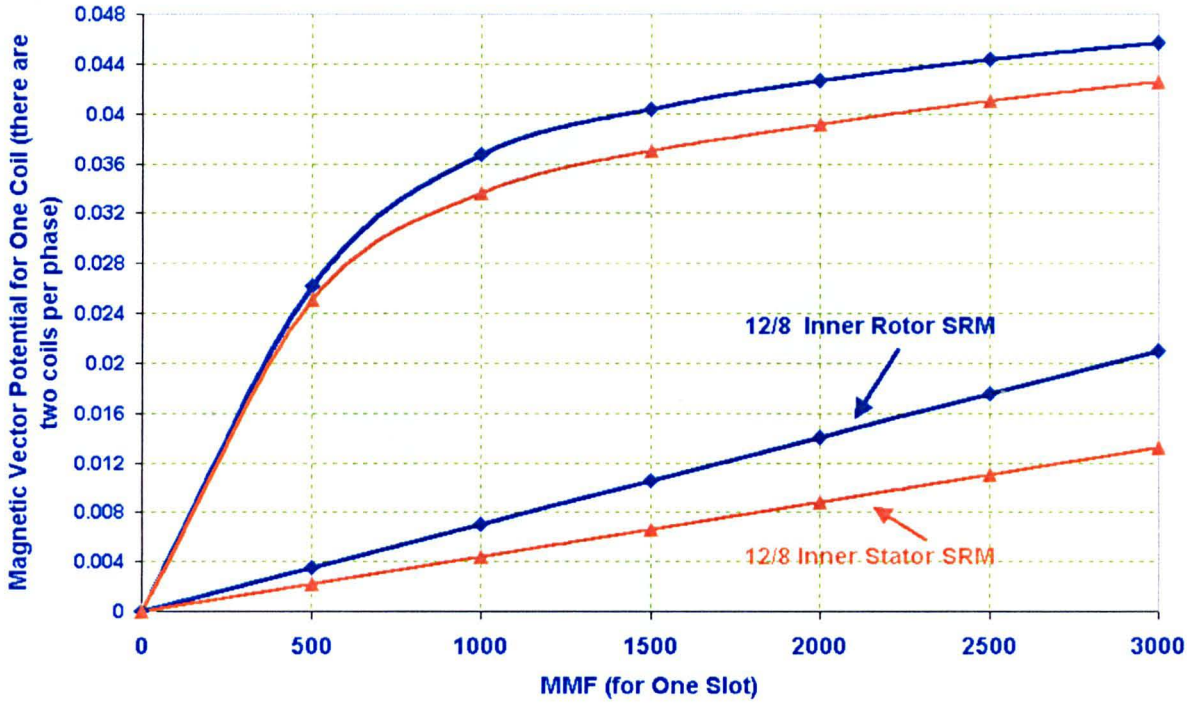

d) The comparison between the inner rotor and the outer rotor (same W)

Fig. 3.17 Design of the Inner Stator Segmented-Rotor SRM

Fig. 3.17 shows the design of the inner stator segmented-rotor SRM. For the purpose of comparison the machine was selected to be the same outside diameter as the inner-segmented rotor. The circle around the machine in Fig.3.17 (b&c) is just to model the boundary with the adaptive finite elements. The general design rules, which were developed in chapter (2), were applied here. The stator core back the overlapping, the tooth width and the height of the segment all are equal. The t/λ used here is the same for the optimum design of this inner segmented rotor (t/λ=0.67). The aligned and unaligned positions are shifted down for the outer rotor. This result was expected because when the rotor became the outer the separation between the segments increased so the reluctance increased in the unaligned position; the unaligned position came down. Also the aligned position was not reduced quite as much as the unaligned because the length of the flux path increased a little in the aligned position so that the aligned inductance increased. The slot area of the outer rotor machine is 424 mm^2 and in the inner rotor is 272 mm^2. The conclusion here for this comparison is that the inner stator allows more slot area for the conductors and the torque may be higher than with the inner rotor design.

3.12 Comparison between the Torque Capability of the Segmented-Rotor SRM and one with an Axially Laminated Rotor

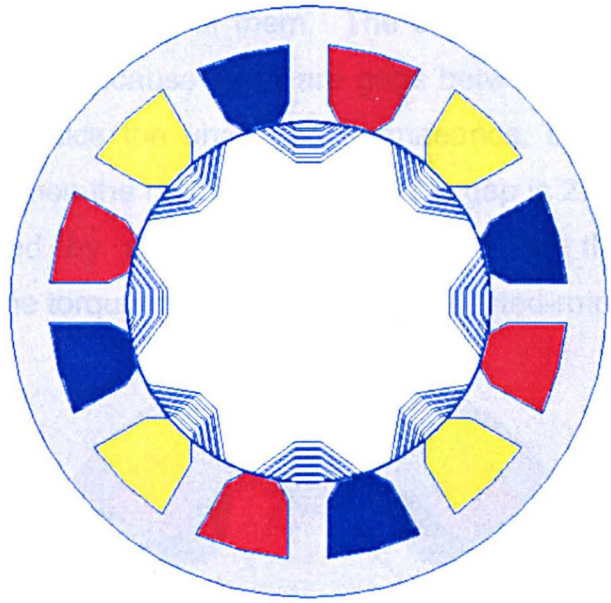

Fig. 3.18 Axial Laminations SRM to Compare with Model W=0.01 Segmented Rotor SRM (One Phase Energised)

Fig. 3.18 shows an axially laminated SRM. The segments are the same size as the previous model3 of the new segmented-rotor 12/8 fully pitched SRM.

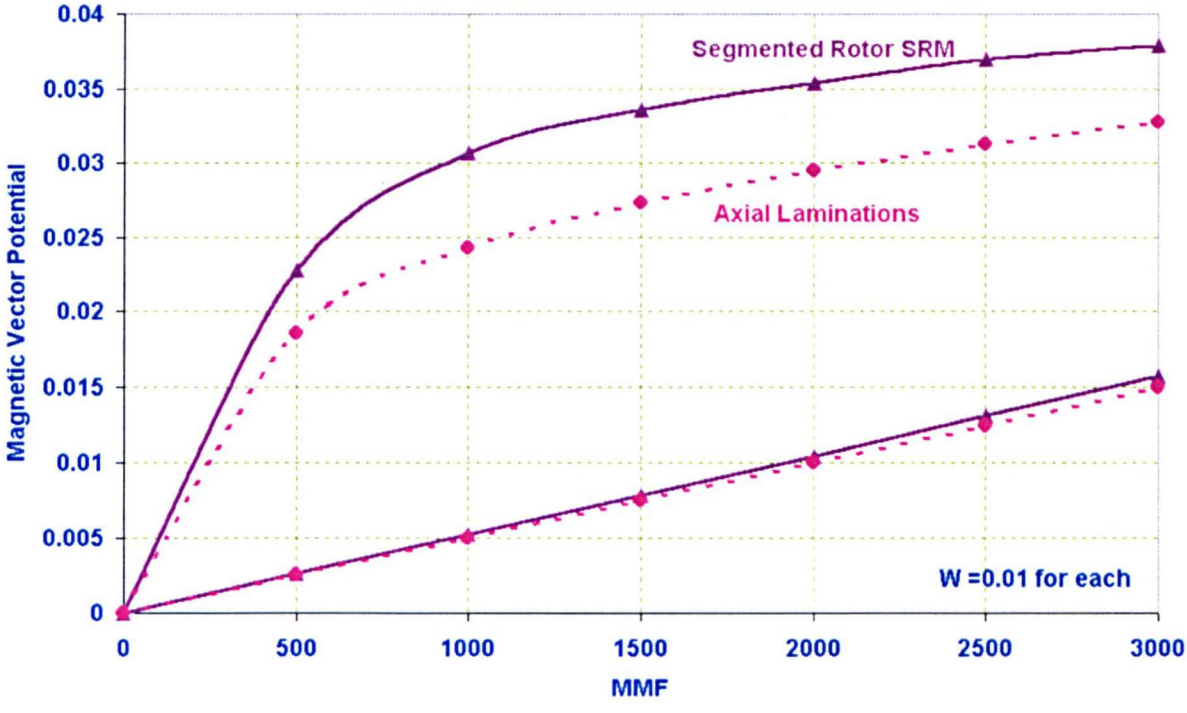

Fig. 3.19 Comparison between the Segmented-Rotor and Axial Laminations

Fig. 3.19 shows a comparison between the segmented-rotor SRM and an axially - laminated SRM. Both have three phases with fully pitched windings and the size of the segment is the same in both of them. The axial laminations gave less torque than the segmented rotor because there are gaps between the laminations. These gaps are needed to reduce the unaligned permaeance, but they also reduce the aligned permeance. When the ratio of the iron to the gap is 2:1 the aligned saturated flux-linkage is reduced by approximately one third, so the motor will deliver approximately 2/3 of the torque of its equivalent segmented-rotor SRM [116-120].

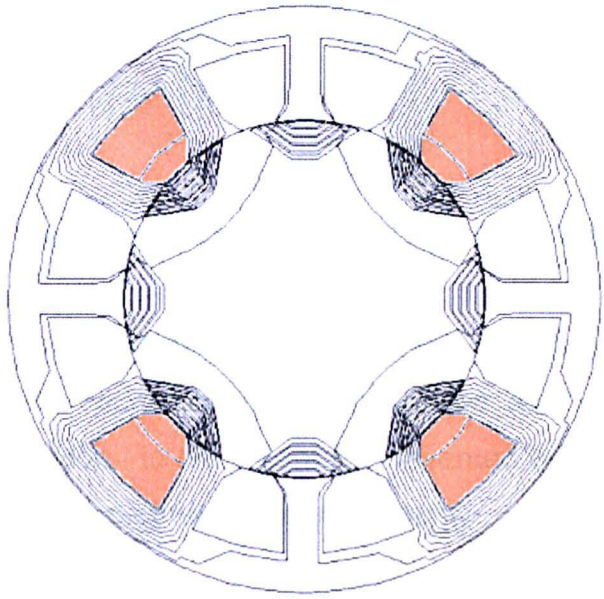

Fig. 3.20 The Flux Follows the Same Shape of the Bent Iron Lamination It may not be the minimum path (aligned position)

Fig. 3.20 shows that the flux is forced to cross through the segments following the path defined by the bent iron of the axial lamination.

3.13 Two Phase Segmented-Rotor SRM

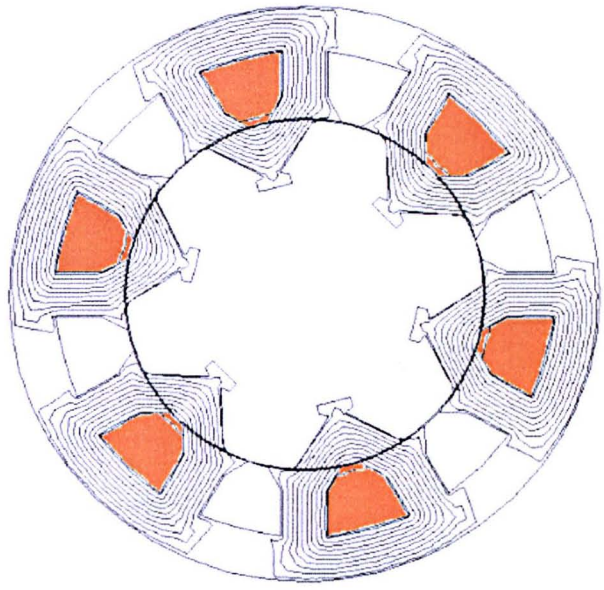

Fig. 3.21 Two Phase Segmented-Rotor Fully Pitch SRM

Fig. 3.21 shows how the segmented-rotor can be used for a two phase machine. In the aligned position all the segments are energised (i.e. all the 6 segments are able to produce torque [121]. Horst in his patent [97] invented his SRM to be 2-phase so that he could energise all the segments simultaneously.

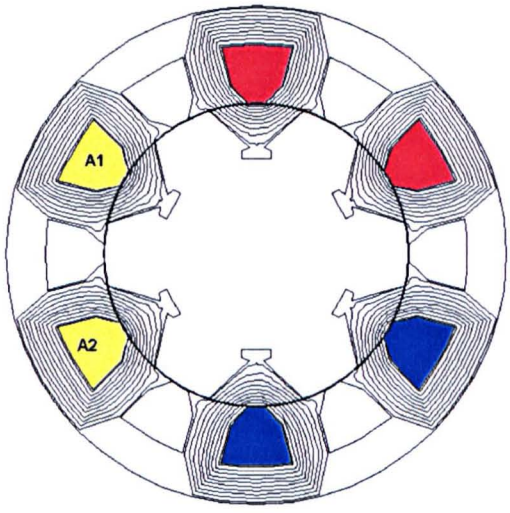

12/6 fully pitched SRM.
Three coils per phase
Two phases only
All the segments are
energised in the aligned position

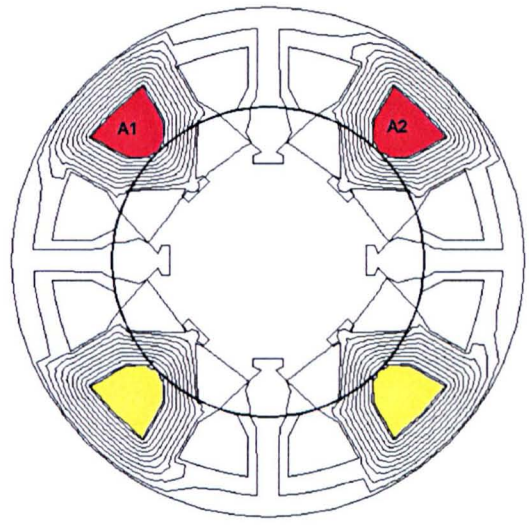

12/8 fully pitched SRM,
Two coils per phase
Three phases
Half the segments energised are
energised in the aligned position

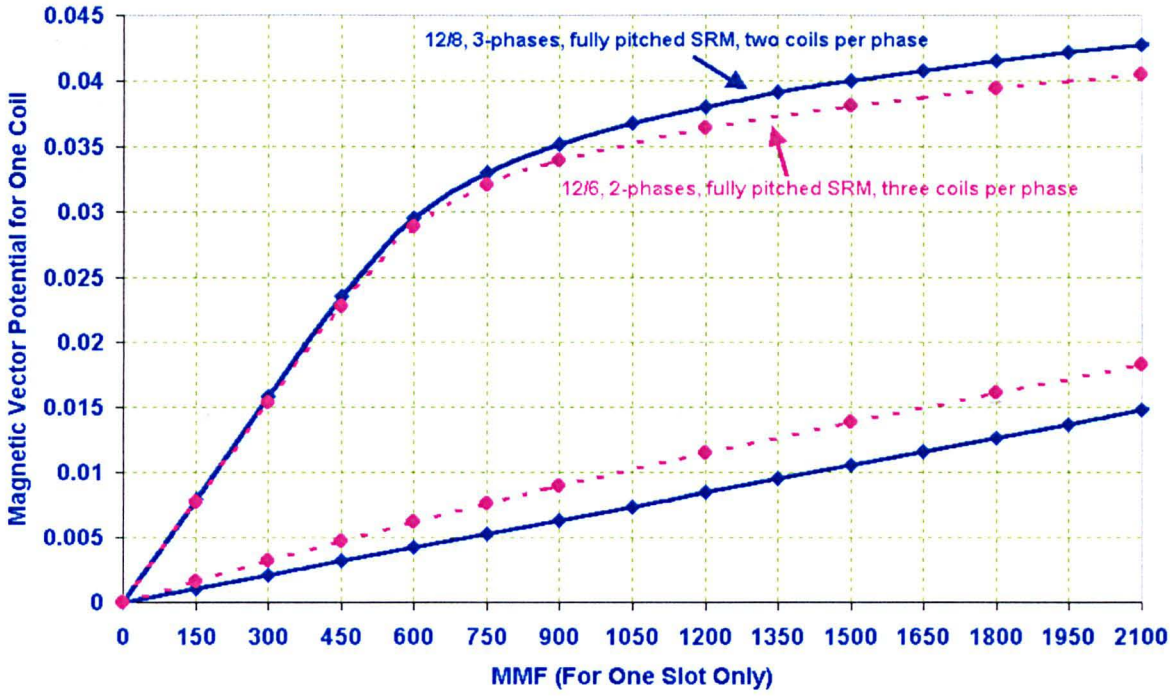

Fig. 3.22 Comparing the SRM Designed in this Thesis wit that of the Horst Invention

Fig. 3.22 shows the area enclosed by the 12/6 is less than that of the 12/8. In addition there are eight energy loops per cycle in the new SRM design discussed in this thesis and only six energy loops per cycle for the 12/6 (similar to the Horst design). So the new SRM presented in this thesis gives more torque than the Horst design.

3.14 Conclusion

This chapter develops the segmental concept of a three phase segmented-rotor SRM. It starts from the basis of segmental design and develops magnetic circuit parameters as a function of the stator tooth width for the 12/8 fully pitched segmented-rotor SRM. Different models were built for different values of stator tooth width and compared with two conventional models of the SRM. The models of the new design did not give precisely the best stator tooth width, consequently comparison was used to discriminate between the best two models of the new design. The optimum value of the tooth width was found to be between the two best teeth widths from the new design models. From this result the value of $t/\lambda=0.67$ was

selected as a basis for the rest of design. The chapter discusses some items regarding the choice of the stator pole arc between the magnetic circuit (tooth) and the electric circuit (the windings) plus the way of fitting the segments in the rotor. An axial lamination design was compared with one model of the new design to prove that the new design performs better. The chapter presents another design of this motor which uses the entire volume of the machine to produce torque by introducing the inner stator segmented-rotor SRM, which allows more area for the conductors.

4 Analysis and Design of 12/10 Short Pitched Segmented-Rotor SRM

4.1 Introduction

Single phase machines were initially considered in chapter (2) and it was shown to be possible to create greater air-gap force densities than with conventional toothed rotors, once the ratio of effective tooth width to pole pitch exceeded 0.5. In chapter (3) the general concept of the segmented-rotor was applied to three phase machines, which naturally led to a design in which the coils span a number of slots. The simulation has shown much more torque than a conventional SRM for a given frame size. However, the machine has substantially longer end-windings that will reduce the electric loading, and make it impractical for applications which combine a short lamination stack length with a large pole pitch. This chapter seeks to solve this problem by introducing a new machine topology, which permits the use of short pitch windings, placed around a single tooth. This concept maintains the torque capability of the previous design, but uses a much lower volume of copper. The chapter develops the theoretical basis for the machine configuration and then presents simulated results for a new 12/10 segmented-rotor SRM; illustrating both static torque and flux linkage profiles [122-135].

4.2 The Concept of a 3-Phase, Short Pitched, Segmented-Rotor SRM

To develop a three phase design which is suitable for short stack length machines it is essential that the winding spans a single tooth to keep the end-windings short, whilst maintaining the condition that only the conductors of a single phase occupy any one slot. To see how this can achieved, Fig. 4.1 shows the multi tooth winding design in rectilinear form, illustrating the conductors of a single phase [136-145].

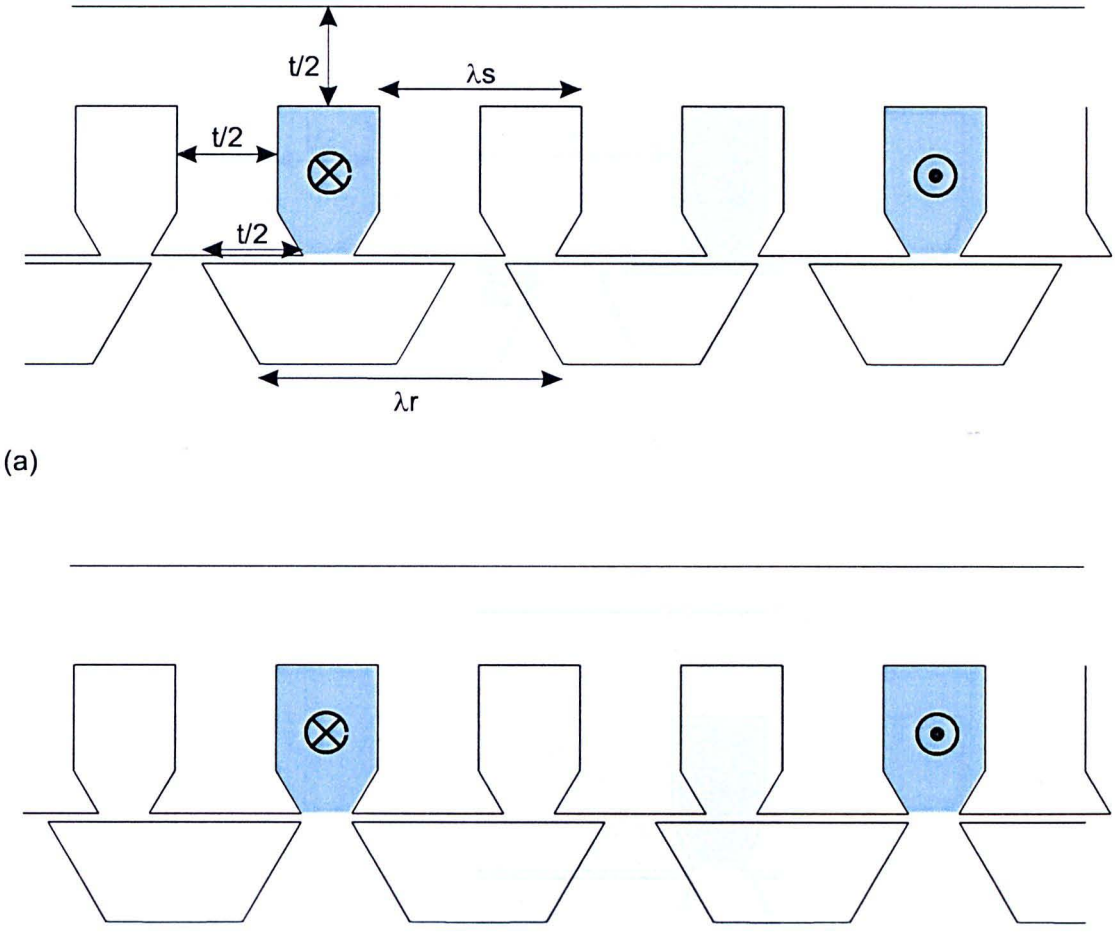

Fig. 4.1 Rectilinear Representation of the Multi Tooth Winding Segmental SRM, Showing First, Aligned Position and then Unaligned Position

It can be seen that each coil actually spans two rotor segments. If the region shown shaded in Fig. 4.1 were removed then the coil would span a single rotor segment and would have a shorter end-winding, wrapped around a single tooth. In the resulting "single toothed winding" arrangement, which is illustrated in Fig. 4.2, the stator teeth form two separate groups: double width teeth, which are enclosed by a winding, and standard width teeth which are unwound.

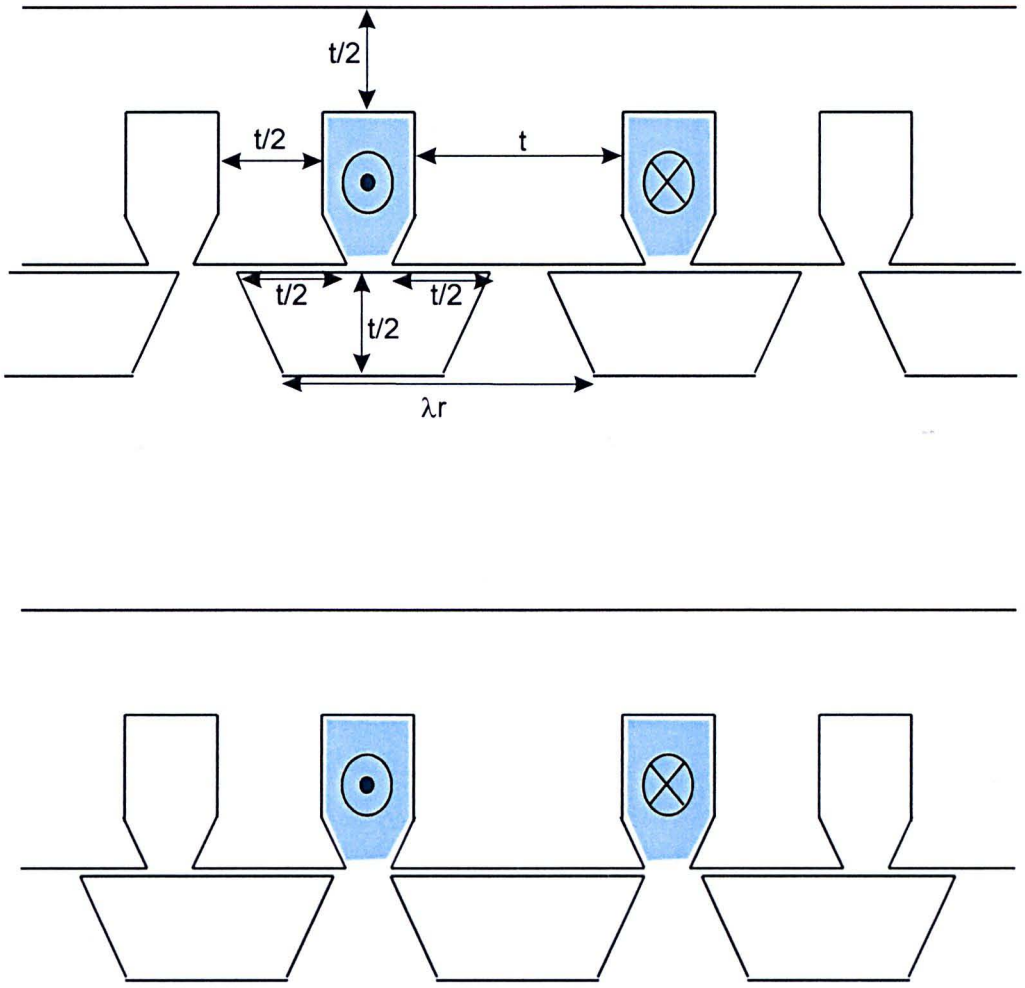

Fig. 4.2 Rectilinear Representation of the Single Tooth Winding Segmental SRM Design, Showing First the Aligned Position and Then the Unaligned Position

The unwound teeth still have a function, as they act as return paths for the magnetic flux. Excitation of a single phase now excites two adjacent slots and the phase permeance is the sum of the two slot permeances. The tooth pitch of the wound stator teeth must be equal to the rotor pole pitch, so that the permeance variation of these two slots with respect to rotor position is in phase [122-124].

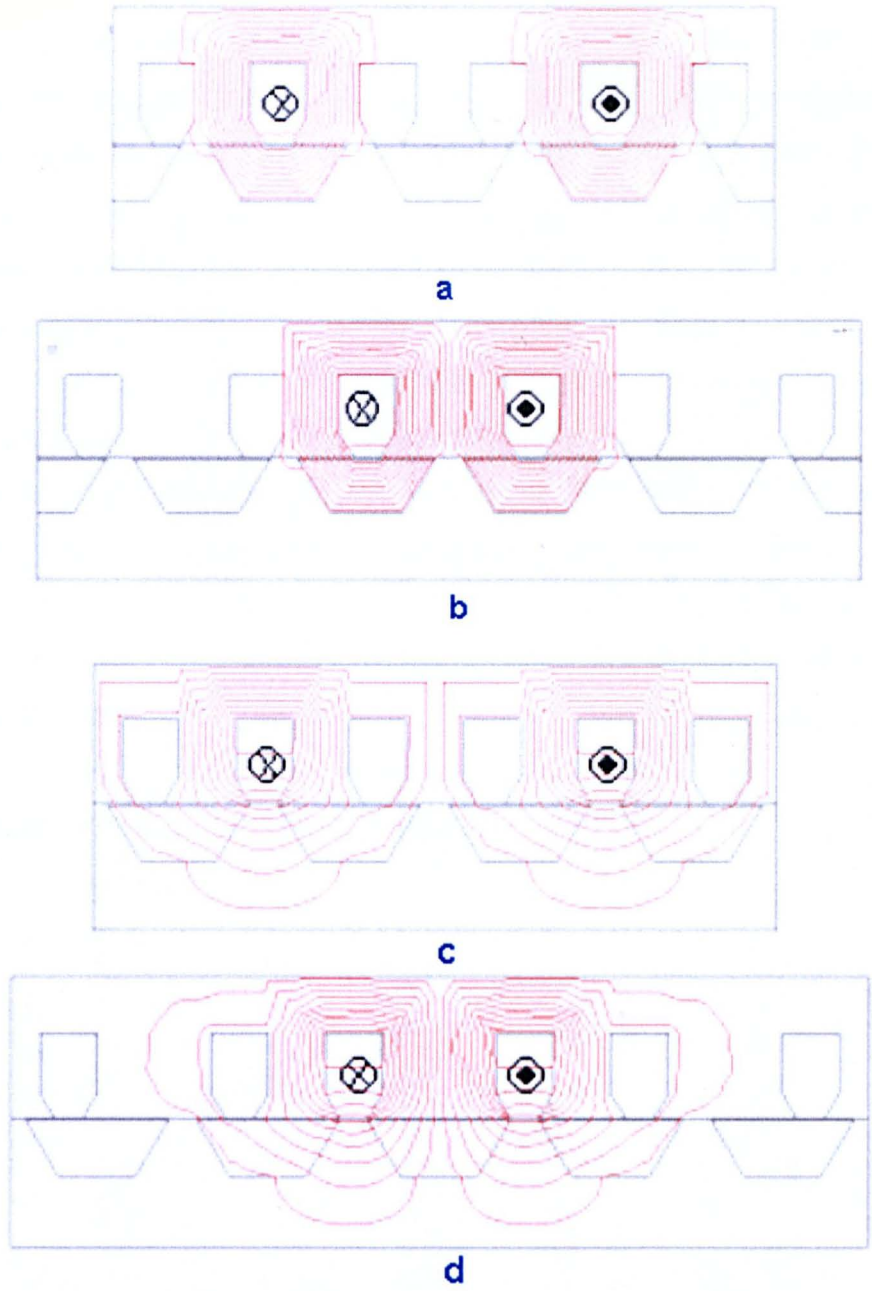

Fig. 4.3 Flux Plots Showing the the Magnetic Flux Distribution in Both Three Tooth and Single Tooth Winding Segmental Rotor SRMs

(a) Multi tooth design, aligned position (b) Single tooth winding design, aligned position

(c) Multi tooth design, unaligned position (d) Single tooth winding design, unaligned position

Fig. 4.3 shows the flux distribution in both the multi tooth winding design and the single tooth winding design, with a single phase excitation. Both the aligned position and the unaligned position are shown. In both cases the rotor pole pitch is maintained at 20 mm, the air-gap length 0.3 mm and the effective ratio of t/λ is 0.67. (In conventional toothed-rotor SRMs the ratio of tooth width, t, to rotor pole pitch, λ, is used because it gives a measure of the magnetic utilisation of the machine. In a segmental rotor machine the concept of tooth width is not so applicable, since the rotor has no teeth. However, the notation t/λ will continue to be used to denote the wider definition of the proportion of the machine air-gap over an excited rotor pole which carries air-gap flux in the aligned position.)

The two designs have identical slot shapes, cross-sectional areas and identical core back depths. The unwound teeth of the single tooth winding design are the same width as each of the teeth of the multi tooth winding design, whilst the wound teeth are double this width. The flux plots for the two machines are very similar, except for the fact that two stator slots and one stator tooth have been removed in the single tooth winding design. As these regions carried no flux, their removal does not significantly influence the level of flux-linkage [122-124].

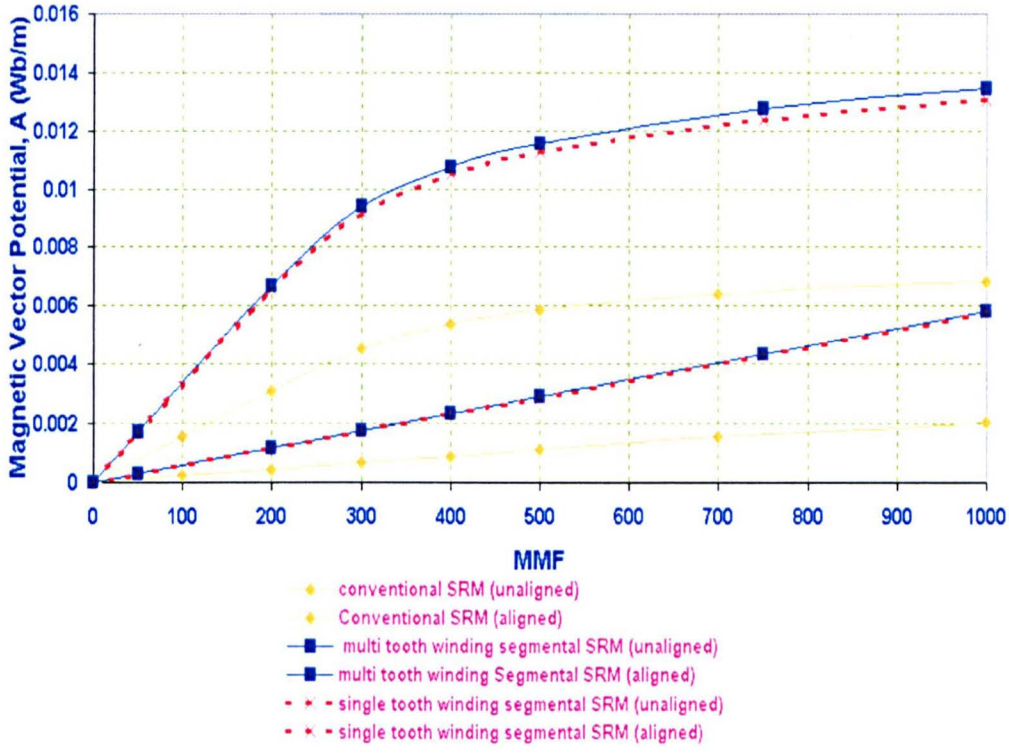

Fig. 4.4 Magnetic Vector Potential of a Phase Coil as a Function of Coil MMF for Both Segmental Designs and a Conventional SRM

Fig. 4.4 shows the flux-linkage curves per unit axial length for the two designs, as might be expected, they are virtually identical. Indeed, in the unaligned position the two permeances are within 1% of each other, whilst in the aligned position the unsaturated permeances are almost identical and the saturated values are within 3%. As the flux-MMF curves are identical, so is the force produced by any one phase. Fig. 4.4 also shows flux-linkage curves for the equivalent conventional SRM with a toothed rotor, indicating how its flux-linkage amounts to only one half of the segmental designs.

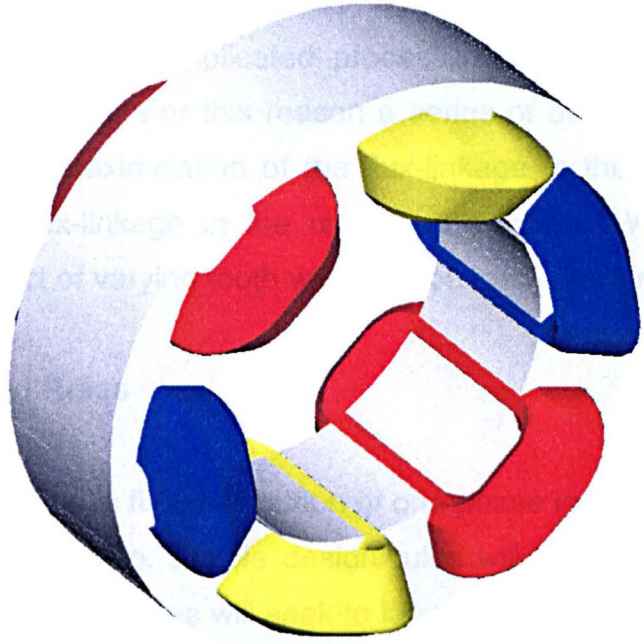

Fig. 4.5 General Machine Arrangement for a 12/10 Three Phase SRM with Single Tooth Windings

The reasoning above seems to suggest that the single tooth winding design has all the advantages of the multi tooth winding design, but with shorter end-windings. However, in reality the comparison is more complicated. The three phase coils of the multi tooth winding design occupy a peripheral length of four rotor segments, whilst the three phase coils of the single tooth winding design occupy five segments because the wound teeth are increased in width. Consequently, in the single tooth winding design the force exerted per unit area of air-gap is reduced to only 80% of the multi tooth winding design when the MMF per phase is fixed. It can now be seen that the single tooth winding design has much shorter end-windings, thereby

permitting an increased phase MMF for a given loss, but utilisation of the magnetic circuit is reduced, so that the force density per unit MMF is reduced by 20% [122-124].

4.3 Design of a 12/10 Segmented Short Pitched 3-Phase SRM

The relationship between the output torque of the new motor and its dimensions, number of poles, number of turns per phase, excitation current, current conduction angles etc. is complex. Optimisation of each parameter in the magnetic circuit of this motor separately is a very complicated process, requiring lots of adaptive finite element models to be built. For this reason a series of design rules are produced, based around intuitive maximisation of the flux-linkage in the aligned position and minimisation of the flux-linkage in the unaligned position. Working within these design rules the impact of varying tooth width will be once more explored.

4.3.1 General Design Rules

Fig. 4.6 shows the magnetic flux distribution of one phase in both the aligned position and in the unaligned position. Simple design rules will be produced with regard to these flux distributions. The rules will seek to keep equal flux density in all flux paths when in the aligned position, as shown by the dimension "W" in Fig 4.6.a. Rules concerning the size of slot openings and segment widths are also generated with regard to the unaligned position of Fig. 4.6.b, making sure that neither the permeance of the stator slot opening or the permeance between rotor segments is unduly large.

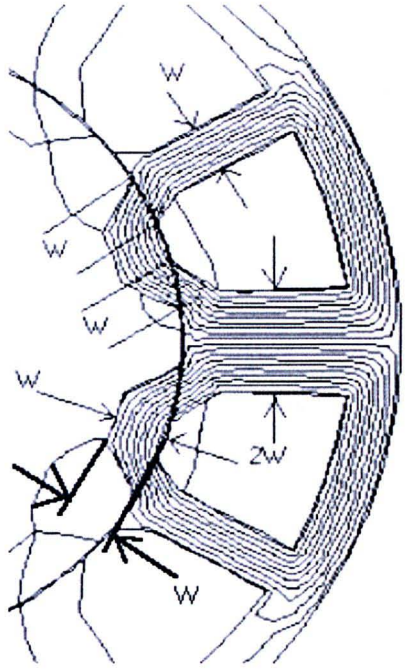

Fig. 4.6.a One Section of the 12/10 SRM (aligned position)

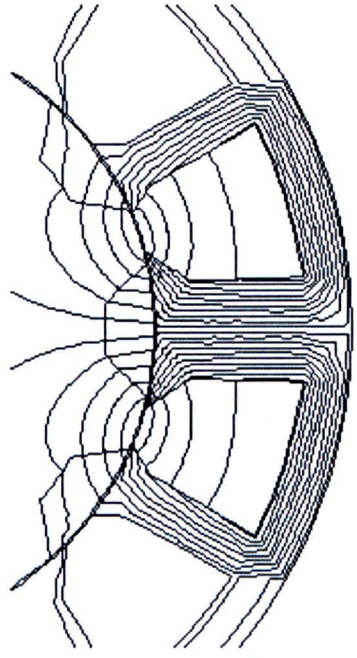

Fig. 4.6.b One Section of the 12/10 SRM (unaligned position)

For clarity a complete set of design rules for the single tooth winding design are given below [122-124].

1. Only one phase winding is contained in any one slot.
2. All coils span a single slot.

3. Only every other slot is wound in order to satisfy rules 1 and 2.
4. The pitch between two adjacent slots carrying the MMF of one phase is equal to the rotor pole pitch so that the slot permeances of each phase all vary in phase with each other.
5. The width of the gap between rotor segments is equal to that of the stator slot openings. This ensures that neither the rotor nor stator contribute unnecessarily to the unaligned permeance.
6. The width of the body of the wound stator teeth is equal to twice the width of overlap between one rotor segment and the tooth tip in the aligned position. This ensures that the flux density in the body of the tooth is equal to that in the tooth tips.
7. The width of the body of the unwound teeth is equal to one half that of the wound teeth, as two unwound teeth carry the return flux of one wound tooth.
8. The radial depth of both the stator core back and the rotor segments is equal to the width of the unwound tooth as they only ever carry the flux of one unwound tooth.

4.3.2 The Impact of Stator Tooth Width

The previous section has described some general design rules. Now the same question arises that appeared when designing the 12/8 segmented-rotor SRM - what is the optimum value of the tooth width?

A series of finite element models were built for different values of the parameter "W" in Fig. 4.6. As with the earlier 12/8 machine the area between the aligned and the unaligned flux-linkage curves can then be used to estimate performance capability and will be compared with that of a conventional SRM [126-127].

As in earlier work the rotor outside diameter will be selected to be 60% of the outside diameter of the stator. The shaft and all the material between the segments will be modelled as having free space permeability.

The rotor pole arc for the example 12/10 machine, which has a 150 mm outside diameter, is given by: $\lambda_r = 2*\pi*0.0454/10=0.0285$ m.

Table 4.1 shows the range of stator tooth widths used for three models of the new 12/10 SRM. The values are selected to correspond to values of t/λ varying from 0.33 to 0.7 [128].

W	0.00475	0.007	0.01
2*W/Rotor Pole Pitch = t/λ	0.33	0.49	0.7

Table 4.1 Tooth Widths of the New Design and the Ratio of t/λ

Figures 4.7, 4.8 and 4.9 illustrate these three models in both the aligned position and the unaligned position.

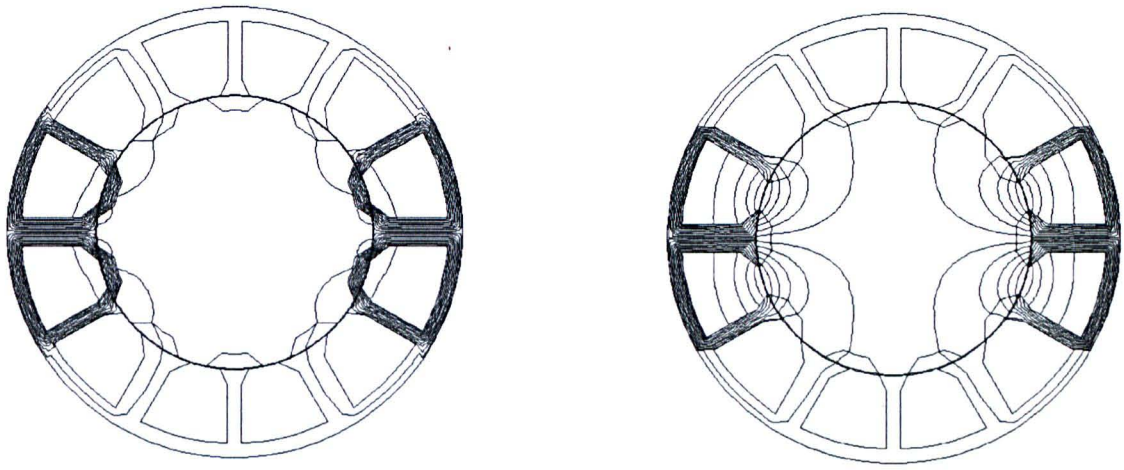

a (aligned position) **b (unaligned position)**

Fig. 4.7 12/10 Segmented-Rotor SRM (Model1: W=0.00475 m, t/λ=0.33)

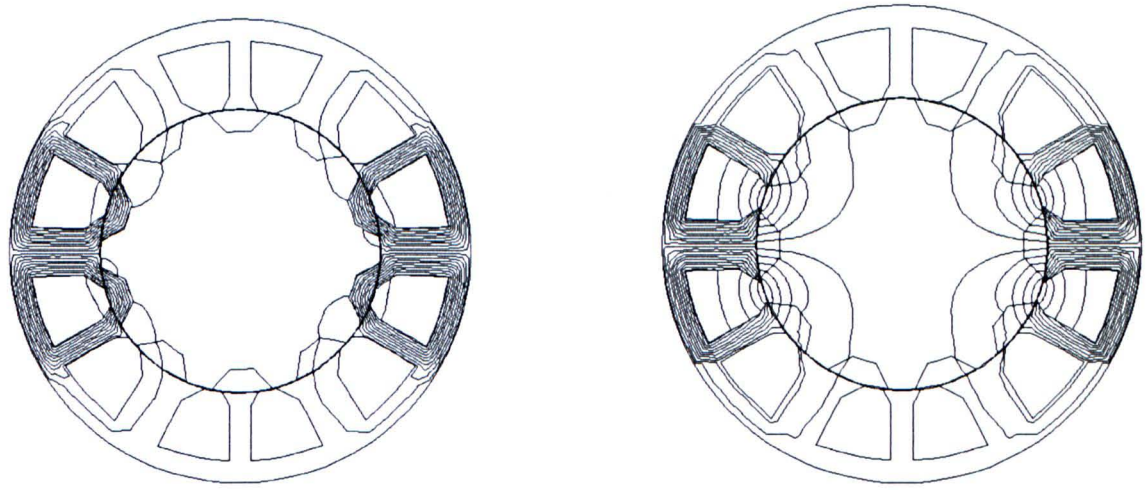

a (aligned position) **b (unaligned position)**

Fig. 4.8 12/10 Segmented-Rotor SRM (Model 2: W=0.007 m, t/λ=0.49)

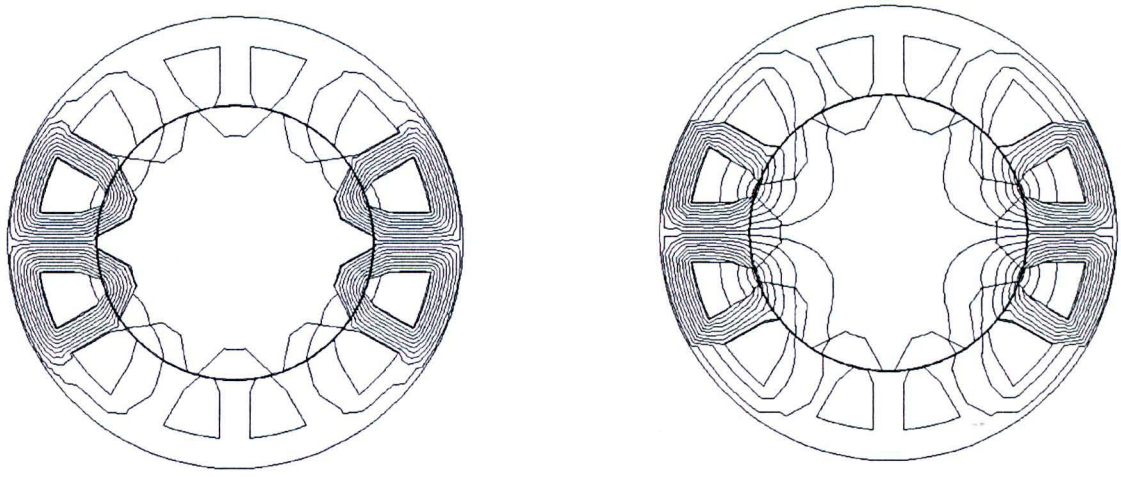

a (aligned position) **b (unaligned position)**

Fig. 4.9 12/10 Segmented-Rotor SRM (Model 3: W=0.01 m, t/λ=0.7)

Fig. 4.10 shows a comparison between the aligned and the unaligned flux-linkage characteristics (per meter of axial length) for the three tooth widths, alongside those of a conventional 12/8 SRM with short pitched windings. Clearly model 1 has teeth which are too narrow, leading to a low aligned flux-linkage and hence a low torque capability. As the teeth are widened, the co-energy per unit MMF increases until it is much greater than that of the conventional 12/8 SRM. It should also be remembered that each phase of the new 12/10 machine traverses this loop 10 times per revolution, whilst each phase of the 12/8 only does so 8 times per revolution. Taking this into account, the new designs of models 2 and 3 (in which $t/\lambda=0.49$ and $t/\lambda=0.7$) both give more torque than the conventional SRM.

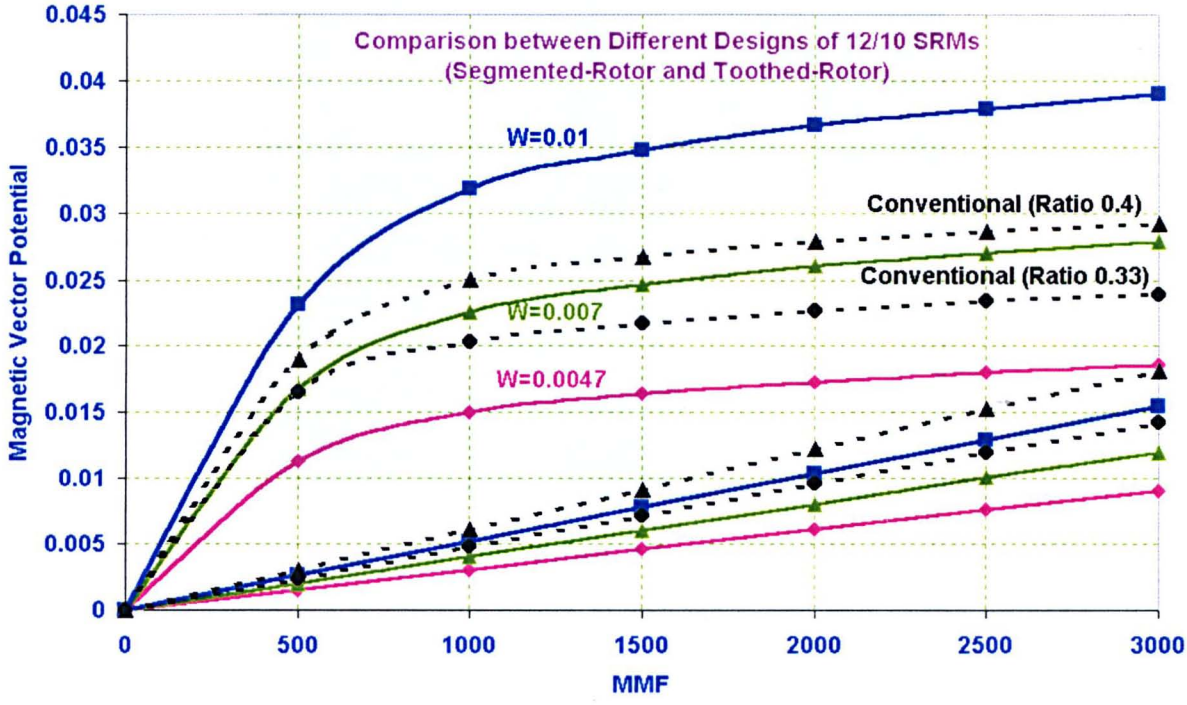

Fig. 4.10 Comparison between the Different Models of the New Design of 12/10 and the Conventional One

New Short Pitch Segmented Rotor 12/10 SRM			
Model Number	1	2	3
W	0.0047	0.007	0.01
Slot Area(mm^2)	548	392	257
Area between the aligned and the unaligned positions Unit Co-energy MMF = 3000	28.9	48.4	69.5

Table 4.2

Conventional Short Pitch 12/8 SRM		
Model Number	1	2
θ_1/λ	0.33	0.4
Slot Area(mm^2)	430	344
Area between the aligned and the unaligned positions Unit Co-energy MMF = 3000	42.1	50.3

Table 4.3

Table 4.2 and Table 4.3 show the areas of the slots and the areas enclosed by the aligned and the unaligned positions for the models of the new design and the conventional design in order to assess the new design.

The above comparison is based upon a fixed MMF per phase, but takes no account of the varying slot area. In order to give a more valid evaluation, comparisons based on fixed current density and fixed losses will be used in a similar manner to that of chapter (3).

4.4 Comparison between the New SRM and the Conventional for Fixed Current Density and Fixed Losses

4.4.1 Comparison Based on Fixed Current Density for each case

Assume the current density $J_{rms} = 10A/mm^2$

Assume the fill factor =0.4

Assume two coils per phase.

New 12/10 short pitch 12/10 SRM.

Model1

$$MMF1 = \sqrt{3} * 10 * 2 * 548 * 0.4 = 7593.3$$

Model2

$$MMF2 = \sqrt{3} * 10 * 2 * 392 * 0.4 = 5431.71$$

Model3

$$MMF3 = \sqrt{3} * 10 * 2 * 257 * 0.4 = 3561$$

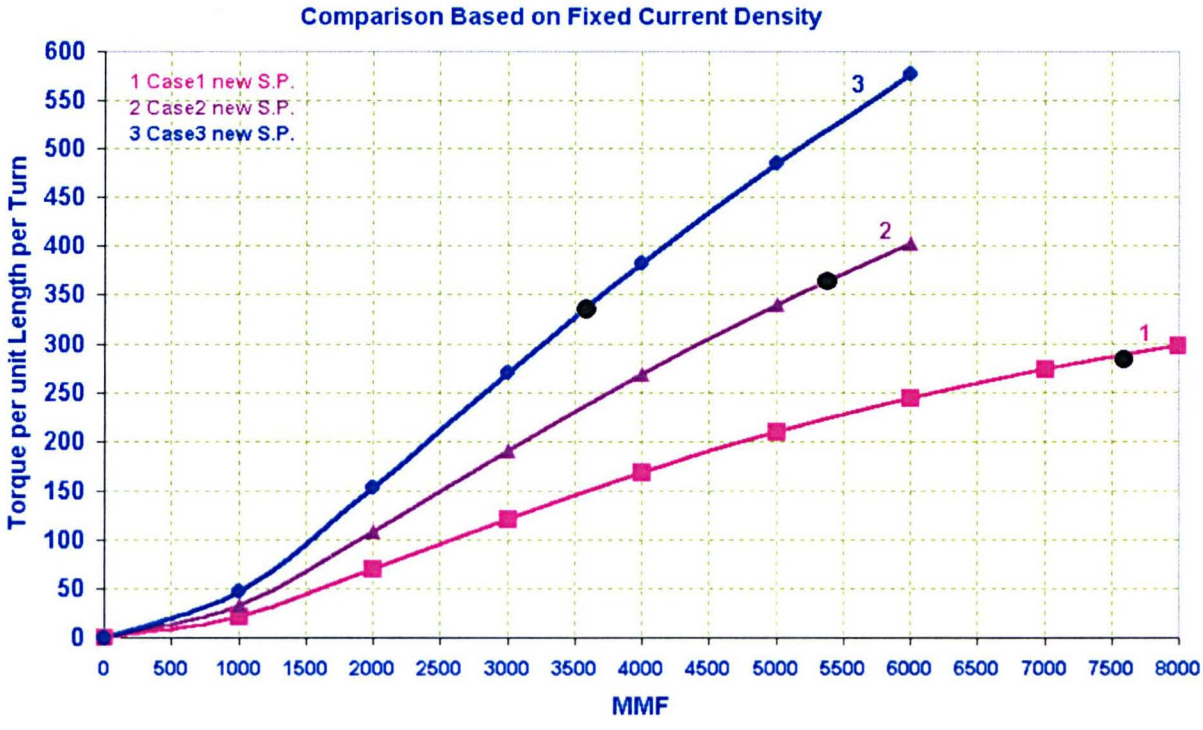

a

4.4.2 Comparison based on Fixed Loss

$$\text{Copper Losses} = J^2 * \rho * \text{copper volume} = \text{Constant}_1.$$

For constant loss $J^2 * \text{copper volume} = \text{Constant}_2$.

$$J^2 * \text{Slot Area} = \text{Constant}$$

$$J \alpha \sqrt{\frac{1}{\text{slot area}}}$$

Calculation of the Current Density:

$$J_1 \alpha \sqrt{\frac{1}{10^{-3} * 0.548}} \alpha \quad 42.71$$

$$J_2 \alpha \sqrt{\frac{1}{10^{-3} * 0.392}} \alpha \quad 50.5$$

$$J_3 \alpha \sqrt{\frac{1}{10^{-3} * 0.257}} \alpha \quad 62.37$$

Taking the conventional machine with t/λ = 0.33 as a reference and using a peak MMF of 3500 AT it is now possible to determine the MMF in the other machines for the same loss, as follows: -

$$MMF_5 \alpha J_5 A_5 \quad \& \quad MMF_1 \alpha J_1 A_1$$

So $$\frac{MMF_5}{MMF_1} = \frac{J_5 A_5}{J_1 A_1}$$

$$MMF_1 = \frac{3500 * 42.71 * 548}{48.22 * 430} = 3950.77$$

MMF(s) for the new fully pitched 12/8 Models

Model 1 3951

Model 2 3342

Model 3 2706

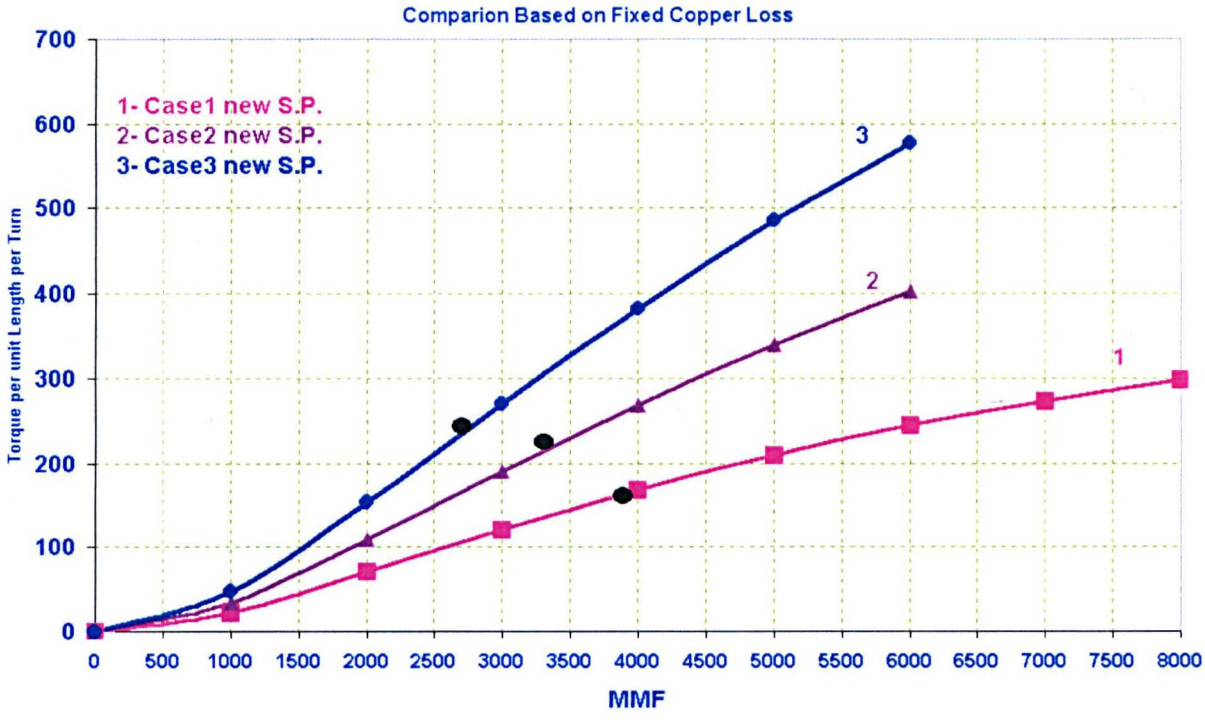
Comparion Based on Fixed Copper Loss
1- Case1 new S.P.
2- Case2 new S.P.
3- Case3 new S.P.
Torque per unit Length per Turn
MMF
0
100
200
300
400
500
600
700
0 500 1000 1500 2000 2500 3000 3500 4000 4500 5000 5500 6000 6500 7000 7500 8000
1
2
3

b

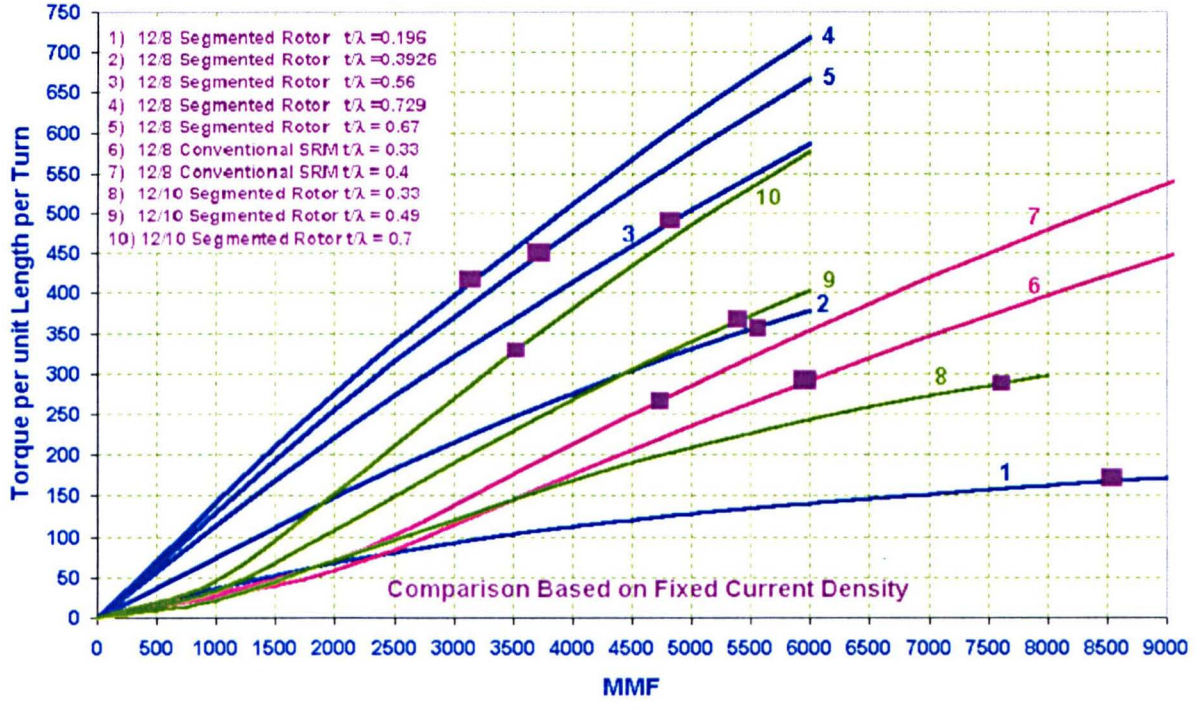
1) 12/8 Segmented Rotor t/λ =0.196
2) 12/8 Segmented Rotor t/λ =0.3926
3) 12/8 Segmented Rotor t/λ =0.56
4) 12/8 Segmented Rotor t/λ =0.729
5) 12/8 Segmented Rotor t/λ = 0.67
6) 12/8 Conventional SRM t/λ = 0.33
7) 12/8 Conventional SRM t/λ = 0.4
8) 12/10 Segmented Rotor t/λ = 0.33
9) 12/10 Segmented Rotor t/λ = 0.49
10) 12/10 Segmented Rotor t/λ = 0.7
Comparison Based on Fixed Current Density
Torque per unit Length per Turn
MMF
0
50
100
150
200
250
300
350
400
450
500
550
600
650
700
750
0 500 1000 1500 2000 2500 3000 3500 4000 4500 5000 5500 6000 6500 7000 7500 8000 8500 9000
1
2
3
4
5
6
7
8
9
10

c

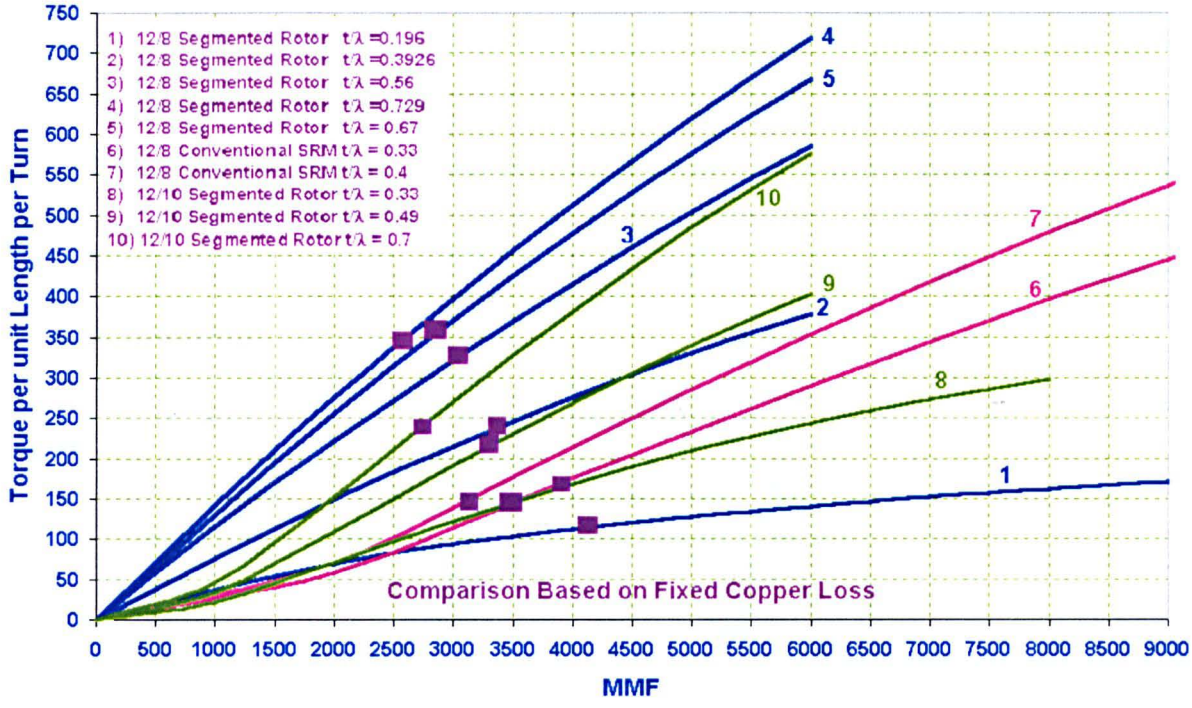

d

Fig. 4.11 Comparison between all the Models of the New SRMs and the Conventional SRM

Fig. 4.11 shows the torque per unit axial length for each tooth width as a function of slot MMF. In Fig. 4.11 black dots are placed on each curve to represent the MMF equivalent to a winding r.m.s. current density of 10 A/mm^2. The large slot area of Model 1 gives a high MMF, but still gives a low torque because of the low flux-linkage. Model 2 gives a marginally greater torque than Model 3, the lower torque per unit MMF is compensated for by its increased MMF capability. Fig. 4.11.b has black dots to represent points of equal total windings loss. In this case Model 3 has the higher value of the torque per unit length per turn (Appendix 2).

Fig 4.11 (c) and (d) give a comparison with both a conventional 12/8 SRM and the fully pitched windings design of chapter (3). The 12/10 segmental design appears to perform much better than the conventional SRM, but is worse than the 12/8 segmental design with fully pitched windings. However, the comparison continues to take no account of endwindings effects: in the fully pitched windings design this will substantially reduce performance, with the impact depending upon the axial length of the laminations.

4.5 Detailed Characteristics of the chosen12/10 SRM

Fig. 4.12 shows the final design of the 12/10 machine, with t/λ = 0.7. The rotor segments are retained onto the shaft in the same manner as earlier and the rotor "dove tails" are also illustrated. As in the 12/8 segmental design these features are chosen to minimise any impact upon the magnetic performance whilst still ensuring adequate retention.

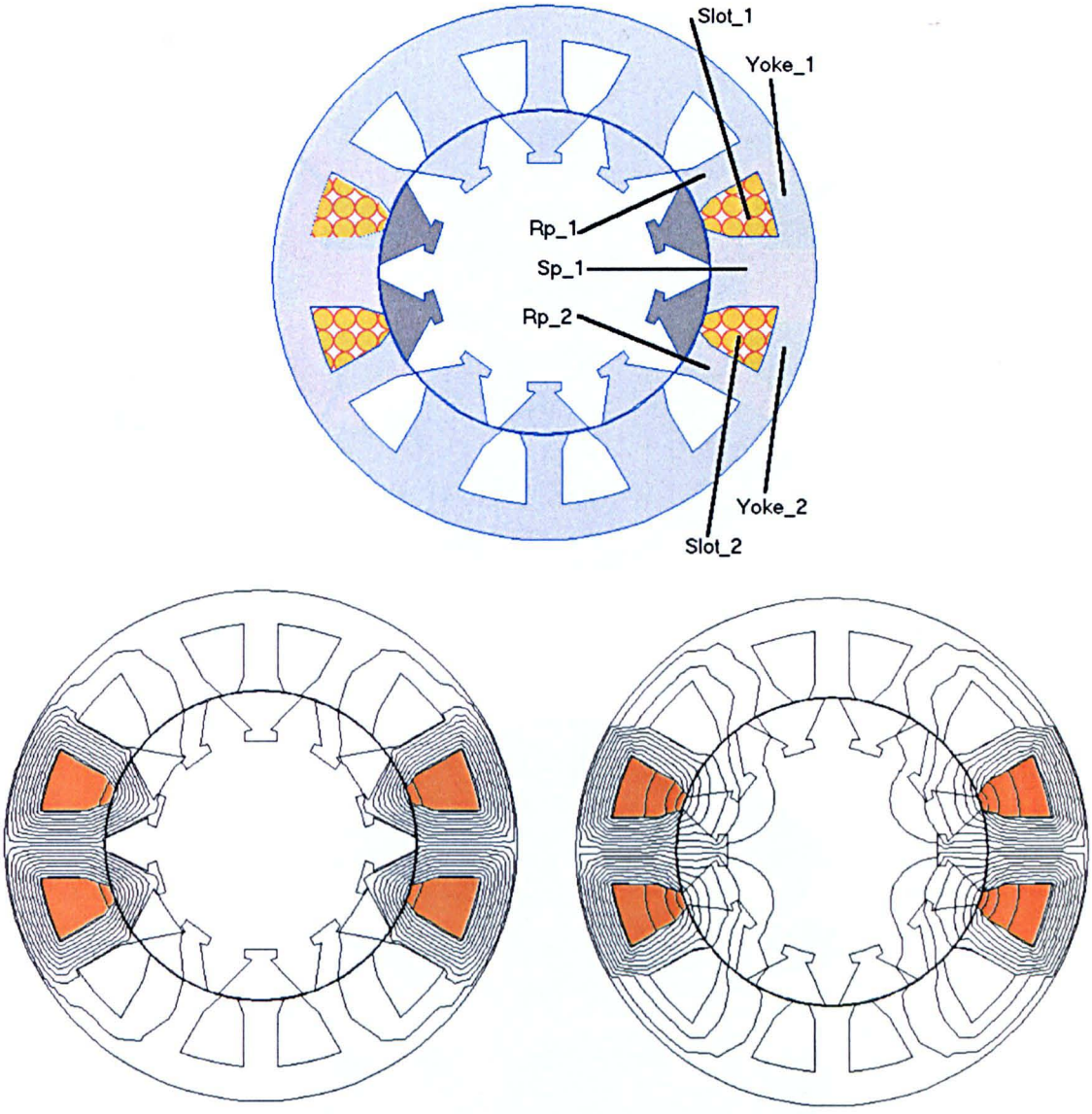

a-aligned position **b-unaligned position**

Fig. 4.12 Magnetic Flux Plot of the Chosen 12/10 SRM (one phase excited)

Fig. 4.13.a and Fig. 4.13.b shows shading plots indicating first the magnetic flux density and then the regions of magnetic saturation. In all cases a single phase is

excited in isolation: red shows areas of high flux density (or saturation) and blue indicates areas of low flux density (or saturation). In the aligned position similar flux densities occur throughout the magnetic flux plot, though the saturation plot shows how greatest values (and therefore the greatest points of saturation) actually occur in the stator tooth tips and in the rotor segment. In the unaligned position there are relatively low flux densities throughout [129-143]. The MMF/Slot for the figures shown =3000.

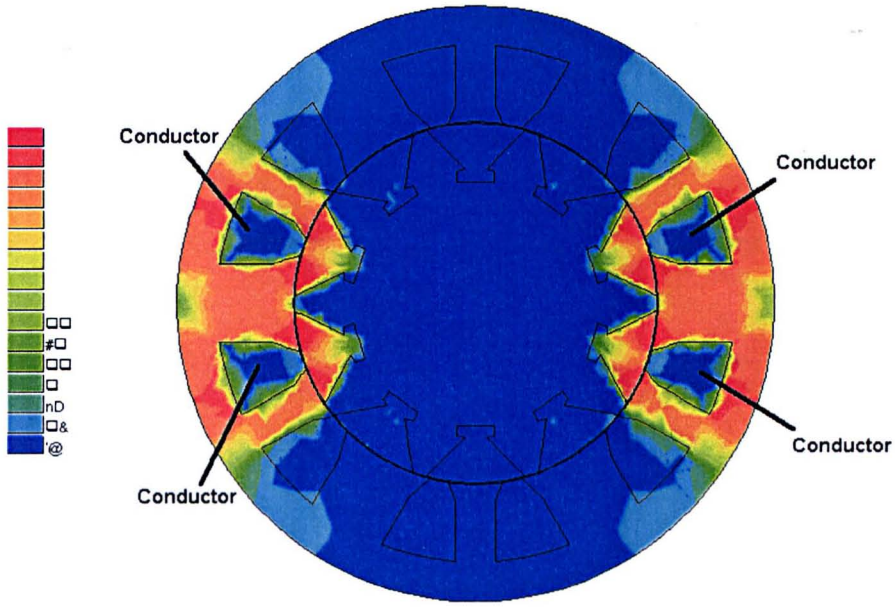

Fig. 4.13.a Flux Density in the Aligned Position of the Designed 12/10 Segmented-Rotor SRM (Model 3)

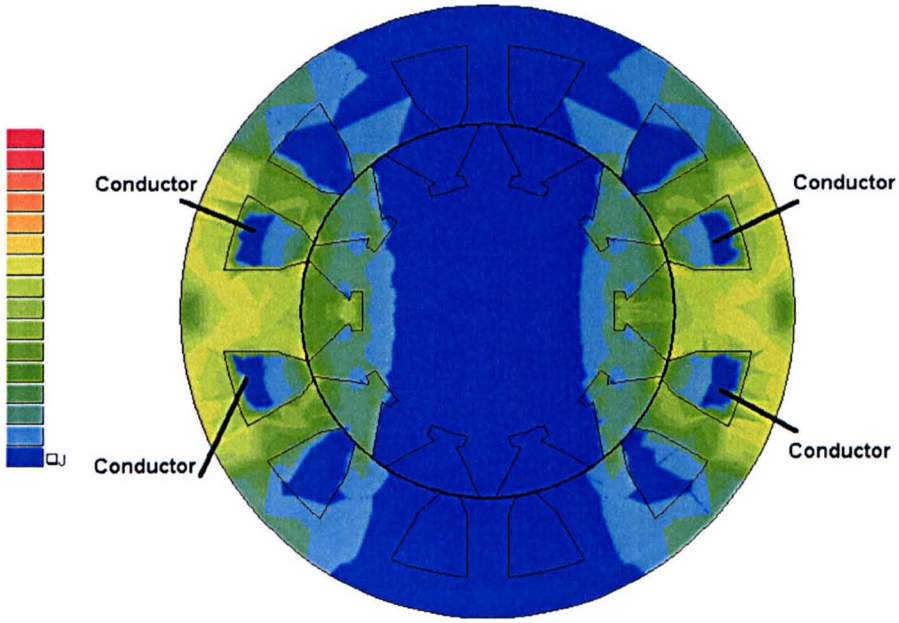

Fig. 4.13.b Flux Density in the Unaligned Position of the Designed 12/10 Segmented-Rotor SRM (Model 3)

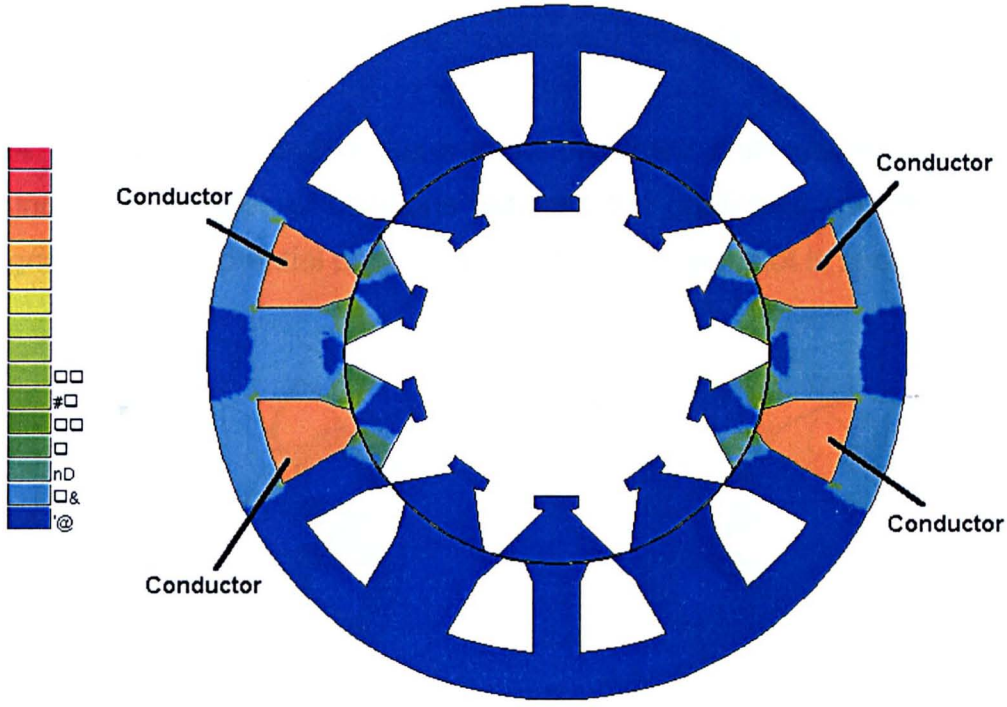

Fig. 4.13.c Saturation in the aligned position 12/10 Short Pitched (Model 3)

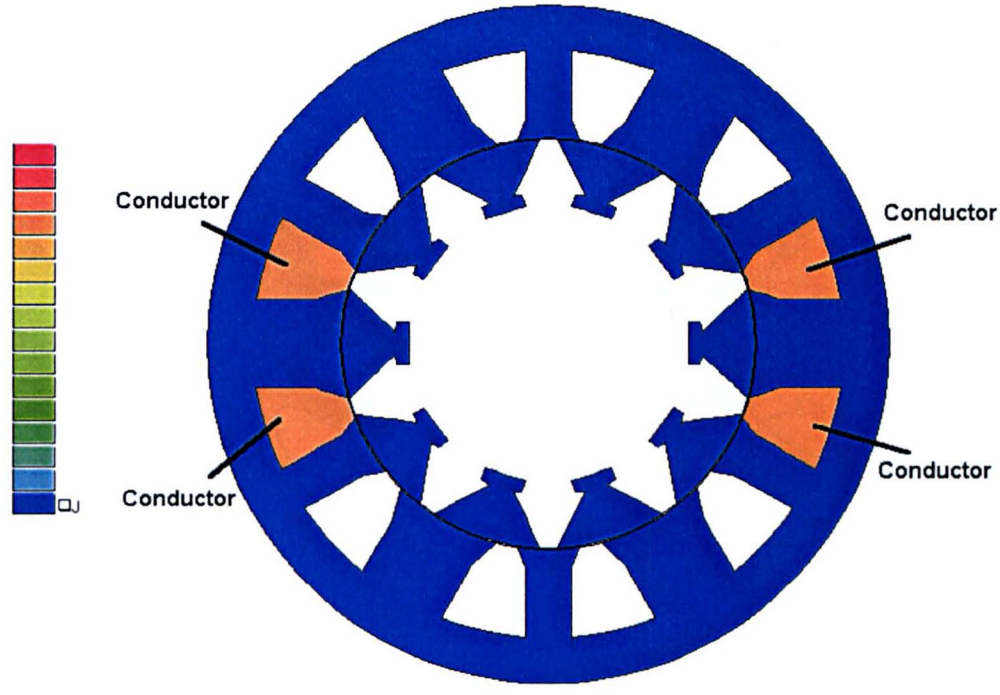

Fig. 4.13.d Saturation in the unaligned position 12/10 Short Pitched (Model 3)

4.6 The Predicted Characteristics of the New Optimised Short Pitched 12/10 Segmented-Rotor SRM (adaptive finite element model)

Fig. 4.14 shows the predicted flux-linkage predicted characteristics of the 12/10 design, including a series of positions between the unaligned and aligned position. The magnetic vector potential per coil versus the MMF per slot is shown.

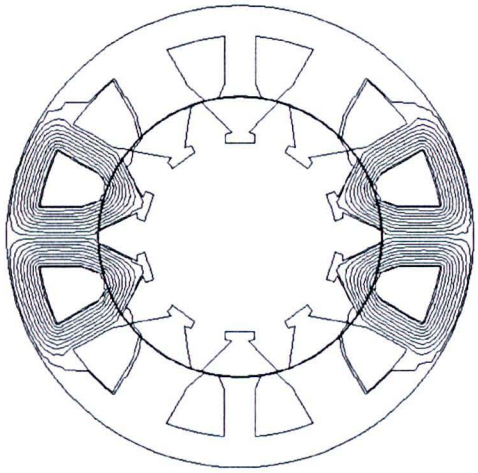

Zero

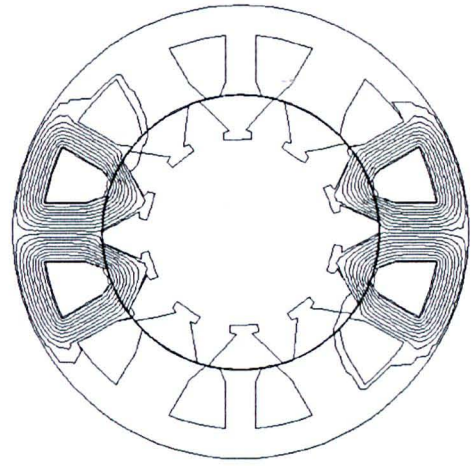

2

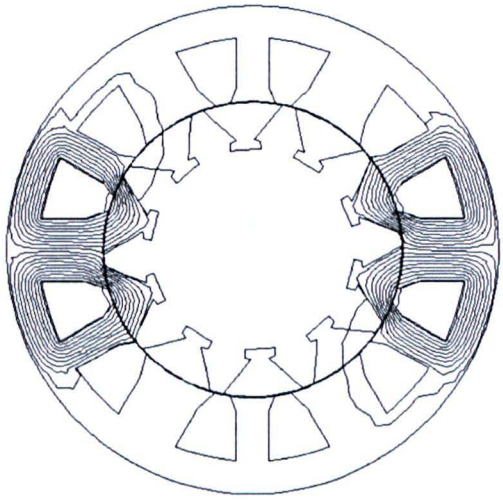

4

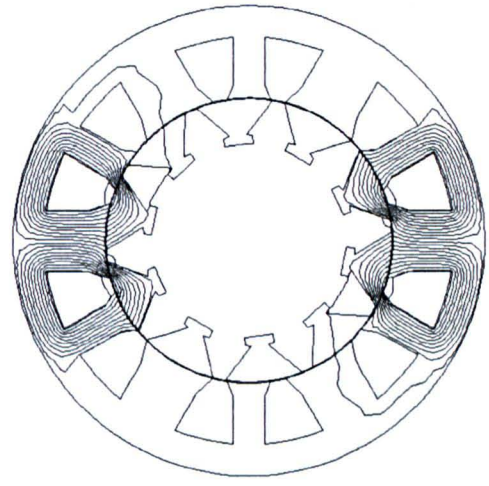

6

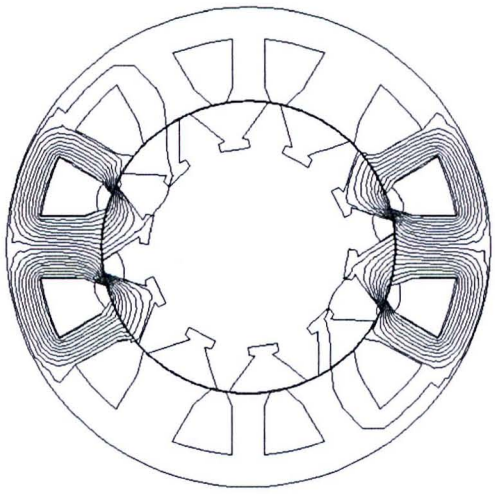

8

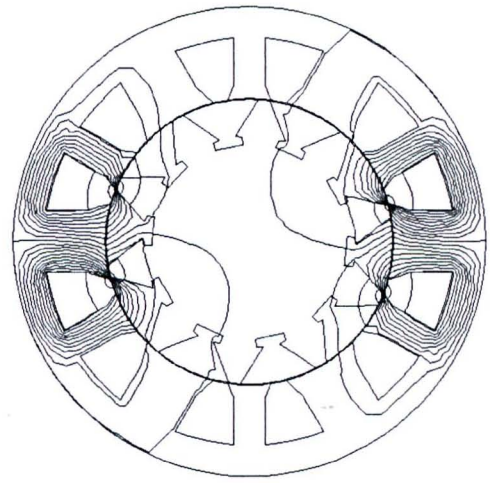

10

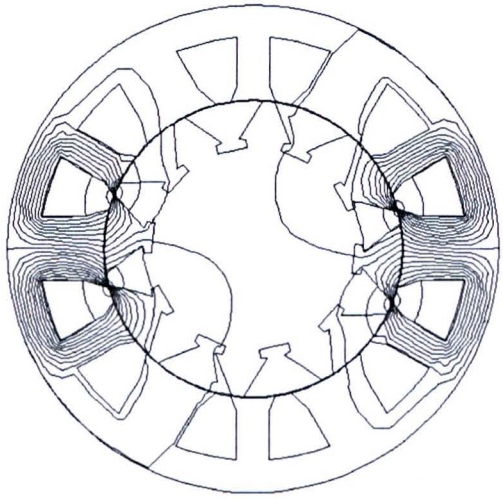

12

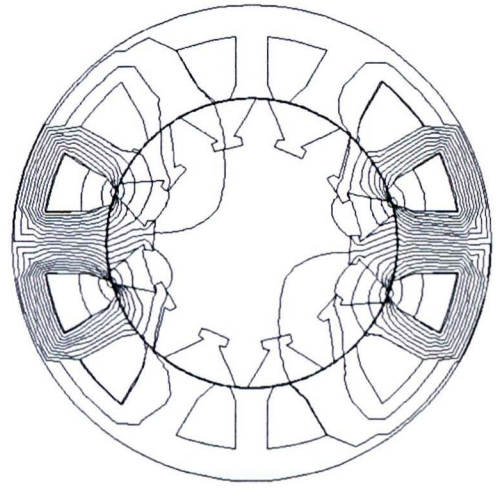

14

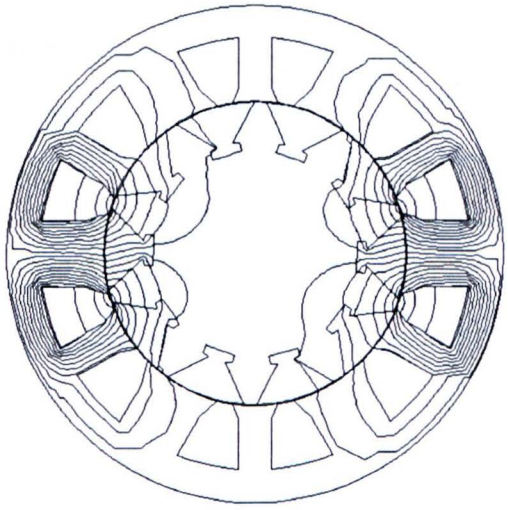

16

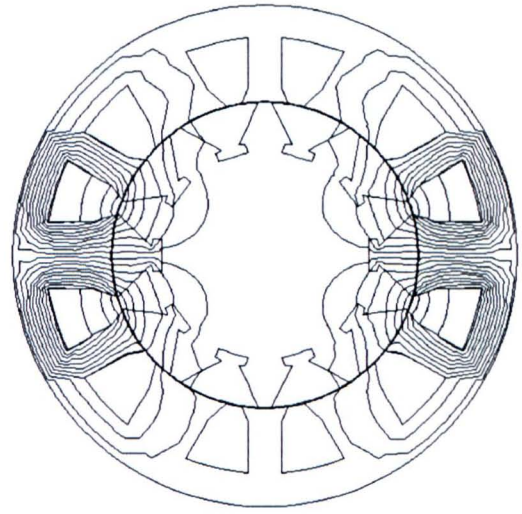

18

Magnetic Flux Plot for Different Position for the 12/10 Short Pitched SRM

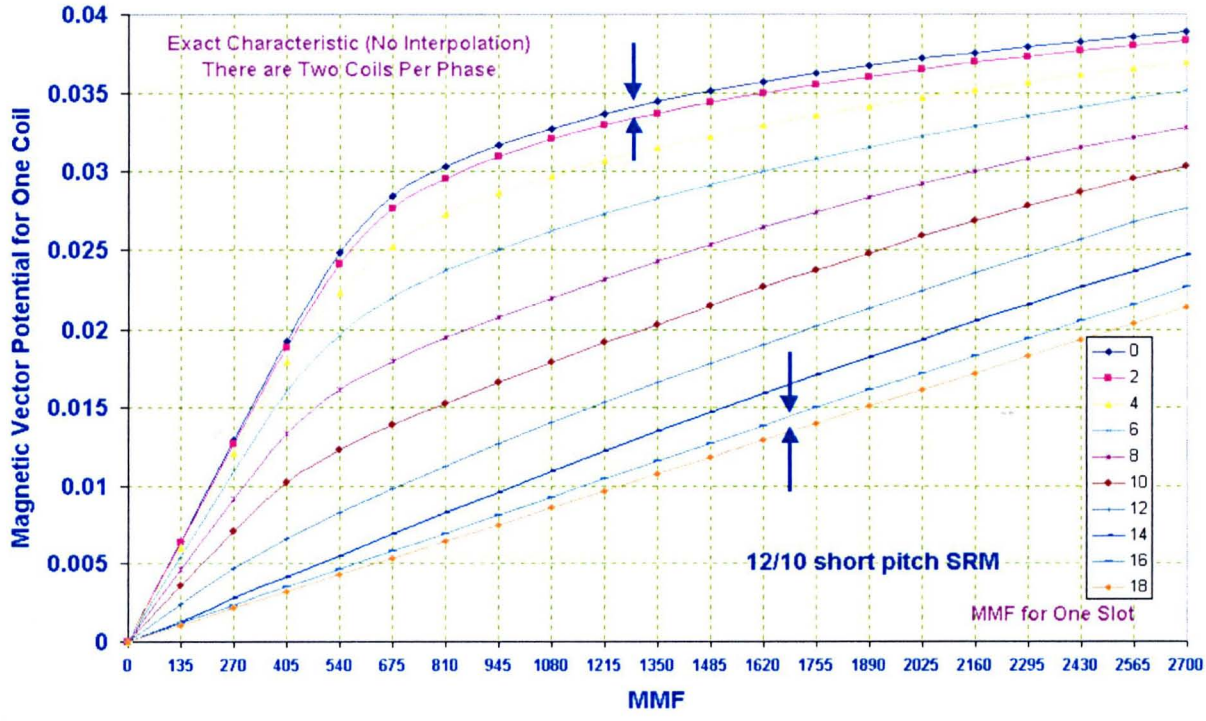

Fig. 4.14 New 12/10 SRM Characteristic

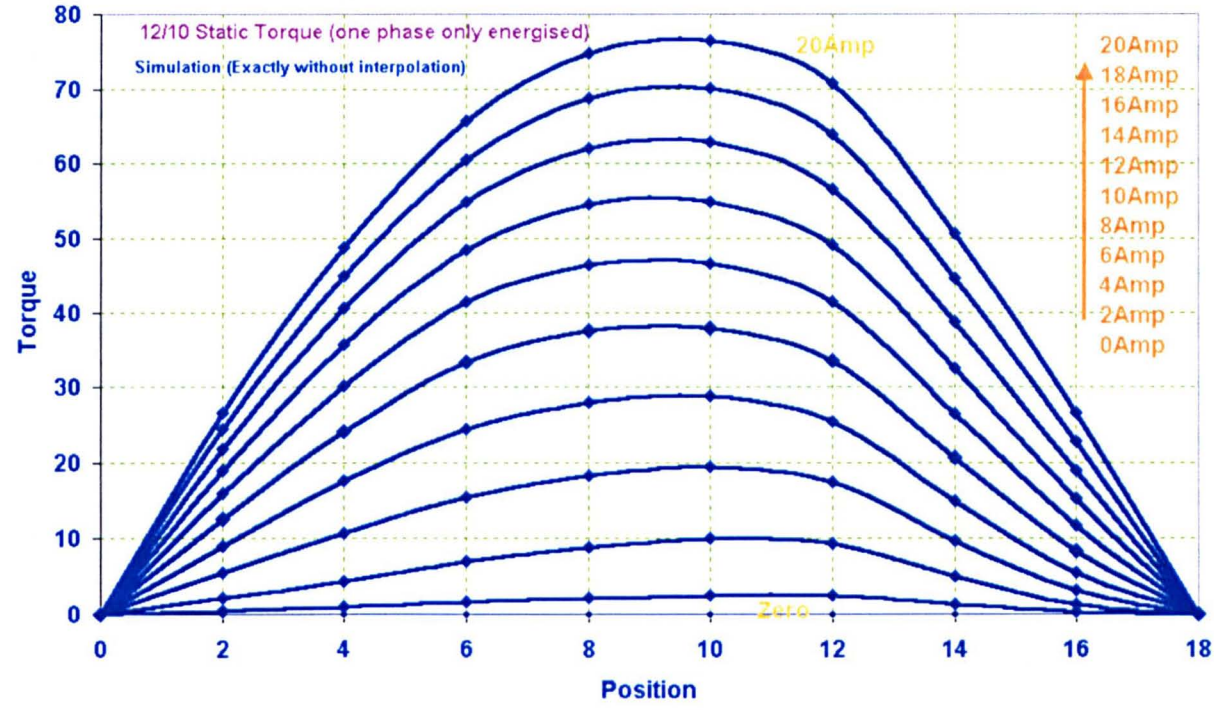

Fig. 4.15 The Predicted Static Torque Characteristic

Fig. 4.15 shows the predicted static torque characteristic based on the magnetic vector potential in Fig. 4.14. This figure uses 270 turns per coil.

4.7 Orientation of Magnetisation

There is the freedom to choose the magnetic orientation of each coil, and the effect of this can be understood by initially considering excitation of a single phase. Each phase is constructed from two coils, positioned at opposite sides of the machine. The magnetic flux plots of Fig. 4.12 show that there is minimal coupling between the individual coils of a phase. Consequently the magnetic characteristics of any one phase are independent of the polarity of the two coils: both may have an MMF directed radially inwards, both outwards, or one in each direction without having a measurable effect upon the phase parameters [144].

Consider now the situation when two phases are simultaneously excited. There are two mechanisms by which the two phases can interact; either due to mutual magnetic coupling or due to cross saturation of their common magnetic flux paths. The mutual inductance between phases is minimal, leaving only the cross saturation effect. In conventional SRMs the rotor and stator core backs carry the flux of all phases: to prevent cross saturation when multiple phases are excited it is often necessary for the core back to be deeper than that magnetically required by one phase acting alone. In the segmental machine the situation is somewhat different. Each portion of stator core back and each wound tooth carries only the flux of one phase and therefore can be sized accordingly. Only the unwound teeth, forming the flux return path, contain the flux of two phases. If the phase coil MMFs all act inwardly then the return fluxes of two excited phases are both outward and the flux in the unwound tooth will be the sum of the two phase fluxes. The teeth have been dimensioned to only take the flux of a single phase, and hence there is the possibility of cross-saturation between phases reducing the torque. This is most likely to occur when the machine is operating under voltage control and positive voltage is applied for more than one third of a cycle. Under all other operating conditions the cross-saturation effect will be negligible.

The above effect can be removed completely if the MMFs of adjacent stator coils are directed in the opposite direction i.e. inwards, outwards, inwards, outwards etc. When this occurs the unwound teeth carry the difference between the flux of adjacent coils, and hence simultaneous excitation of two phases will actually reduce the saturation conditions in this region. Note that with this arrangement the unwound teeth carry bi-directional flux. In addition to having a minor influence upon the torque

capability of the machine, the direction of the stator coil MMFs influences the iron loss in the machine. This is covered in more detail in a later chapter.

4.8 Conclusion

This chapter has introduced a new machine design which seeks to overcome the problem of high end-windings copper losses, encountered in the first design of a segmented-rotor SRM. The new design has short pitched windings placed around a single tooth, with only every other tooth having a winding. The reasoning behind the design was first explained and then a series of design rules generated and used as a basis for creating a design with a 150 mm outside diameter. The impact of tooth width was then investigated and it was shown that optimum performance can be produced when t/λ is greater than 0.5. A design with $t/\lambda=0.7$ was then developed and flux/MMF characteristics calculated for a series of rotor positions.

5 Comparison between the New Segmental Machines and Conventional SRMs

5.1 Introduction

In Chapters 3&4 two different concepts of the new segmented-rotor SRM were developed. These machines were compared with two designs of a conventional SRM, using criteria of equal winding loss in the slots or equal current density to represent different thermal situations. The comparisons made were rather simplistic, neglecting many important effects, such as end-windings loss and torque ripple. In this chapter a more detailed comparison is made, in which models for all the machines are refined.

5.2 Basis of Comparison

Three machines are compared: the conventional design and the two segmental designs. All three machines will have the same outside diameter (150 mm) and lamination stack length (150 mm). It will also be assumed that the slot fill factor is kept at constant value equal 0.46 for all three machines. Experience has shown that this is the upper bound of what can be achieved in practice. End-winding length will be estimated for each machine and incorporated into the models.

Each design will be developed on the basis of an equal number of turns (150 per slot). The machines will be evaluated principally in terms of their torque capability for a fixed winding loss of 300W. This loss is of the order of magnitude that can be sustained by machines of this size without exceeding their steady state thermal limit.

By modelling the Flux-Linkage characteristics at a series of rotor positions the static torque profiles will also be estimated. These will be used as a basis for estimating torque ripple when operating under current control.

5.3 Characteristics of the Conventional 12/8 SRM

The two conventional SRM models used in earlier chapters corresponded to different values of the tooth width to pole pitch (t/λ). In this chapter the comparison focuses

upon the design with $t/\lambda=0.33$, as this design gave the highest average torque capability of the two designs. The design had a core back width of one half the tooth width, as it was considered that such a design should give the maximum magnetic capability. However, such a narrow core back depth would not generally be chosen for drive applications because the mechanical stiffness of the core is very low. This results in high levels of acoustic noise, which is a generally known disadvantage of SRMs. For this reason the core back depth of the design used in this chapter is increased to 85% of the tooth width. The increased core back depth reduces the slot area; hence the winding volume and MMF capability are also reduced [145]. Dimensions of the machine modelled are given in Table 5.1.

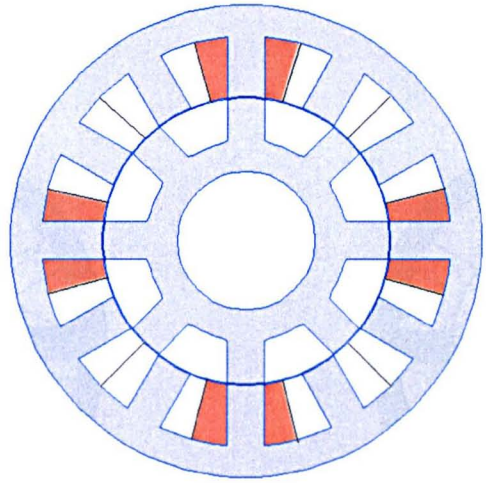

Fig. 5.1 12/8 Conventional SRM (wide core-backs)

Stator Outside Diameter	150 mm
Shaft Diameter	43.64 mm
Rotor Diameter	90.8 mm
Air Gap Length	0.3 mm
Stator Core-Back	10 mm
Rotor Core Back	10 mm
Stator Tooth Width	11.76 mm
Rotor Tooth Width	11.76 mm

Table 5.1: Dimensions of Wide Core-Back Conventional SRM

Using 2D finite elements the machine was modelled at 10 discrete rotor angles, ranging from the aligned to unaligned positions. Fig. 5.2 shows example magnetic flux distributions for each of these angles.

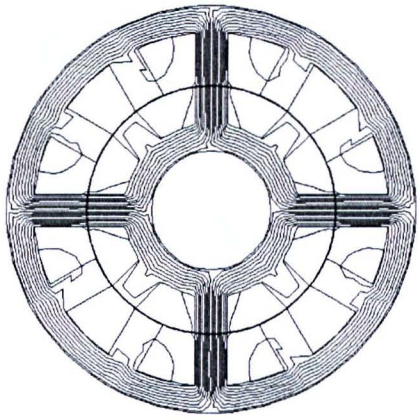

Zero

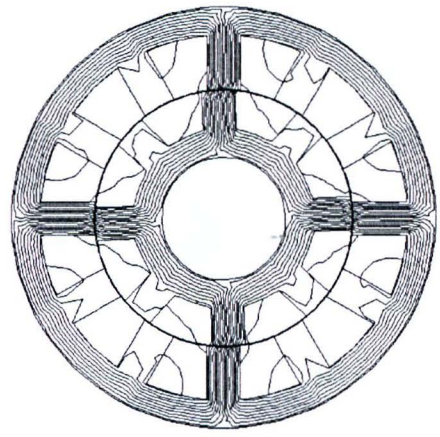

2.5

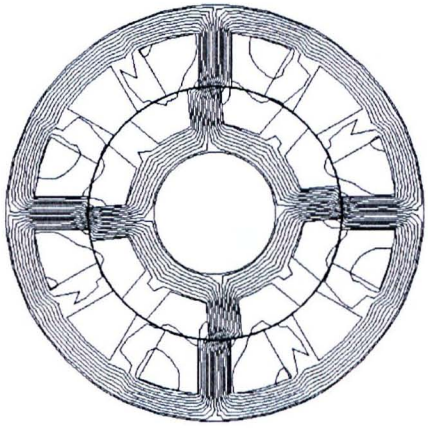

5

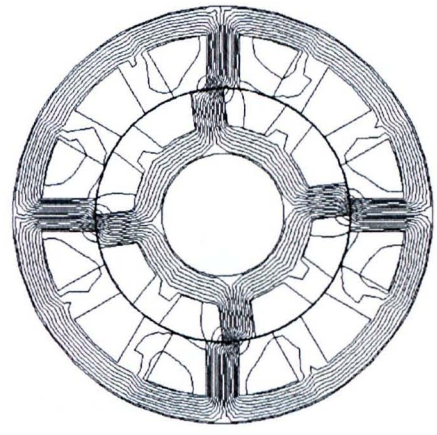

7.5

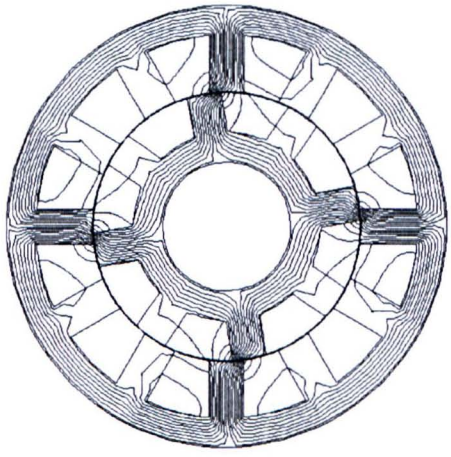

10

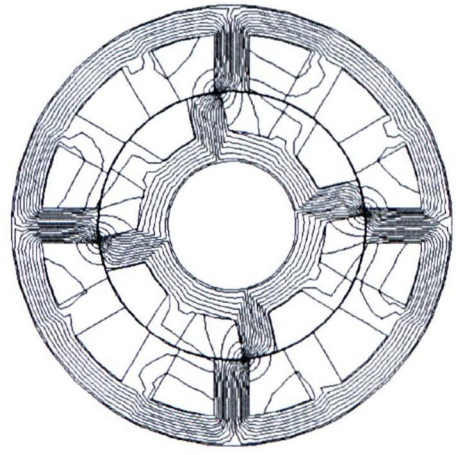

12.5

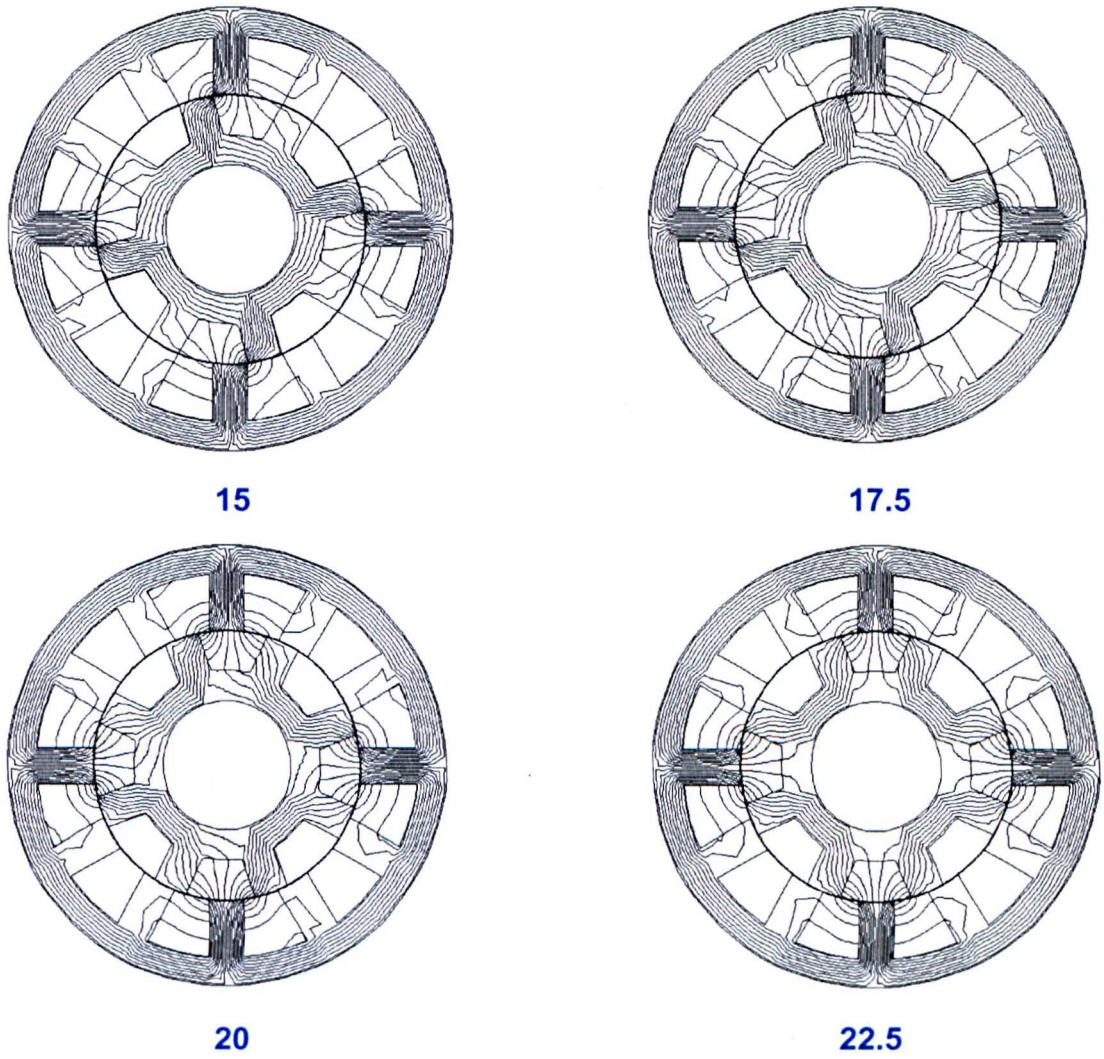

Fig. 5.2 Conventional SRM Models for a Range of Rotor Positions

Fig. 5.3 shows the Flux-Linkage characteristic resulting from the above models. The vertical axis represents the flux-linkage per phase, whilst the horizontal axis represents the current per slot [146-147]. Each slot is assumed to contain 150 conductors.

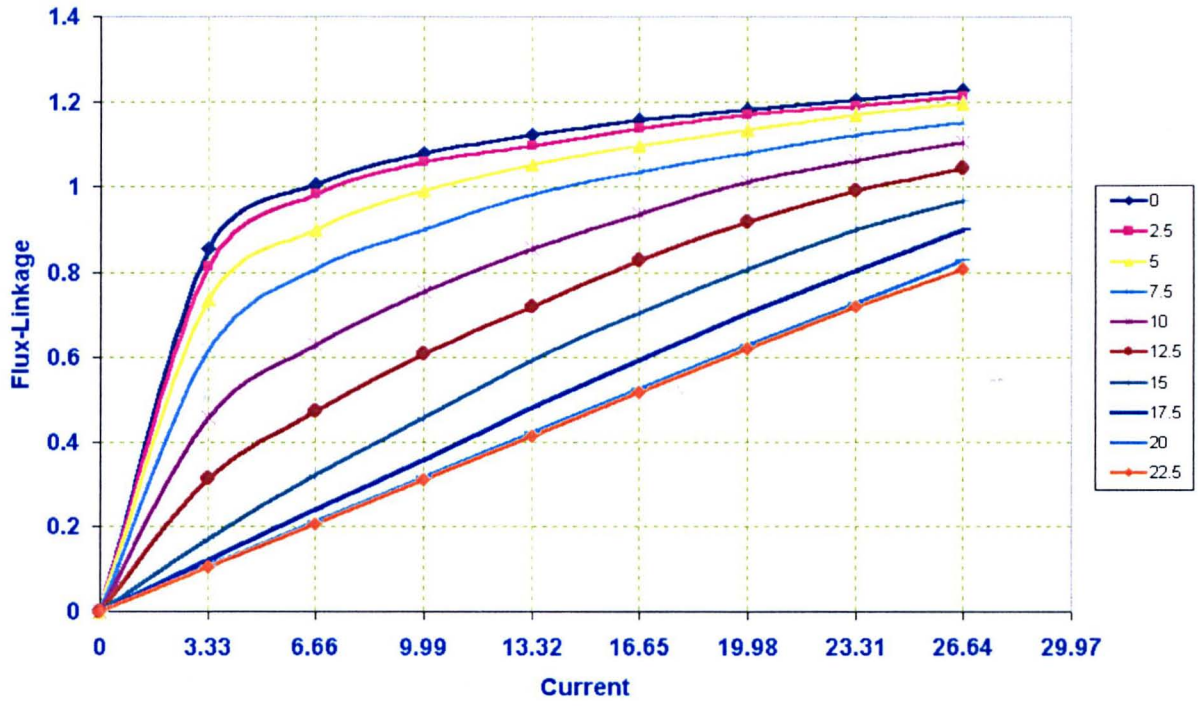

Fig. 5.3 Flux-Linkage Characteristic versus the Current for the Wide Core-Backs Conventional SRM

For completeness, Fig. 5.4 shows a comparison between the current design of SRM, with its wide core-back and the earlier model employing a narrow core-back. The increased core back depth has resulted in increased flux-linkage at high excitation levels in the aligned position, so the machine is capable of more torque per unit MMF. Note: however, that the stator slot area is decreased by $\frac{430-332.43}{430}$=22.69%, resulting in a lower MMF capability.

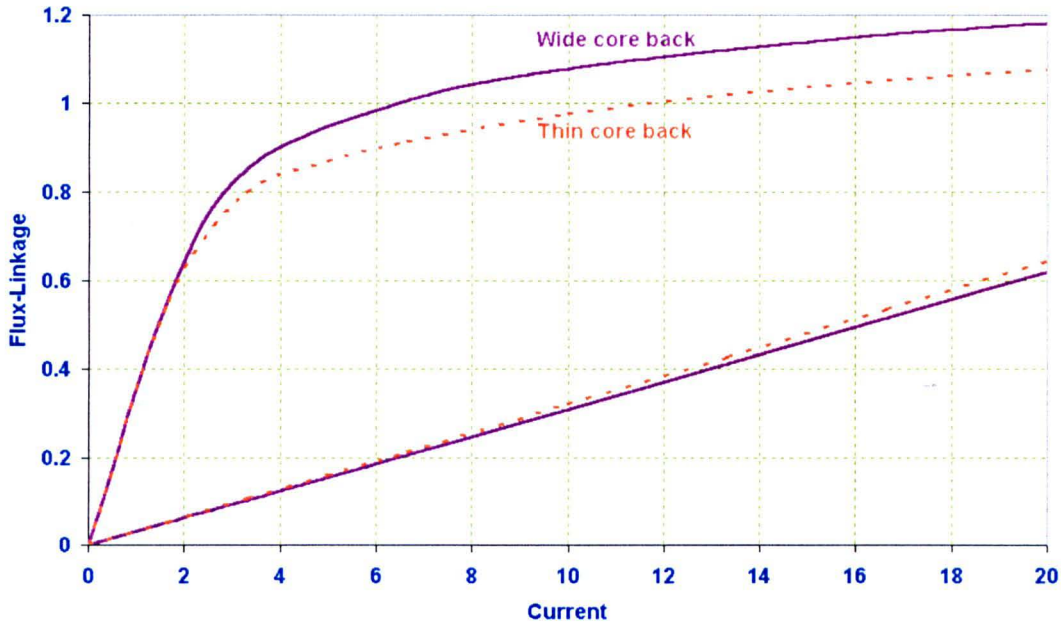

Fig. 5.4 Comparison between the Wide Core Back and the Thin Core Back SRMs

The static torque characteristics for this machine can be derived from the Flux-Linkage characteristic of Fig. 5.3 by determining the instantaneous variation of co-energy and differentiating this with respect to position.

Static torque characteristics, derived for this machine in the above way, are shown below.

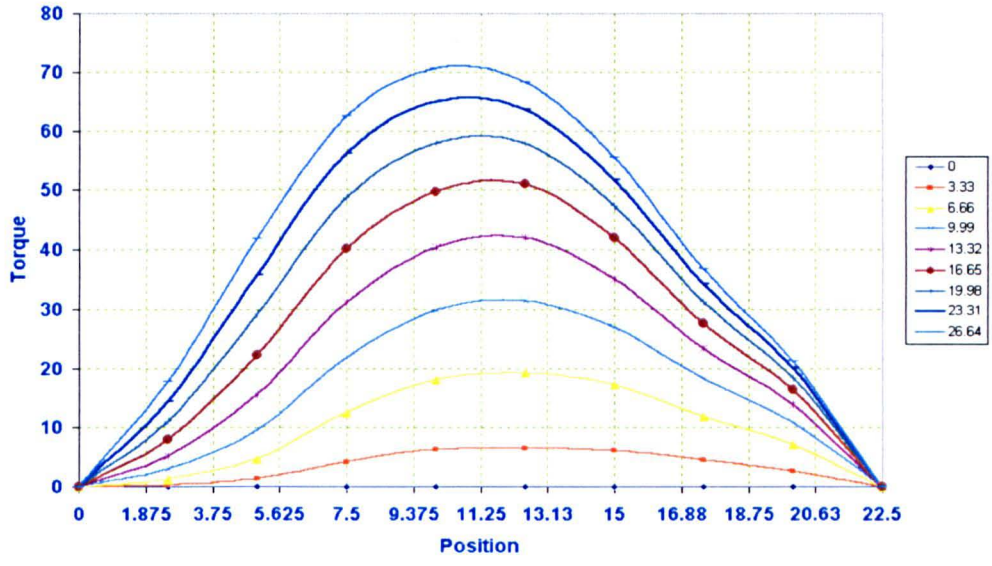

Fig. 5.5 Predicted Static Torque Characteristic for the 12/8 Conventional SRM

5.4 Characteristics of the Segmented-Rotor 12/8 SRM

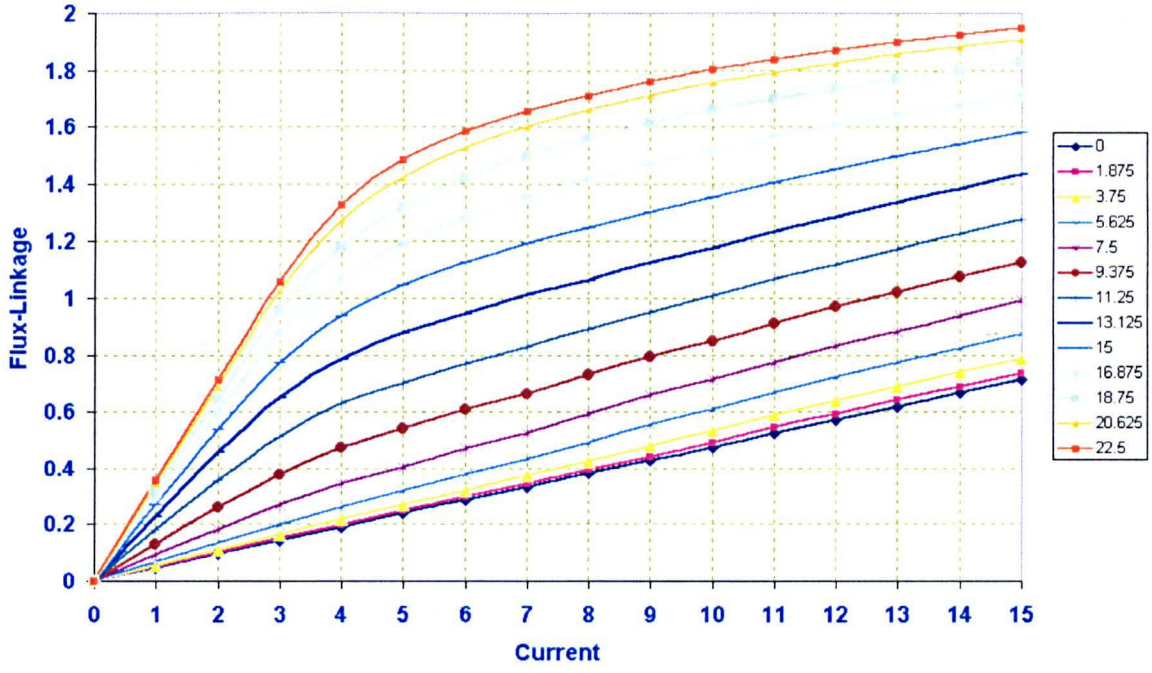

Fig. 5.6 Flux-Linkage Characteristic of the 12/8 Segmented-Rotor SRM (150 conductors/slot)

This characteristic (Flux-Linkage for this assumed number of turns) was determined from the magnetic vector potential characteristic which was produced in chapter (3)

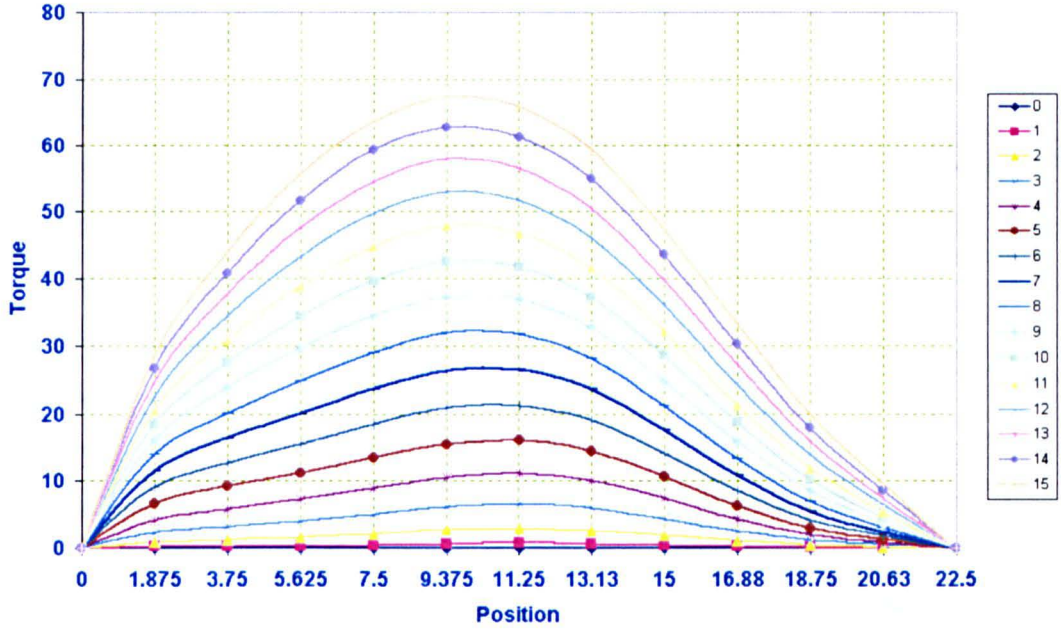

Fig. 5.7 Static Torque Characteristic of the 12/8 Segmented-Rotor SRM (150 conductors/slot)

Fig. 5.7 shows the static torque characteristic of 12/8 segmented-rotor SRM based on predicted Flux-Linkage characteristic using the 2D-FE.

5.5 Characteristic of the Segmented-Rotor 12/10 SRM

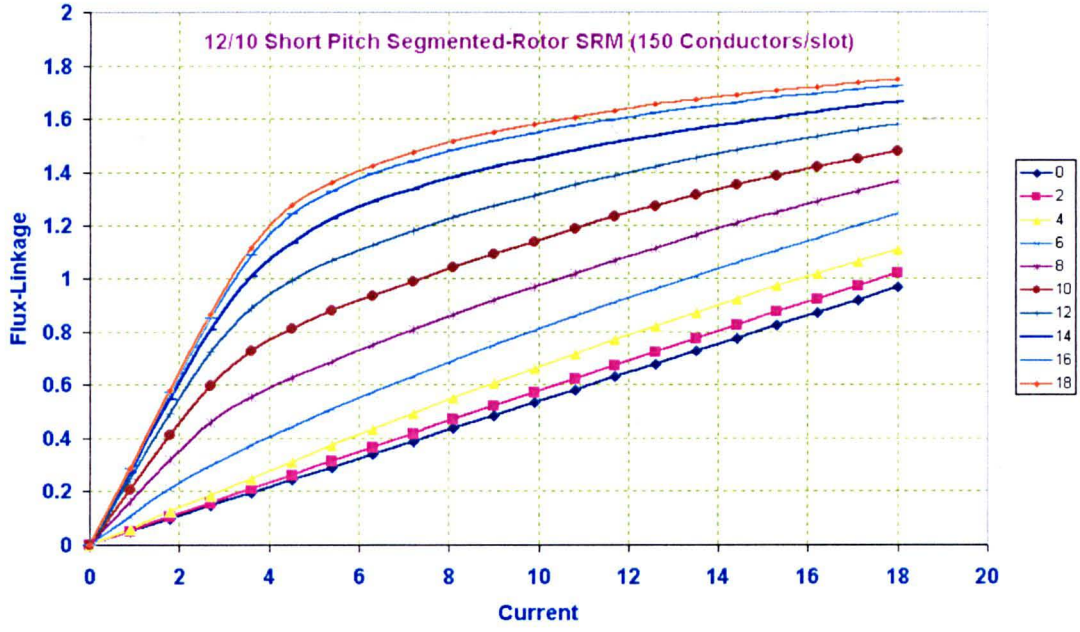

Fig. 5.8 Flux-Linkage Characteristic of the 12/10 Segmented-Rotor SRM

This characteristic was determined from the magnetic vector potential characteristic which was produced in chapter (4).

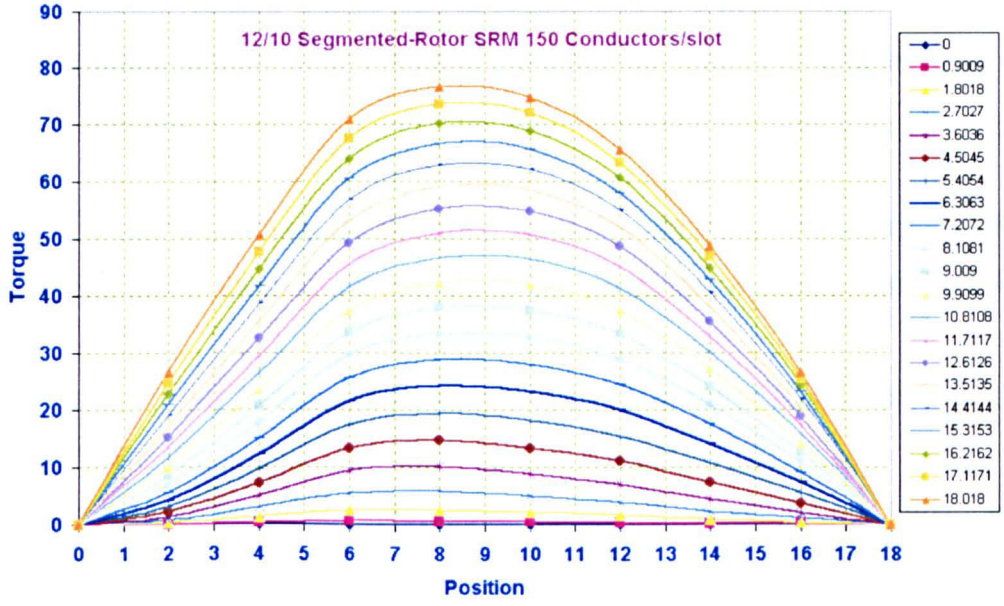

Fig. 5.9 Static Torque Characteristic of the 12/10 Segmented-Rotor SRM

Fig. 5.9 shows the static torque characteristic of 12/10 segmented-rotor SRM based on predicted Flux-Linkage characteristic using the 2D-FE.

5.6 Evaluation of Winding Turn Length

5.6.1 Conventional 12/8 SRM

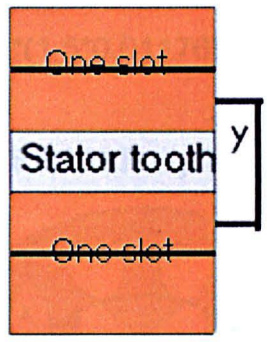

Fig. 5.10 One Stator Tooth and Two Stator Slots

Fig. 5.10 shows one stator tooth and two stator slots. There are four coils per phase. Each coil fills two halves of two stator slots, as shown below:

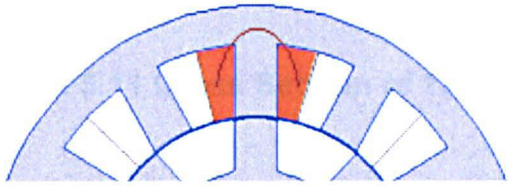

The circumferential length of the section shown (y) from the end-winding turns is estimated as follows:

1-The length is taken as average distance from the centre of the windings of the coil on the right side of the tooth to the centre of the windings of the coil on the left side of the tooth.

2-Rst_inner is the inner radius of the stator, Lps is the stator tooth height and t is the stator tooth width.

3-The mean circumferential distance for one endwinding arc $=(2\pi/12)^*(R_{st\_inner}+L_{ps}/2)$. Subtracting the stator tooth width from this value approximately gives the mean circumferential length between winding centres.

$$y=(\frac{(2\pi(Rst\_inner+Lps/2)/12)-t}{2}+t)=0.02037m.$$

The axial length of the end-winding is assumed to equal 1.5 times the stator tooth width [62]. This is based on measurements on some prototypes of the conventional SRM.

Total length of one turn=2*0.15+2*(1.5*0.01176)+2*0.02037=0.37708m

5.6.2 New Segmented-Rotor 12/8 SRM Fully Pitched 12/8

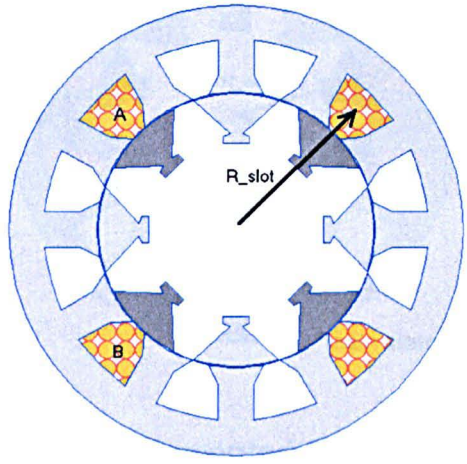

Fig. 5.11 Cross Section of 12/8 Segmented-Rotor SRM Showing the Position of R_Slot

R_slot is the radius of the centre of the slot = inner radius of the stator + half the height of the stator pole=0.0457+0.0175/2=0.05445 m

S (the circumfrential length between the centre of slot A and slot B) = $\frac{2\pi*0.05445}{12}*3=0.0855m$

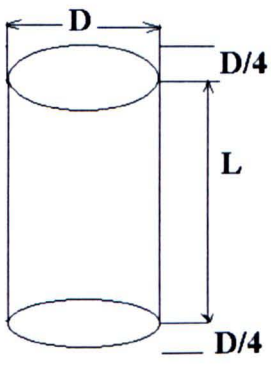

Assume the axial length of the end-windings (from one end only)=D/4, where D is the outer diameter of the machine [62] (once more this is based on measurements of prototype conventional SRM with fully pitched windings).

Total length of one turn=4*D/4+2L+2S = 0.15+2*0.15+2*0.0855=0.621m.

5.6.3 New Segmented-Rotor Short Pitched SRM 12/10

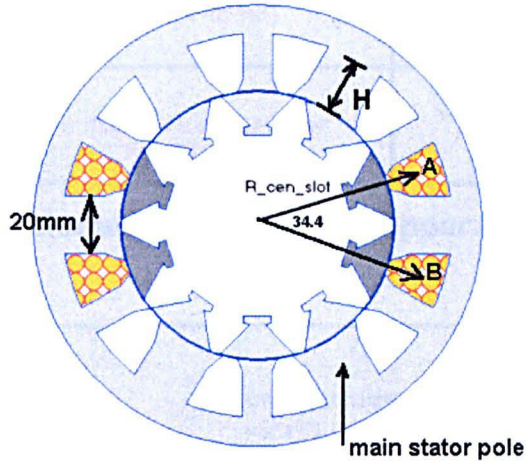

Fig. 5.12 Cross Section of 12/10 Segmented-Rotor SRM showing the Position of R_cen_slot

Assume once more that the axial length of the end-winding length in the short pitched segmented-rotor SRM is 1.5 times the main tooth width [62].
The main tooth width = 20mm
The mean circumferential arc of the endwindings is determined to be 34.4 degrees. This gives a circumferential length of 33.3 mm at the mean radius of the slot.

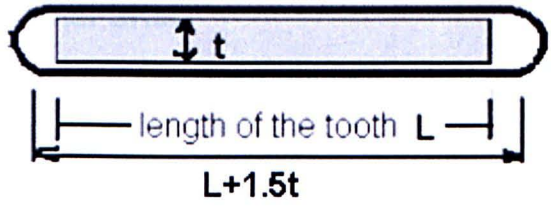

Fig. 5.13 One Stator Tooth and the Conductor

Hence the total length of one turn = 2*0.15 + 2*(1.5*0.02) +2*0.03332=0.426m

	Volume of the Copper	Weight of the Copper
12/8 Conventional SRM	$6*(0.377*0.46*332*10^{-6})=345.52*10^{-6}m^3$	$8940*345.52*10^{-6}=3.08$ kg
12/8 Segmented-Rotor SRM	$6*(0.62*0.46*272*10^{-6})=466.24*10^{-6}m^3$	$8940*466.24*10^{-6}m^3=4.168$ kg
12/10 Segmented-Rotor SRM	$6*(0.42665*0.46*257*10^{-6})=302.634*10^{-6}m^3$	$8940*302.634*10^{-6}=2.706$ kg

Table 5.2: Volume and Weight of Copper in Each SRM

	Volume Including End-Winding Turns $=\pi*r^{2}*L$(including end-winding)
12/8 Conventional SRM	$\pi*(0.075)^2*(0.15+1.5*0.01176)=2.9624*10^{-3}m^3$
12/8 Segmented-Rotor SRM	$\pi*(0.075)^2*(0.15+0.075)=3.976*10^{-3}m^3$
12/10 Segmented-Rotor SRM	$\pi*(0.075)^2*(0.15+1.5*0.02)=3.18*10^{-3}m^3$

Table 5.3: Volume of Each SRM

5.7 Current Capability for 300w of Winding Loss

5.7.1 The 12/8 Conventional SRM

Assuming four coils per phase each coil links one stator tooth and a fill factor of 0.46.

Copper loss for 3-phases

$$P = 3J^2\rho V_{cu}$$

$300=3*2*(J)^2*0.0178*10^{-6}*0.37708*0.46*332*10^{-6}$

$J=6.98$ Amp/mm^2

If the phase is excited with constant current for one third of a cycle then the peak value of current is given by

$I=\sqrt{3}*6.984*10^{6}*0.46*332*10^{-6}/150=12.3Amp$

5.7.2 The 12/8 Segmented-Rotor SRM

Copper losses of 3-phase $P = 3J^2\rho V_{cu}$

$300=3*2*(J*10^{6})^{2}*0.0178*10^{-6}*\ 0.621*0.46*272*10^{-6}$

So $J=6.00\ Amp/mm^2$

$I=\sqrt{3}*6*10^{6}*0.46*272*10^{-6}/150=8.68Amp$

5.7.3 The 12/10 Segmented-Rotor SRM

Copper loss for 3 phase 12/10

$P = 3J^2\rho V_{cu}$

Area of one slot = $0.257*10^{-3}\ m^2$.

$300=6*[J^{2}*0.0178*10^{-6}*(0.42665*0.46*0.257*10^{-3})]$

$J=7.463A/mm^2$

$I=\sqrt{3}\ J*A_{cond}=\sqrt{3}*7.463*10^{6}*0.46*0.257*10^{-3}/150=10.18\ Amp.$

5.8 Mean Torque Capability

This section is dedicated to determine the average torque corresponding to the calculated current based on 300W copper loss in each machine. It assumes ideal excitation for each machine (rectangular pulse for 1/3 of a cycle).

5.8.1 The 12/8 Conventional SRM

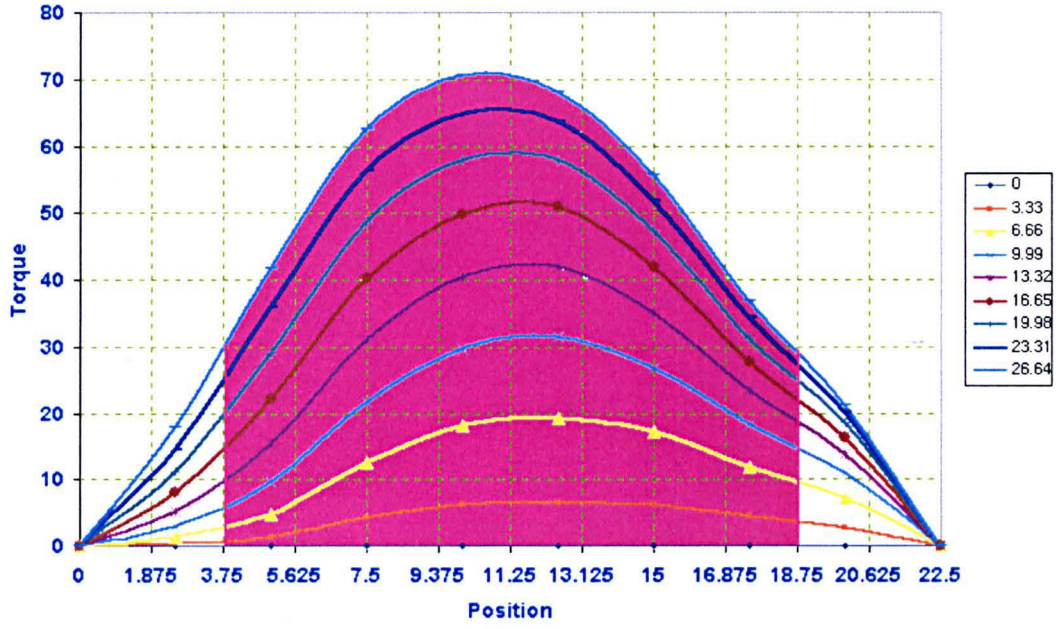

Fig. 5.14 Area which Gives Highest value of Torque During Running (Assume ideal excitation, rectangle pulse for 15 mechanical degrees)

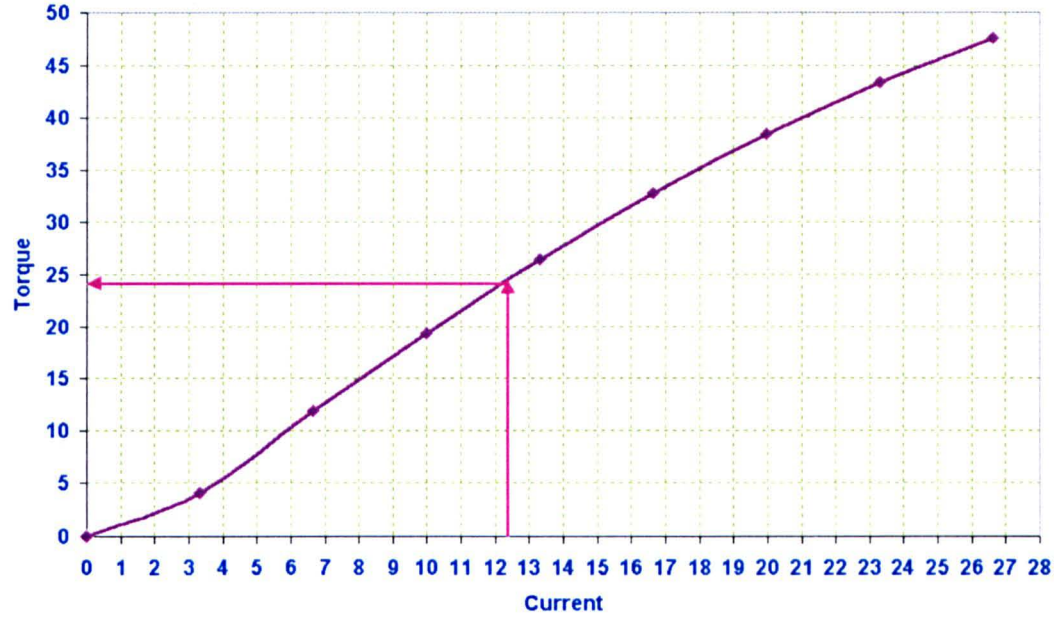

Fig. 5.15 Average Torque versus the Current, 12/8 Conventional SRM (15 mechanical degrees)

From Fig. 5.15 at current =12.3 Amp the torque is 24 Nm.

5.8.2 The 12/8 Segmented-Rotor SRM

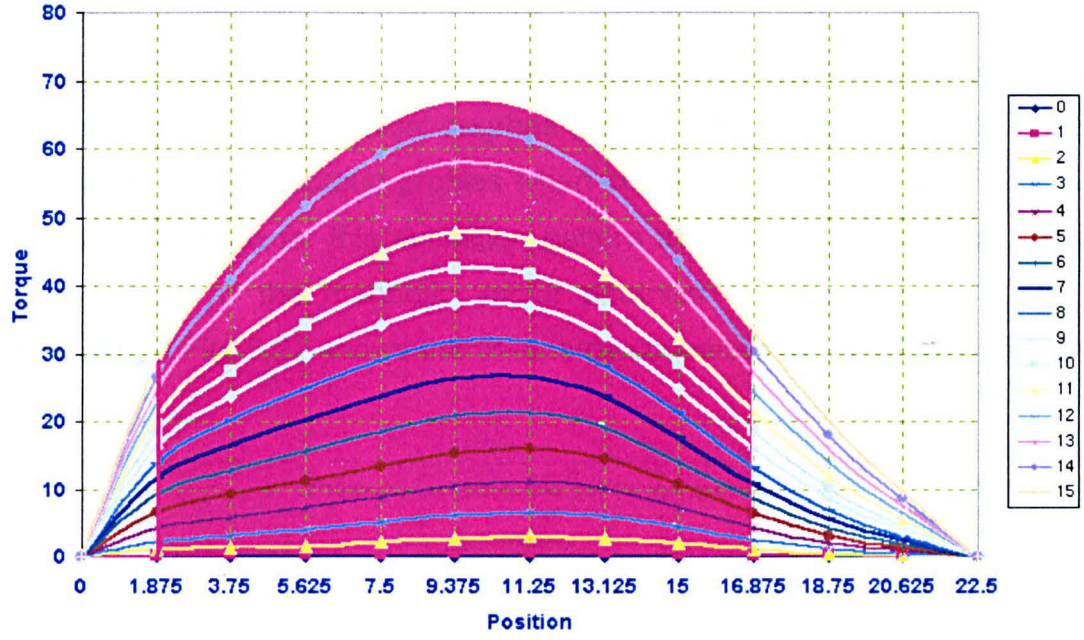

Fig. 5.16 Area which Gives Highest value of Torque during Running (Assuming ideal excitation, 1/3 of the cycle rectangle pulse)

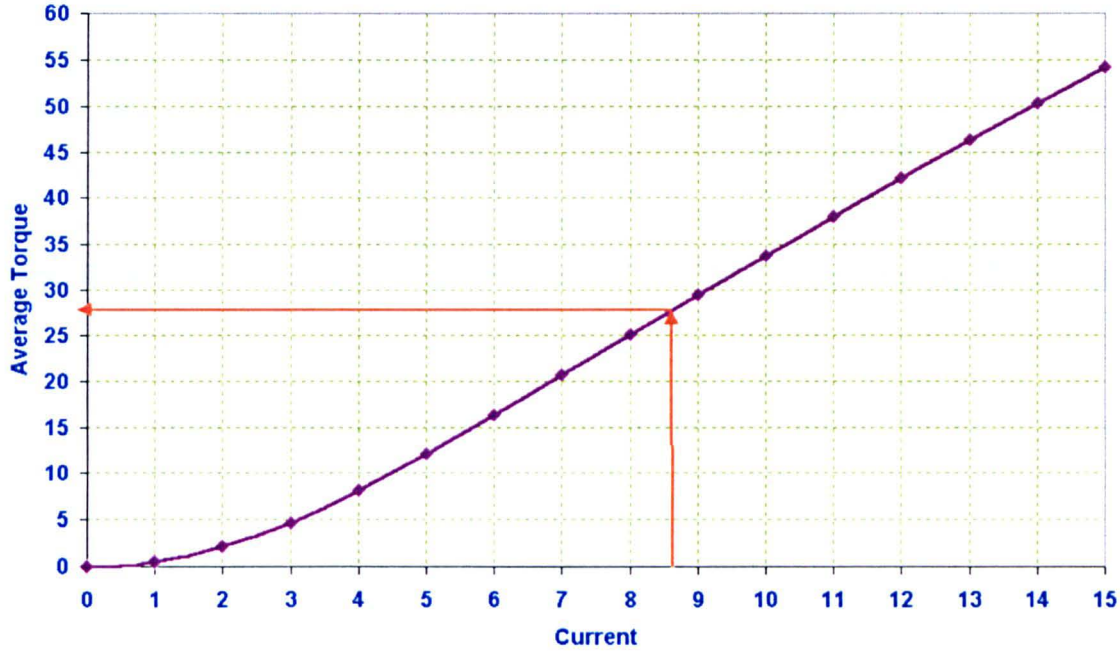

Fig. 5.17 Average Torque versus the Current 12/8 Segmented Rotor the (torque for 15 mechanical degrees)

From Fig. 5.17 at current = 8.68 Amp the torque is 28 Nm.

5.8.3 The 12/10 Segmented-Rotor SRM

Assuming ideal excitation (1/3 of the cycle rectangle pulse) so the effective running torque occurs over 12 mechanical degrees only (2/3 the cycle). Fig. 5.18 shows the predicted instantaneous torque profiles when constant currents flow. Fig. 5.19 then gives the mean torque for this excitation pattern as a function of current. Fig. 5.20 and Fig. 5.21 show the magnetic vector potential and flux-linkage in the three machines, whilst Fig. 5.22 shows the co-energy converted per electrical cycle in each case.

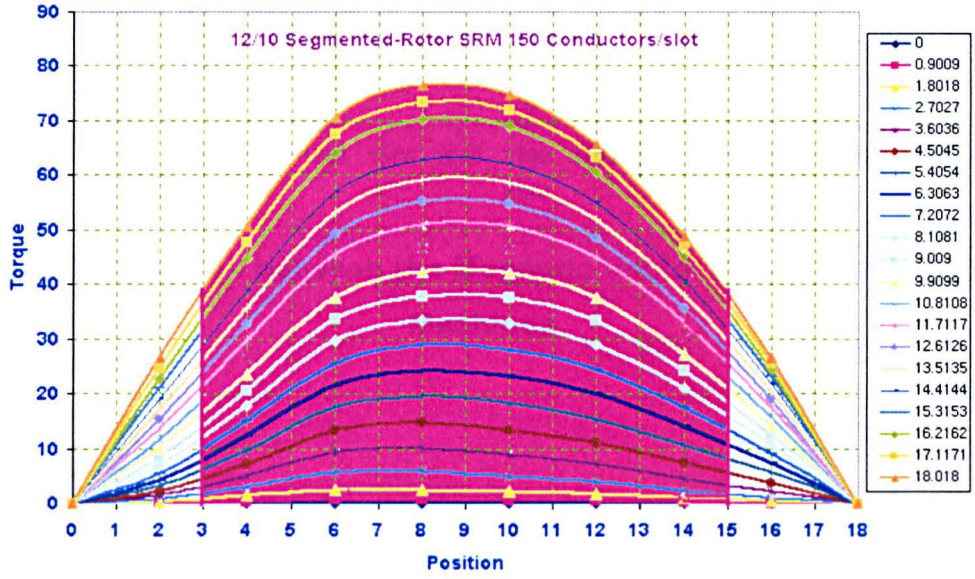

Fig. 5.18 Area which gives the Highest Value of Torque during Running

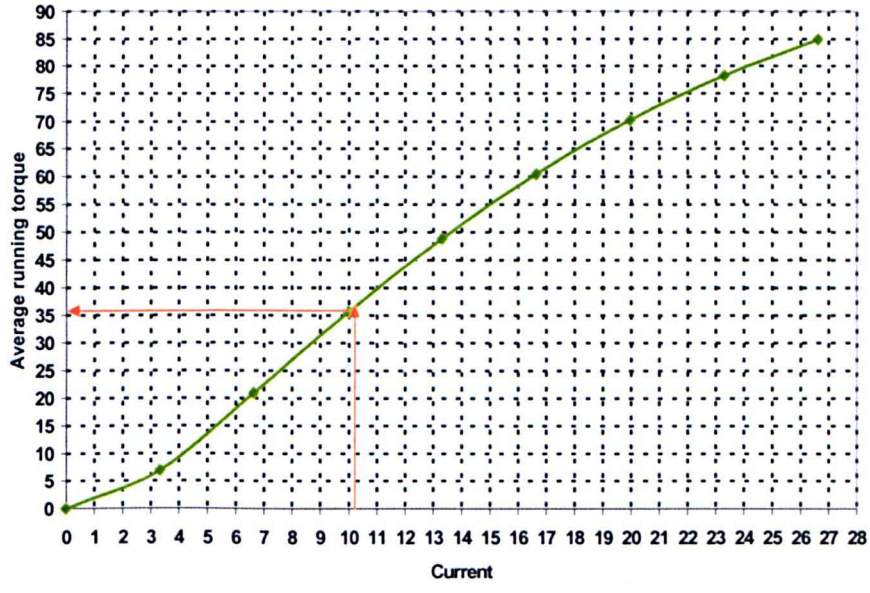

Fig. 5.19 Average Torque versus the Current (T for 12 degrees only)

From Fig. 5.19 at current = 10.18 Amp the torque is 36 Nm.

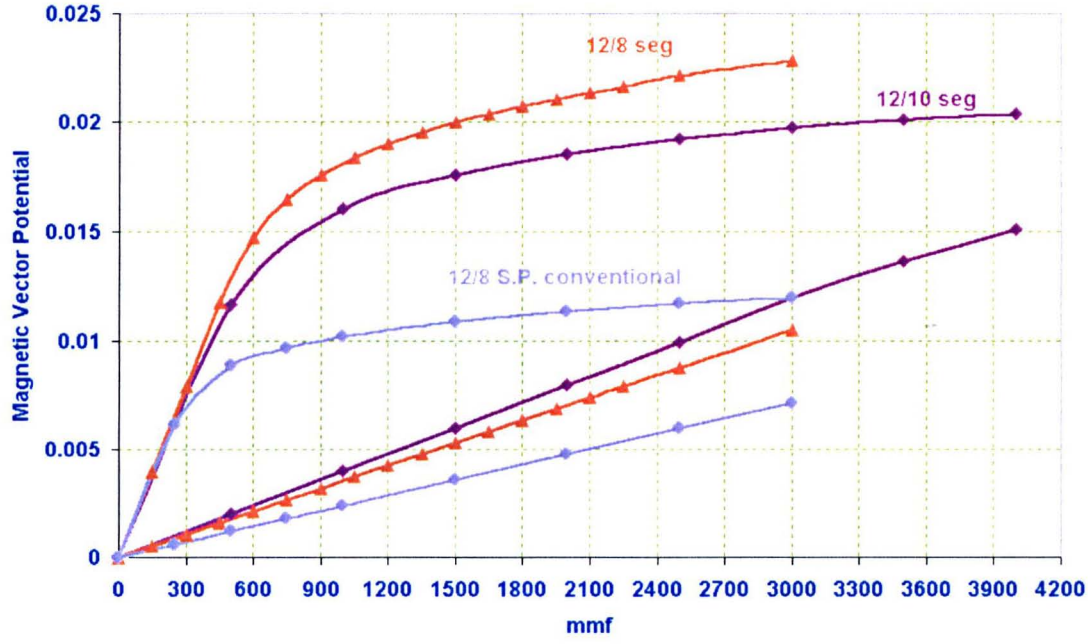

Fig. 5.20 Comparison between the Magnetic Vector Potential for the three Machines

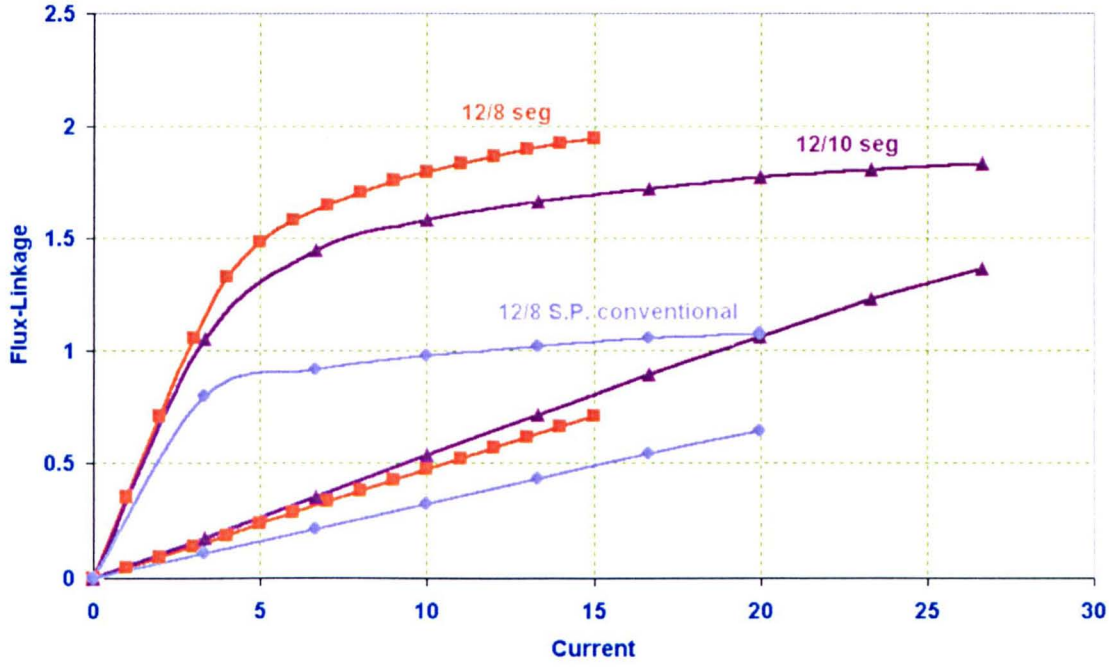

Fig. 5.21 Comparison between the Flux-Linkage for the three Machines (Assuming 150 Conductors / Slot)

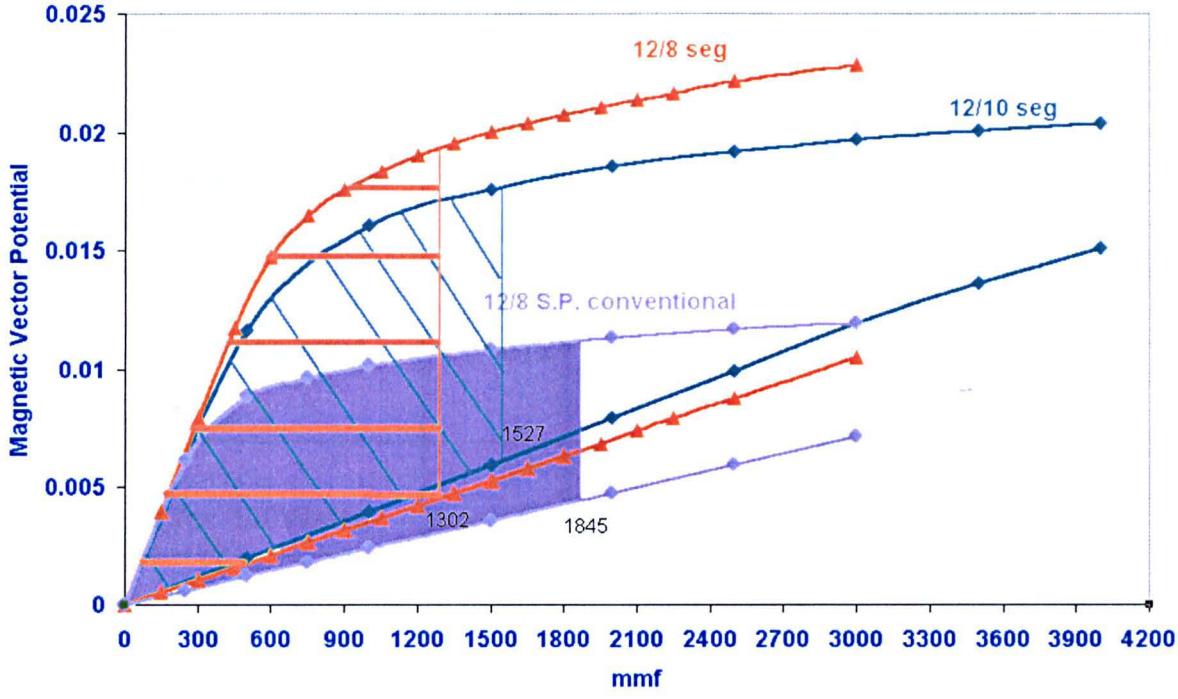

Fig. 5.22 Areas Enclosed between the Aligned and the Unaligned Positions for Fixed Copper Loss 300 Watts (Under Voltage Control)
Magnetic Vector Potential per Slot versus the MMF per Slot for each SRM

The area between the aligned and the unaligned positions is proportional to the output torque. This area must be multiplied by eight for the 12/8 SRM and by 10 for the 12/10 SRM in order to determine the energy converted to torque when rotating through a complete revolution.

	New segmented rotor 12/8	New segmented rotor 12/10	Convention 12/8
Average length Of one turn	0.621m	0.426m	0.377m
Slot area mm^2	272	257	332
J for 300Watts	6	7.463	6.98
MMF per Slot	150*8.683= 1302.48	150*10.18= 1527	150*12.3= 1845
Average torques NM	28	36	24
Specific torque (torque/copper volume)	6790.74	11320.75	81015.39
Specific torque (torque/mass of the copper)	6.478	13.3	7.79

Table 5.4: General Comparison between the three SRMs

5.9 Torque Ripple

Torque ripple in the three machines will be compared at high current, assuming that each machine is excited with constant current in a conducting phase, with each phase conducting for one third of a cycle. The machine is assumed to be operating at very low speed, so that commutation between phases is instantaneous. Torque ripple is calculated using the predicted static torque characteristic [148-162].

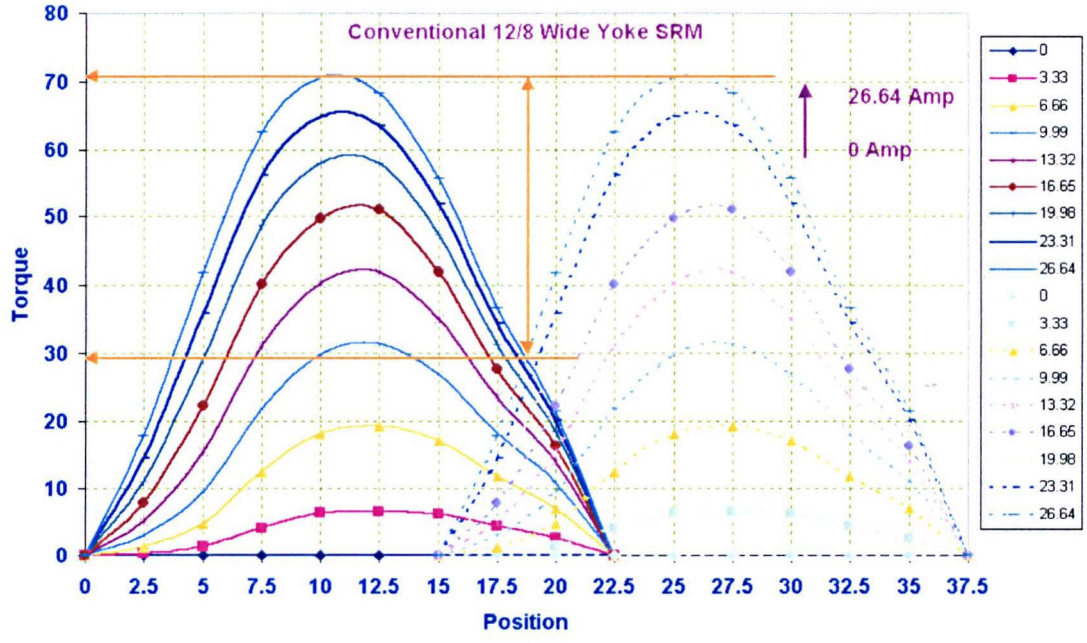

Fig. 5.23 Torque Ripple in the Conventional 12/8 SRM

$$\text{Percentage Ripples} = \frac{T_{maximum} - T_{intersection}}{T_{maximum}} \quad [154]$$

Percentage ripple = 59.15%

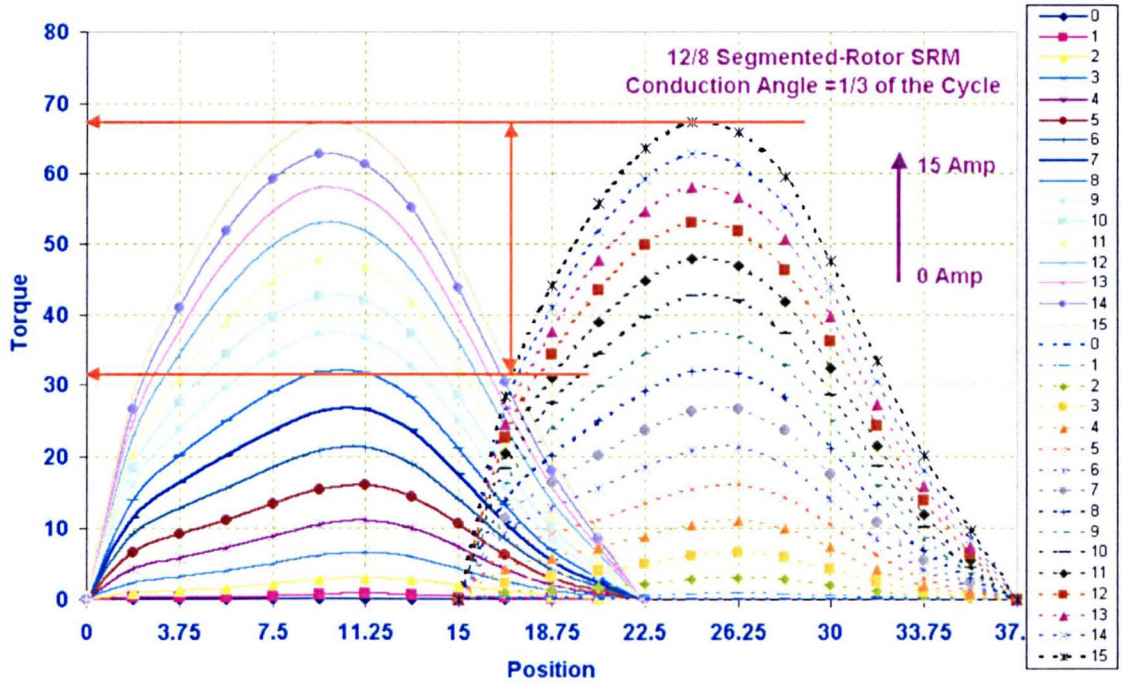

Fig. 5.24 Torque Ripple in 12/8 Segmented Rotor SRM

Percentage ripple = 54.41%

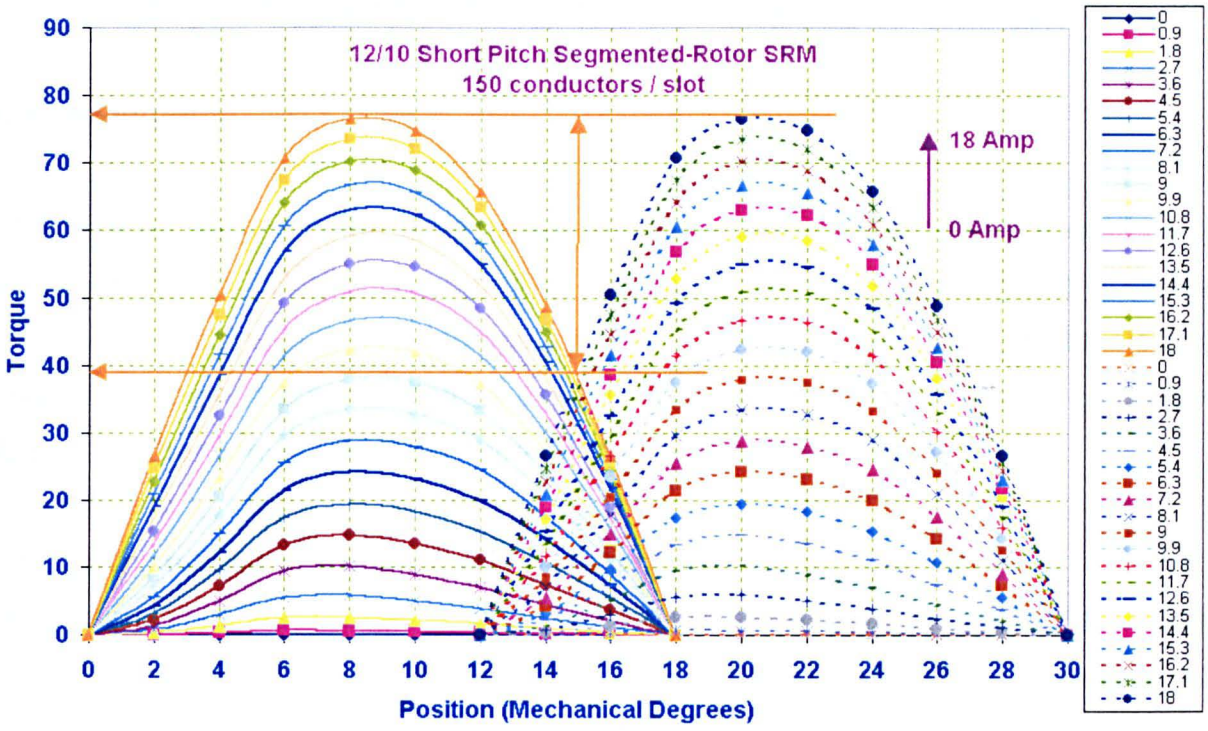

Fig. 5.25 Torque Ripple in 12/10 Segmented Rotor SRM

Percentage Ripple = 49.31%

5.10 Conclusion

This chapter makes a comparison between the different SRMs, taking endwinding effects into account. The output of each machine was calculated to assess the gain from the new design before building any prototype. Whilst both segmental machines are predicted to outperform a conventional SRM, the new short-pitched 12/10 segmented-rotor SRM has shown the best results, although it appears that torque ripple is increased in the segmental designs.

6 Building and Testing the New 12/8 SRM Prototype

6.1 Introduction

This chapter describes the construction and static testing of a prototype of the new segmented-rotor SRM, as designed in chapter 3. Measurements made upon the prototype machine are then compared with those predicted using finite element analysis. Finally the overall torque capability of the machine is assessed in relation to that of other conventional switched reluctance machines [166-167].

The machine has three phases with an inner rotor and outer stator. Rotor and stator laminations were laser cut and use a standard 0.5 mm lamination steel, often used in induction motors, with the manufacturer's trade name "Scotsil 400". The laminations were then coated with an insulation coating with the trade name "Kor-C" [178-179]. The rotor diameter, the outside stator diameter, the air gap length and the axial length for the new design are equal to the same equivalent physical parameters of a conventional 12/8 SRM which was built previously at the University of Newcastle. This enables an experimental comparison of the results for the new segmented-rotor SRM with an equivalent conventional SRM.

6.2 Manufacturing of 12/8 New Segmented-Rotor SRM

The prototype three phase segmented-rotor SRM has 12 teeth on the stator and 8 rotor segments. The windings are fully pitched in that they span one complete magnetic pole of the machine. However, the machine should not be confused with a SRM with fully pitched windings. Unlike the segmental machine, these latter machines use the changing mutual coupling between phases to produce torque and therefore require more than one phase to be excited at any one position. The segmental machines have virtually no mutual coupling between the phases, operating on a changing self inductance like a conventional short pitched winding SRM. As the coils must span three stator teeth this topology requires each end-winding of the machine to span one quarter of the machine, i.e. it is a four pole winding. This gives substantially shorter end-windings than a 6/4 segmental

machine, in which the end-windings would have to span one half of the machine, however they are still very substantially longer than those of a conventional short pitched winding SRM. This is important for end-winding copper loss [69-70].

The new optimised SRM has a of ratio t/λ =0.67. This ratio requires the stator teeth to be of the same width as that of a conventional SRM with a t/λ of 0.33. An experimental machine with this t/λ already exists, making comparison between the two machine types much easier, as slot areas and stator magnetic dimensions are similar.

6.2.1 Rotor Assembly

The eight rotor segments are constructed from stacks of separate laminations, assembled onto a non-magnetic shaft and held by a non-magnetic steel wedging system. It is essential that these components are non-magnetic so that they do not affect the static characteristics of the machine. Of course eddy currents may affect the dynamic performance, but it was judged that this would be of minor importance since the wedges and shaft are well away from the areas of high flux density. The rotor segments require both circumferential location and retention against centripetal and magnetic radial forces when rotating. Circumferential location was achieved by using flat bottoms on the rotor segment laminations, matched into channels in the shaft. The wedges fit into dovetails in the segments, and are then bolted to the shaft. The segments are also clamped axially using end-rings [170-171].

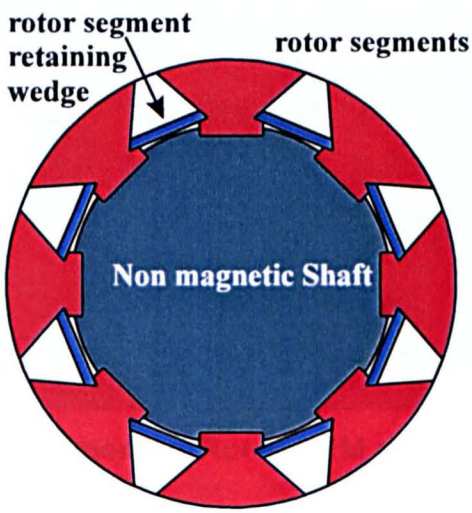

Fig. 6.1 Wedging System used to hold the Rotor Segments onto the Rotor Shaft

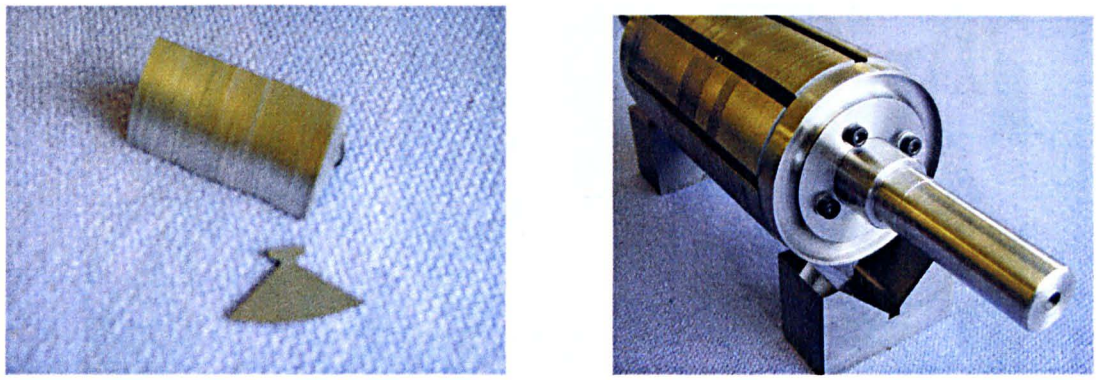

Fig. 6.2 Segment Stack and Assembled Rotor

Fig. 6.2 shows a photograph of the assembled rotor. To further increase mechanical rigidity the rotor was then potted using an epoxy compound, before turning in a lathe to give the required final outside diameter. The assembly arrangement was calculated to give safe operation up to a maximum of 30,000 rpm. Higher speeds would be possible if larger bolts were employed to hold the wedging system [172-173].

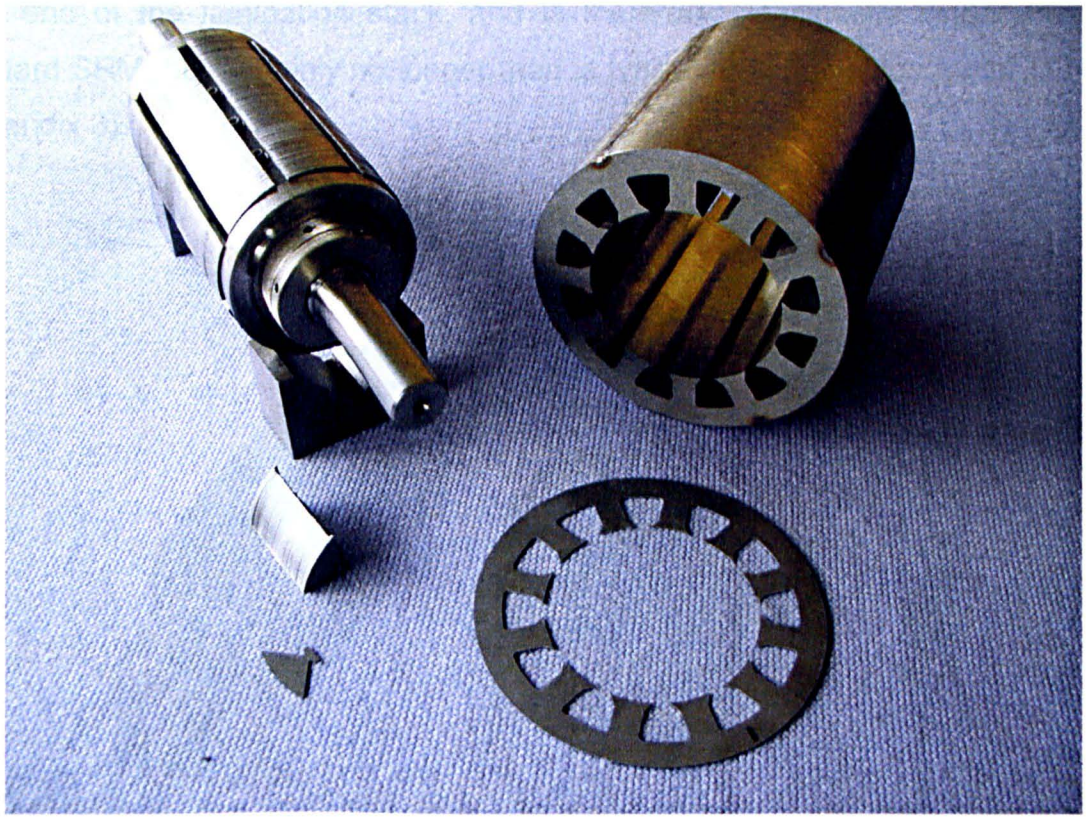

Fig. 6.3 12/8 Segmented-Rotor SRM during its Building

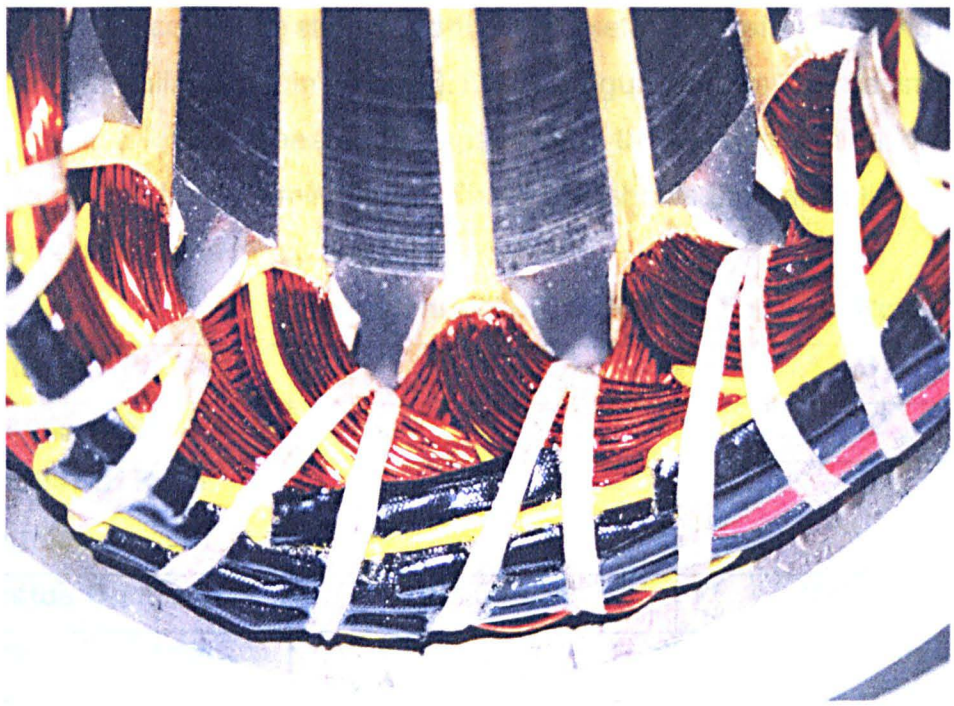

Fig. 6.4 End-Windings Turns

Fig. 6.4 shows the details of the stator end winding. It is a standard double layer winding, commonly used in AC machines. The end winding stands out 37 mm at each end of the lamination stack, and is therefore significantly longer than in a standard SRM, but certainly no longer than is typical in an induction motor [174-175] (Appendix 3).

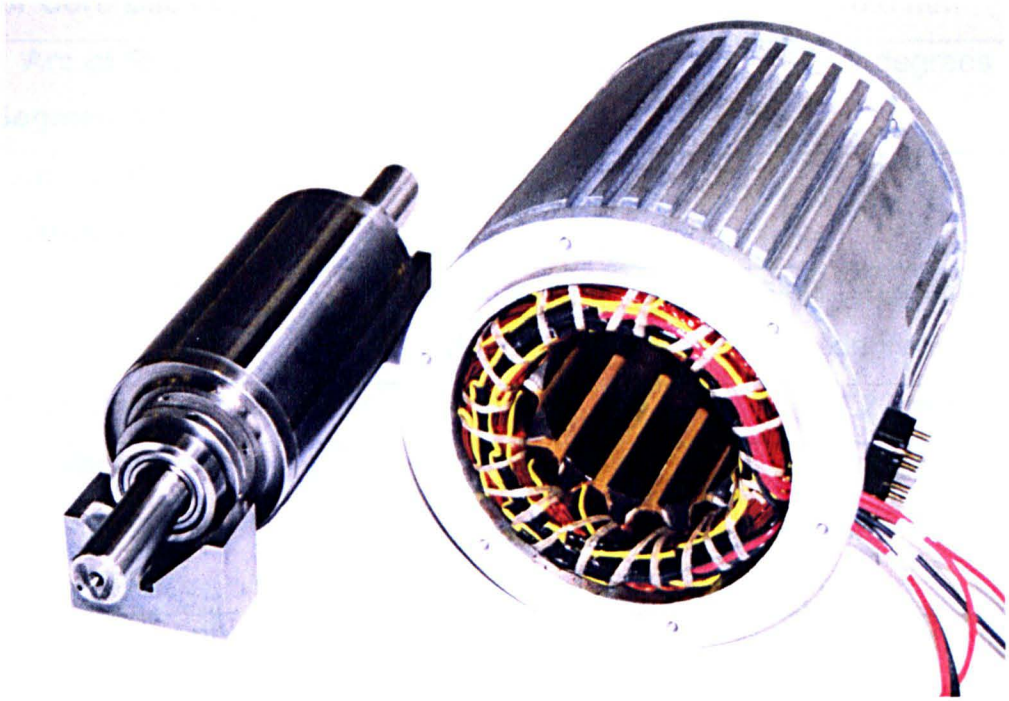

Fig. 6.5 Complete Rotor and Stator

Fig. 6.5 shows the complete stator and the complete rotor after building [176-180], with measured details given in Table 6.1. The figure shows the casing fitting the welded laminations. It was heated to expand then the welded laminations were put in and left to cool to fit the laminations. The figure shows the ventilation ducts in the stator casing and the fins for cooling.

	Segmental Rotor SRM	Toothed Rotor SRM
Number of Phases	3	3
Number of Stator Slots	12	12
Number of Rotor Segments/teeth	8	8
Outside Diameter	150.0 mm	152.6 mm
Stack Axial Length (rotor and stator)	150.0 mm	150.00 mm
Rotor Outside Diameter	90.8 mm	89.6 mm
Air-gap Length	0.3 mm	0.25 mm
Stator Tooth Width	11.93 mm (parallel sided)	12.05 mm at tip, with 12 degree taper
Arc of Stator Tooth Tip	22.5 degrees	15.0 degrees
Stator Core Back depth	11.9 mm	10.6 mm
Arc of Rotor Segments/teeth.	37.5 degrees	16.2 degrees
Number of Series Turns/Phase	300	204
Coil Span	3 slots (90 mechanical degrees)	3 slots (90 mechanical degrees)
Wire Diameter	1.0 mm	1.20 mm
Slot fill-factor (copper area to overall slot area)	46%	42%
Resistance per phase @ 20 degrees C	3.58 Ω	1.825 Ω

Table 6.1 Dimensions of the Prototype Machine and a Fully Pitched Winding Toothed Rotor SRM, Used for Comparison.

6.3 Static Test of the 12/8 Segmented-Rotor SRM

Because the magnetic field in an SRM is not significantly affected by eddy currents, the static and dynamic characteristics should be effectively identical. Furthermore, because there is very low coupling between phases, excitation of one phase in isolation should be enough to measure the major parameters. However, the characteristics are substantially complicated due to the highly non-linear form of the magnetic characteristics.

Rather than use inductance, it is more appropriate for analysis to use the variation of flux-linkage with current in a SRM. The flux-linkage of any one experimental machine is only a function of excitation current and rotor position. This section will present measurements of the flux-linkage characteristics of this machine. It will also show measurements of the shaft torque, indicating how that varies with both position and excitation current.

6.3.1 Thermal Testing

Before proceeding with the magnetic testing the machine was first excited with d.c. current to ascertain it's thermal performance. The machine was stationary for this test, with all three phases connected in series and carrying a current of 3.05 amps. Average temperature rise in the winding was derived from measurement of the winding resistance and knowledge of the thermal coefficient of resistivity, whilst that in of the case was measured using a thermocouple. Although the aluminium casing is finned, there was no fan ventilation. It is interesting to see how approximately 60% of the temperature rise is between the casing and ambient, with a time constant of close to 80 minutes, and 40% between the winding and casing, with a time constant of 3 minutes.

Based upon these results it was determined that 100 degree centigrade rise corresponded to a loss of 272W and r.m.s current of 4.67 A.

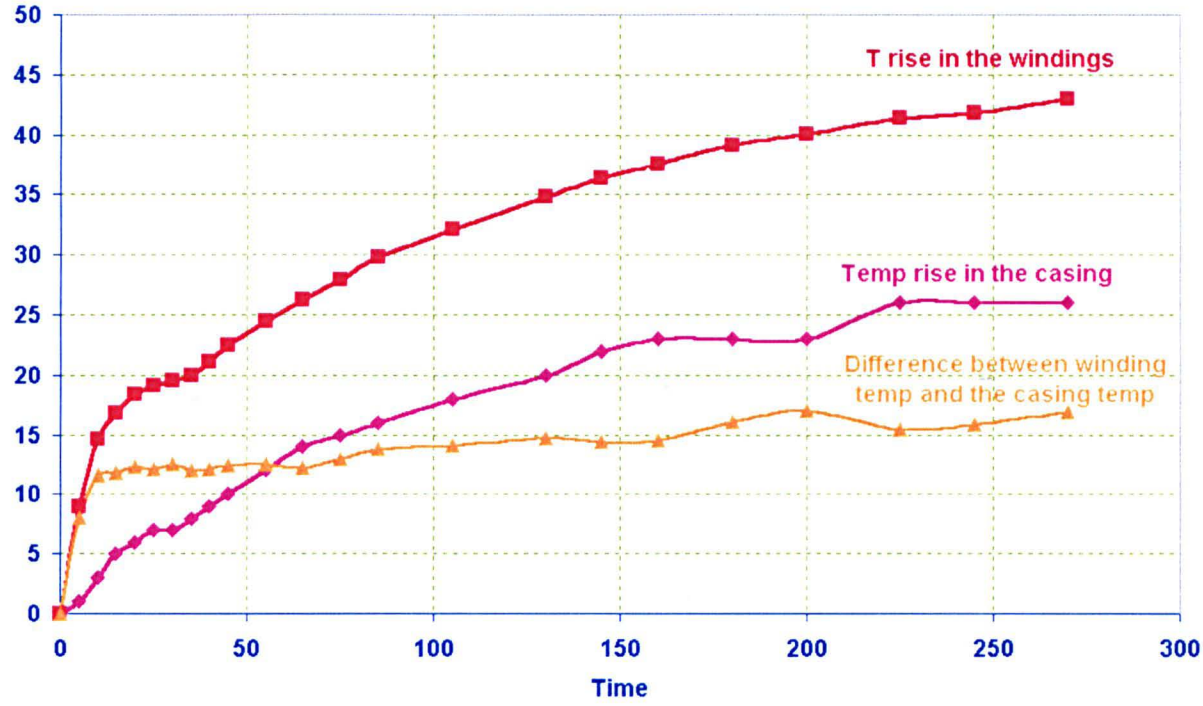

Fig. 6.6 Thermal Test of This Machine

6.3.2 Static Torque Characteristic

The torque production in a SRM comes from the tendency of the rotor poles to align with the excited stator poles. The rotor moves from zero-torque unstable position (unaligned position) to a zero-torque stable position (aligned poles). Between these two positions, the value of static torque varies assuming a particular shape. The torque versus rotor position characteristic (static torque characteristic) gives useful information about the capability of the magnetic structure to generate average torques during normal motor operations and gives an indication of likely torque ripple [69-70][181].

The torque production as a function of rotor angle and phase current was examined through a series of locked rotor tests. The torque produced in the SRM depends only on angle and current and is independent of the speed. Initially these tests were performed using a torque transducer coupled to the machine shaft via flexible couplings at one end and clamped at the other. At some currents and angles the

machine torque was large enough to significantly twist the couplings so the angle must be read with each reading [69-70][181]. The results are displayed in Fig. 6.7.

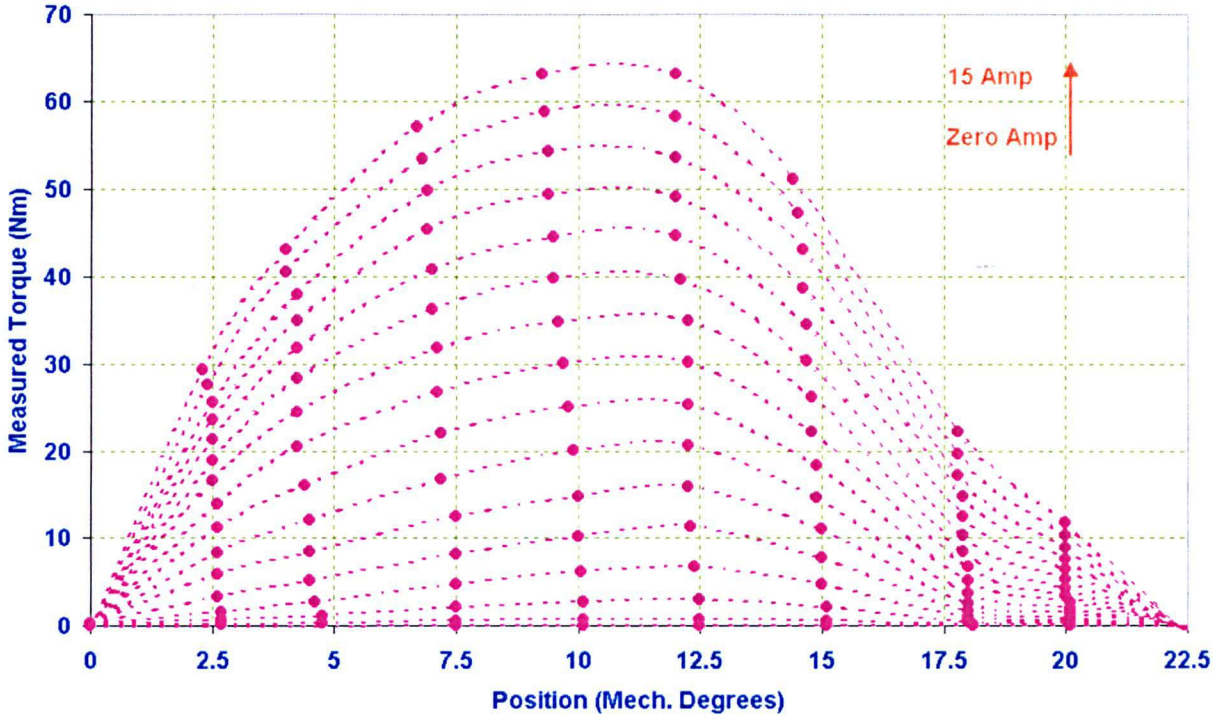

Fig. 6.7 Experimental Measurement of Static Torque Characteristic

The general form of the static torque curves is similar to that of a conventional SRM when the machine is saturated, but differs significantly at low currents. In an unsaturated conventional SRM the magnetic permeance rises almost linearly with angle of overlap of the teeth, resulting in an almost constant torque during this period. In the segmental machine the permeance does not vary in such a simple manner: as the area of overlap on one side of the magnetic circuit increases, it decreases on the other. This results in a static torque which rises to reach a peak at approximately 12.5 degrees from the aligned position [69-70][181].

In toothed rotor SRMs the magnetic flux crosses two air-gaps of identical form. At full alignment the permeance is at a maximum, and as the rotor moves away from alignment the permeance falls linearly. For a standard 12/8 motor in which the teeth of rotor and stator occupy an arc of 15 degrees, the simple approximation outlined above predicts that the permeance falls to zero when the rotor is displaced 15 degrees from alignment, and remains so until the unaligned position is reached at 22.5 degrees. This variation is shown in Fig. 6.13. Because the rate of change of

permeance is linear over most of the current stroke the torque produced at constant current is predicted to be linear.

With the segmental SRM the variation of air-gap permeance with position is more complex. Magnetic flux flows down one tooth, into a rotor segment and returns via an adjoining stator tooth. In the aligned position the reluctance of the two air-gaps linking a rotor segment to adjoining stator teeth are equal but, as the rotor moves from the aligned position, the reluctance of one air-gap falls whilst that of the other rises. Hence, as shown in Fig. 6.13, the initial rate of change of permeance is zero but, as the asymmetry rises, the rate of change of permeance also rises, until it reaches a maximum at a rotor displacement of 15 degrees. Consequently the torque increases rapidly up until 15 degrees away from alignment, at which point there ceases to be any overlap between the rotor segment and one of the stator teeth. This type of torque variation can be seen in the measurements of Fig. 6.7. The static torque profiles of the two SRM types are compared and differences explained in terms of permeance variation. The segmental rotor machine is likely to lead to slightly higher torque ripple under current control with flat current waveforms [69-70][181].

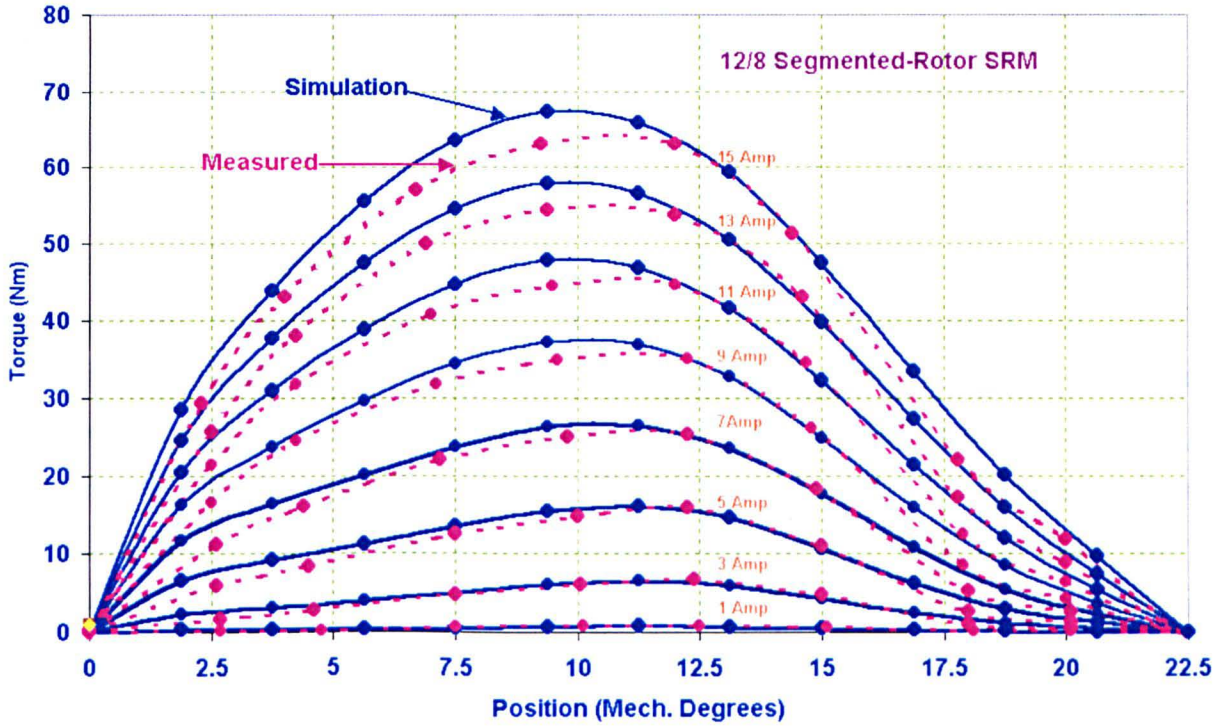

Fig. 6.8.a Comparison between Predicted and Measured Torque Characteristics

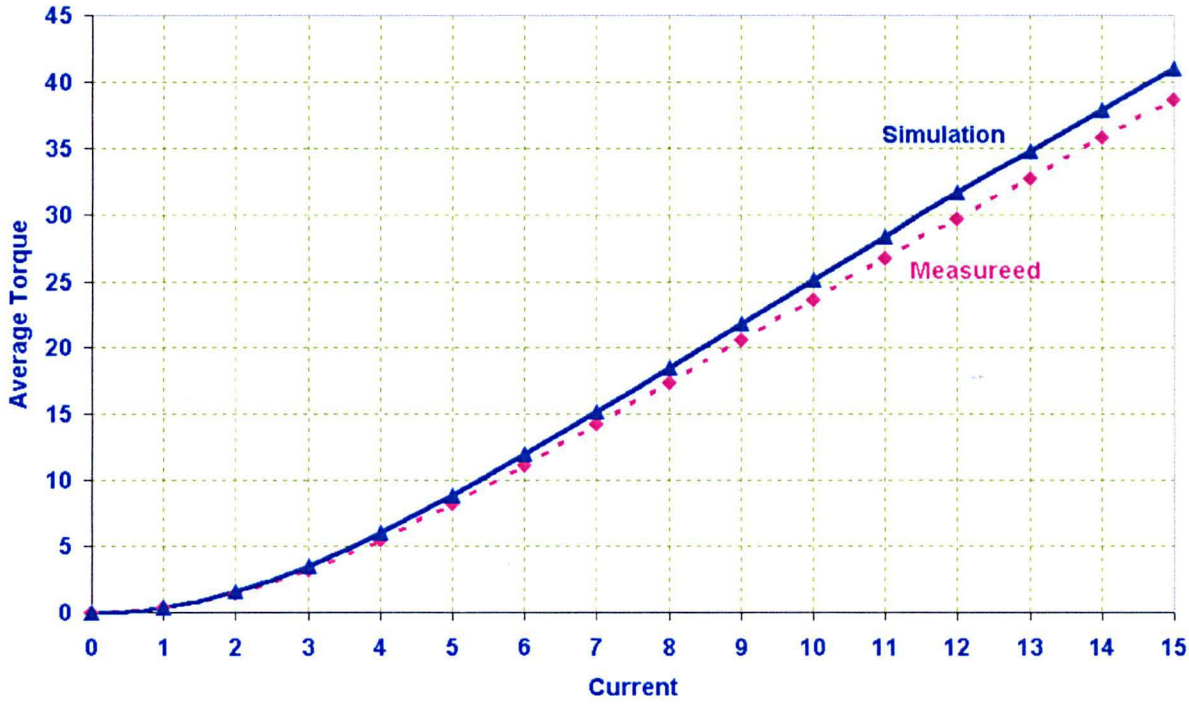

Fig. 6.8.b Difference between the Measured and Simulated Torque

Fig. 6.8.b gives a comparison between measured static torque and those predicted using two dimensional finite element analysis. The comparison is generally good, both in terms of the shape of the curves and their magnitude. The simulation has taken no account of three dimensional end effects, and so this comparison is certainly as good as can be expected. At very large currents the discrepancy is larger, when the simulation tends to overestimate the mean torque by about 3%.

Calculation of the static torque from the predicted Flux/MMF curves is accomplished by integrating the flux linkage curves at a series of discrete positions as shown in Fig. 6.9, to determine the co-energy variation with current and position. This integration is performed using first order approximations to the flux-linkage, thereby introducing some numerical error into the solution. If a large number of discrete positions are calculated then there is the danger of rounding error being introduced as the torque is proportional to the rate of change of flux-linkage. Equally, if too few positions are used then the calculated torque does not include the higher order variations with respect to position [69-70].

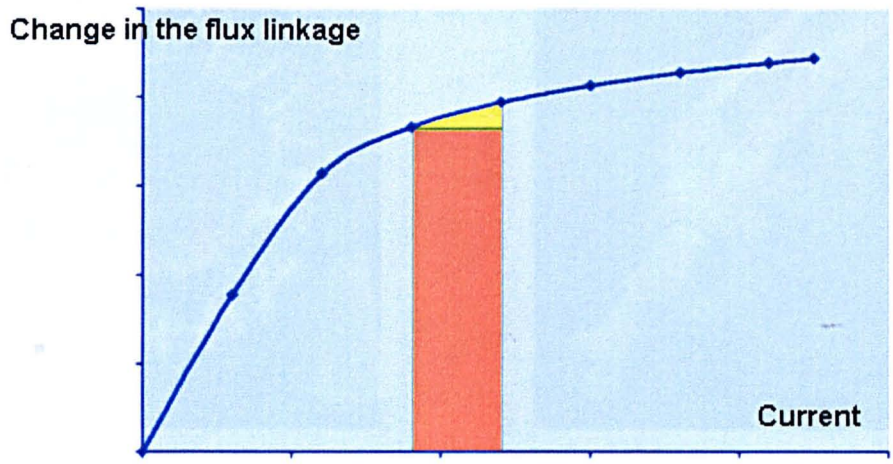

Fig. 6.9 Each Step is Approximated to Rectangular Plus Triangular Sections

6.3.3 Mean Torque Capability

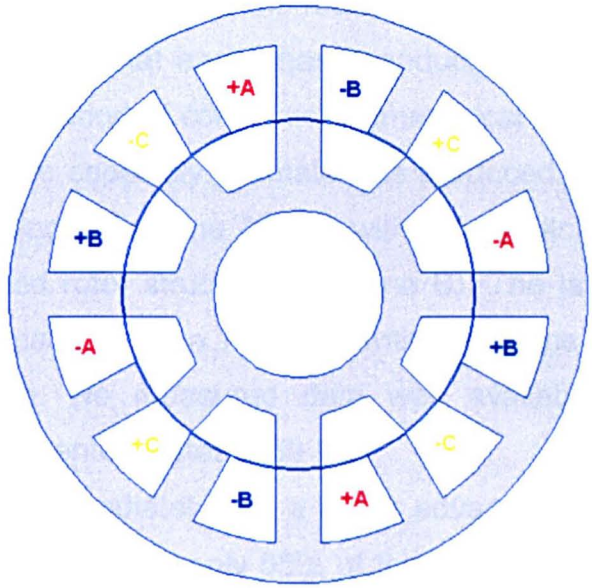

Fig. 6.10.a Winding Connection in 12/8 Fully Pitched Toothed-Rotor SRM

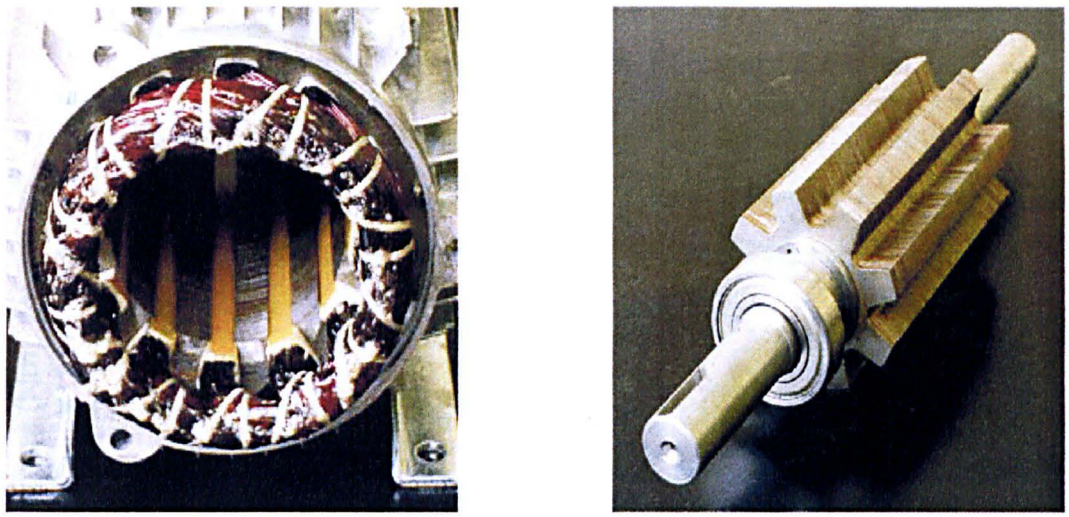

Fig. 6.10.b The Fully Pitched conventional SRM which is included in the Comparison of the Torque Capability and was Built before in the Lab of the Newcastle University

The variation of mean torque as a function of total machine winding loss was determined, the loss being found from the measured machine's electrical resistance. This loss estimate assumed that each phase conducted a constant current for one third of a cycle, with the period of conduction symmetrical about the position of peak torque. The same torque capability estimate was produced for a conventional SRM with short-pitched windings (machine A) and with a fully pitched winding SRM (see Fig. 6.10) with a toothed rotor structure (machine B). The latter was taken directly from measurements, made upon a machine with the same outside diameter and lamination stack length. No measured data was available for machine A, so simulated results are presented instead [69-70].

The short pitched SRM immediately had a major advantage due to its smaller end-windings: this resulted in it having only 65% of the total winding mass. Hence for a given loss it could operate with $1/\sqrt{0.65}$ =1.24 times greater r.m.s. current density. The machine has the same magnetic geometry as machine B, corresponding to t/λ=0.33.

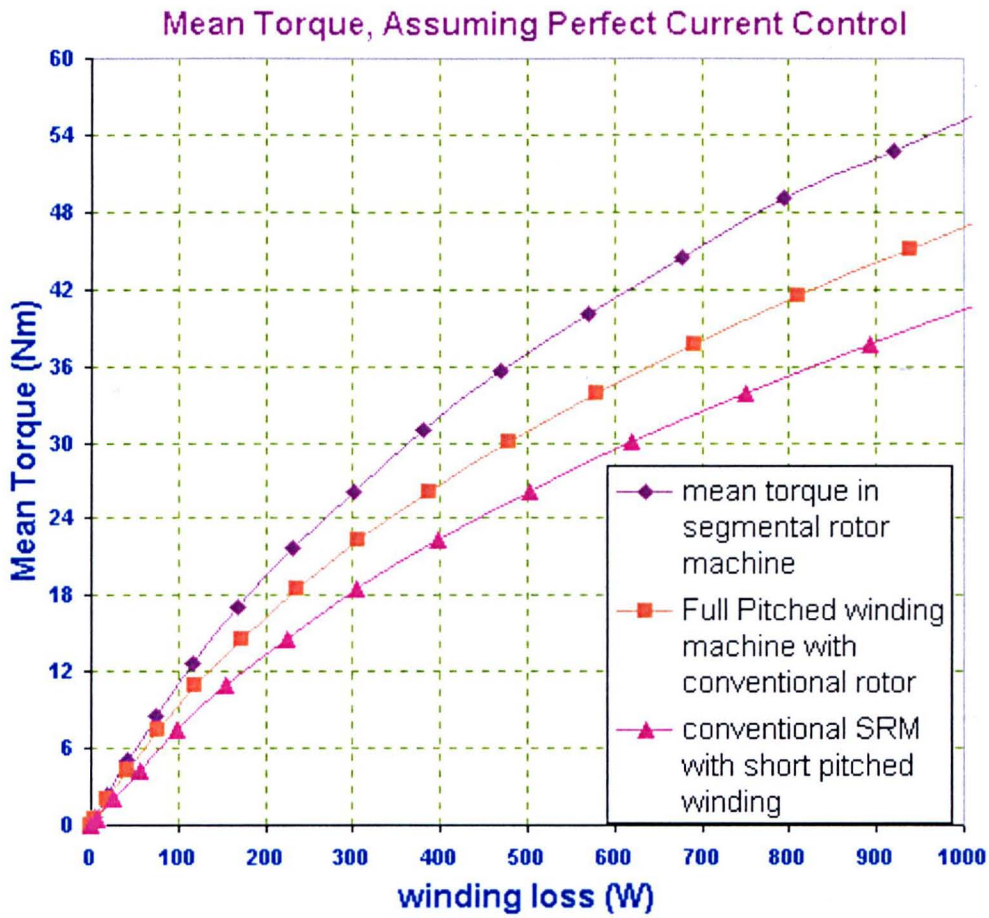

Fig. 6.11 Comparison between the Conventional (both the Short Pitched and the Fully Pitched) and the Segmented-Rotor SRMs

Fig. 6.11 give a comparison of mean torque capability as a function of winding loss for the three machines under unipolar current control. Comparisons take into account differing end-winding lengths and excitation periods. Curves for the segmental and conventional fully pitched winding machines are by measurement, whilst that for the conventional short pitched winding SRM is based upon simulation [69-70].

In comparing machines account is taken of the requirement to have two phases simultaneously conducting in the conventional fully pitched winding SRM, and the subsequent increase in winding loss. Fig. 6.11 shows how this machine has 340 W of winding loss when delivering a mean torque of 24 Nm [69-70].

The segmental rotor machine has been shown to offer increased magnetic flux – linkage over the other machines. It has an identical winding pattern and very similar copper mass to machine B, but each phase needs to conduct for only one third of a

cycle. It can deliver 24Nm of torque with only 260W of loss, which is well within the steady state thermal capability of the machine.

If the three machines are viewed in terms of torque capability for a given loss, then for 300W of winding loss (about 100 degree rise without forced ventilation); machine A can deliver 18.4Nm, machine B 22.0 Nm, and the new segmental machine 26.1 Nm. Fig. 6.11 shows how these gains are apparent over a wide range of winding loss values.

Two factors are dominant when comparing the torque capability of the machines.

1. The MMF capability of the segmental SRM is reduced because of the additional length of the end-windings. The fully pitched windings increase the length of each turn by approximately 55%. For both machines to have the same winding loss this corresponds to a reduction in MMF capability to $\sqrt{1/1.55}$ =80% of the conventional toothed-rotor SRM.
2. Each turn of the segmental winding SRM links the flux of two stator teeth and is therefore has approximately double the flux-linkage of the conventional SRM.

The combination of the above results in 40% more torque in the segmental machine. Note however that there will be additional space and extra copper cost resulting from the long end-windings.

6.3.4 Measurement of Flux-Linkage Characteristic

A range of experimental methods may be used for measurement of the flux-linkage characteristics [182-186]. These include:-

1-Direct measurement using magnetic sensors that measure the flux inside the motor. This method is not usually applied, as it is very expensive. It requires sensors to be installed when the motor is assembled, thus complicating the motor design. Furthermore, any one sensor can only give the flux density at one location, rather than the desired mean flux-linkage of a coil.

2-Measurment of inductance using ac bridge methods. However, these are limited effectively to low-power rated machines, since they require additional equipment to superimpose an ac signal onto a large dc current that must be passed through the

phase winding. At each angle a number of measurements must be made, which makes the procedure time consuming.

3-Measuring the flux linkage indirectly: The preferred method of obtaining the motor's magnetisation characteristics is to indirectly measure the stator flux linkage from voltage and current measurements on the phase winding circuit. In these methods, a voltage source is applied to the phase winding, and the terminal voltage and current are measured. If the phase resistance is known, then the flux linkage can be found from integration of the voltage.

In most integration techniques, the general principle is to apply a voltage pulse to the motor winding with the rotor clamped to some fixed position. The current will rise up to some level, and then the voltage is turned off. Through this time, integration takes place to determine the instantaneous flux linkage, and, in practice, analogue or digital integration can be employed.
These latter, locked rotor tests were undertaken to determine the flux-linkage variation with current and position. A step change in voltage was applied to the winding of a single phase and the current waveform measured. From integration of the difference of the applied voltage and the resistive drop the flux-linkage was then determined and is illustrated in Fig. 6.12 & Fig. 6.13.

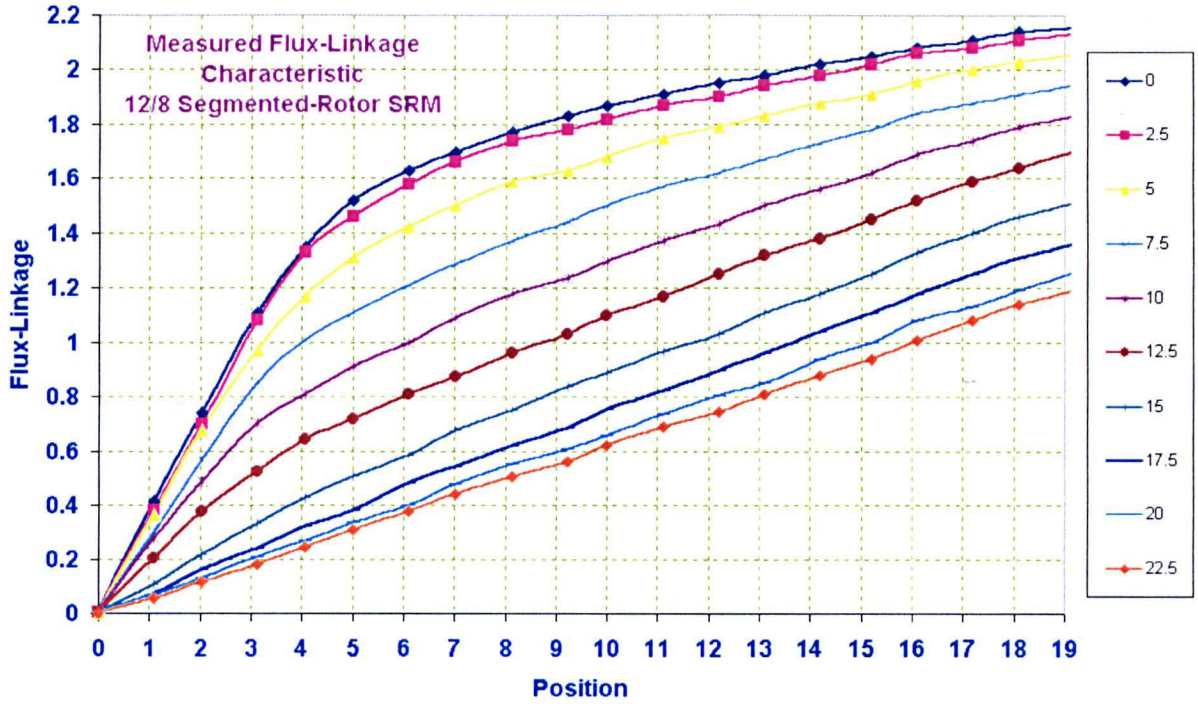

Fig. 6.12 Measured Flux-Linkage Characteristic of the 12/8 New SRM versus the Current

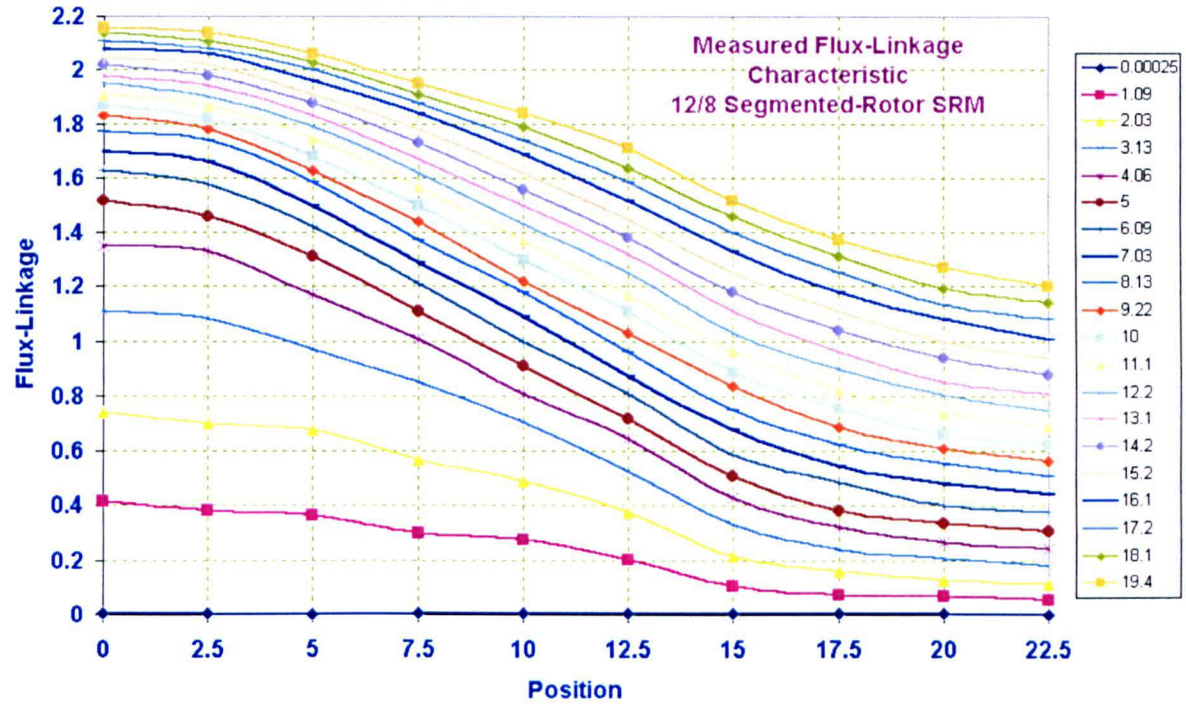

Fig. 6.13 Measured Flux-linkage curves as a Function of Current for a Single Phase in Steps of Equal Angle, Running from the Unaligned Position to the Aligned Position

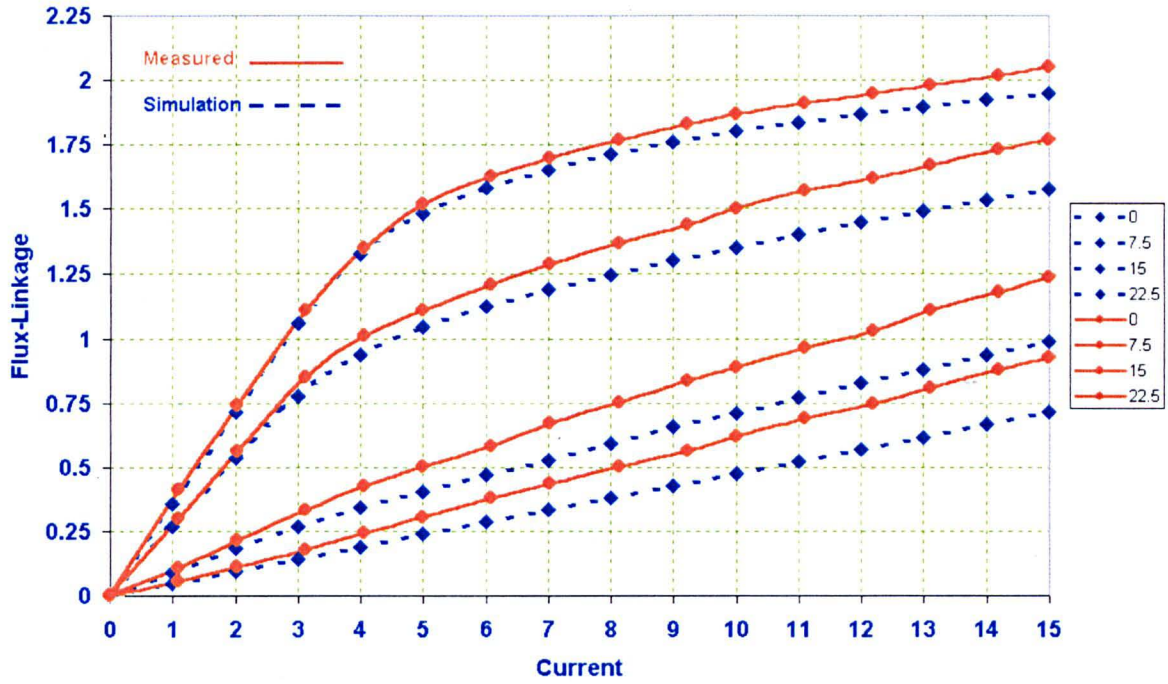

Fig. 6.14 Comparison between the Measured and Simulated Flux-Linkage Characteristic

Fig. 6.14 shows a direct comparison between measured flux-linkage curves and those predicted using two dimensional finite element analysis. The measured curves are of similar form to the predicted ones, but display an increased flux-linkage, particularly in the unaligned position. This is a direct result of the end-winding leakage inductance, which has not been included in the two-dimensional finite element model. Since the end windings are relatively long this effect is significant.

6.4 Conclusions

The chapter presents the design details of the first prototype of the segmented-rotor SRM. A three phase version has been built and tested. Torque has been measured as a function of both current and position, showing good agreement with predictions. Comparisons with a conventional switched reluctance machine of the same outside diameter and core length has shown a 41% increase in torque per unit copper loss at thermal limit. The increased end-winding length requires more copper and so the torque per unit copper mass is not increased. Measured flux-linkage characteristic were well predicted but show some differences due to the end-winding effect not being included in the two dimensional finite element model. The greatest difference

between measured and predicted Flux-Linkage curves occur in the unaligned position where the phase end-effects are most significant.

7 Building and Static Testing of the 12/10 Segmented Rotor SRM Prototype

7.1 Introduction

A three phase rotating demonstrator has been designed in accordance with the rules developed in chapter (4). The machine has twelve stator teeth, with six coils (two per phase), wound round every other tooth. The rotor comprises ten magnetically isolated segments. This chapter briefly describes construction of the machine and then presents the results of static tests.

7.2 Machine Construction

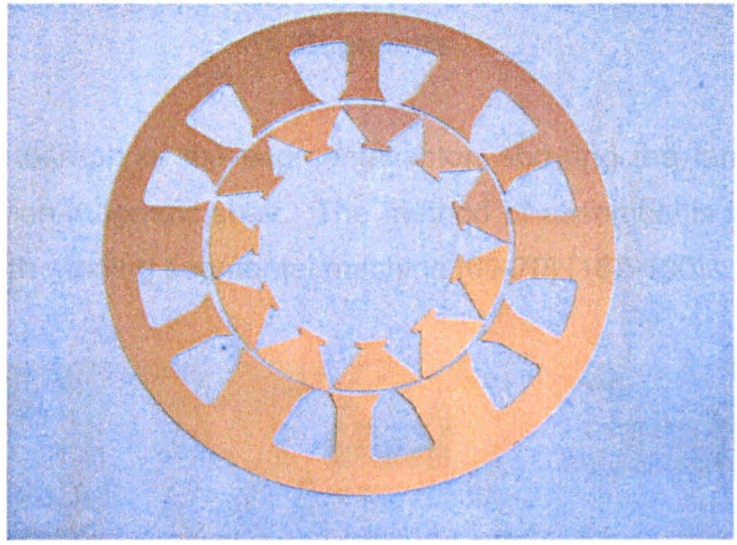

Fig. 7.1 One Set of Stator and Rotor Laminations before Assembly

Fig. 7.1 shows the cross section of the new 12/10 segmented-rotor short pitched SRM. One stator lamination and ten rotor segments are shown.

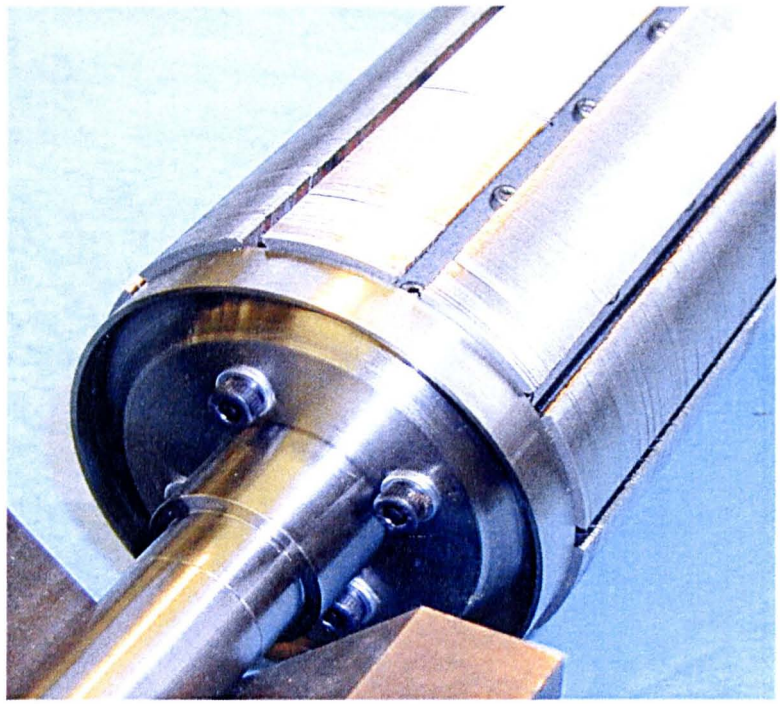

Fig. 7.2 Rotor of the 12/10 Single Tooth SRM, Showing the Individual Rotor Segments

Fig. 7.2 is a photograph of the segmental rotor, showing the laminated segments mounted onto a non-magnetic shaft. The method of assembly is identical to that of the 12/8 multi tooth winding segmental machine [69-70] [187-190].

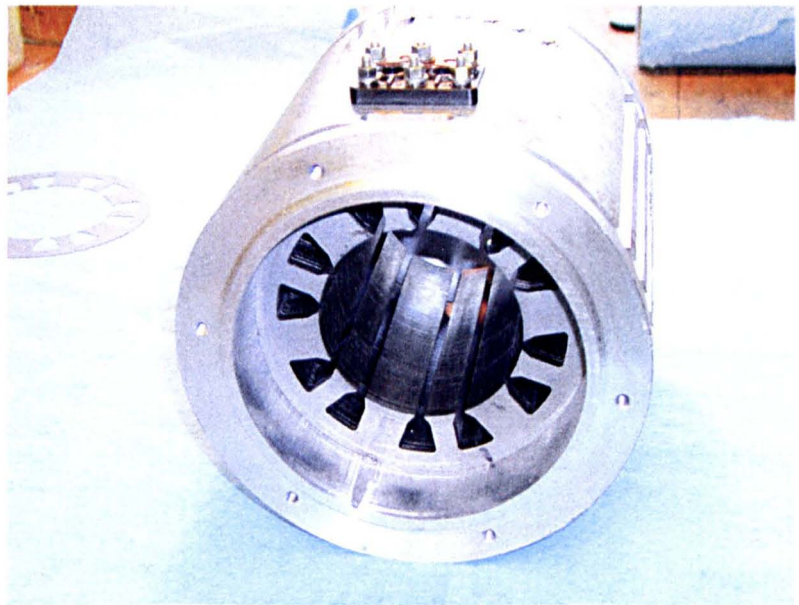

Fig. 7.3 Casing fitted with the Stator after welding the Stator Laminations Together

Fig. 7.3 shows the casing of the new SRM, it was heated to expand then the welded stator laminations was inserted inside it. The casing was then left to cool so it shrink fitted the stator laminations.

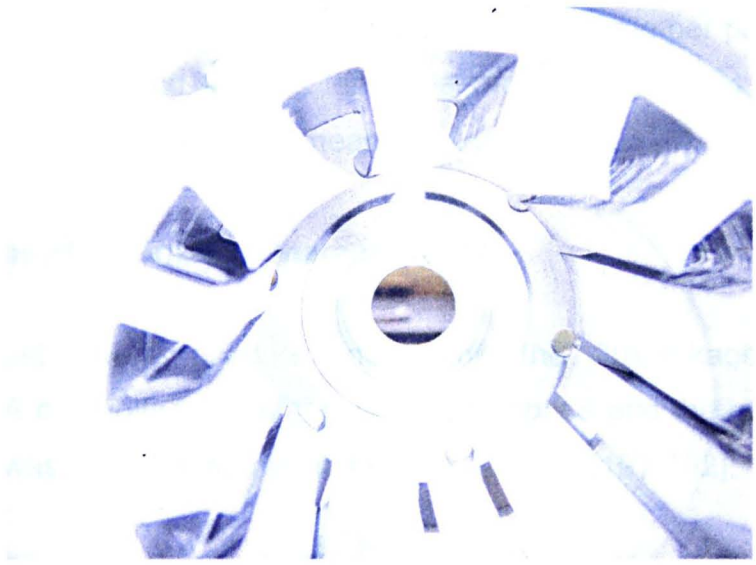

Fig. 7.4 Fixing the Bearing within the Stator

Fig. 7.4 and Fig. 7.5 are photographs of the single tooth winding stator, clearly showing the winding arrangement, with each coil wound around a single tooth, and only every other tooth wound. [122-124].

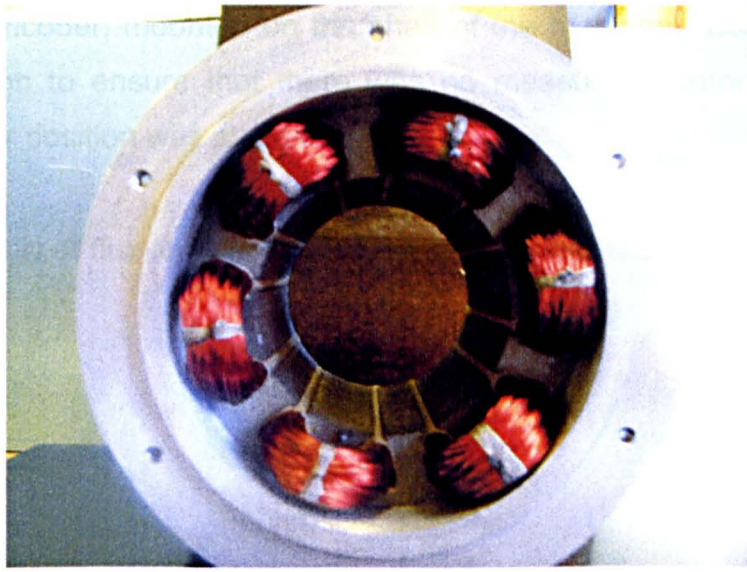

Fig. 7.5 Close up of the Stator of the 12/10 Segmental Rotor SRM, Showing the Non Overlapping Windings, Placed around every other Tooth

The machine was wound with 1.0mm diameter conductors, as in the multi tooth winding segmental SRM. The two machines have virtually identical slot areas but, because the effective slot fill factor fell from 0.46 to 0.41 there was a 10% reduction in the number of series turns per phase, falling from 300 turns per phase to 270 turns per phase. The mean end-winding length is reduced from 124 mm to 67 mm, resulting in a reduction of 20% in the mean turn length [122-124]

7.3 Measuring the Flux-Linkage Characteristic

Locked rotor tests were used to determine the flux-linkage-current-position characteristics. A d.c. voltage was applied to one phase and the current monitored. The flux-linkage was then determined using the equation [191-192]:

$$\psi = \int_0^t [V - iR]dt \qquad (6.1)$$

The resistance used in the above calculation was based upon d.c. resistance tests made at 20 degrees centigrade, giving a resistance of 2.56 Ω. During the test it was assumed that the temperature remained constant and that during the transient the effective resistance was unaffected by the changing magnetic field in the stator slots. The rotor was mechanically locked at one end and the rotor position monitored using a 12 bit digital encoder, mounted on the shaft of the machine. Locking of the rotor was good enough to ensure that there was no measurable rotor twist during the transient, so rotor position was constant.

The resulting family of flux-linkage/current curves is illustrated in Fig. 7.6

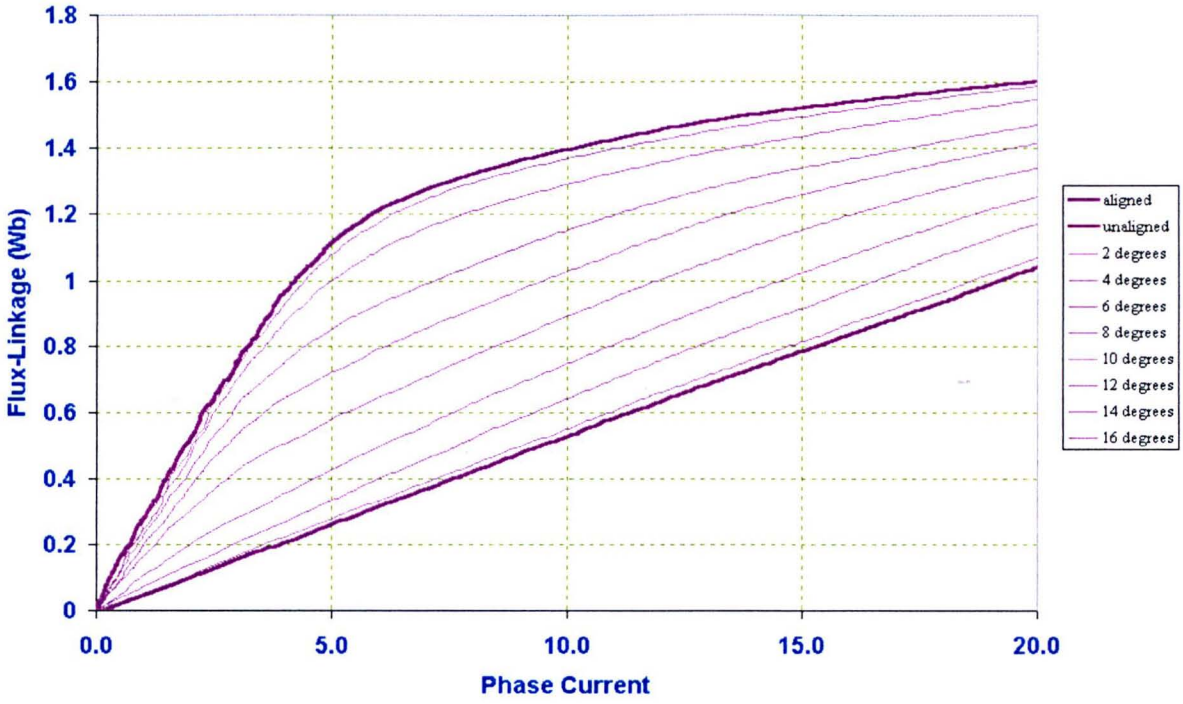

Fig. 7.6 Measured Flux-Linkage Curves for the 12/10 Single Tooth Prototype with a Single Phase Excited. Each Curve is at Constant Position, Running from the Unaligned to the Aligned Position in 2.0 Mech. Degrees Steps

7.4 Measuring the Static Torque Characteristic

The prototype machine has also been subjected to static torque testing. Once more the rotor was locked at one end, with a torque transducer placed between the locking plate and the rotor shaft, with the rotor position measured as above. Measured torque/position curves are shown in Fig. 7.7.

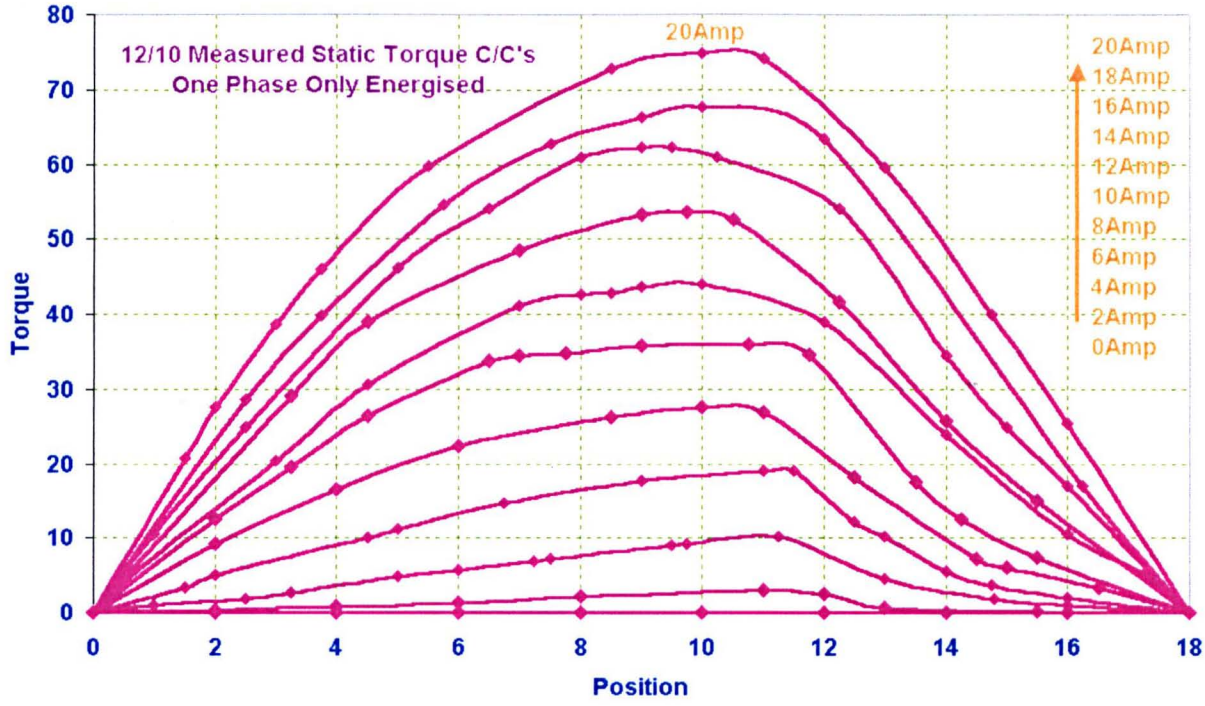

Fig. 7.7 Measured Static Torque Curves for the 12/10 Single Tooth Prototype with a Single Phase Excited. Each Curve is for a Constant Current, Rising in 2.0 Amp Steps to 20.0 Amp

At high currents the torque variation with position is almost sinusoidal in shape, in a manner consistent with conventional SRMs operating with high magnetic saturation. At low currents the machine is operating in a magnetically linear mode, and significant torque is produced between the aligned position and a displacement of 12 mechanical degrees, corresponding to one third of an electrical cycle. Once more this is typical of any SRM, but unlike conventional machines the torque profile is not flat within the torque producing region: it rises with displacement from the aligned position, producing a peak at approximately twelve degrees. This is because the permeance of a phase winding does not change linearly with position. This effect was also encountered on the multi tooth winding segmental SRM (see chapter (6)).

7.5 Comparison between Measured and Predicted Flux-Linkage Characteristics

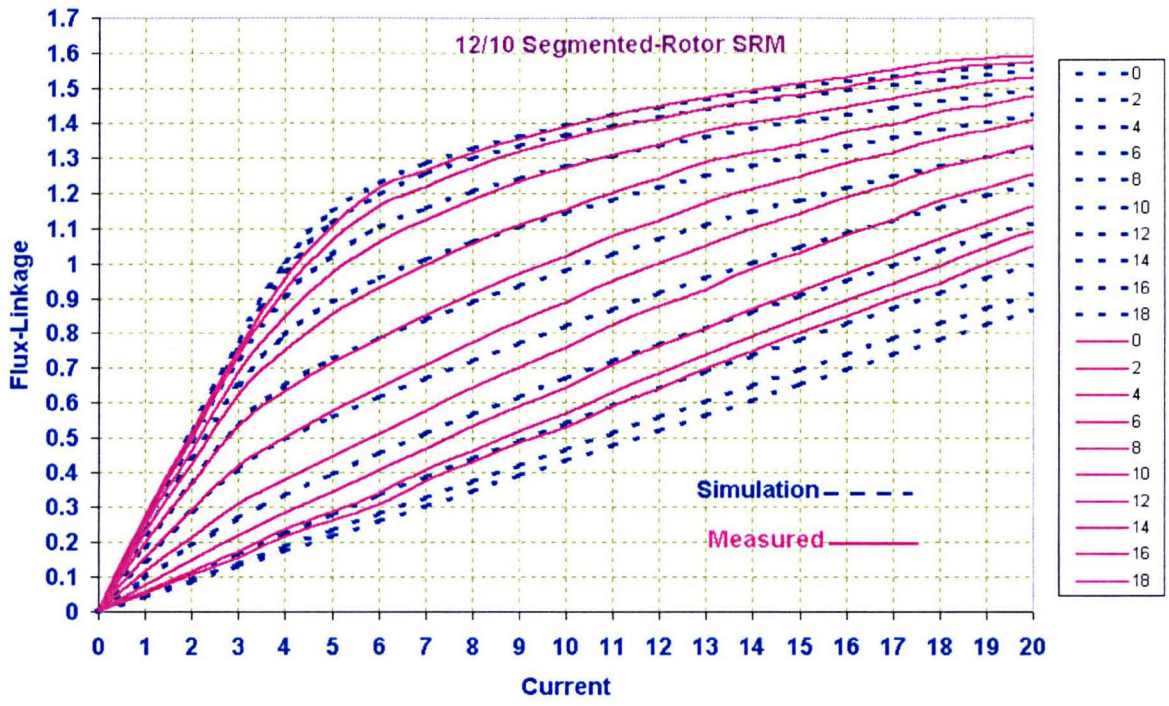

Fig. 7.8 Comparison of Measured and Predicted Flux-Linkage Characteristics (predicted values shown dashed)

Fig. 7.8 compares the measurements with those predicted using two dimensional finite elements. The measured and predicted curves for the aligned position are within 2% of the peak flux-linkage, but the predicted unaligned flux-linkage is 17% less than the measured value. Predicted values take no account of end-winding leakage inductance, and this is judged to be the major cause of this error. This leakage component is also present in the aligned position, but is reduced in its influence at high excitation currents by saturation of the machine core [192-193].

7.6 Comparing the Predicted and the Measured Torque Characteristic

Finite element analysis was also used to predict the static torque performance indirectly from the flux-linkage curves. Comparisons with measured values are shown in Fig. 7.9 for different excitation levels.

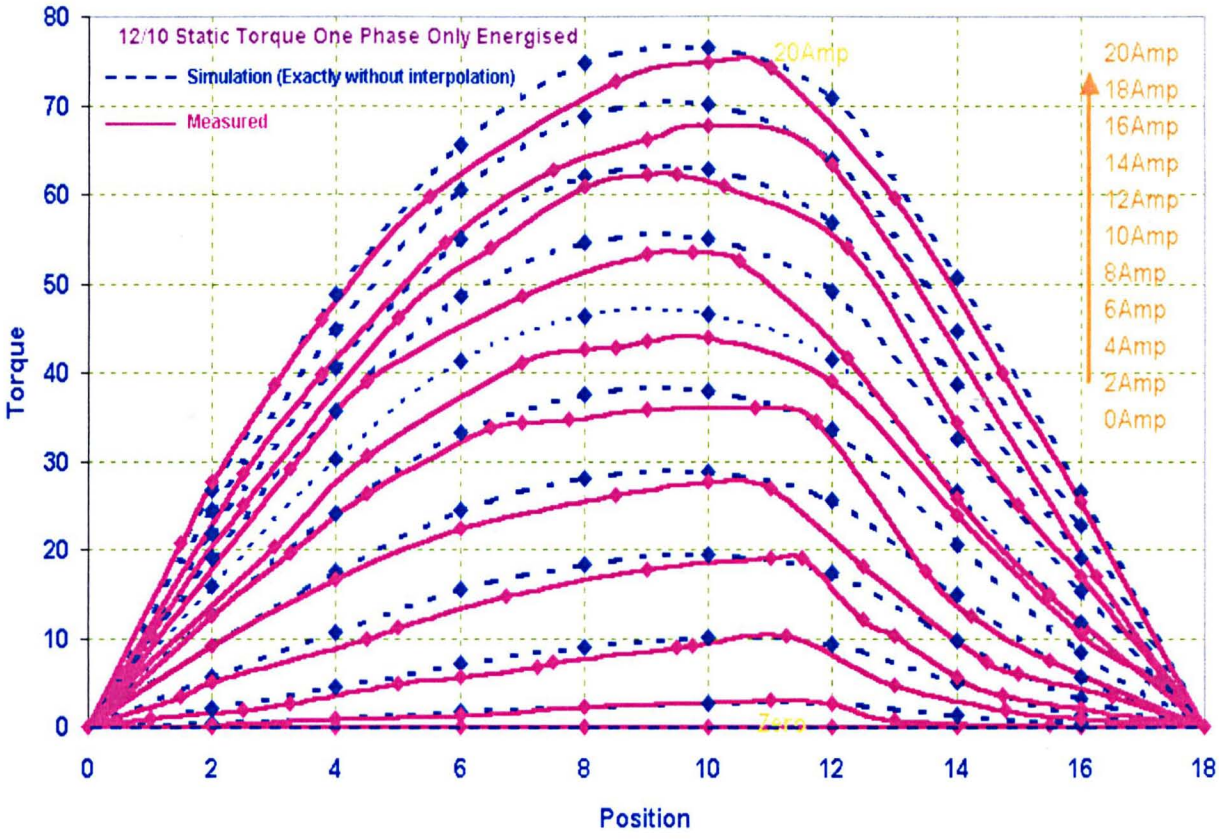

Fig. 7.9 Comparing the Static Torque Characteristic

In all cases the agreement between predicted and measured values is good, with the predicted torques having the correct shape of the torque profile, but typically overestimating the torque produced by 5%. This is a direct result of underestimating the unaligned permeance, as discussed above [194-195].

7.7 Thermal Test Results

The machine was subjected to thermal testing whilst both static and when running at constant speed under current control, fed from an asymmetric half bridge inverter. Static test results indicated that a loss of 542 watts in the winding corresponded to an overall temperature rise of 100 degrees centigrade, of which 52% was due to the convection drop at the casing surface and 48% to a conduction drop in the winding and core. Fig. 7.10 shows results taken from running tests with a r.m.s. current of 4.38 Amps at a speed of 512 rpm, corresponding to a winding loss of 177 W. This indicated that a winding loss of 370 W would give 100 degrees rise. The disparity

between static and running tests suggested that there are significant other loss mechanisms whilst rotating – these will include iron loss, bearing loss and windage. Note how, like the first prototype, the machine can be modelled by two thermal time constants; one of three minutes associated with conduction and one of 45 minutes associated with convection.

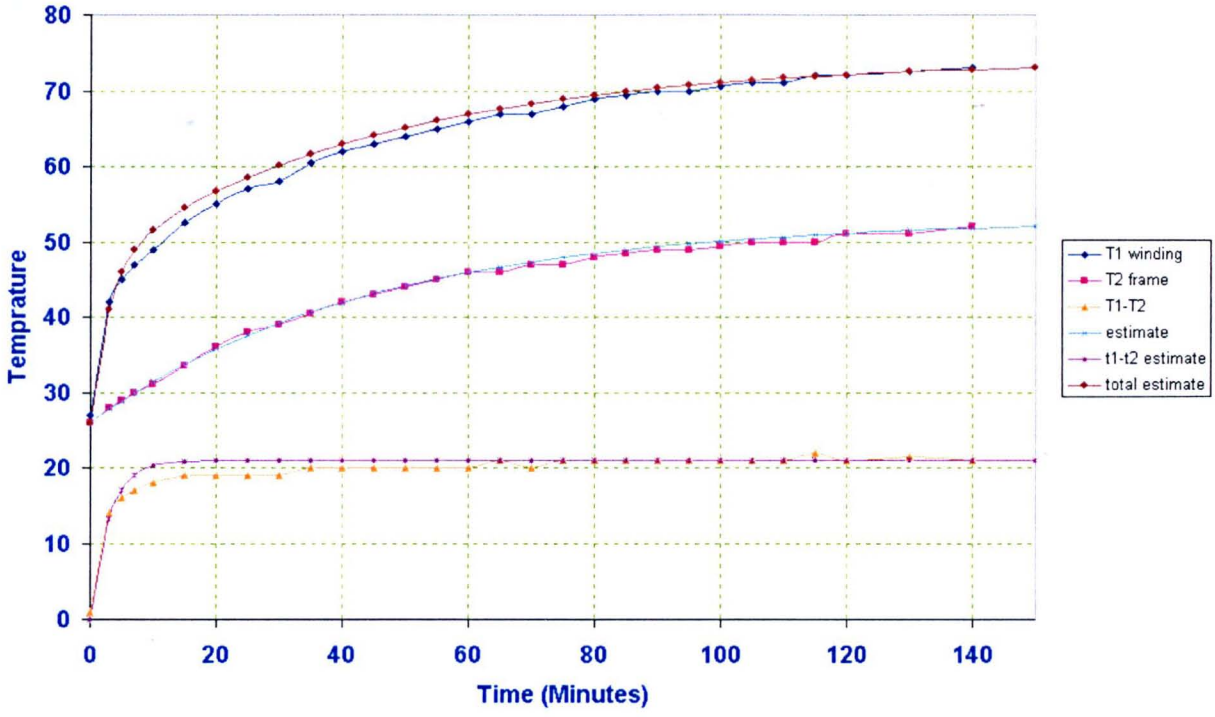

Fig. 7.10 Thermal Test

	Single tooth winding Segmental Rotor SRM	Multi Tooth Winding Segmental Rotor SRM	Toothed rotor SRM
Number of Phases	3	3	3
Number of Stator Slots	12	12	12
Number of Rotor Segments/teeth	10	8	8
Outside Diameter	150.0 mm	150.0 mm	152.6 mm
Stack Axial Length (rotor and stator)	150.0 mm	150.0 mm	150.00 mm
Rotor Outside Diameter	90.8 mm	90.8 mm	89.6 mm
Air-gap Length	0.3 mm	0.3 mm	0.25 mm
Stator Tooth Width	20.0/10.0 mm	11.93 mm (parallel sided)	12.05 mm at tip, with 12 degree taper
Arc of Stator Tooth Tip	30.25/18.5 degrees	22.5 degrees	15.0 degrees
Stator Core Back depth	10.00	11.9 mm	10.6 mm
Arc of Rotor Segments/teeth.	30.25 degrees	37.5 degrees	16.2 degrees
Number of Series Turns/Phase	270	300	204
Coil Span in Mech. Degrees	1 wide tooth: 36	3 slots: 90	3 slots: 90
Effective Wire Diameter	1.0 mm	1.0 mm	1.20 mm
Estimated turn length	435 mm	547 mm	591 mm
Slot fill-factor (copper area to overall slot area)	41%	46%	42%
Resistance per phase @ 20 degrees C	2.56	3.58 Ω	1.825 Ω

Table 7.1. Dimensions of the Prototype Machines and a Fully Pitched Winding Toothed Rotor SRM, used for Comparison.

7.8 Torque Capability

Based upon measured torque capability, Fig. 7.11 shows the mean torque produced as a function of winding loss for the prototype machine, alongside those for the multi tooth winding segmental SRM and two conventional SRMs, one with short pitched windings and one with fully pitched windings, detailed in table 7.1. All four machines have the same outside diameter and lamination stack length and all results are based upon measured static torque performances. For the purposes of this comparison it is assumed that each machine is operating under current control with one phase conducting at a time. Throughout the phase conduction period the phase is assumed to conduct a constant current and the torque output is based upon the mean measured torque over the period of conduction. Losses presented are based solely upon winding losses, using the winding resistance of each machine when running at an average winding temperature of 100 degrees centigrade.

At all loss levels the segmental machines produce substantially more torque than the conventional SRMs. For 300W of winding loss, which is comfortably within the thermal limit of all four machines, the conventional SRM produces 18.4 Nm, the fully pitched winding conventional SRM 22.0 Nm, the multi tooth winding segmental SRM 26.1Nm and the new single tooth winding segmental SRM 26.5 Nm. Hence, in broad terms the single tooth winding segmental machine is producing the same torque as the multi tooth winding segmental machine. Whilst it has the same core volume as the earlier segmental design, it is achieving the same performance with only 71% of the copper volume [122-124][196].

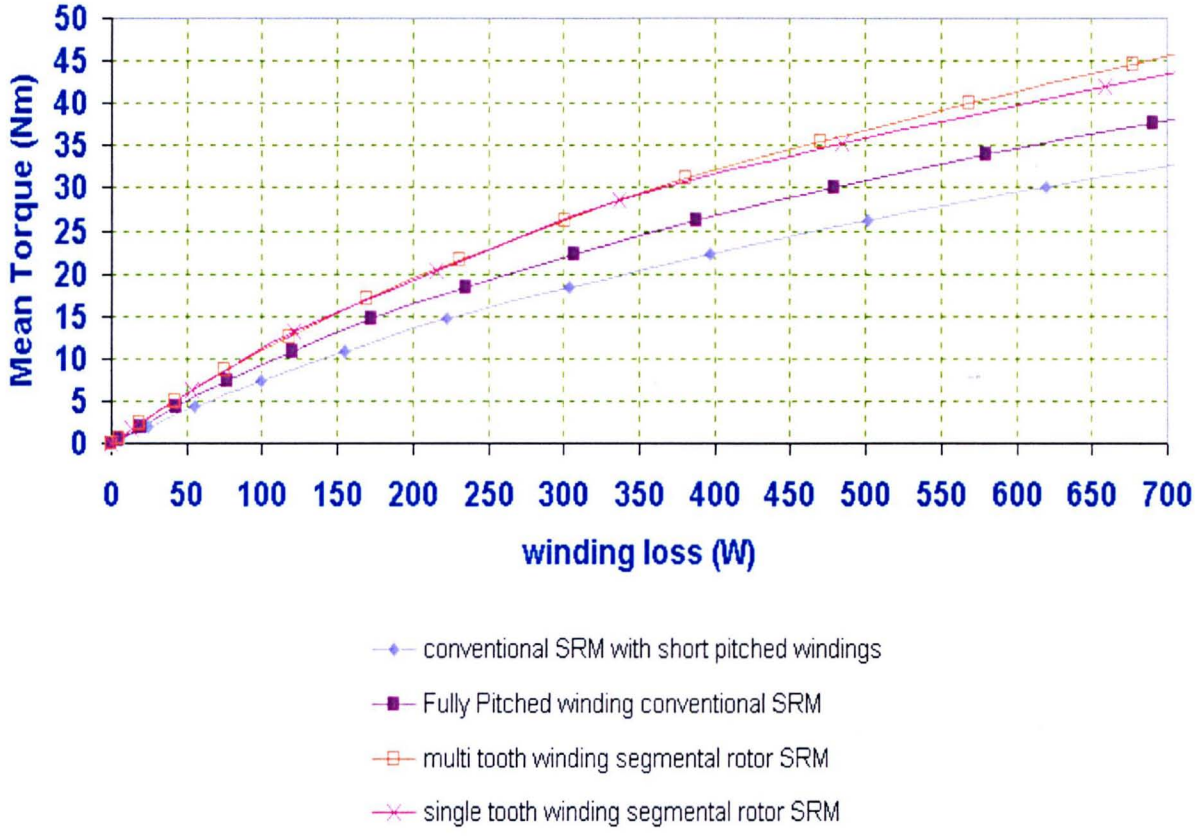

Fig. 7.11 Mean Torque Production as a Function of Winding Loss for Conventional and Segmental SRMs, assuming Perfect Current Control with each phase Conducting for one Third of a Cycle. (Winding Temperature of 100 Degrees centigrade)

7.9 Conclusion

A novel design of switched reluctance motor, combining a segmental rotor with short pitched windings has been built and extensively tested. Measured torque and flux-linkage characteristics have been compared with those predicted using the finite element method. The concept enables a large increase in the flux linking each turn of the machine, thereby creating a large increase in torque density. The machine delivers 44% more torque than a conventional SRM and equals the torque capability of the previous segmental SRM design in which the windings span three teeth, whilst using 29% less copper volume. In comparison to the earlier segmental design the windings are used more efficiently because of the shorter end-winding length, but the magnetic performance is reduced: these two effects approximately balance out to give equal torque capability.

The design offers an advantage over segmental rotor SRMs, with windings spanning multiple teeth, due to the short length of the end-windings. This makes the concept particularly suitable for machines of a relatively short axial length and removes this limitation of the earlier multi tooth segmental designs.

8 Mutual Interaction between Phases

8.1 Introduction

The chapter investigates the mutual interaction between phases in the new segmented-rotor SRM with two different modes of operation. First, when the motor operates with switched excitation in one phase and the second phase has a fixed MMF. Second, when the motor operates with two phases excited simultaneously. These two modes of operation are sometimes used in the conventional SRM to increase the output torque and decrease the torque ripple. In addition, the chapter tests these modes with the different possible connections in the short pitched segmental SRM. Mutual inductance between phases can increase or decrease the output torque according to the level of saturation in the teeth used by the two phases, so the flux density in the teeth between the phases is investigated.

8.2 Testing the12/8 Segmented-Rotor SRM

8.2.1 Simulating the Machine when there is a Fixed MMF in another Phase

In practical operation there is often overlap of conduction between phases, and so it is necessary to determine whether the presence of current in one phase affects the characteristics of the other phases. In this section the 12/8 machine is simulated using finite elements; one phase is excited whilst a fixed MMF is maintained in the second phase. There are three things to be examined here [144][197-199]. First, will the motor give significant output torque or will the torque production collapse? Second, is the value of torque more or less than the case of no MMF in the second phase? Third, what is the impact of the polarity of this MMF on the output and the characteristics?

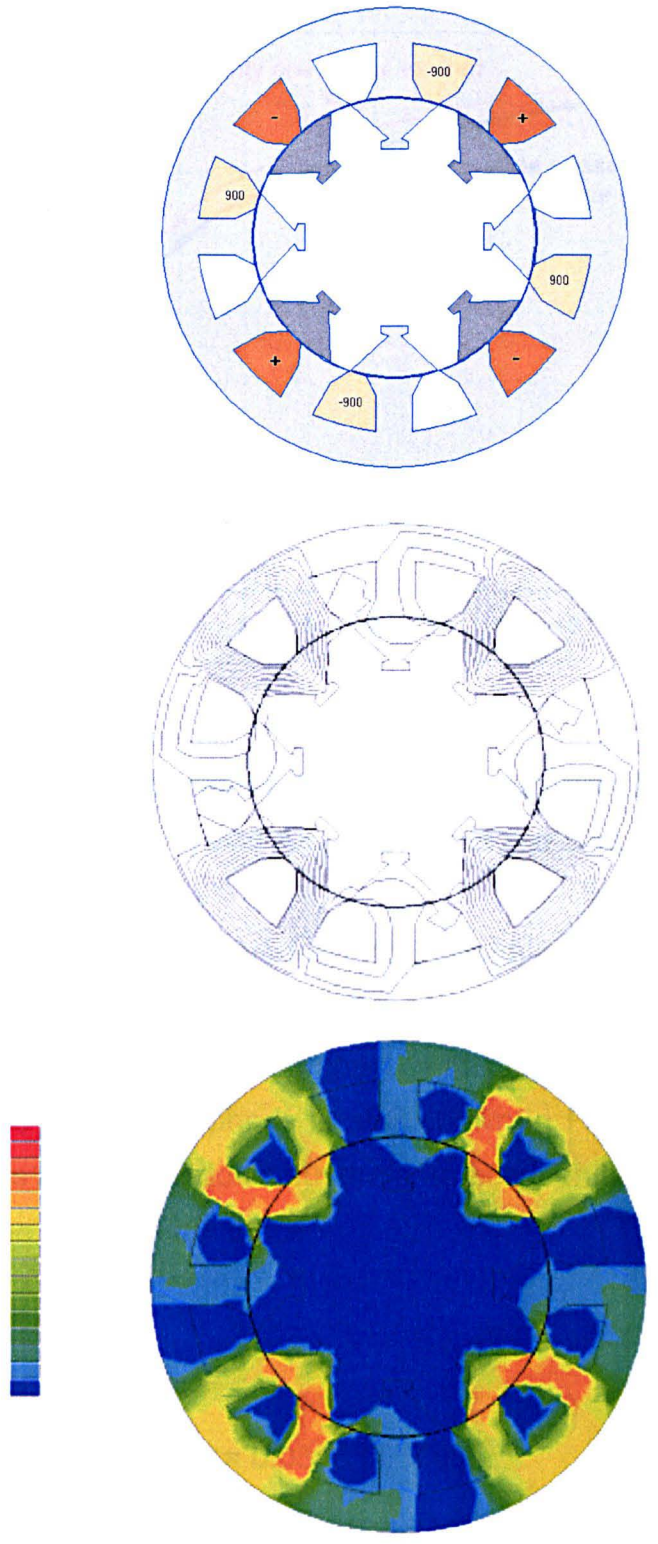

Fig. 8.1 (a) Excitation of one Phase Whilst a Second has Fixed MMF, Showing the Magnetic Flux Plot and the Flux Density Distribution

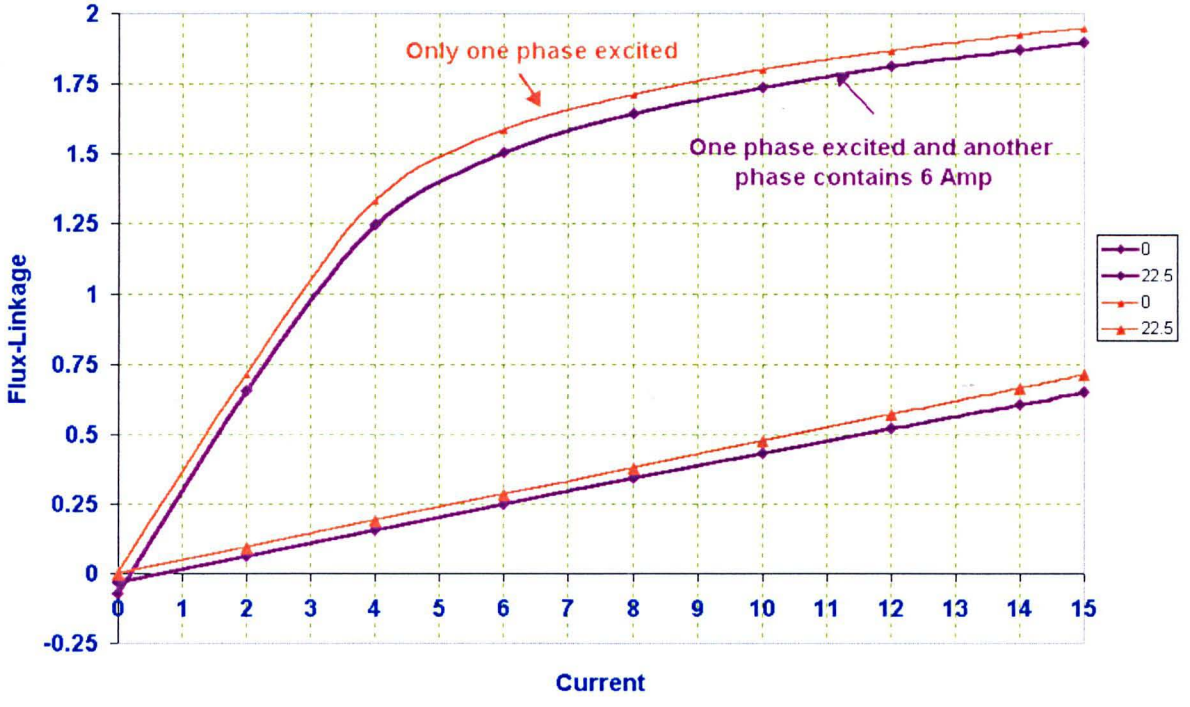

Fig. 8.1 (b) Impact of Operating the SRM with Another Phase has a Fixed MMF of 900 Ampere Turns per Slot

Fig. 8.1 shows the 12/8 segmented-rotor SRM with one phase excited and the other containing a fixed MMF. The fixed MMF is selected to be 900 (equivalent to 6 Amps, a medium level of excitation). The impact of this fixed MMF in the second phase on the characteristic of the first phase is also shown in Fig. 8.1. The aligned and the unaligned curves are shifted down but the area between them remains the same.

Calculation of the mutual inductance:

$$M = \frac{\Psi_2}{i_1} = \frac{\Psi_2}{900/N}$$

N=150 conductors/slot.

The unsaturated Flux-Linkage = 0.0316 ($i_2 = 0$).

The saturated Flux-Linkage = 0.0702 ($i_2 = 0$).

M (unsaturated) =0.0316 = 5.26 mH

M (saturated) =0.0702/6=11.7 mH.

These values are less than 4% of the unsaturated self inductance in the aligned position.

Suppose the fixed MMF in the second phase has its polarity reversed. Does it have any more influence?

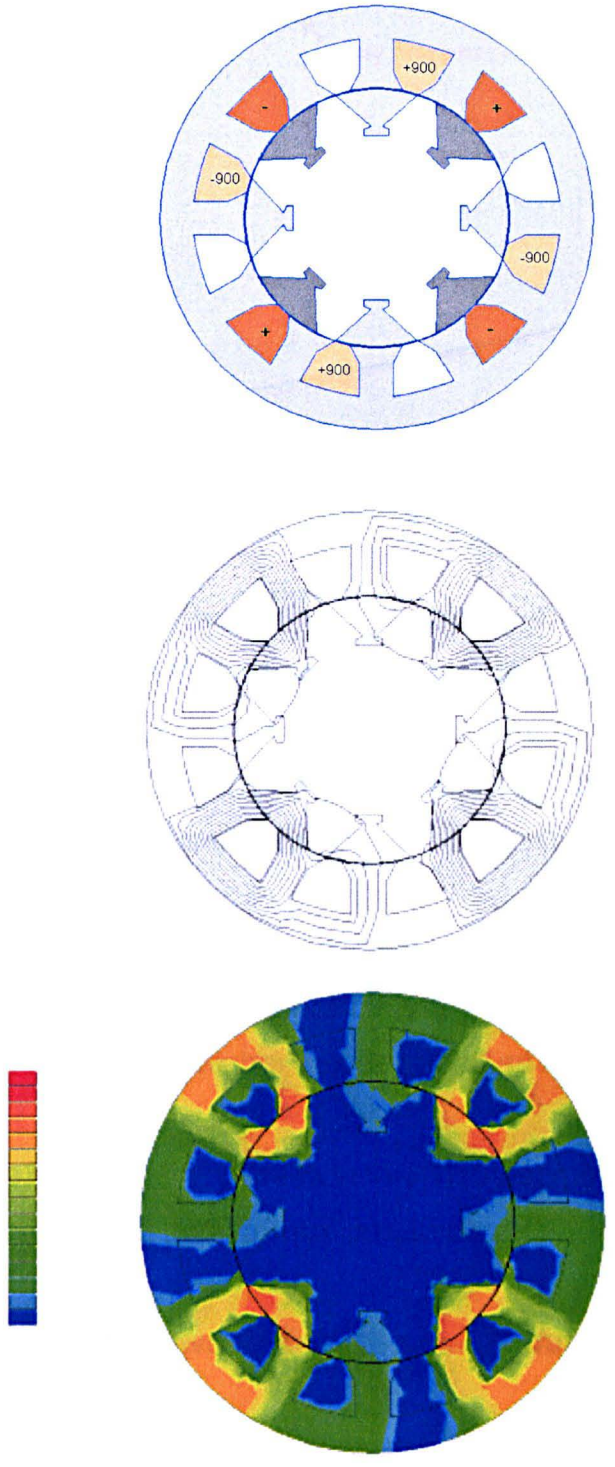

Fig. 8.2 (a) Excitation of one Phase Whilst a Second has Fixed MMF, Showing the Magnetic Flux Plot and the Flux Density Distribution

Fig. 8.2 (b) Changing the Polarity of the Fixed MMF shown in Fig. 8.1

Fig. 8.2 shows the impact of changing the polarity of this fixed MMF on the characteristic. The characteristic is shifted up.

The mutual inductances (saturated and unsaturated) for this reversed connection are unchanged. From the FE plot the flux density in the tooth used by the two phases in the second connection has slightly higher flux density than in the first.

The mutual inductance between the phases in this 12/8 segmented-rotor SRM is very low and has no significant effect upon torque production.

8.2.2 Testing the Machine with two Phases Excited Simultaneously

Occasionally an SRM may operate with two phases excited simultaneously for particular reasons, such as to minimise the torque ripple or to increase the mean output torque [197-202]. This section tests the same concept in the 12/8 segmented-rotor SRM.

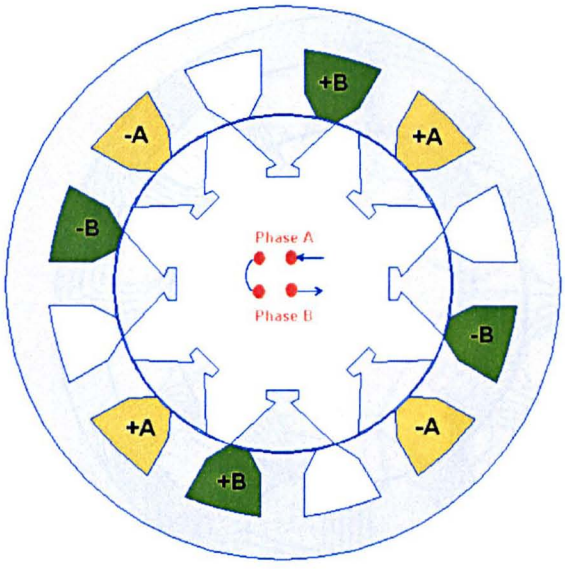

Fig. 8.3 Connection of the SRM

Fig. 8.3 shows cross section of the 12/8 segmented-rotor SRM with two phases excited simultaneously. Wiliest Fig. 8.4 (a-d) shows the magnetic the finite element results for this connection. The aligned and the unaligned characteristics do differ than those of the case of one phase excited only.

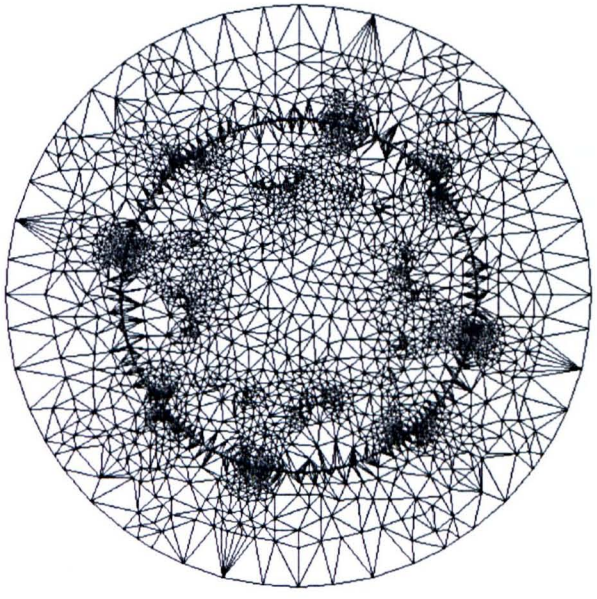

Fig. 8.4.a Adaptive Mesh for a Position between the Aligned and the Unaligned Positions

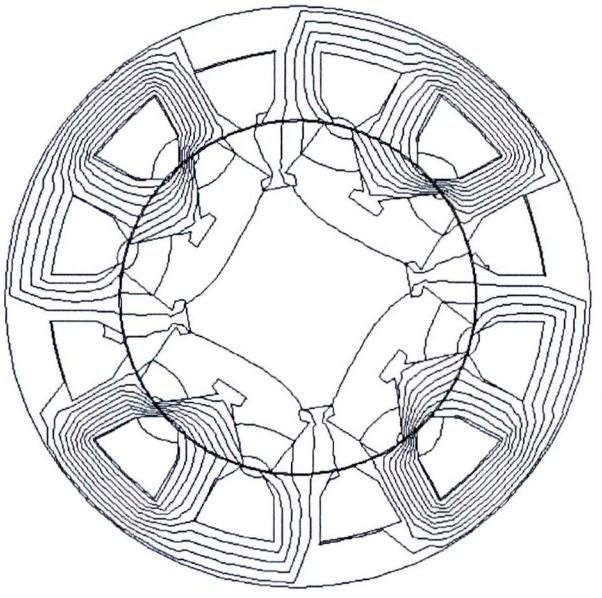

Fig. 8.4.b Flux Plot for a Position between the Aligned and the Unaligned Positions

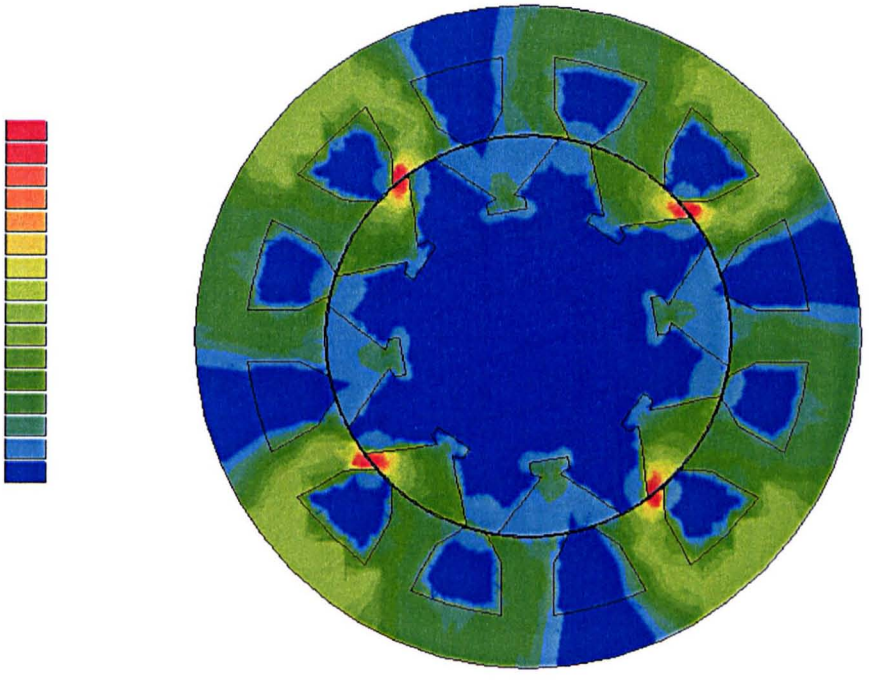

Fig. 8.4.c Flux Density Distribution

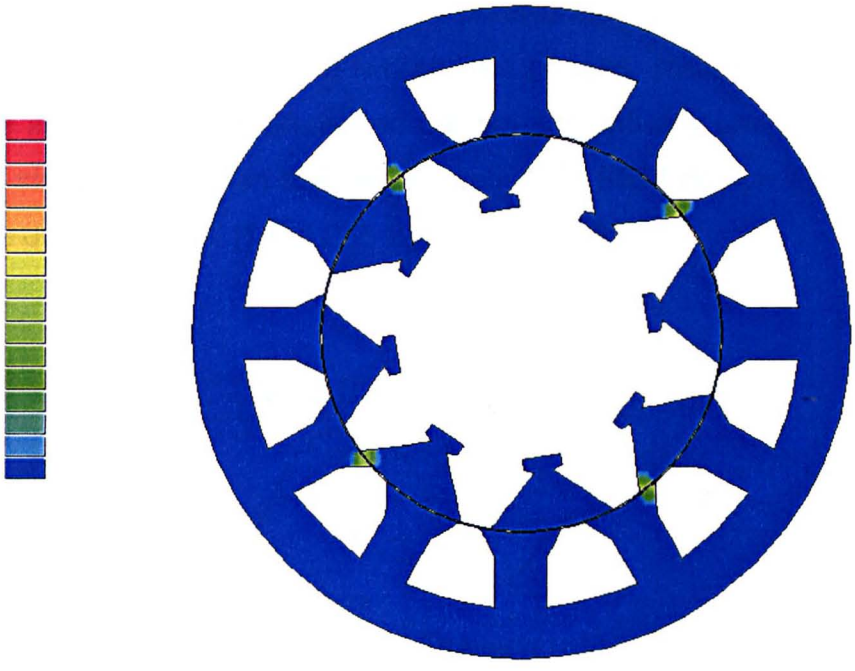

Fig. 8.4.d Saturation

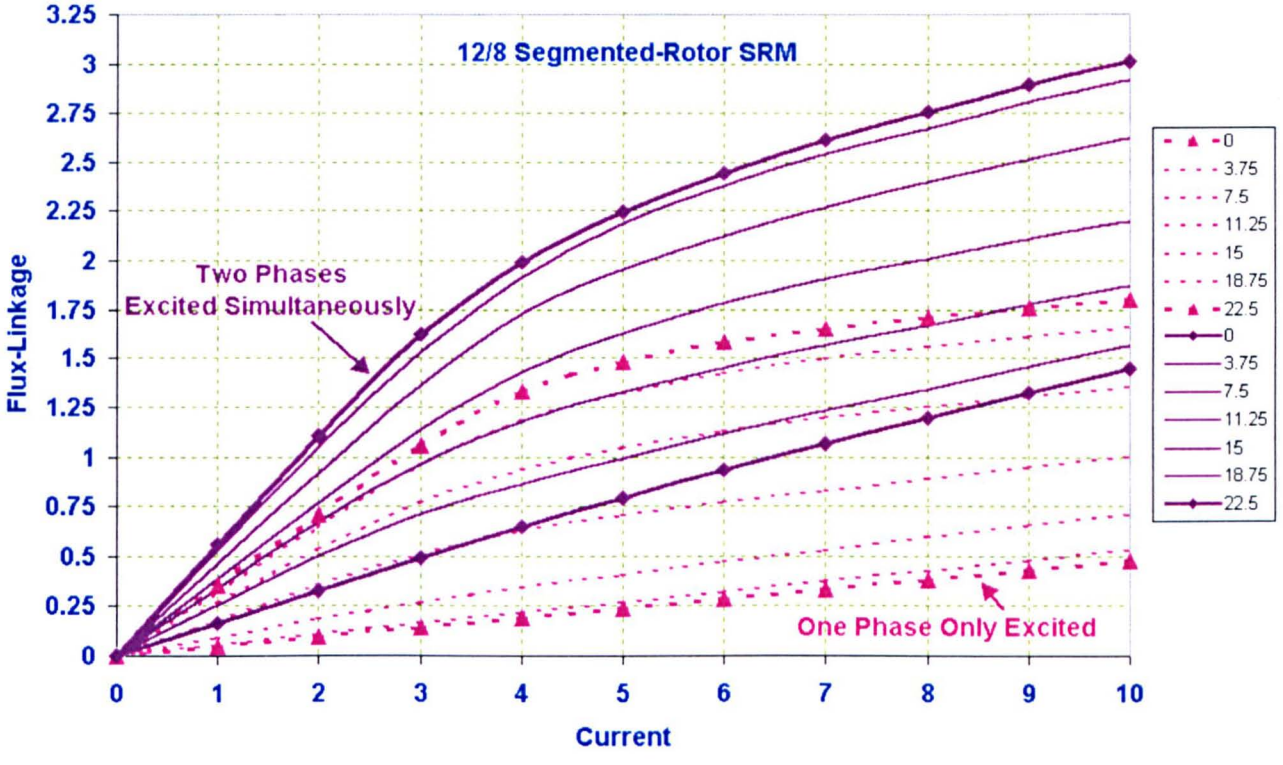

Fig. 8.4.e Flux-Linkage Characteristic when one Phase is Excited alone and when Two Phases are Excited Simultaneously

Fig. 8.4.e shows the impact of exciting two phases simultaneously: the characteristics shown are the sum of those of the two excited phases. Note how the area enclosed between the aligned and the unaligned positions is virtually unchanged. So exciting two phases simultaneously in this segmented-rotor SRM design does not appear to increase the output torque. [144][122-124][179][203-207].

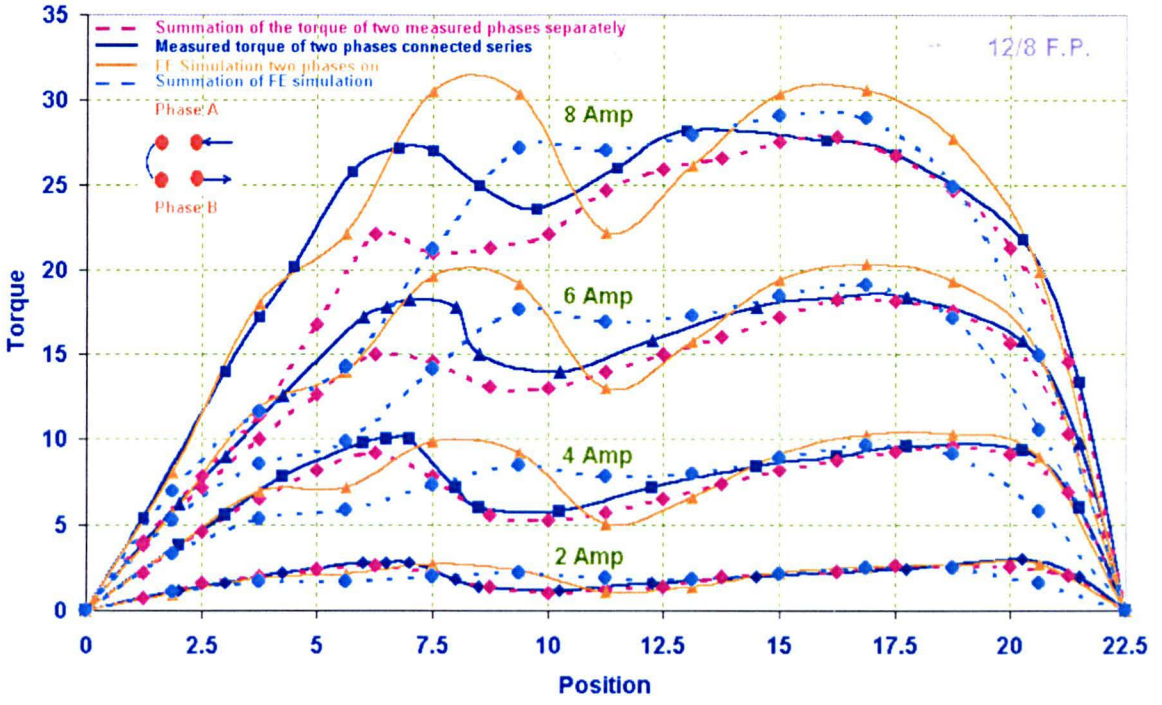

Fig. 8.5 Comparison between Simulated and Measured Torques Results when Two Phases are Excited Simultaneously (first connection).

So exciting two phases simultaneously in the 12/8 segmented-rotor SRM does not increase the output. However, Fig. 8.5 shows the torque ripples decrease when two phases are excited simultaneously. The torque characteristic became flatter than in the case of only one phase excited chapter (6).

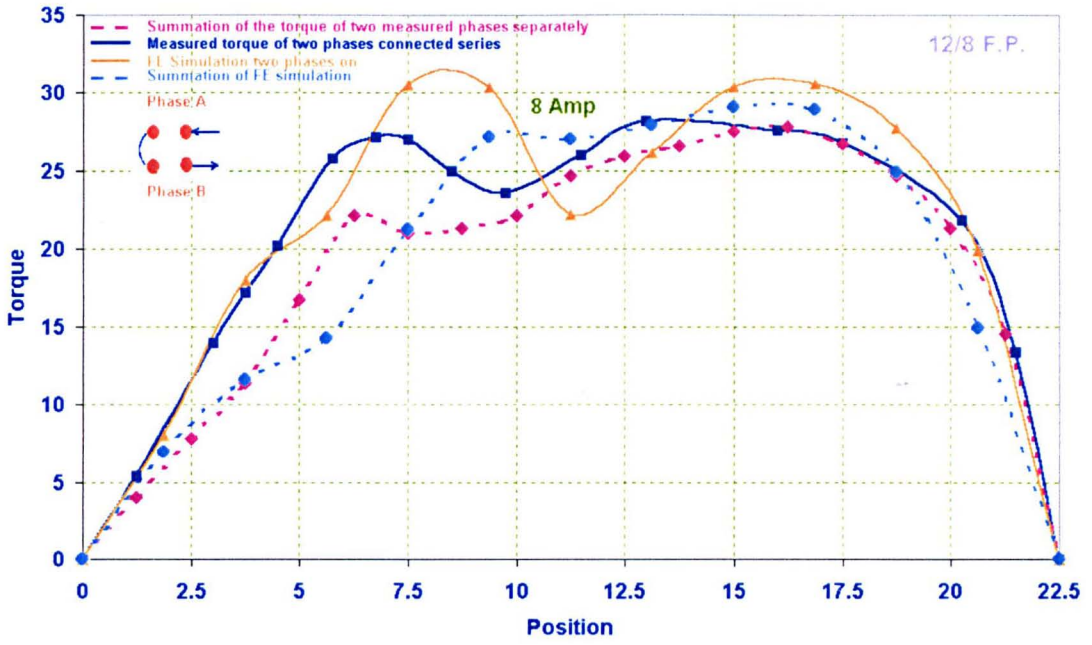

Fig. 8.6 Clarifying one Case of Fig. 8.5 at I=8 Amp

Measured and simulated static torques, first neglecting mutual coupling between phases and then including it (I=8 Amp)

The summation of the torque of two phases when each is excited alone (measured results or simulated results) does not include the mutual inductance effect. When two phases are excited simultaneously (measured results or simulated results) then this includes the mutual effects. The effect of the small value of the mutual coupling between the phases is shown in Fig. 8.6.

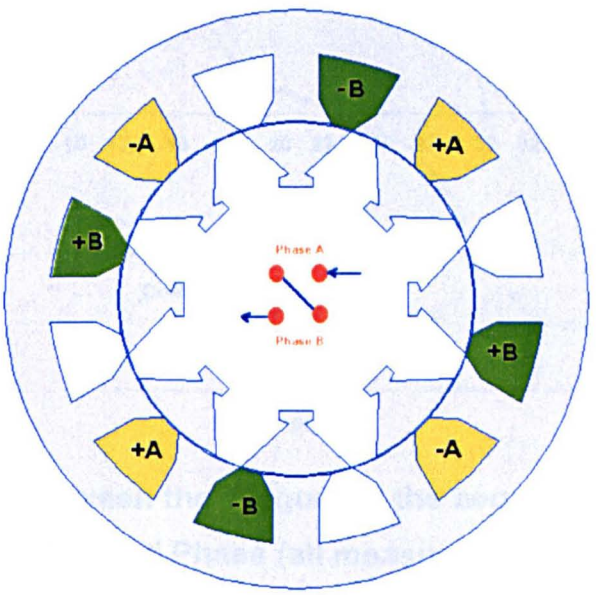

Fig. 8.7 Changing the Connection of the Second Phase

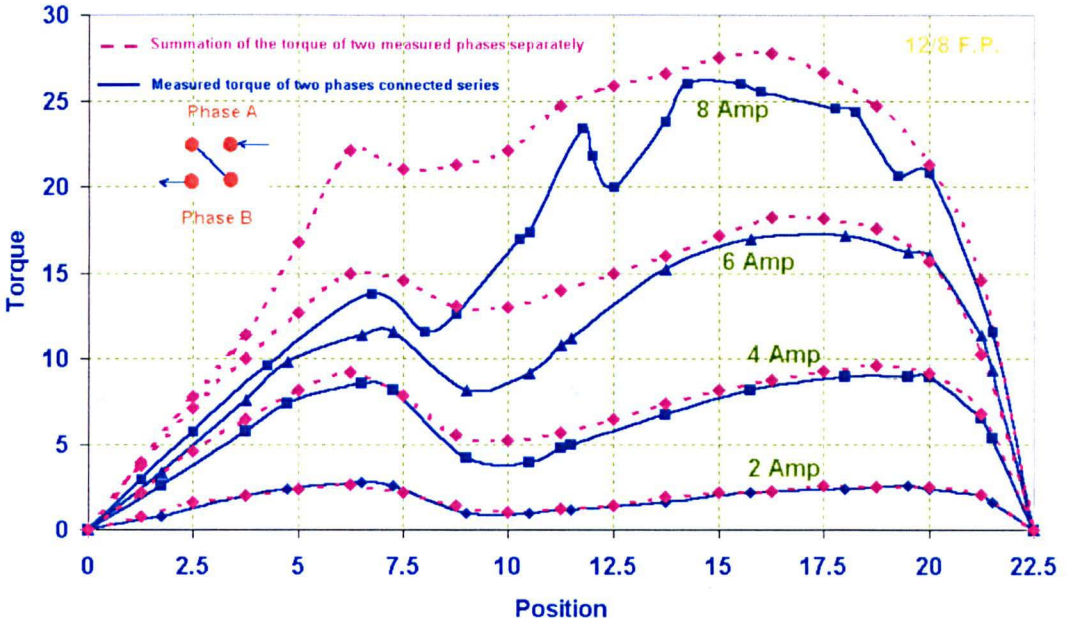

Fig. 8.8 The Impact of Saturation on the Torque for the Second Connection

Fig. 8.7 shows cross section of the 12/8 SRM when the polarity of one connection is changed and Fig. 8.8 shows the torque in this case. The saturation in the teeth between the phases has decreased the torque. So the first connection is best.

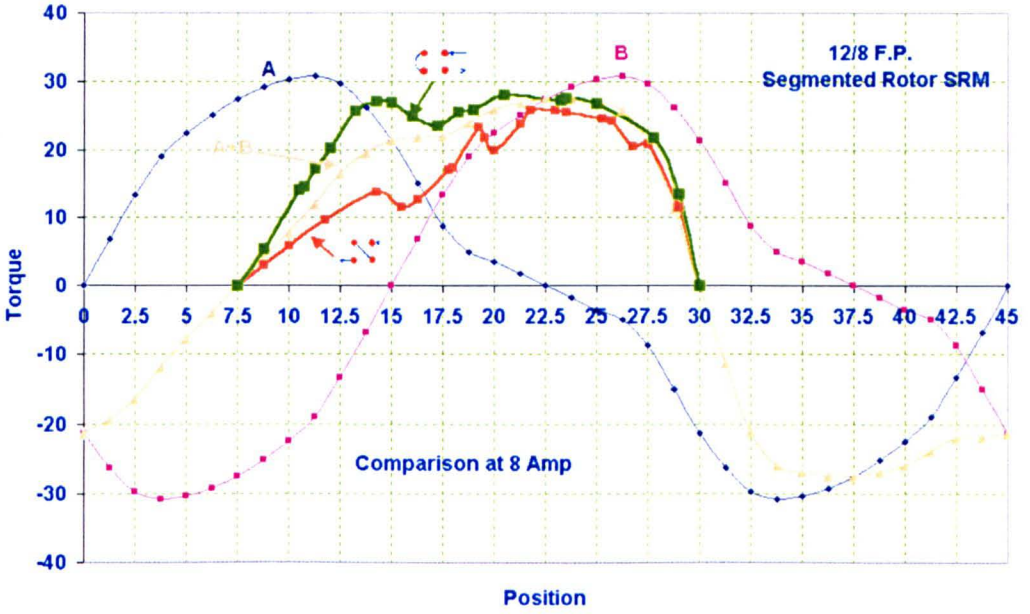

Fig. 8.9 Comparison between the Torque for the two Possible Connections of the Second Phase (all measured results)

Fig. 8.9 shows measured results of the torque for both the possible connections at a fixed current (8Amp) and compares the torque from the summation of two phases

each of them excited separately. The difference between the curves is due to the mutual coupling. For the first connection the torque is approximately that of the case with only one phase excited alone, but with less ripple. In second connection the torque decreased [197].

The importance of the polarity of excitation can be explained by considering the magnetic flux patterns. Two adjoining phases both use the tooth separating them in their flux path. When the two phases have current in the opposite direction (corresponding to connection 1) then the fluxes are in opposite directions and so saturation is actually reduced by the flow of current in two phases. When the phases both carry positive current then the fluxes add in the adjoining teeth, saturation is increased and torque is reduced.

8.3 Testing the 12/10 Short Pitched Segmented-Rotor SRM

The results of the first prototype may not be general since they depend on the construction of the SRM. So this section tests the short-pitched segmented-rotor SRM design for the same two modes of operation.

8.3.1 Testing the Machine when there is Fixed MMF in another Phase

This time the Fixed MMF is given a much higher value of 2700 ampere turns per slot to magnify any effect. This corresponds to 20 amps of fixed excitation in the prototype.

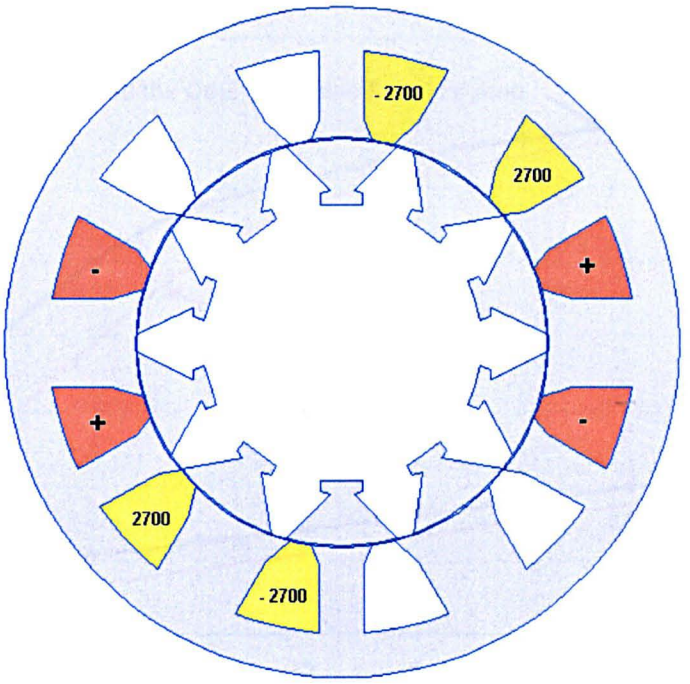

Fig. 8.10.a Cross Section of the 12/10 Segmented-Rotors SRM showing the Connection of the Fixed MMF in the Second Phase

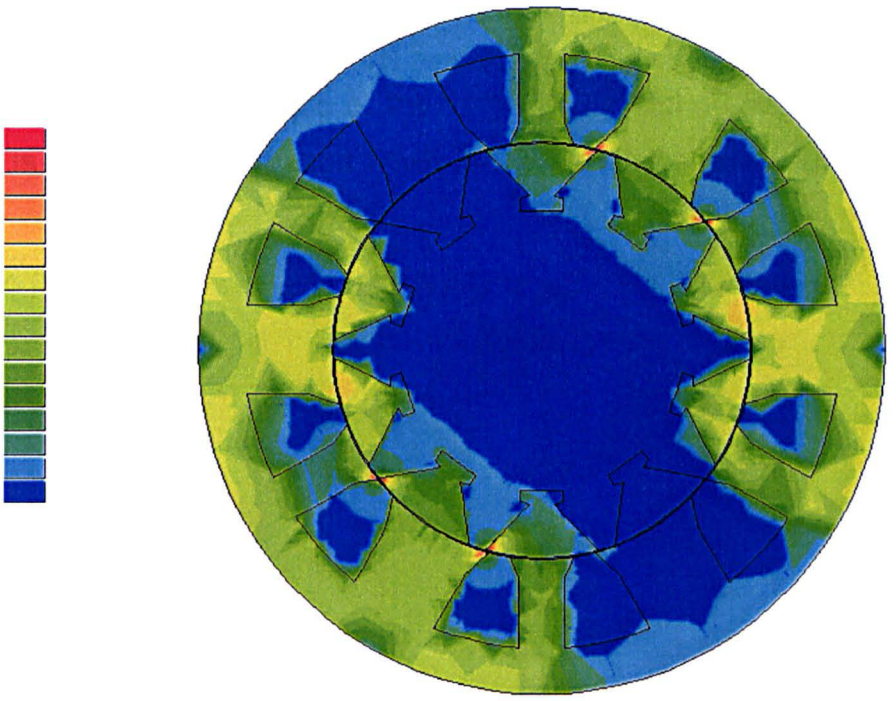

Fig. 8.10.b Flux Density when there is Fixed MMF =2700 in the second Phase

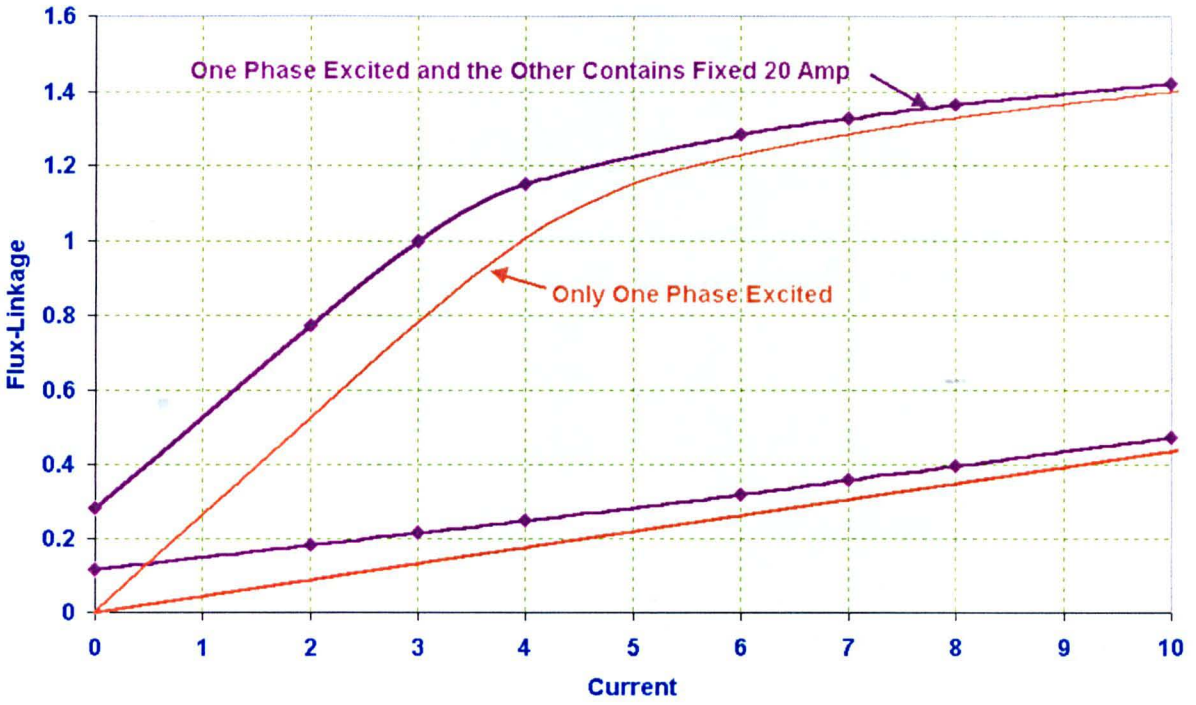

Fig. 8.10.c Comparing two Flux-Linkage Characteristics of the 12/10 SRM: when there is Fixed MMF in the Second Phase and when there isn't

Fig. 8.10 shows the characteristic of the 12/10 short pitched segmented-rotor SRM when there is a high value of fixed MMF in the second phase. The flux density is also shown.

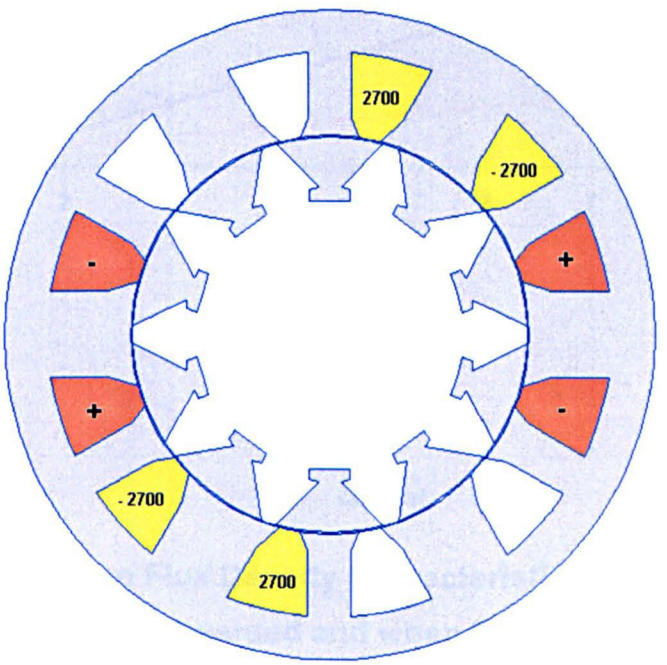

Fig. 8.11.a Connection of the Fixed MMF is Reversed

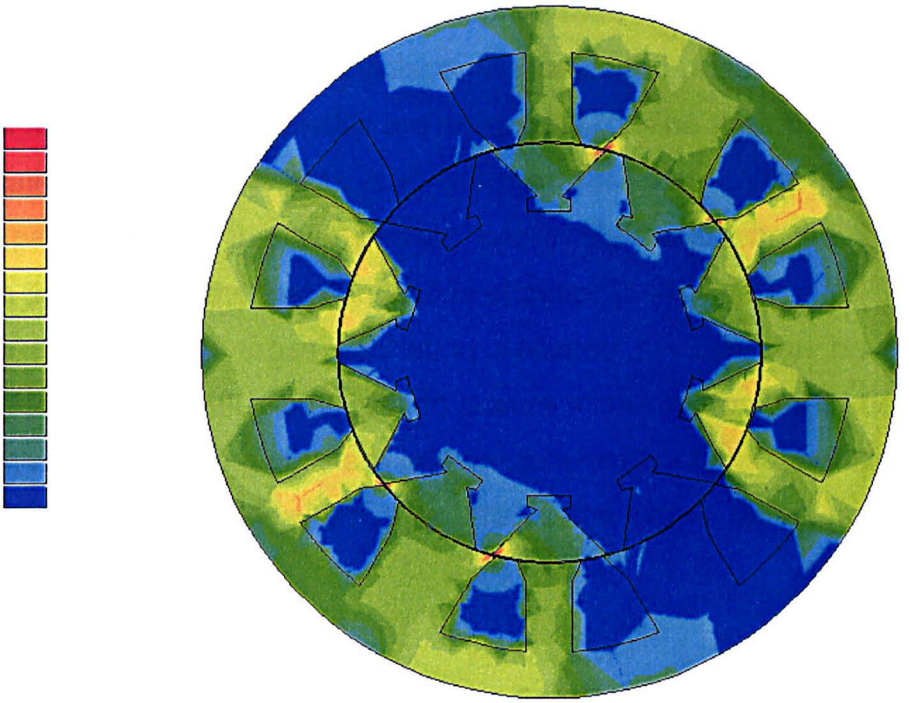

Fig. 8.11.b Flux Density Distribution of the SRM shown in Fig. 8.11.b

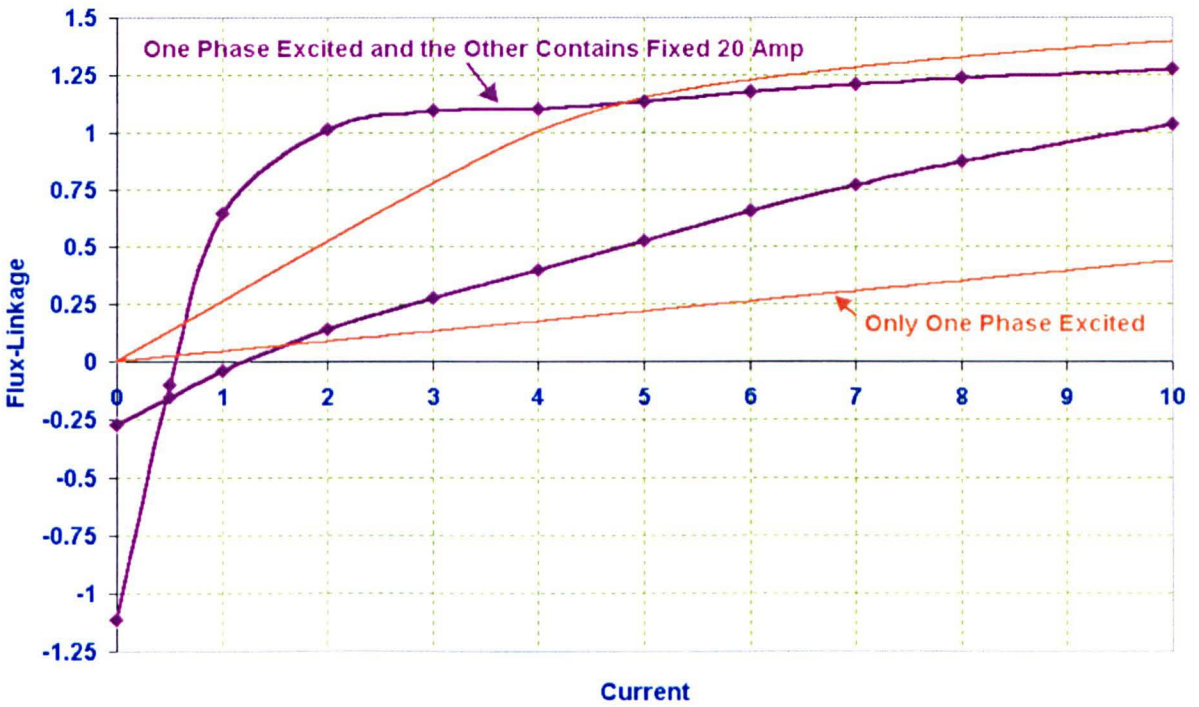

Fig. 8.11.c Comparing two Flux Density Characteristics: when the connection of the Fixed MMF is reversed and when there isn't Fixed MMF

Fig. 8.11 shows the 12/10 short pitched segmented-rotor SRM with a high value of fixed MMF again, but with reversed polarity in the second phase. The FE flux density plot and the magnetic characteristics are shown [197]. The area between the aligned and the unaligned position is less than the previous case. The flux density in the return flux path between the two phases has a high value hence the machine is saturated in this case so the first connection is better [144].

Once more the effect of cross saturation between phases can be explained by examining their common flux path, which occurs in the narrow teeth between them. When the MMFs of adjoining coils are in the opposite directions the fluxes cancel and saturation is reduced, whilst when they are in the same direction they add and saturation increases.

8.3.2 Testing the Machine with two Phases Excited Simultaneously

This section searches for any benefit if the short pitched 12/10 segmented-rotor SRM is operated with two phases excited simultaneously. The copper loss is expected to be the double its normal value so the machine will not normally operate in this way.

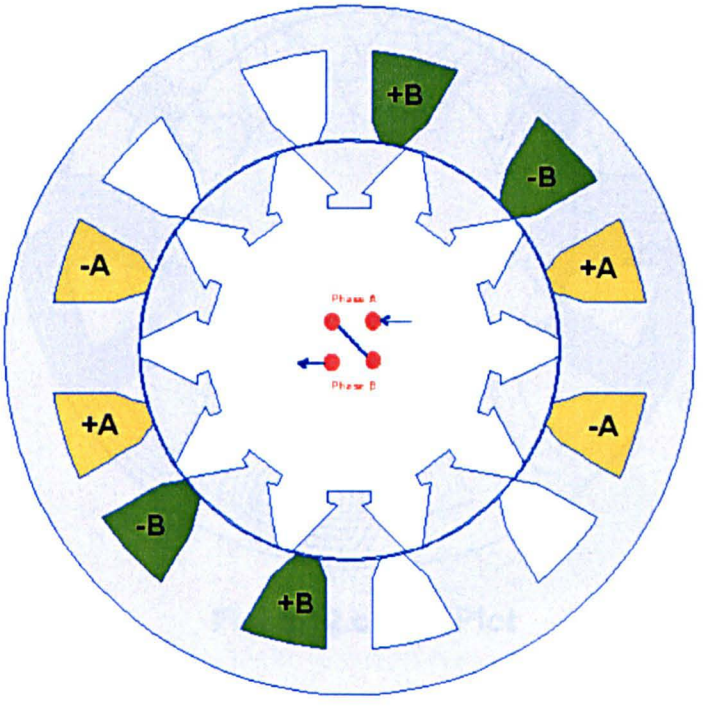

Fig. 8.12.a The Connection of the SRM

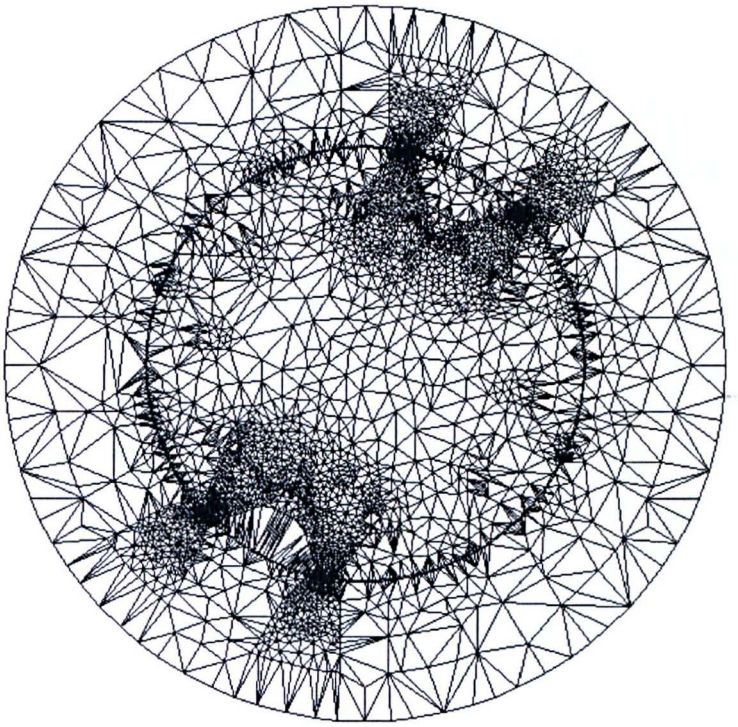

Fig. 8.12.b Adaptive Mesh

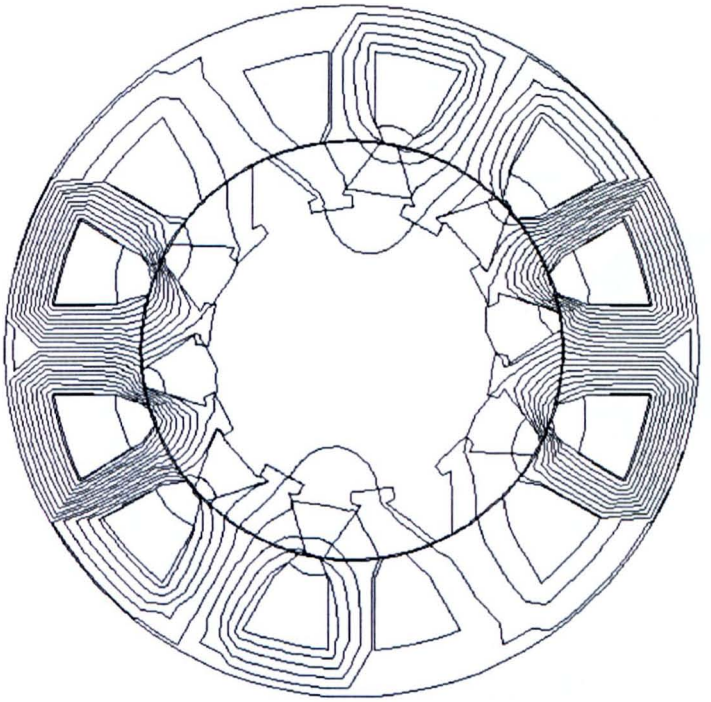

Fig. 8.12.c Flux Plot

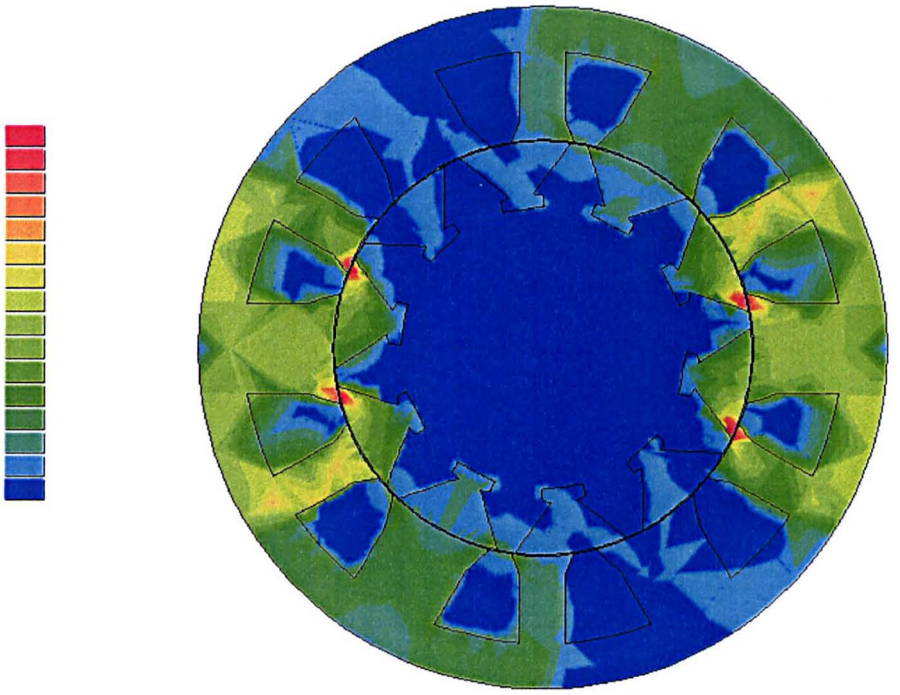

Fig. 8.12.d Flux Density Distribution

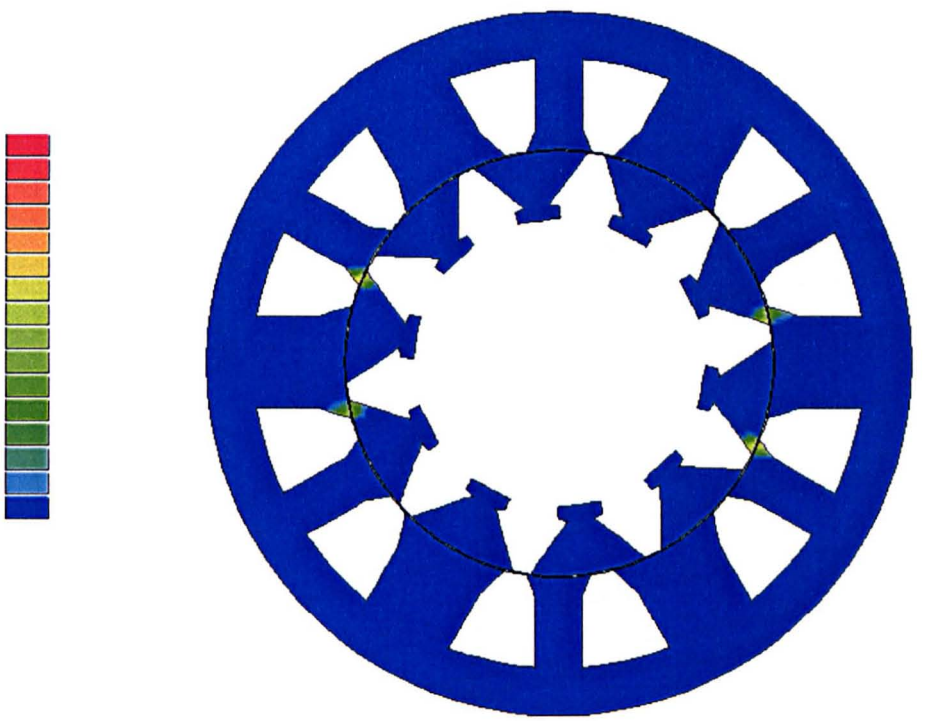

Fig. 8.12.e Saturation

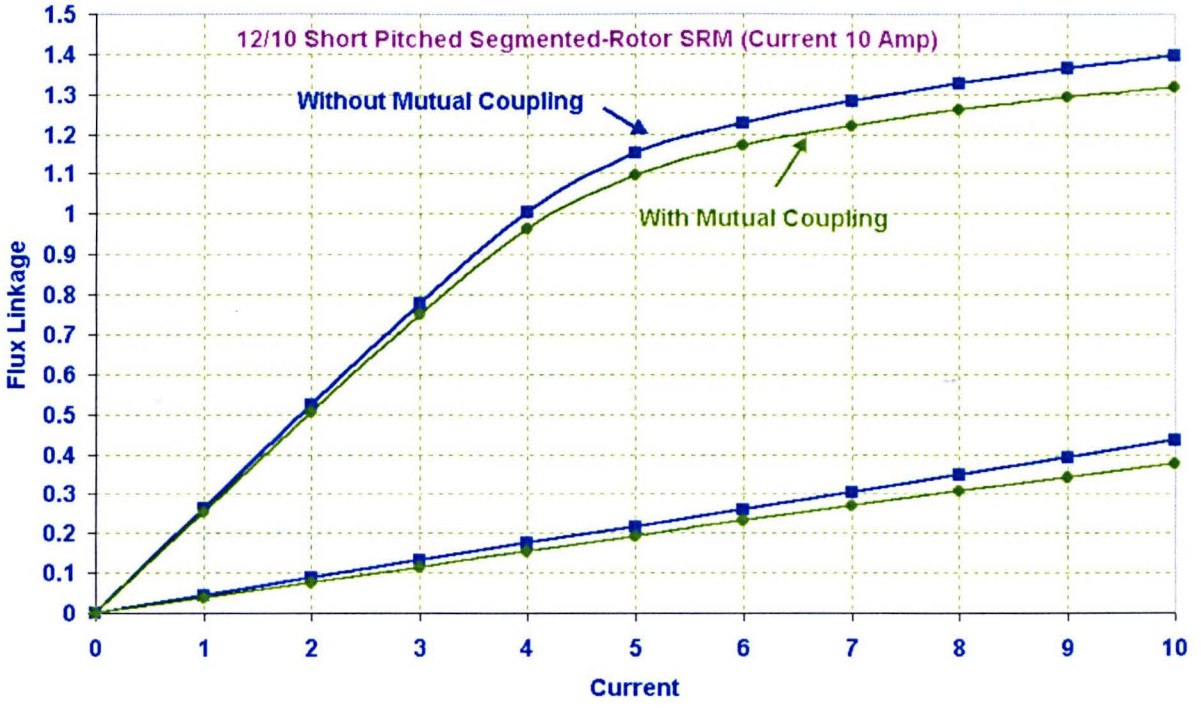

Fig. 8.12.f Impact of the Mutual Coupling on the Flux-Linkage Characteristic of One Phase When Two Phases are Simultaneously Excited with the Same Current

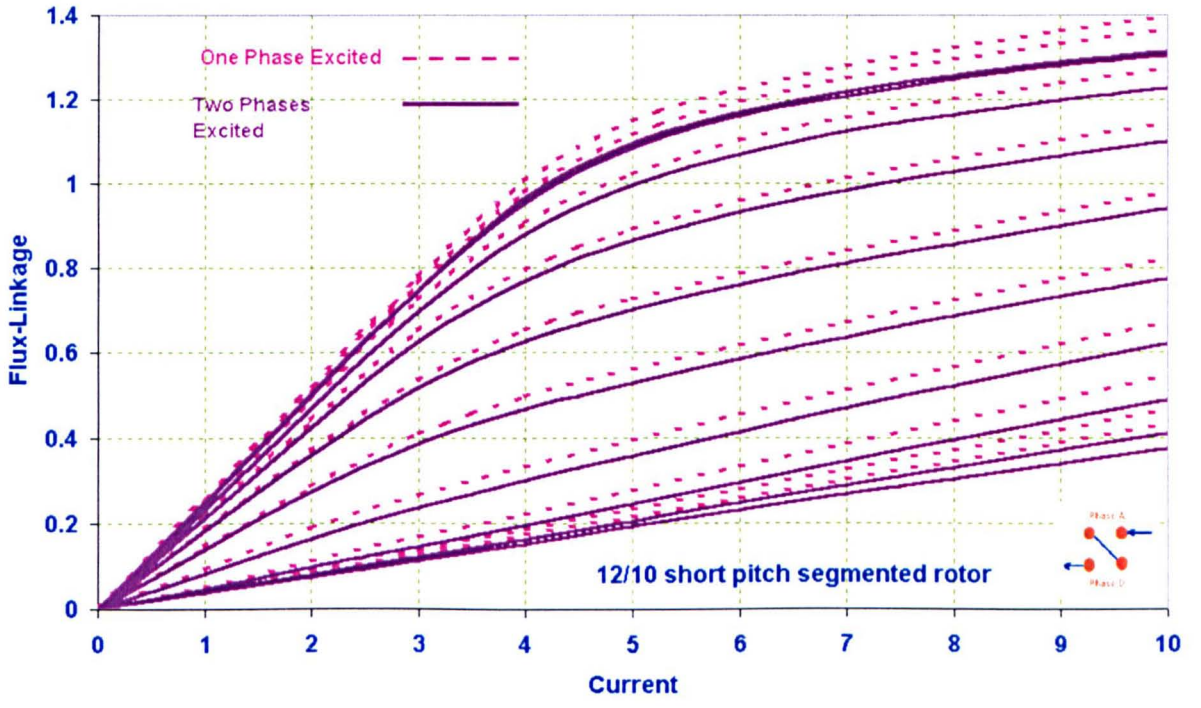

Fig. 8.12.g Comparing Measured and Simulated Flux-Linkage Characteristics

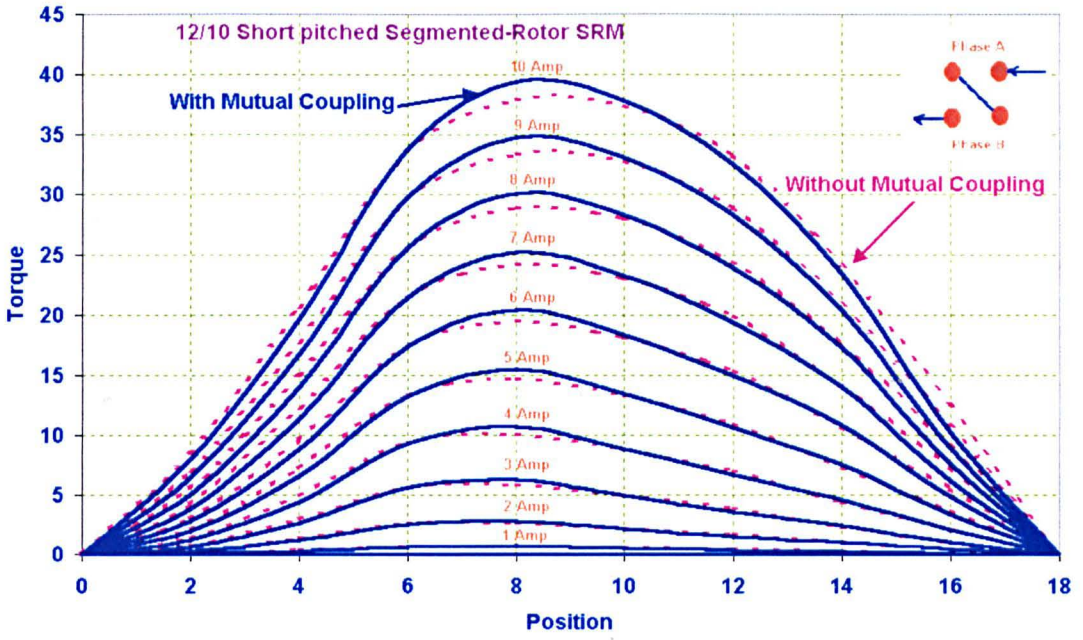

Fig. 8.12.h Comparing Torque Characteristics with Mutual Coupling and without Mutual Coupling (simulated results)

Fig. 8.12 shows the characteristic of the 12/10 segmented-rotor SRM when two phases are excited simultaneously. In the short pitch connection there is little to no mutual coupling between the phases because each coil links one stator tooth.

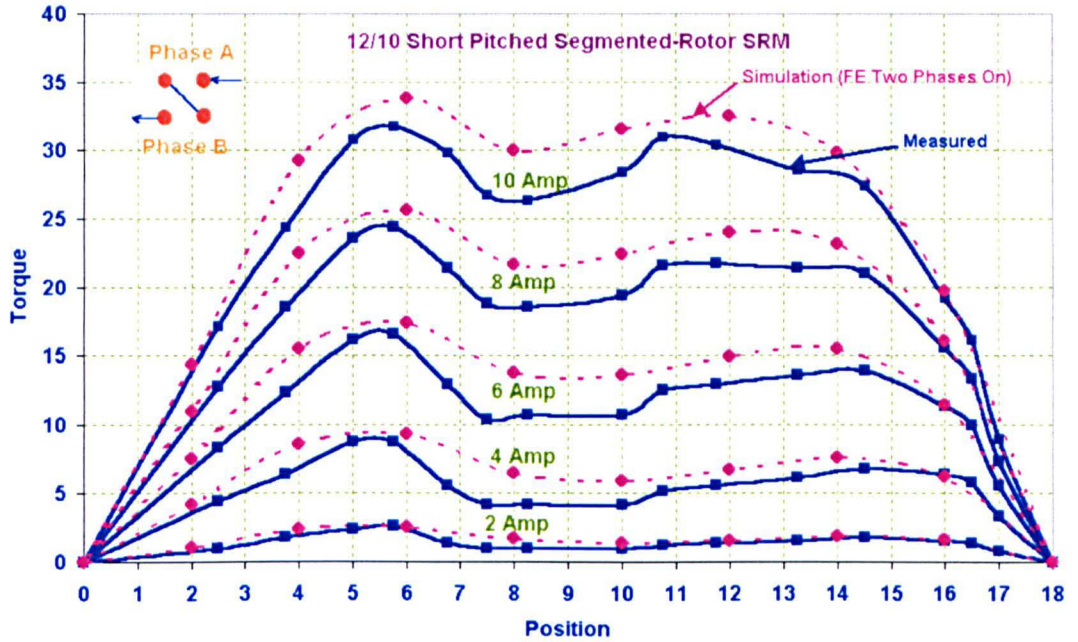

Fig. 8.13 Comparing the Simulated and Measured Torques with Two Phases simultaneously Excited

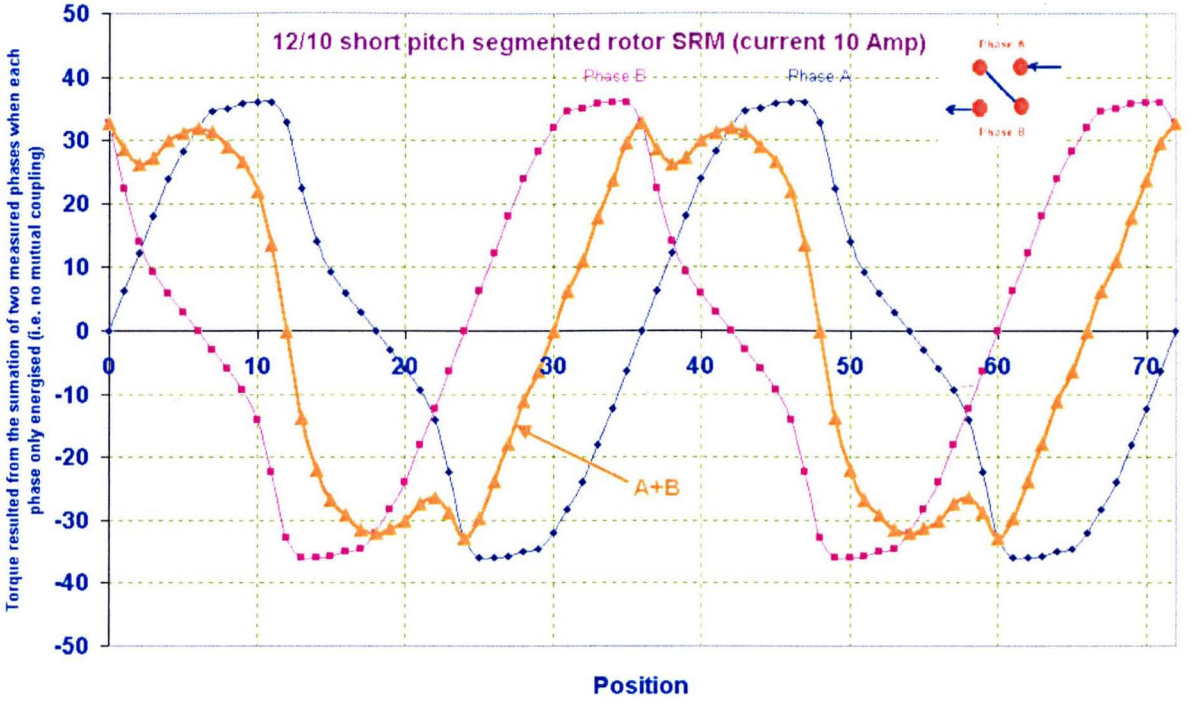

Fig. 8.14.a Summation of Two Phases Torque based on Measurements

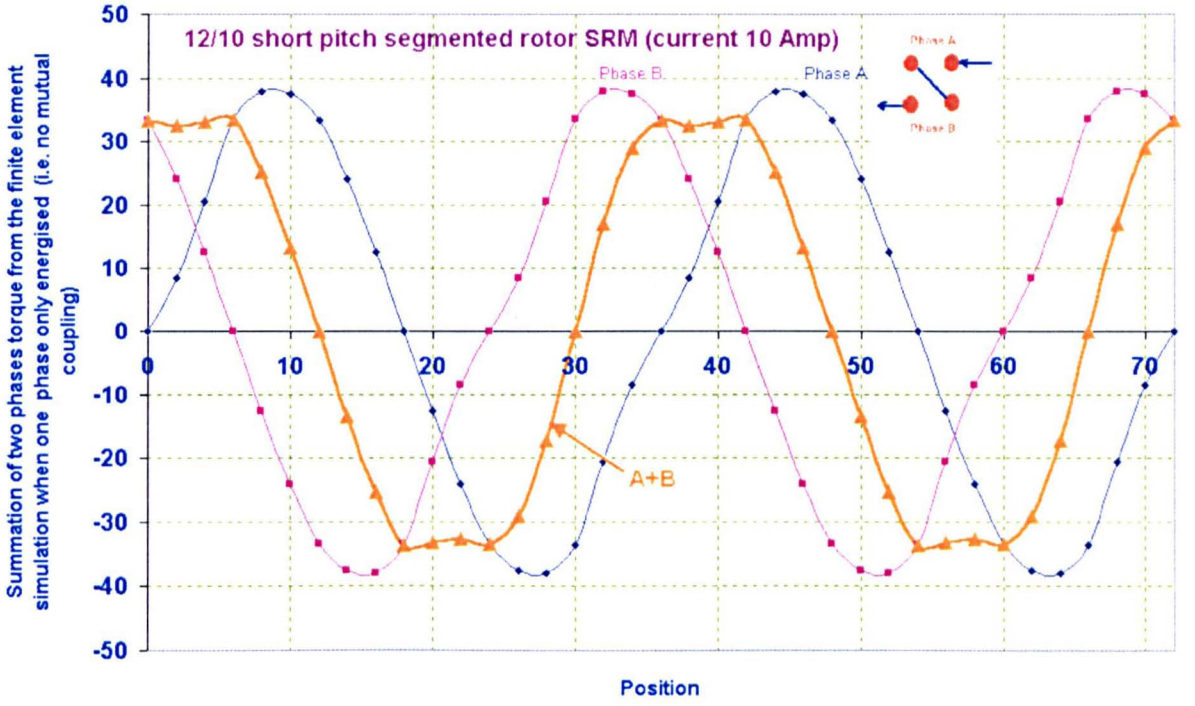

Fig. 8.14.b Summation of two Phases Torque based on Simulated Results

The resultant torque characteristic doesn't include the mutual coupling as only one phase at a time is excited.

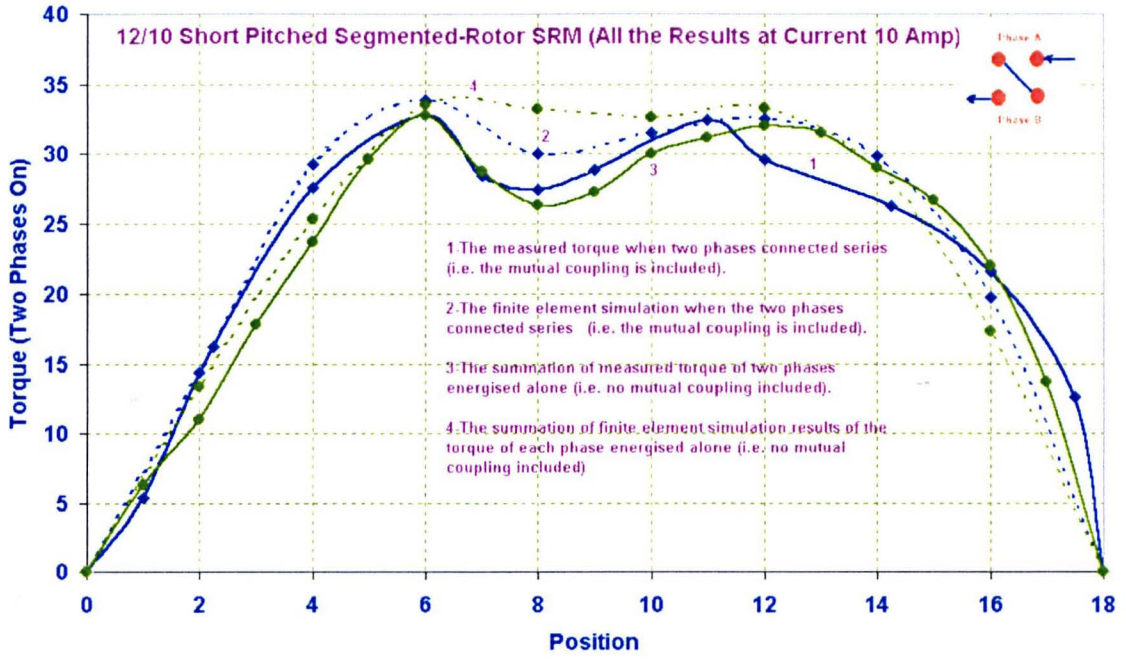

Fig. 8.14.c Comparing the Torque at 10 Amp with and without Mutual Coupling When two Phases are Connected in Series

Fig. 8.14 compares the torque with and without mutual coupling between the phases. It is clear that torque does not increase because the mutual coupling is very small. But the torque ripple is decreased.

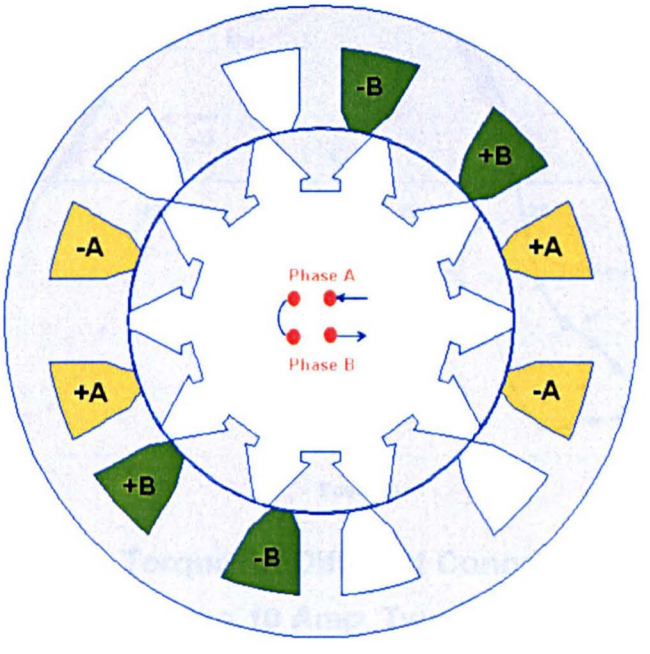

Fig. 8.15 Changing the Connection of the Second Phase

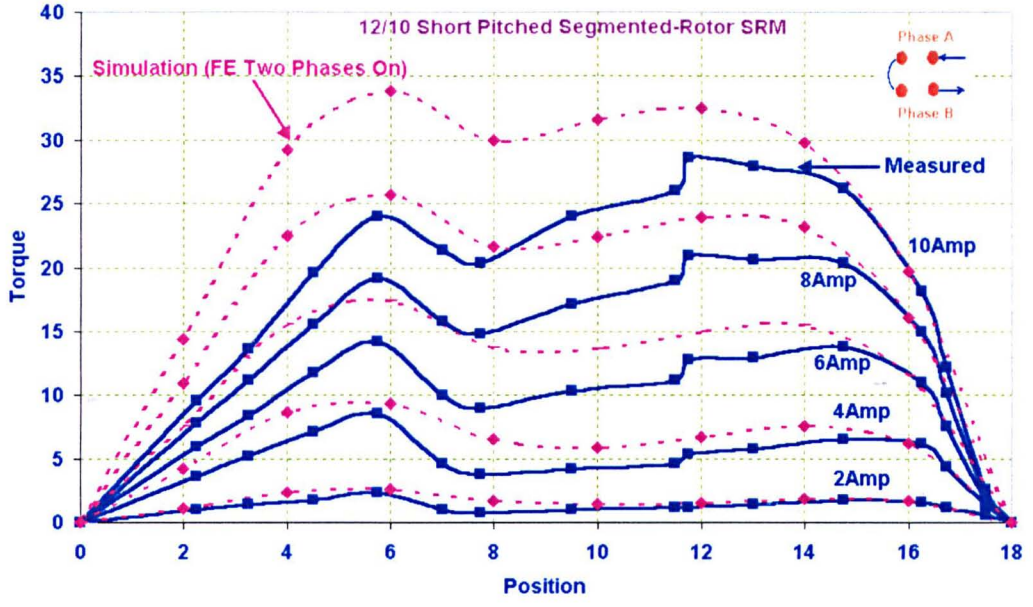

Fig. 8.16 Measured Torque for the two Phases Excited Simultaneously when the Polarity of the Second Phase is Changed

Fig. 8.16 shows the impact of the saturation in the teeth between the phases upon the torque (the second phase connection is reversed).

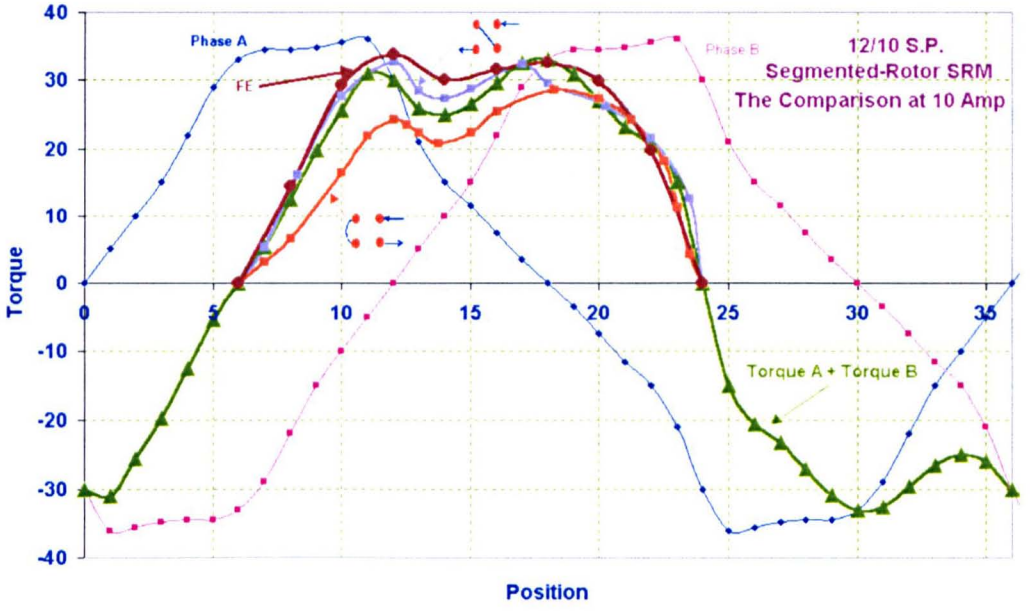

Fig. 8.17 Comparing the Torque for Different Connections with Two Phases Connected in Series and Carrying 10 Amp. Two Different Connection Polarities are Shown

Fig. 8.17 compares the torque for this reversed connection to see the impact of the mutual coupling between the phases and the saturation in the teeth between the phases. In the first connection the torque is similar to when only one phase is excited but has less ripple. In the second the torque is decreased due to the saturation in the teeth between the phases [197].

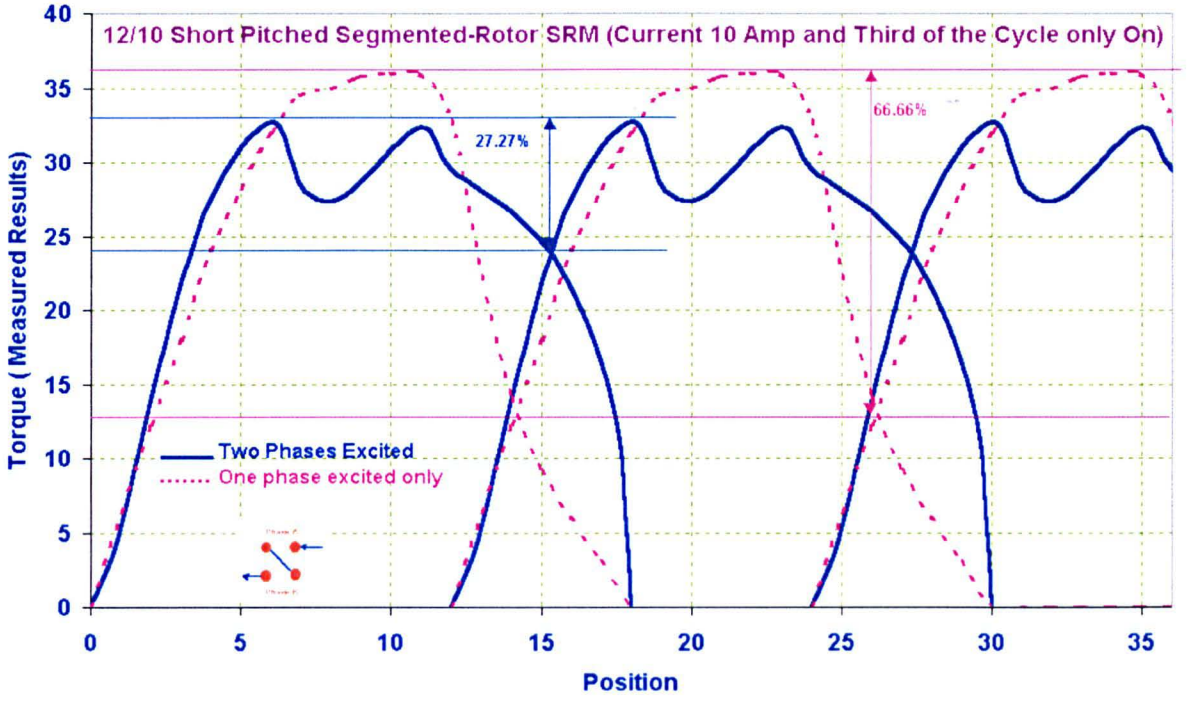

Fig. 8.18 Energising two Phases Simultaneously to Show the Decrease in the Torque Ripple

Fig. 8.18 shows the impact of exciting two phases simultaneously on both the average and the torque ripple characteristic. Exciting two phases simultaneously doesn't increase the average torque but does decreases the torque ripple. The copper loss is double the value when one phase is excited only, so it is unlikely that this will be adopted as an operating mode.

8.4 Conclusion

The chapter tests the new segmented-rotor SRM in two modes of operation with the two new prototypes. First, when there is fixed MMF in the second phase. Second, when there are two phases excited simultaneously. The fixed MMF does not have any significant effect on torque, it just shifts the flux-linkage characteristic up and

down a little according to the connection of this fixed MMF. When exciting two phases simultaneously the output increases slightly with one polarity of connection of the second phase and decreases with the other, due to the saturation in the teeth between the phases. The simulated resulted were validated experimentally using the two new prototypes of the segmented-rotor SRM.

9 Loss Estimation in the new Design and Comparison with a Conventional SRM Design

9.1 Introduction

In previous chapters the design and construction of the new designs of segmented-rotor SRM were described. This chapter is dedicated to estimate the losses in the new designs and comparison of such losses with those in an equivalent conventional SRM.

In addition to winding losses it is necessary to estimate iron loss in each machine type. This calculation is complicated because flux waveforms in SRMs are non-sinusoidal, so the general mathematical formula which is used to estimate the iron loss in conventional electric machines can not be used here [208-209].

9.2 SRM Electromagnetic Losses

The losses in an SRM mainly comprise iron and copper losses, with the latter split into hysteresis and eddy current components. Inclusion of iron loss is of importance when efficiency optimisation is a key-target of the design, particularly in high speed machines where the iron loss can dominate. Models of iron losses can either be empirical or based on the solution of Maxwell's equations. In this chapter the prediction of SRM iron losses is achieved by separating the eddy current losses from those due to hysteresis. The eddy current losses are calculated by rewriting the Steinmetz analytical equation in terms of the rate of change of the square of the flux density rate of change [62][210-218].

The machine is split into three regions: the stator core back or yoke; the stator teeth and the rotor segments. The mean magnetic flux density variation in each region will be calculated and from this the iron loss predicted. The assumption of equal flux densities throughout any one region will lead to some error, but will still enable a reasonable estimate of iron loss to be produced.

9.3 The Basis of the Comparison

The comparison between new and conventional designs can be done in many ways, depending on which operating conditions are fixed and which are varied. The converter d.c. voltage will be fixed at 560 V and the speed of the motors will initially be fixed at 1500 rpm. Rather than use the actual number of turns in each machine, the number of turns used in these calculations is chosen so that each machine just enters full voltage control at a speed of 1500 rpm. The interval between the on/off angles and the angle of advance (or switching on angle) will then be changed to maximise the output torque without allowing the r.m.s. current density to increase beyond $10A/mm^2$ [219-220].

9.4 Estimating the Losses in the New 12/8 Segmented-Rotor SRM

9.4.1 Choice of the Number of the Turns

The number of turns was varied until full voltage control could be achieved at a speed of 1500 rpm, without requiring excessively large winding losses. This ultimately resulted in the choice of 264 turns per phase, which corresponds to the flux-linkage and torque profiles outlined below.

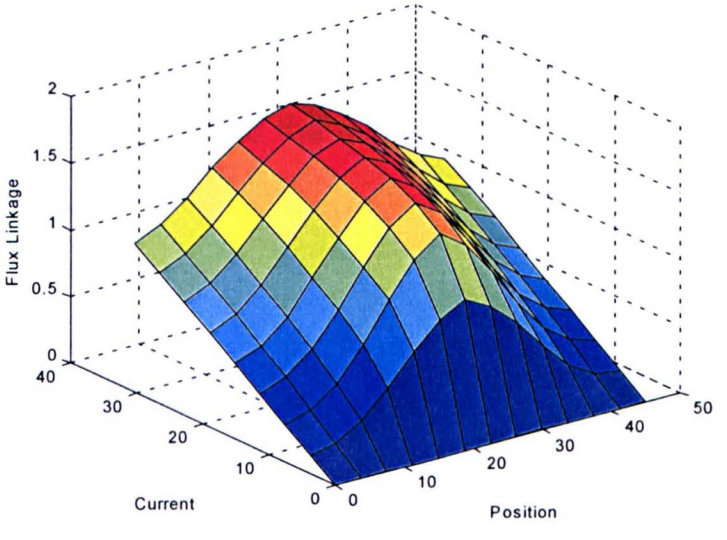

Fig. 9.1 Flux-Linkage Characteristic (264 per phase)

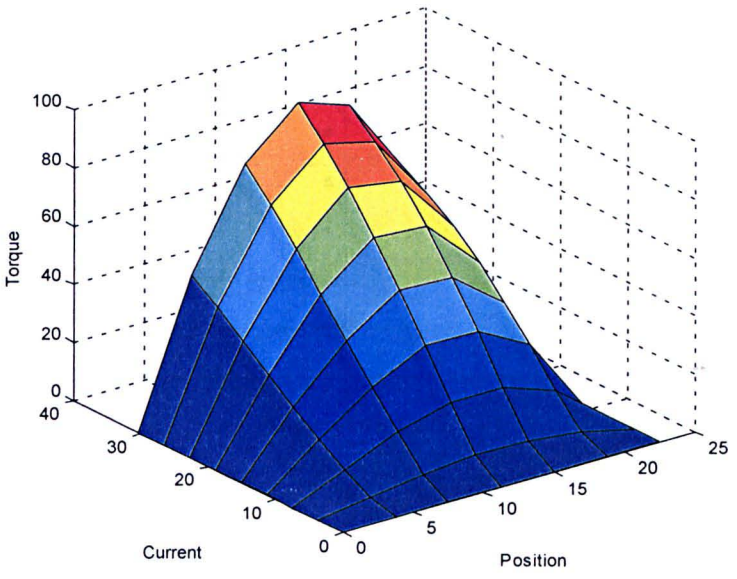

Fig. 9.2 Static Torque Characteristic (264 per phase)

9.4.2 Determination of the Maximum Value of the I_{rms} in the Conductors

Area of one slot=$0.272*10^{-3}$ m^2.

Assume fill factor=0.4 and assume the current density J=10 A/mm^2.

Area of one conductor = $\frac{272*0.4}{132}$ =0.8242mm^2,

I_{rms} (maximum)=10*0.824=8.24Amp.

The influence of the switching on angle will now be studied for three different conduction angles. The torque and the current will be plotted as a function of the switch on angle.

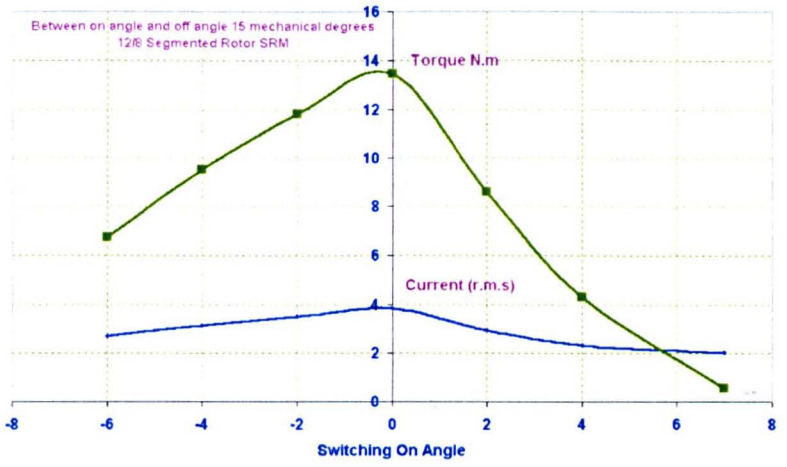

a

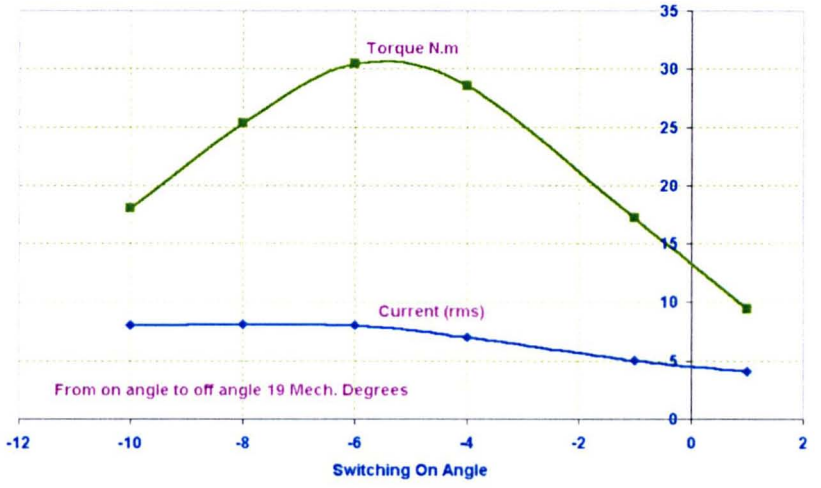

b

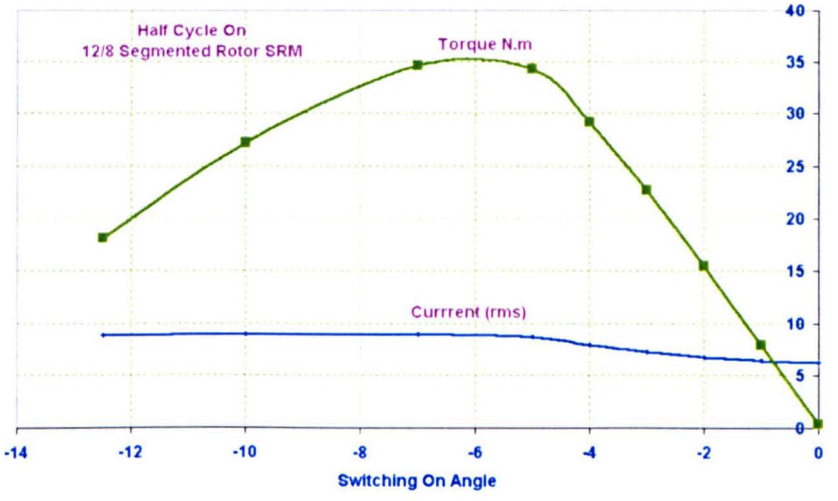

c

Fig. 9.3 Selecting the Switch on Angle that Maximises the Torque without Increasing the Current above 8.24 Amp

Fig. 9.3 shows three charts for different on/off angles and different intervals. A current limiter was used in the simulation to limit the r.m.s. current density to $J \cong 10\text{Amp}/\text{mm}^2$. From these three charts an interval between on/off angles of 22.5° can be seen to give the highest output torque. Fig. 9.4 shows the variation of current density versus switching on angle for a fixed interval between on/off = 22.5° with the current limiter removed. A switch on angle of -4.5 degrees provides the greatest torque capability without requiring current limiting or exceeding a current density of 10Amp/mm^2. This operating point was therefore chosen for iron loss evaluation.

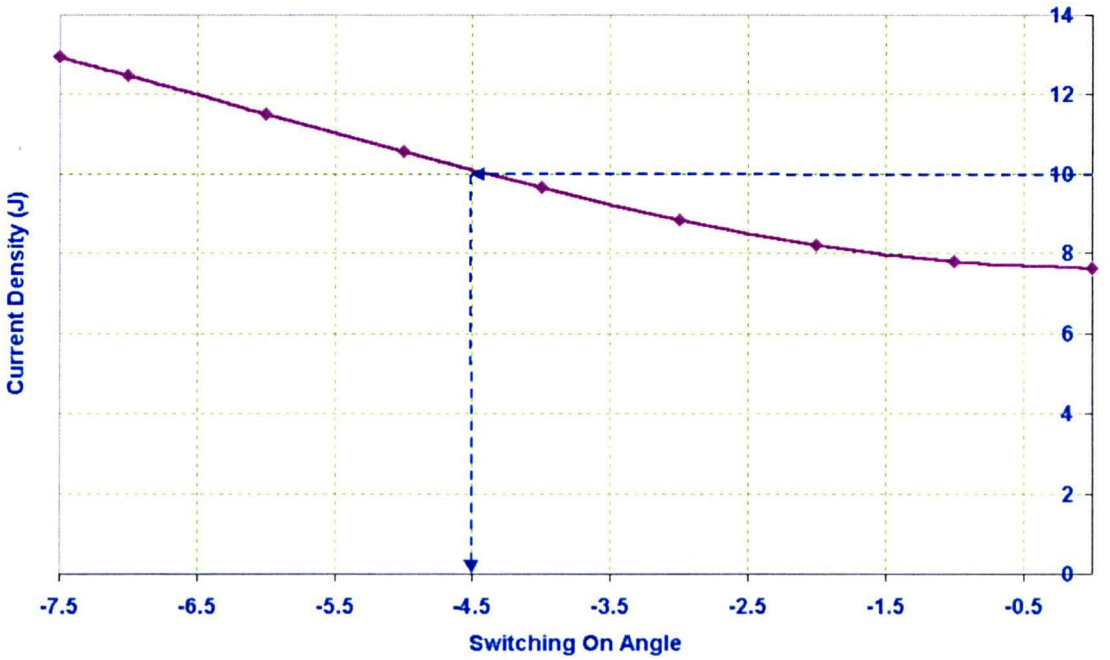

Fig. 9.4 Selection of Switching on Angle for J=10A/mm^2

9.4.3 The Waveforms from the Matlab Simulation of the SRM for these Operating Conditions

Fig. 9.5, Fig. 9.6 and Fig. 9.7 show predictions of current waveforms, torque and flux-Linkage loci under voltage controls with Vdc=560 and speed 1500.

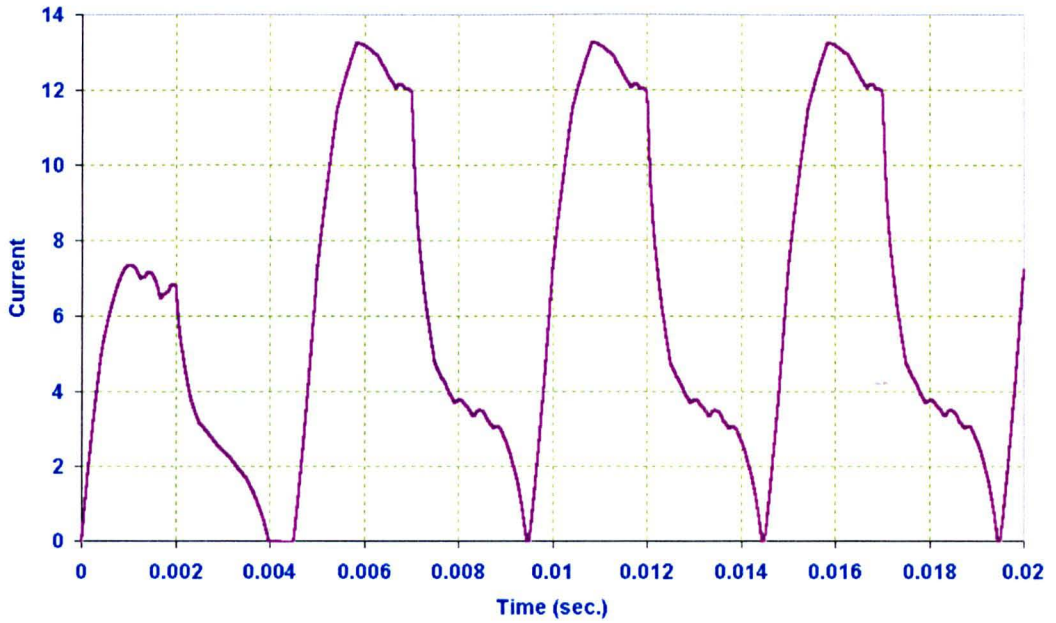

Fig. 9.5 Phase Current

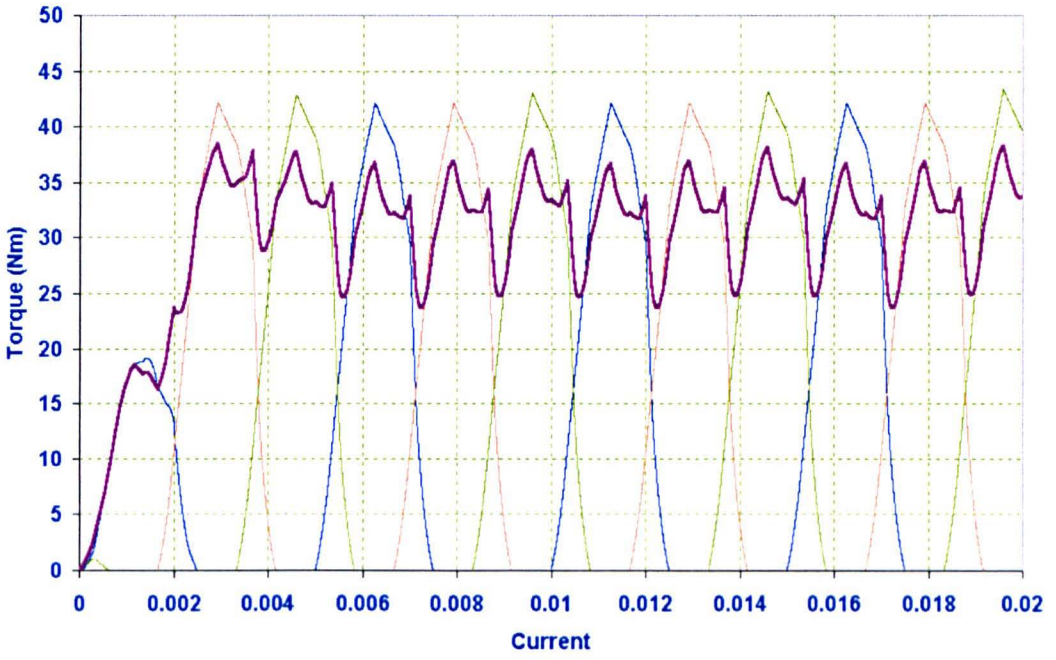

Fig. 9.6 Total Torque

The average torque = <u>31.77 Nm</u>

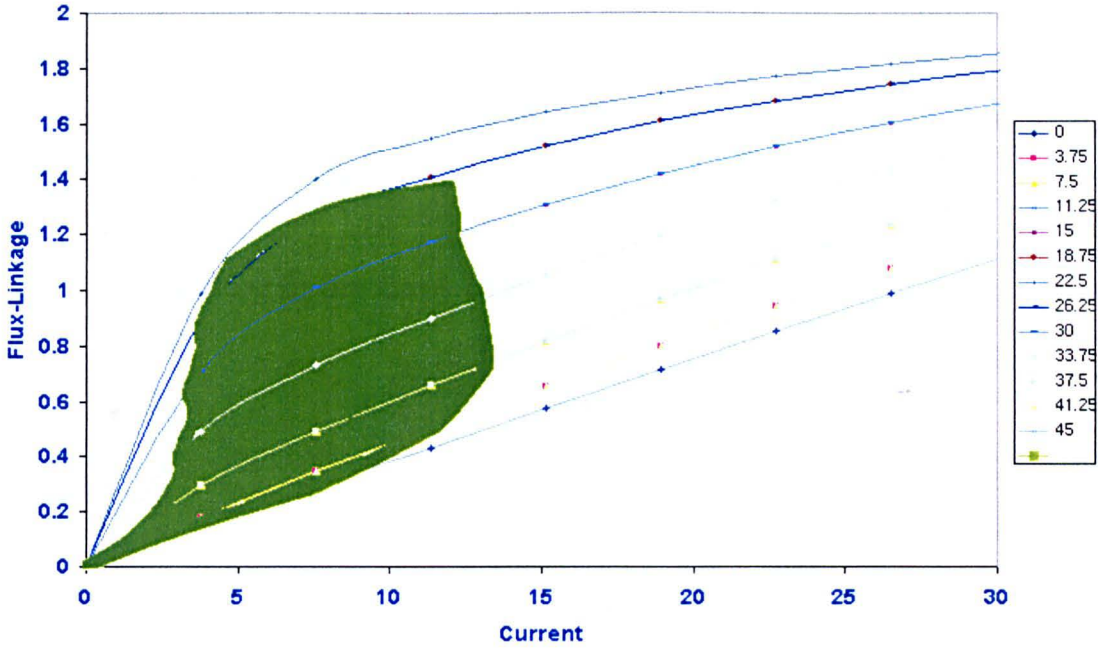

Fig. 9.7 Flux-linkage Trajectory

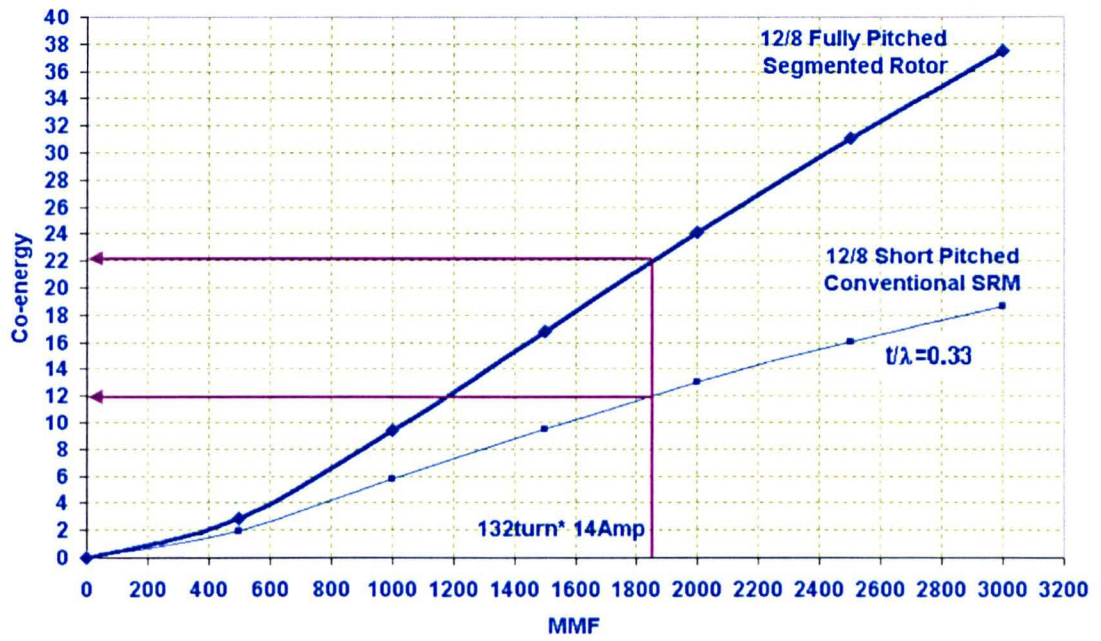

Fig. 9.8 Comparison between the Torque Capability of the New Design and a conventional SRM

Fig. 9.8 shows mean torque predicted under perfect current control. From this figure the ratio between the torques of the new to the old design = 22/12=1.833 at an MMF equal to 14*132=1848 Ampere turns. The approximate maximum value of the torque of the conventional 0.33 short pitched SRM=20 Nm. So for the new fully pitched segmented-rotor SRM the torque is expected to be =1.833*20 = 36.66N.m.

Note: The torque delivered by this machine is less than 36.66Nm because that would represent all the area between the aligned position and unaligned position being filled by the flux linkage trajectory. Here part of the area between the aligned and unaligned positions is not used.

9.4.4 Flux Distribution in the Case of Excitation Overlap

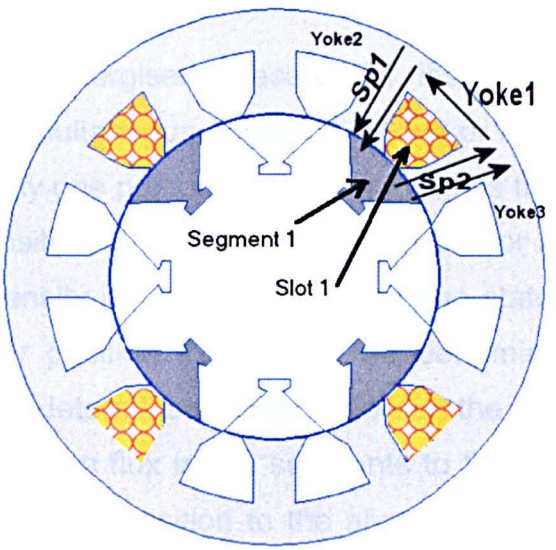

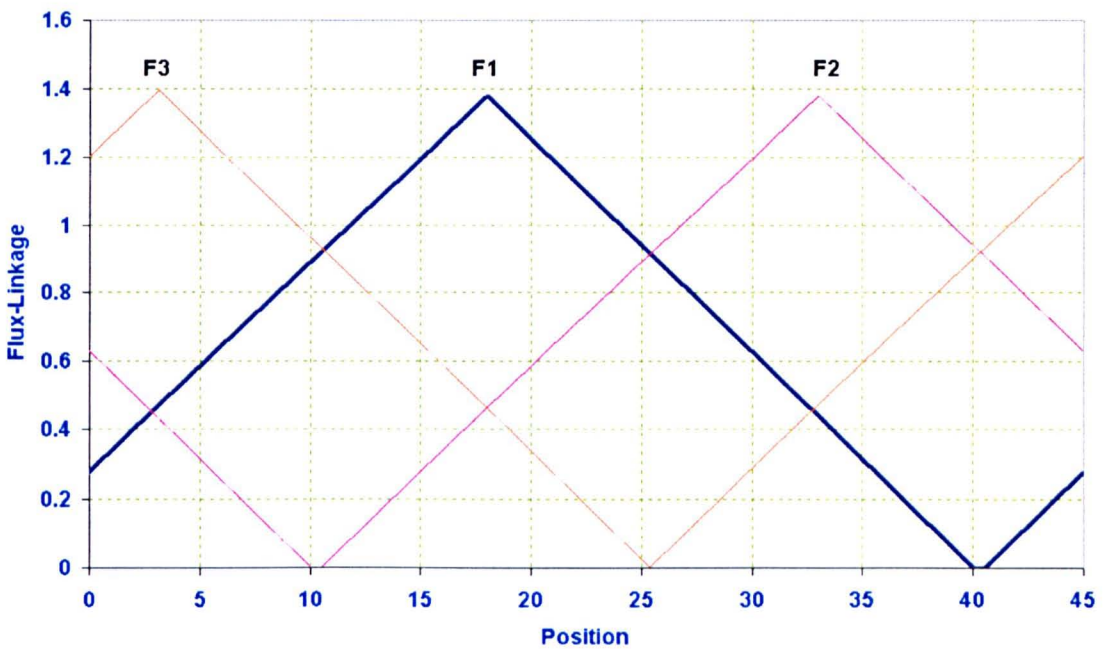

Fig. 9.9 Case when there is an Overlap between the Excitation, the Machine Flux in the Stator Pole will be added

The flux in the yokes is equal to the flux linking the conductor in the slot immediately below the core back portion.

9.4.5 The Ratio of the Flux in the Segment to the Flux in the Yoke

From the fundamental basis of design of the 12/8 fully pitched segmented-rotor switched reluctance motor the width of the stator yoke, width of the stator pole, height of the segment and the overlap are all made equal. From this fundamental choice two important things relating to the flux density in the magnetic circuit follow [69-70]:

1-If the flux of the main energised phase is F1 the flux in the yoke behind the conductor will be F1. Simultaneous excitation of two or more phases will not affect the yoke flux because any one portion of yoke only carries the flux of one phase.
2-Only in the aligned position is the flux density in the rotor segments at a maximum and equal to the flux density in the core back and two stator poles surrounding the conductor. At any other position it needs to be determined. 2-D finite element modelling will be used to determine the ratio between the flux in the segment to that in the yoke. This ratio of the flux in the segments to the flux in the yoke during its movement from the unaligned position to the aligned position will be determined in the absence of saturation; the ratio will then be assumed to be valid at higher excitation levels.

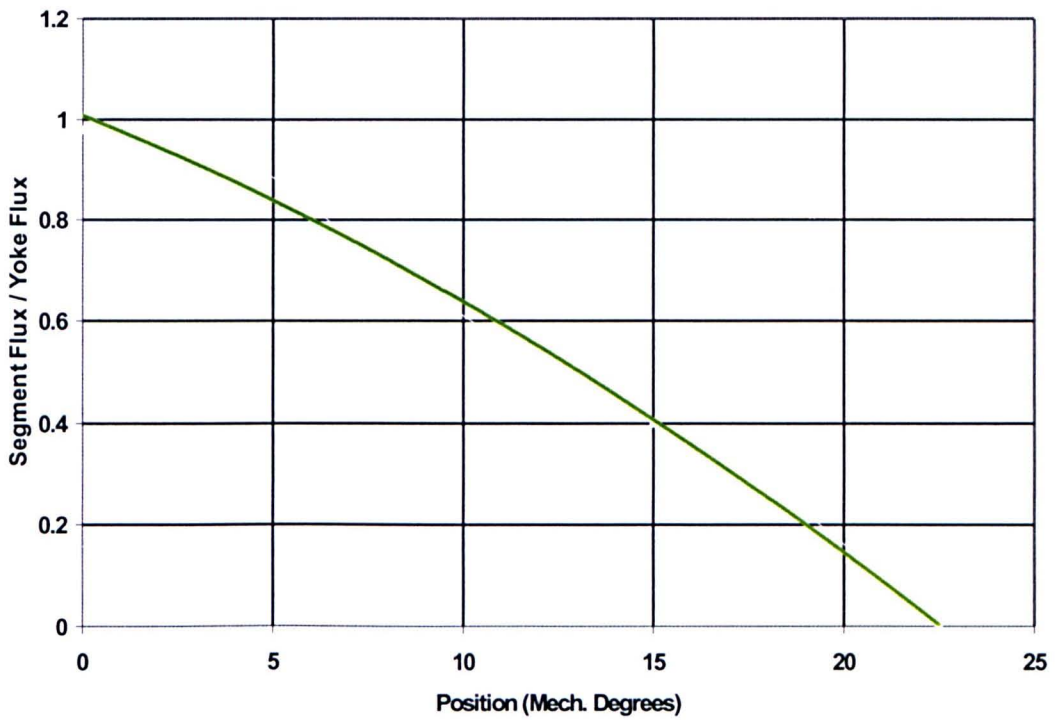

Fig. 9.10 Ratio between the Flux in the Segment to the Flux in the Yoke

The points in Fig. 9.10 were obtained from adaptive 2D-FE solutions for different rotor positions between the aligned and the unaligned positions, thereby giving the ratio of flux in segments/flux in the stator core back).

9.4.6 The Flux in the Stator Poles

With respect to Fig 9.9 the flux in stator pole 1 is the sum of Flux1 and Flux2 Similarly, the flux in stator pole 2 is the sum of excitation of the Flux1 and Flux3 [221]. This results in the curves of Fig 9.10 for the chosen excitation conditions. Note how the peak rate of change of tooth flux density is double that of the core back. This is the opposite to that which occurs in conventional SRMs.

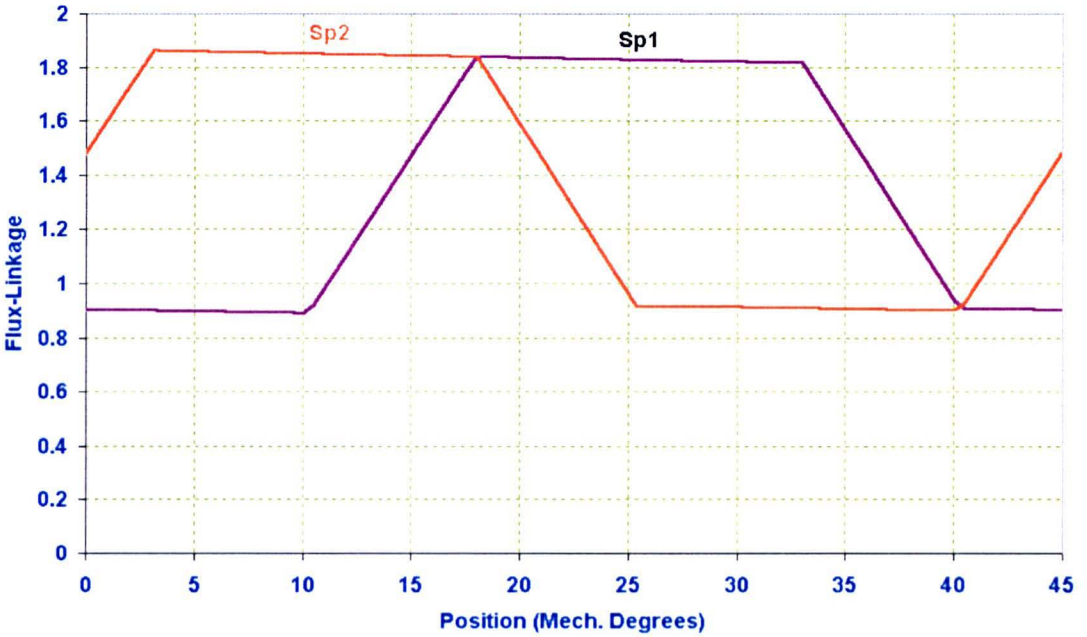

Fig. 9.11 Flux-Linkage in the Stator Poles

9.4.7 The Flux Linkage in Rotor Segments

Fig. 9.12 below shows the amount of each phase flux-linkage which crosses the air-gap and reaches the rotor segments. This is determined from knowledge of the stator flux distribution, combined with the ratio of segment flux to yoke flux given in Fig. 9.10. The flux linking any one segment is then determined from summation of the phase fluxes as it passes under their respective teeth. Note how a segment sees

an oscillatory flux, with alternative positive and negative peaks occurring as it approaches adjacent teeth.

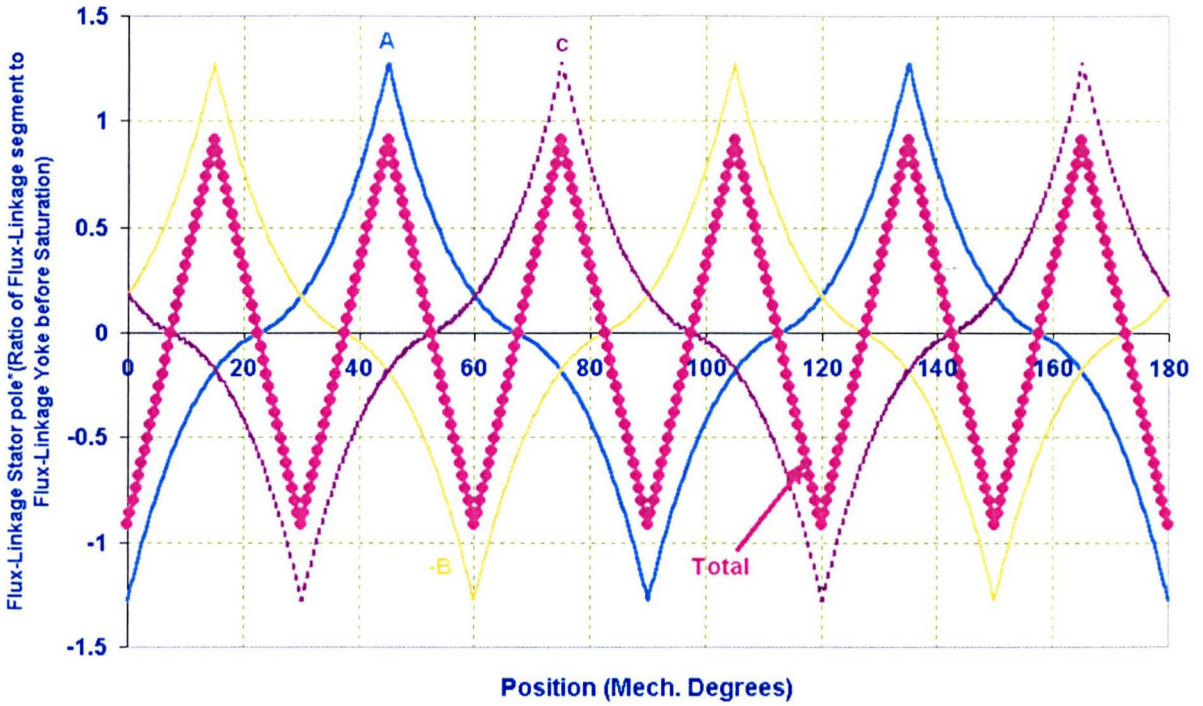

Fig. 9.12 Flux-Linking a Rotor Segment

9.4.8 Calculation of the Flux Density

Peak flux density in the yoke = $\frac{\varphi_{yoke}}{2 * \text{tooth width} * \text{length}} = \frac{\phi_{yoke}}{2 * 0.0118 * 0.15}$

Peak flux density in the two stator poles = $\frac{\varphi_{pole}}{2 * \text{tooth width} * \text{length}}$

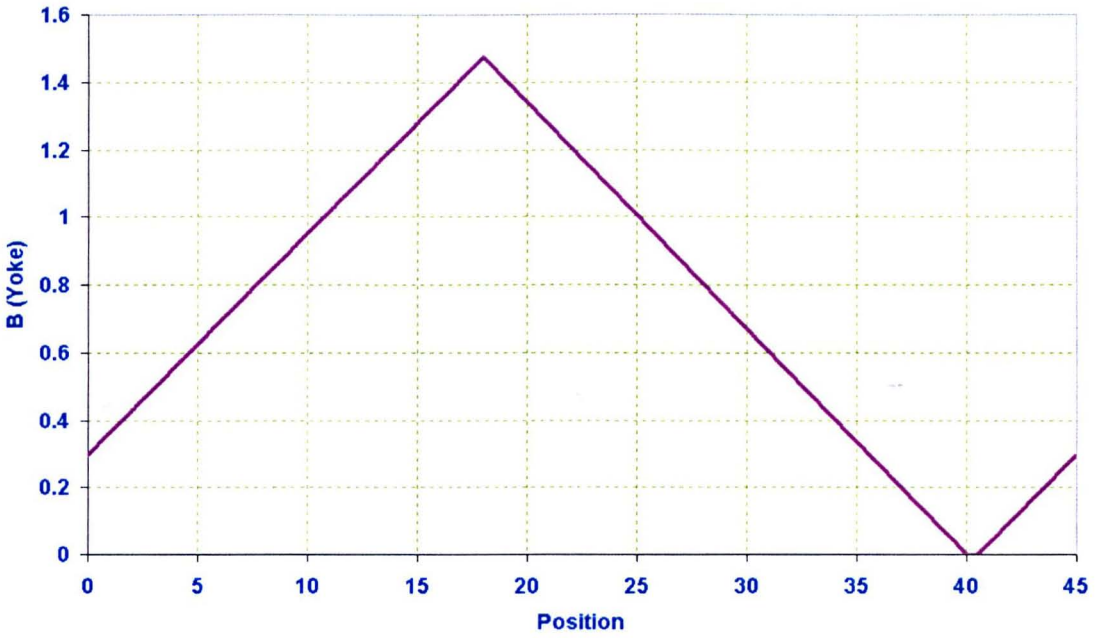

Fig. 9.13 Flux Density in the Yoke

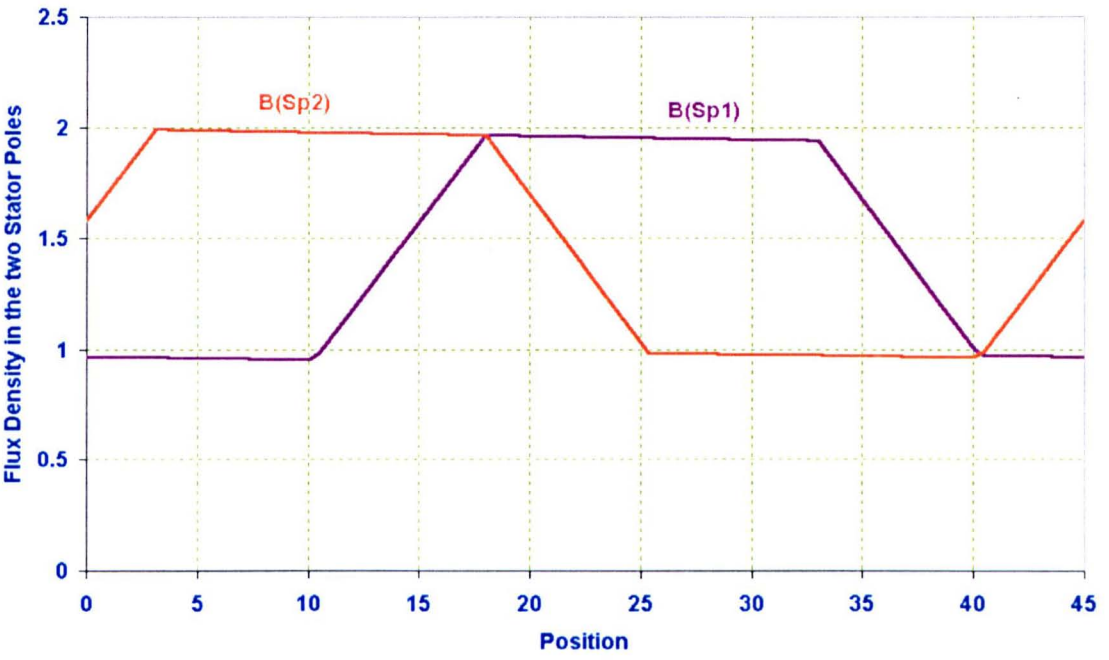

Fig. 9.14 Flux Density in Stator Teeth

The flux density in the segment =

$$\frac{\varphi_{seg}}{2 * \text{tooth width} * \text{length}}$$ *Ratio of the flux in the segment to the flux in the yoke

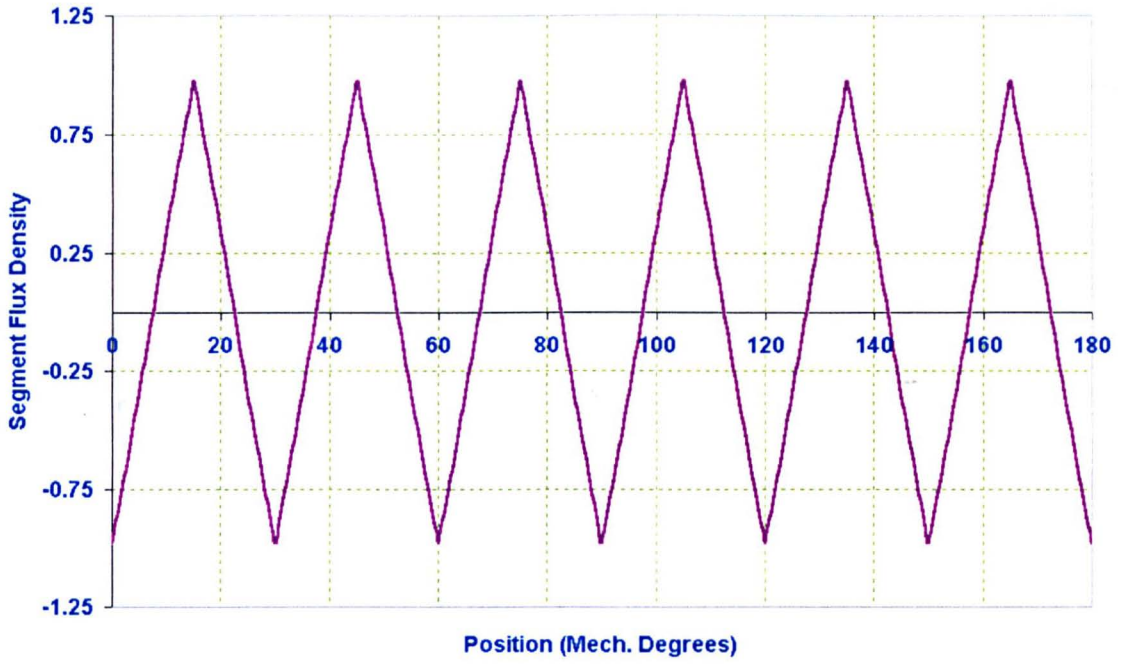

Fig. 9.15 Flux Density in the Segment

9.5 Calculation of Iron Losses

The iron losses consist of anomalous losses, hysteresis losses and eddy current losses. The algorithm for the iron loss estimation has been developed in [62] [222-228] for non-sinusoidal waveforms. The loss constants are dependent on lamination material as well as the machine geometry. Low loss silicon steel, Transil 315-35, is used here for loss estimation and table 9.1 shows the constants [62], which will be used in subsequent calculations:

K_h'	α	K_a'	K_e'
$2.01*10^{-2}$	1.84	$3.43*10^{-4}$	$3.75*10^{-5}$

Table 9.1 Constants of the Iron Loss Equation

9.5.1 Calculation of the Anomalous Losses

The anomalous loss density is instantaneously calculated using the formula:

$$P_a' = \frac{k_a'}{8.76}\left|\frac{dB}{dt}\right|^{1.5}$$

The anomalous loss is then time averaged over an electrical cycle to determine its mean value.

9.5.2 Calculation of the Hysteresis Losses

$P_h^{\backslash} = k_h^{\backslash}.f.\hat{B}^{\alpha}$, where at 1500 rpm $f = \frac{1500*8}{60} = 200\,\text{Hz}$

9.5.3 The Equation for Calculating the Eddy Current Losses

Instantaneous eddy current density is calculated using:

$$P_e^{\backslash} = \frac{k_e^{\backslash}}{(\sqrt{2}.\pi)^2}(\frac{dB}{dt})^2$$

As with the anomalous loss this value is time averages to determine the mean eddy current loss density.

9.6 Calculation of the Iron Loss in each part of the Machine

The table below shows the calculated iron loss components for each part of the machine. Fig. 9.16 shows the results. Note how both the stator teeth and yoke both contribute substantially to the overall iron loss, and how at 1500 rpm the iron loss mechanism is dominated by hysteresis loss. Table 9.2 shows iron loss calculation for this SRM.

	Yoke	Stator Teeth	Rotor Segment
Volume (m^3)	0.000768	0.000031	0.0000255
Anomalous Loss Density (W/kg)	0.5645	0.5453	1.56
Hysteresis loss Density (W/kg)	7.96	13.74	9.04
Eddy Current Loss Density (W/kg)	0.669	0.90	2.58
Total Loss (W)	56.2	44.9	21.4

Table 9.2 Comparison of Machine Iron Losses in Different Sections of the 12/8 Segmented Rotor SRM

Total iron loss = 122.4 Watts

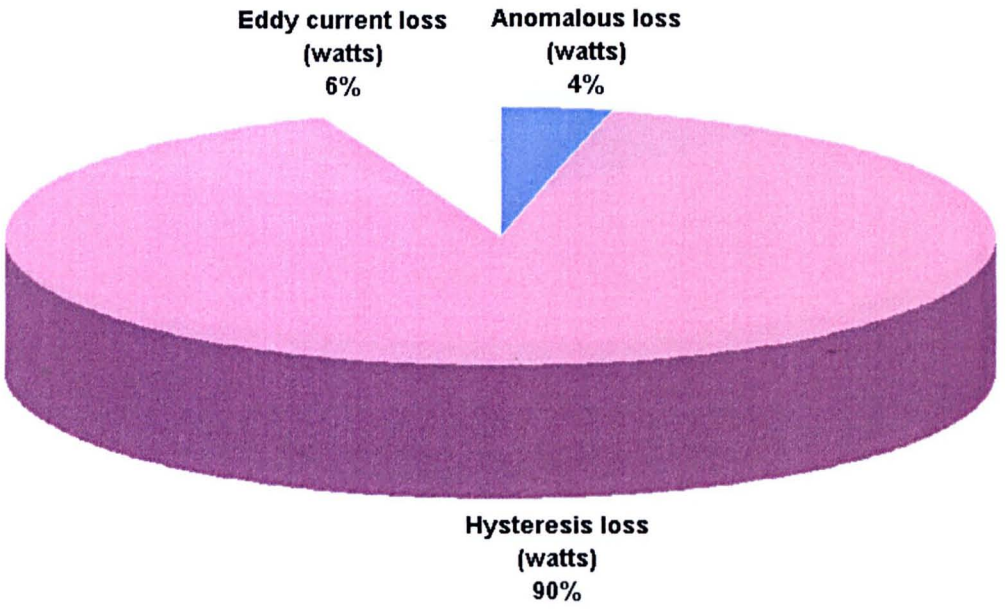

a Distribution of the iron loss in the stator poles

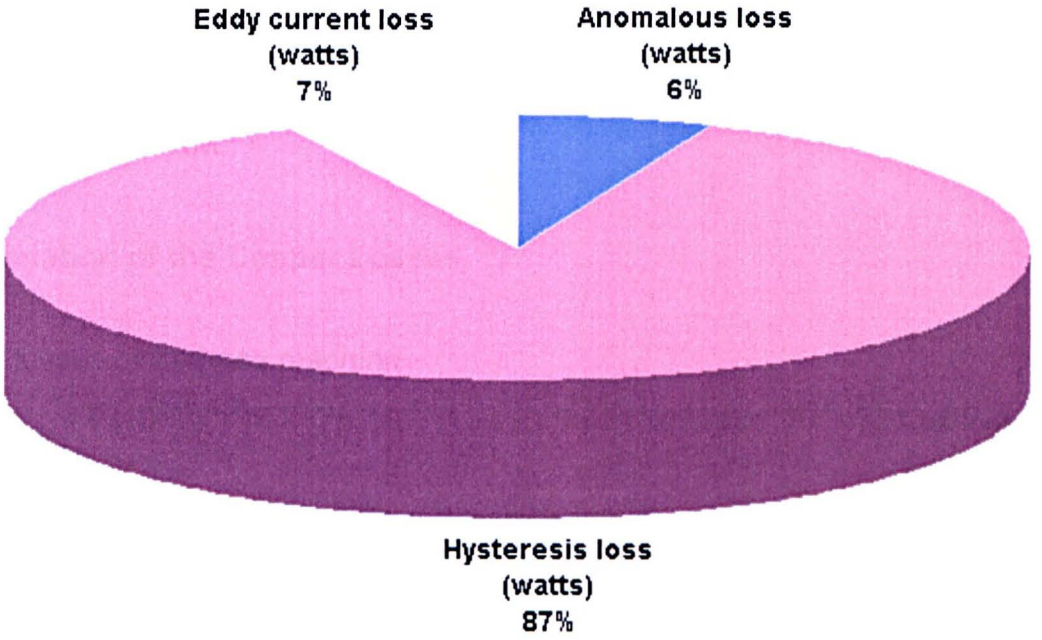

b. Distribution of the iron loss in the yoke

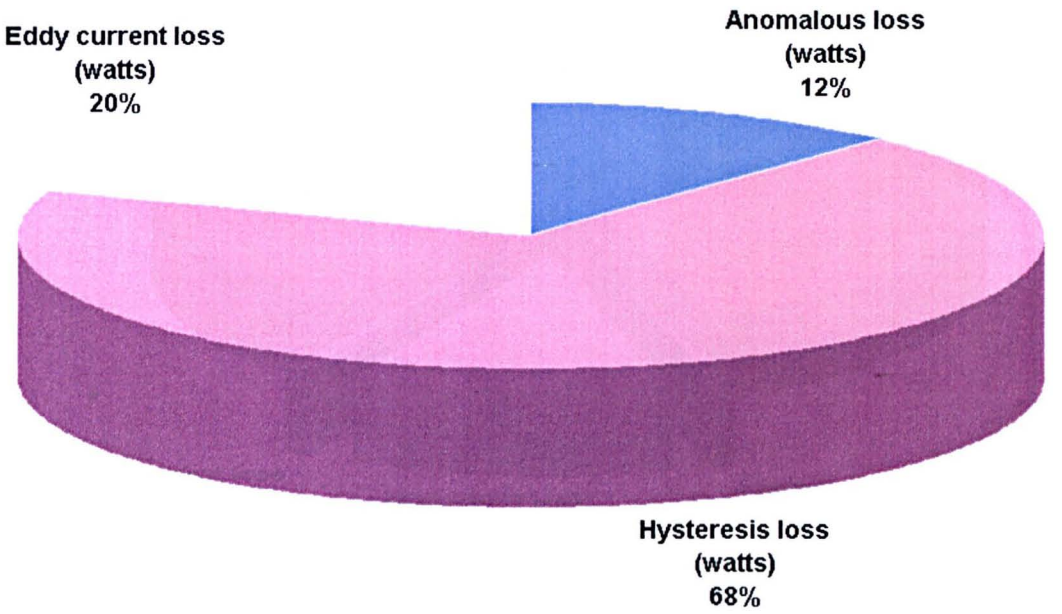

c. Distribution of the iron loss in the segments

Fig. 9.16 Distribution of the Iron Loss in the 12/8 New SRM

Fig. 9.16 shows the relative iron loss distribution in each section of the new 12/8 segmented-rotor SRM.

9.7 Estimation of the Copper Losses

Copper losses of 3-phase machine

$P = 3J^2 \rho V_{cu}$ =3*(10*10^6)^2*0.0178*10^{-6}*(132*2)*0.621*0.82424*10^{-6}=721.65 Watts.

Fig. 9.17 shows the relative distribution of the different loss in the 12/8 new segmented-rotor SRM.

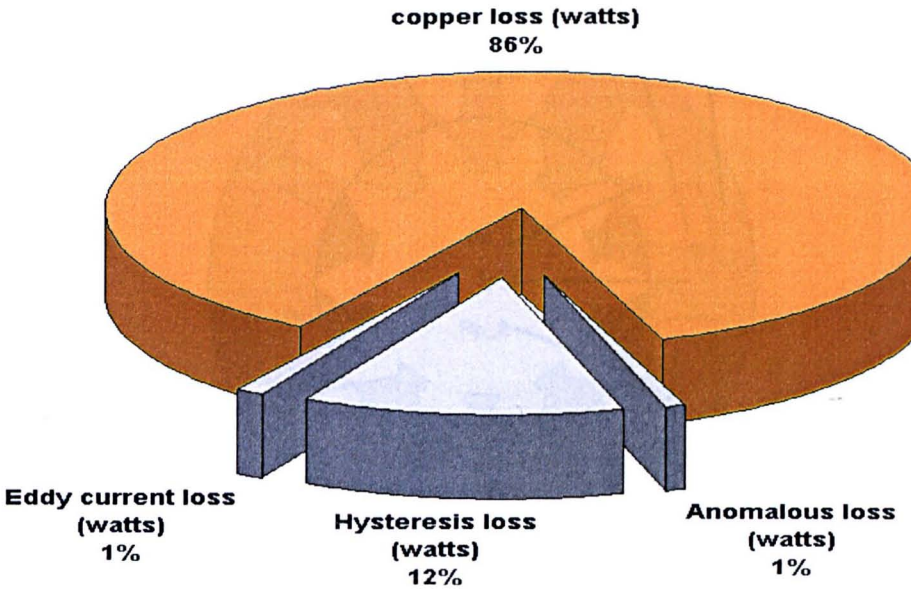

Fig. 9.17 Distribution of the Losses in the 12/8 New SRM

Output power of this motor=31.77*2π*1500/60=**4.99kW**

Total Losses = 844 Watts

9.8 12/10 Segmented-Rotor SRM

The 12/10 segmented-rotor machine is illustrated in Fig. 9.18. This machine has total freedom over the excitation polarity of each coil. The choice of excitation polarity affects only the flux distribution and iron loss in the unwound teeth which act as return paths, because only these teeth see the flux of more than one phase. The coil polarity chosen has the MMF of adjacent coils alternating in polarity i.e. in, out, in, out etc. This results in the flux in unwound teeth being proportional to the difference of the flux between two phases, so overlap between phases will actually reduce magnetic saturation in these teeth.

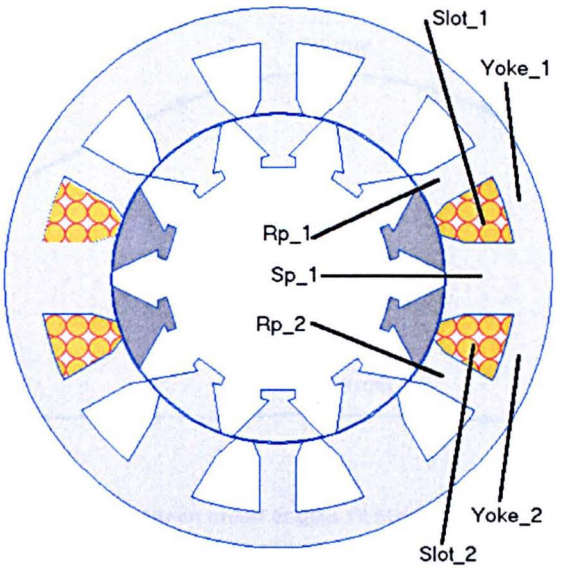

Fig. 9.18 12/10 Short Pitched SRM Segmented-Rotor

9.8.1 Determination of the Number of Turns and the Current Density

A total of 200 turns per phase were required to produce similar operating characteristics to the 12/8 segmental machine, with full voltage control occurring at 1500 rpm. Hence the number of turns per coil is 100, (two coils per slot so 50 turns per slot).

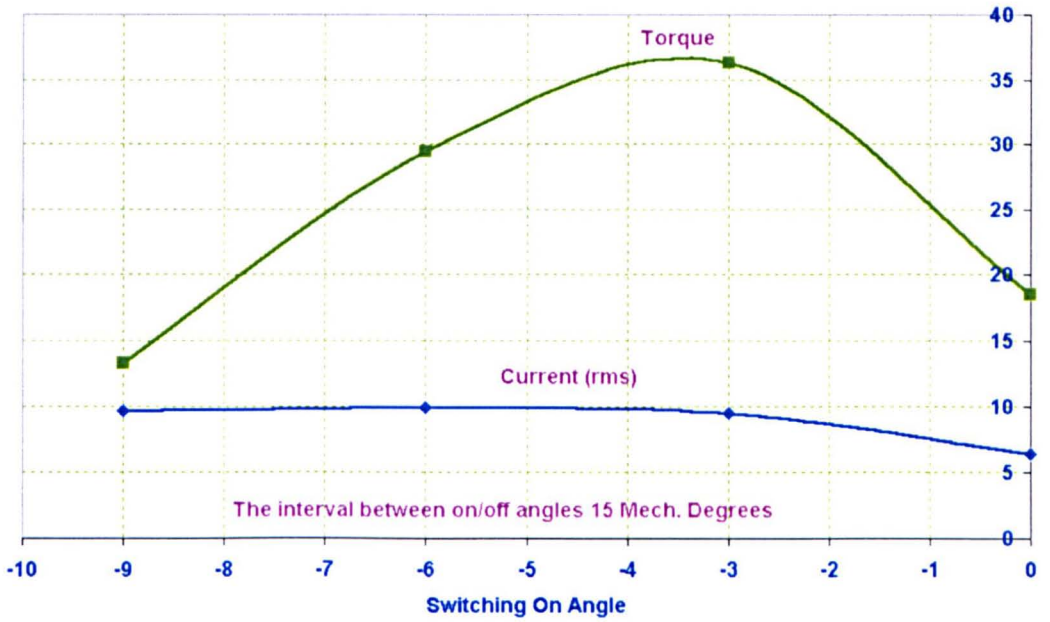

a

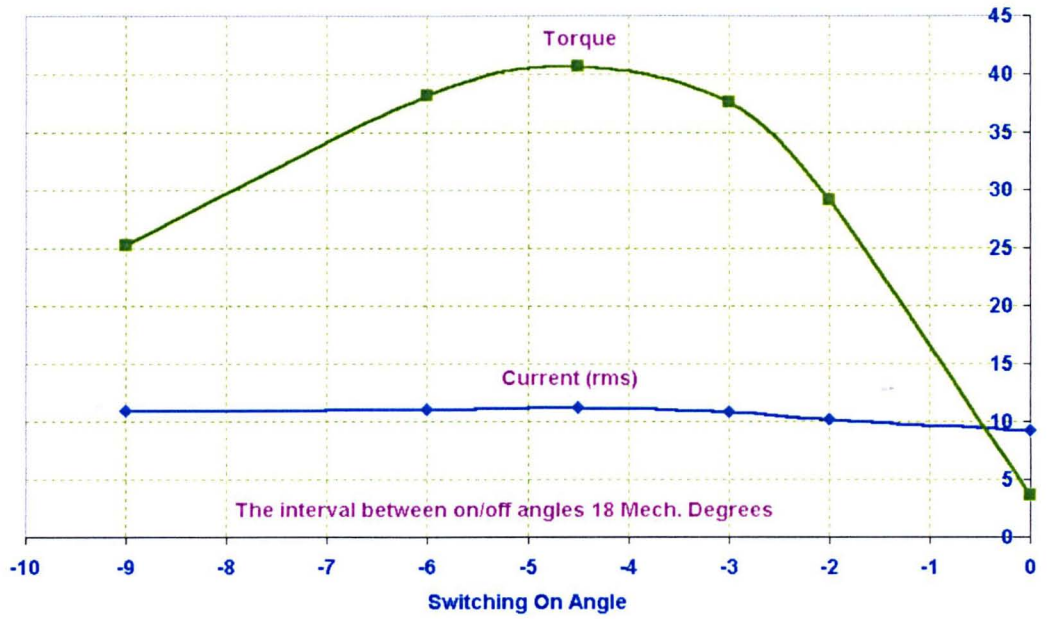

b

Fig. 9.19 Optimisation of the Switching On Angle

Fig. 9.19 shows the results of an investigation to optimise the switching on angles and the interval between on/off angles. The optimum value of switching on/off is -3^{o} / 12^{o}. These values deliver the most torque while keeping the current density to $10A/mm^2$.

9.8.2 Calculation of Current Density

Figures from 9.20 to 9.25 show the performance waveforms using the previous calculated switching on and switching off angles.

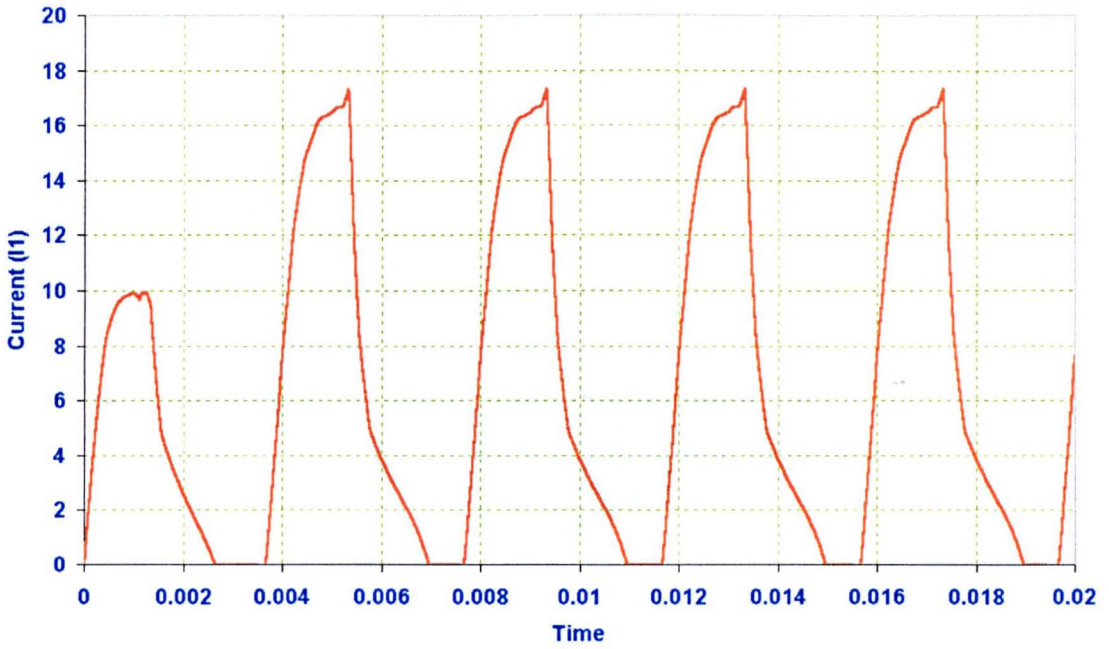

Fig. 9.20 Phase Current

Area of one slot = $0.257*10^{-3}$ m^2 and assume fill factor = 0.4

Area of one conductor = $\frac{257*0.4}{100}$ =1.028 mm^2

$J_{rms}=\frac{\text{Irms}}{\text{A (area of one conductor)}}=\frac{9.469352}{1.028}$ = 9.21143 A/mm^2.

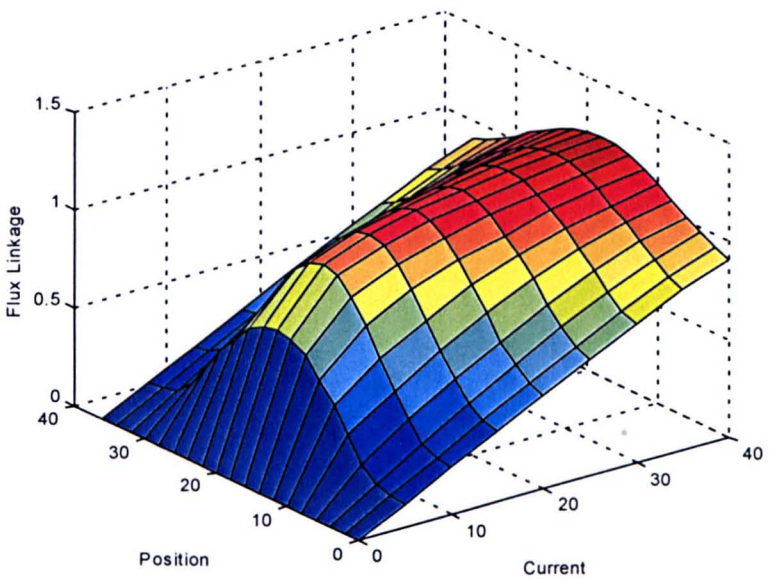

Fig. 9.21 Flux-Linkage Characteristic

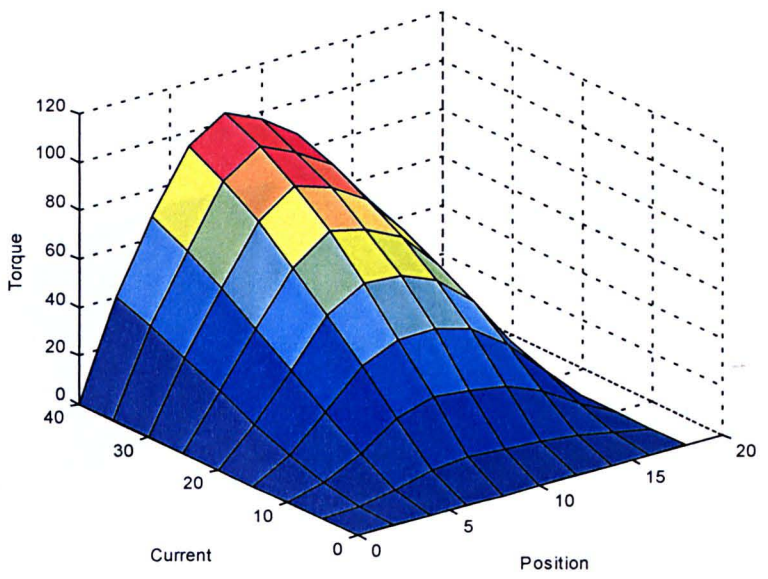

Fig. 9.22 Static Torque Characteristic

9.8.3 Average Torque of the Proposed Machine

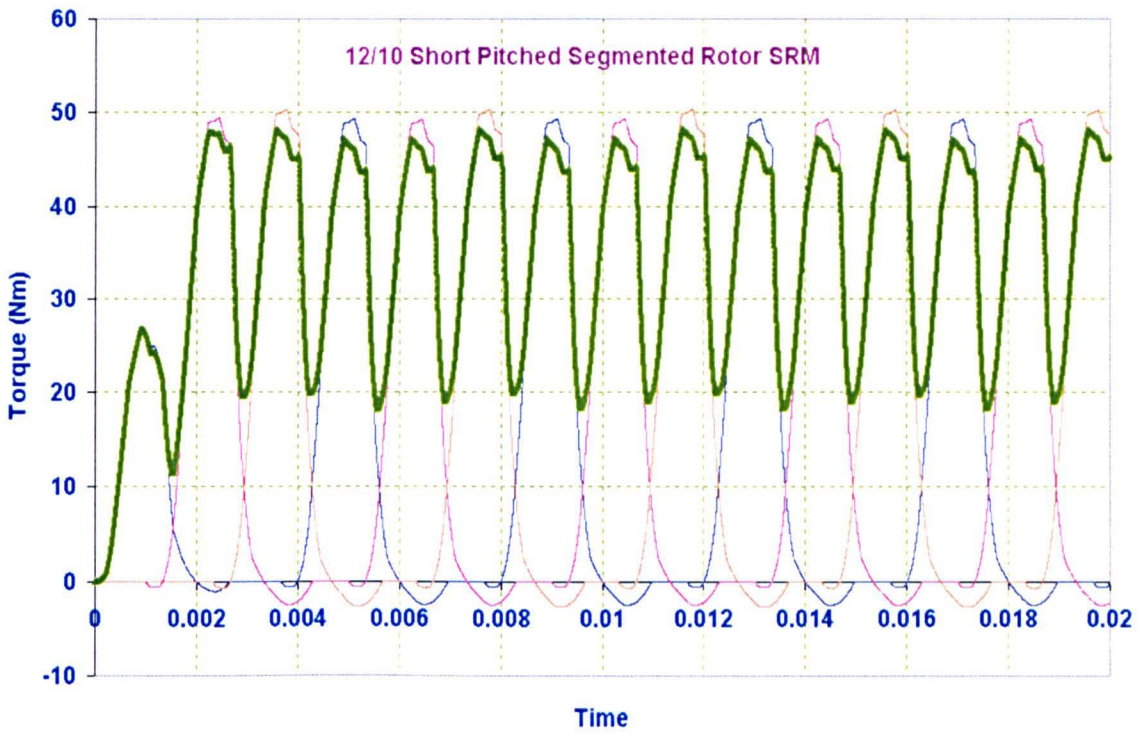

Fig. 9.23 Shape of Each Phase Torque and the Sum

Switching on angle at –3 Mech degrees. Switching off angle at 12 Mech degrees.

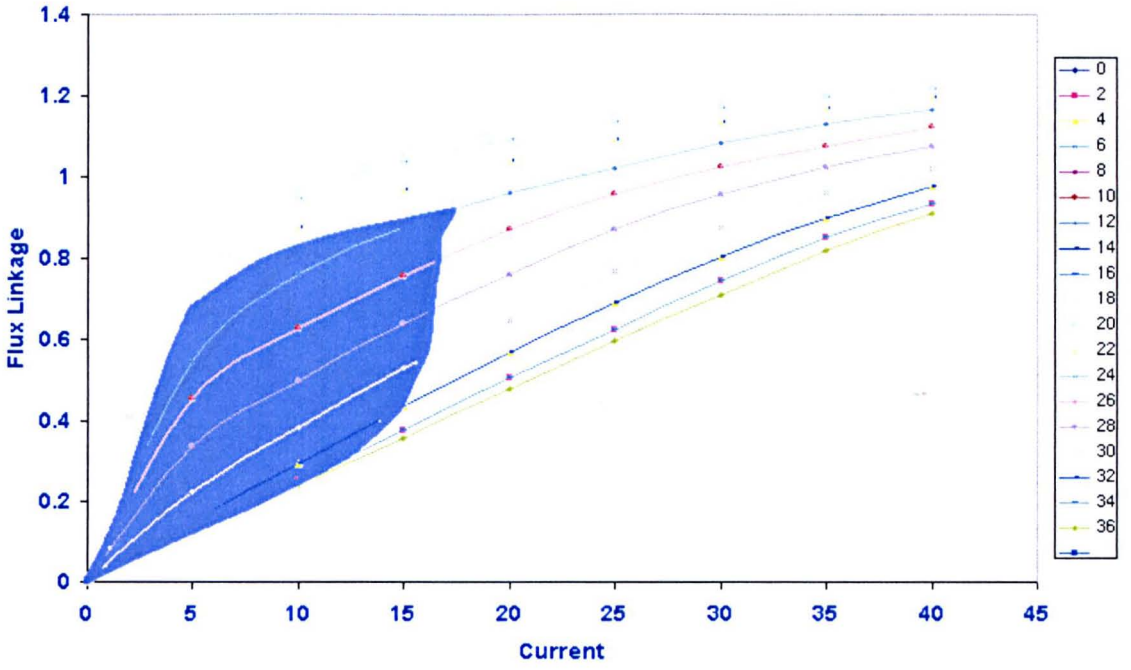

Fig. 9.24 Flux-Linkage Trajectory

The mean torque produced under these conditions is **36.95 Nm**

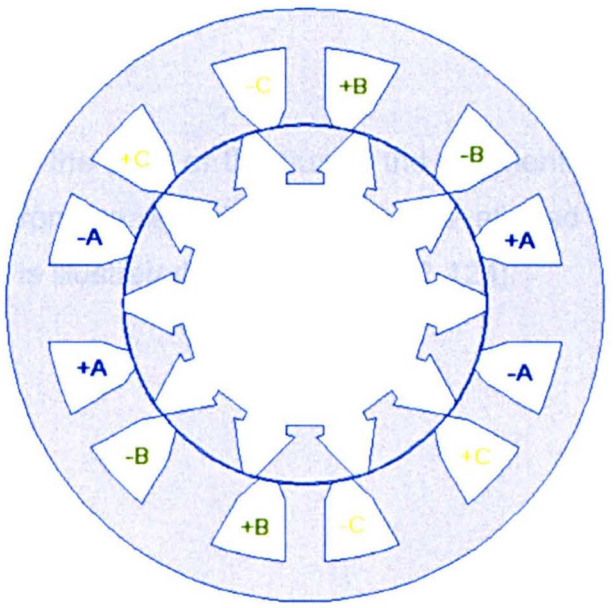

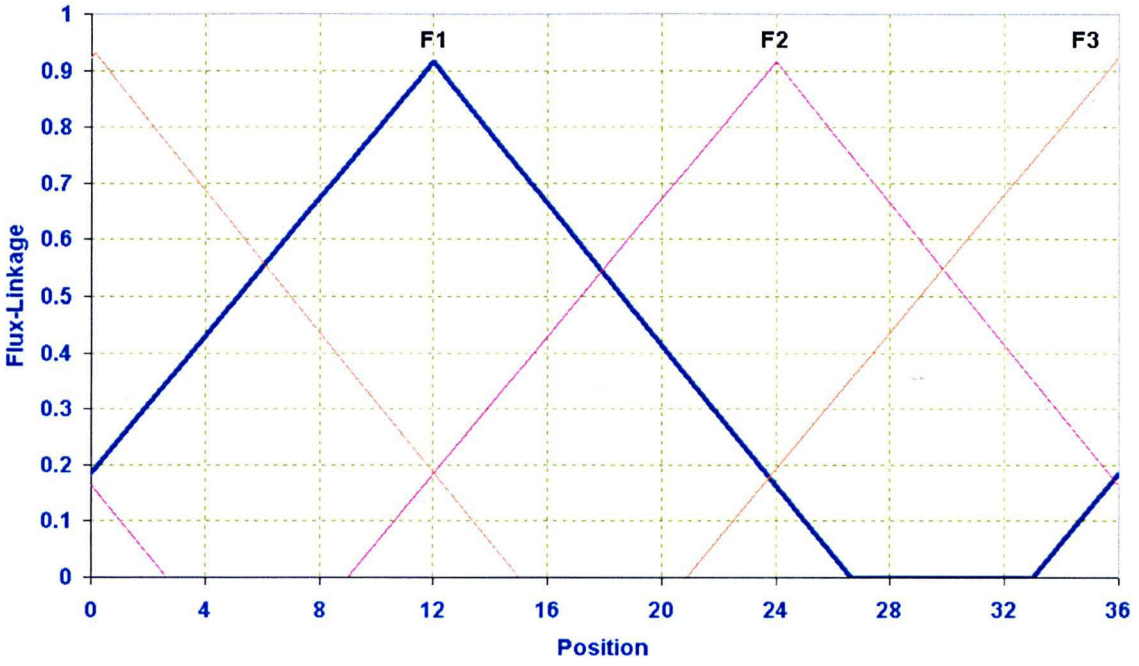

Fig. 9.25 Flux Waveforms

F1 is the flux in stator pole 1.

9.8.4 Determination of the Ratio of the Flux in the Segment to the Flux in the Yoke

As in the 12/8 machine the ratio of the flux in the segments to the flux in the yoke during its movement from unaligned position to the aligned position is determined with no saturation and is illustrated in Fig. 9.26 [122-124].

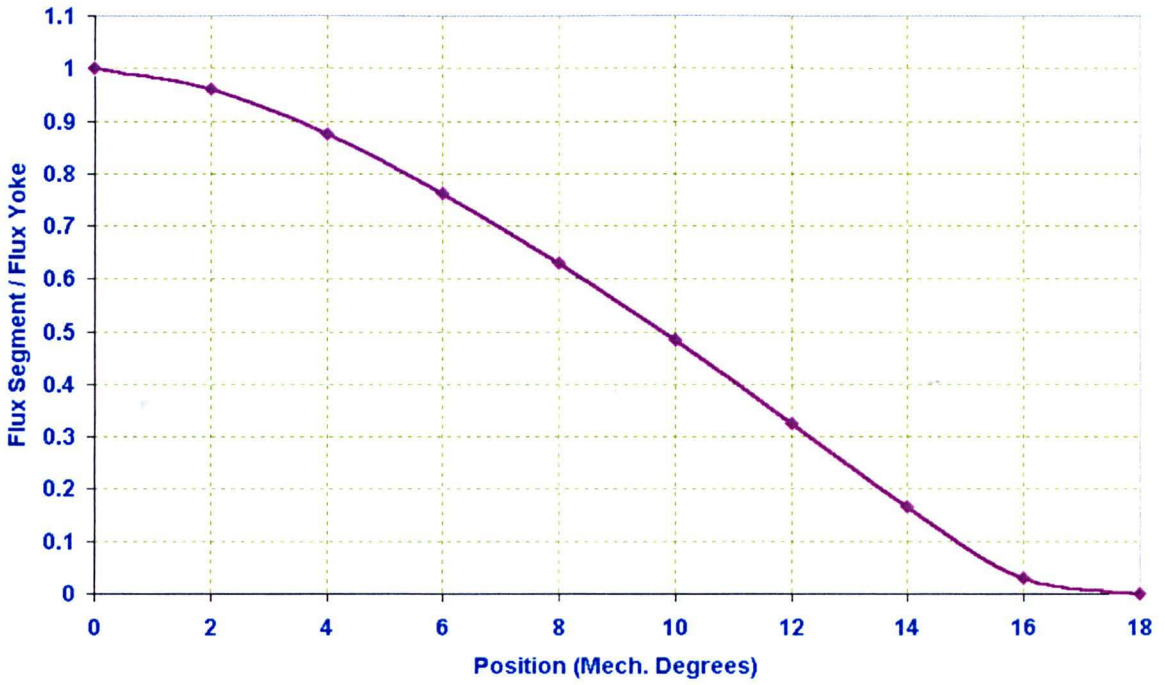

Fig. 9.26 Ratio of the Flux in the Segment to the Flux in the Yoke

Figures from 9.27 to 9.31 show the flux-linkage and flux density distribution in different parts of the machine.

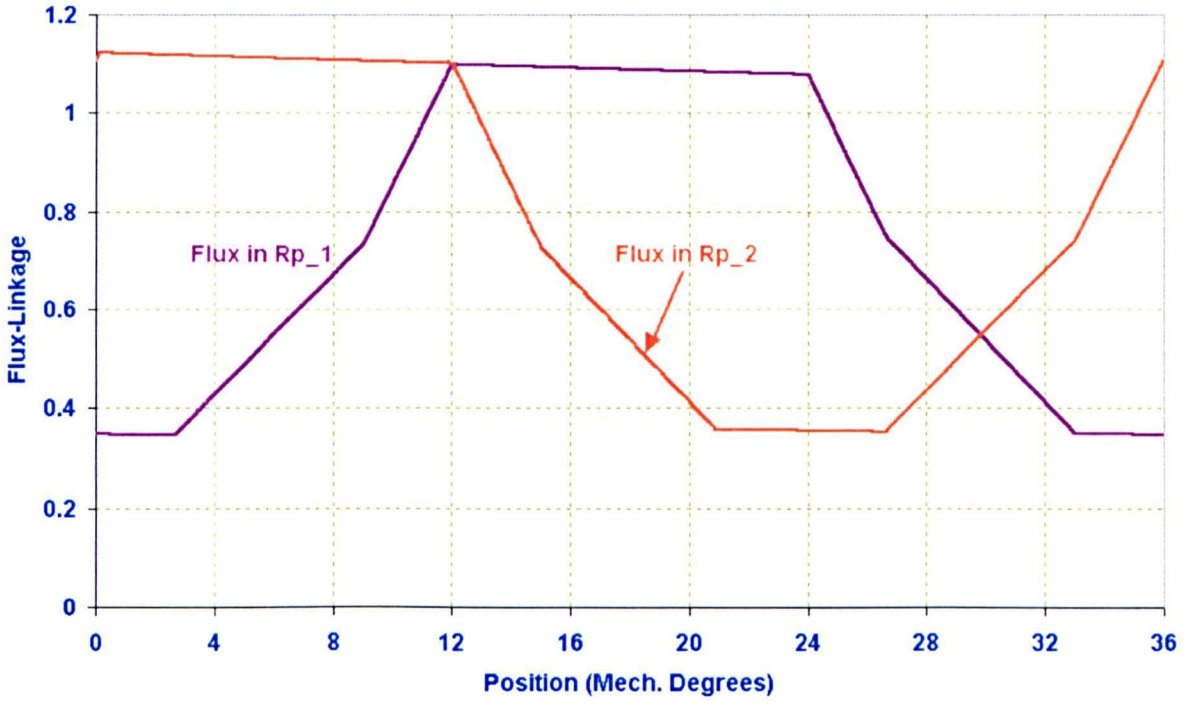

Fig. 9.27 Flux in the two Returning Poles

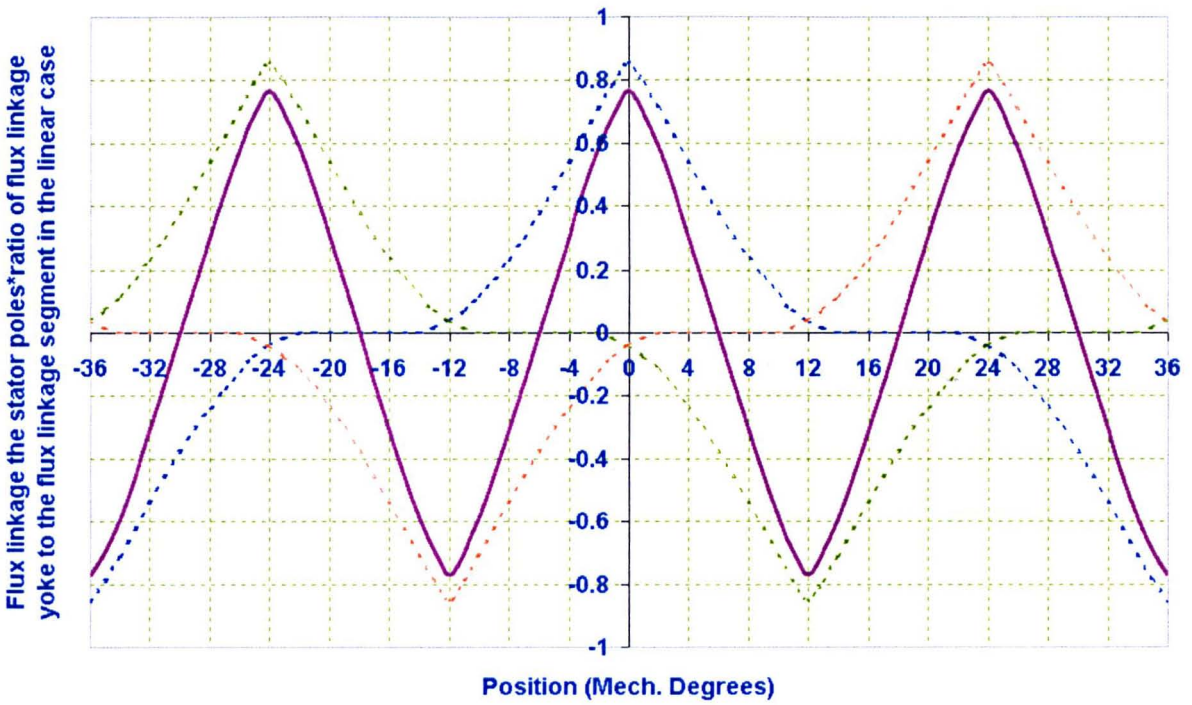

Fig. 9.28 Flux-Linkage the Segment

9.8.5 Flux Density Variation

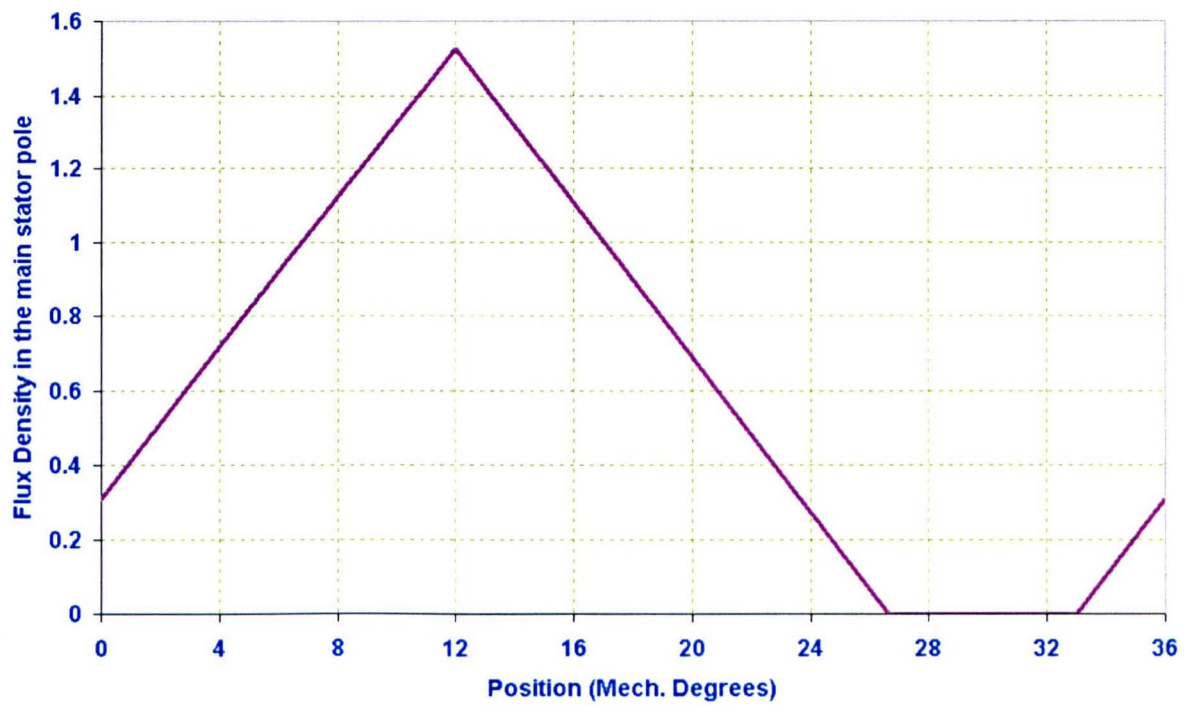

Fig. 9.29 Flux Density in Stator Pole

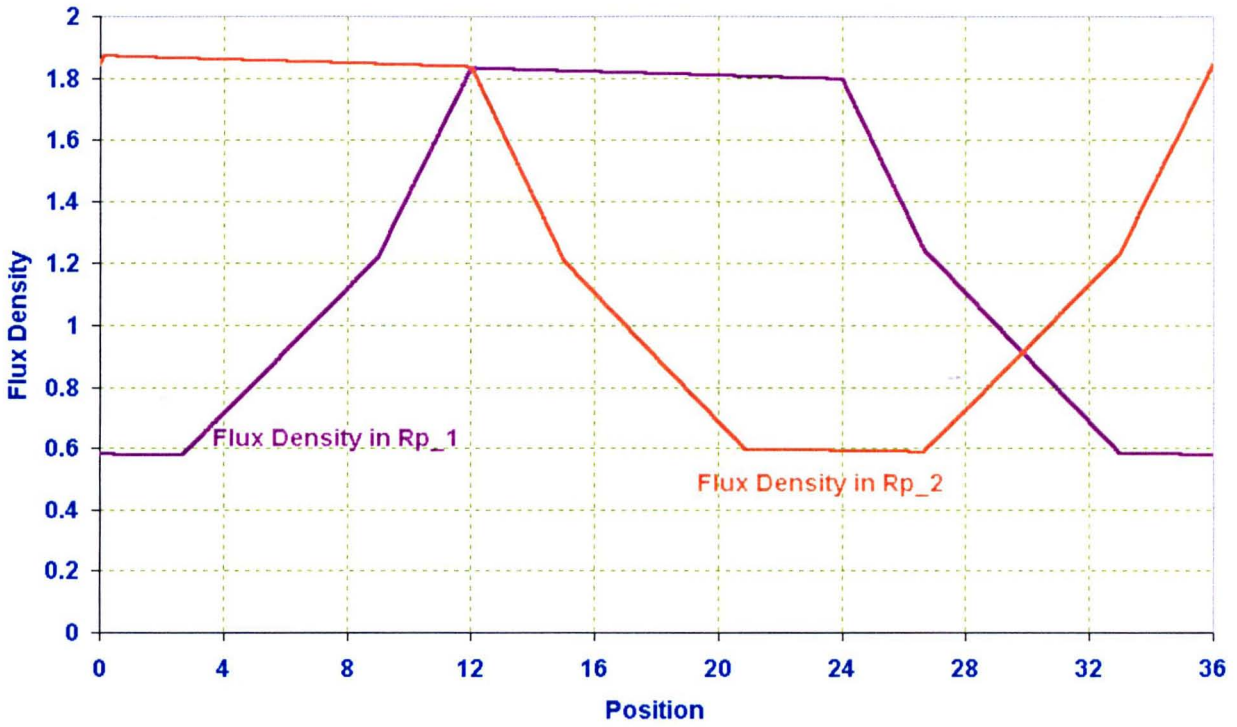

Fig. 9.30 Flux density in Returning Paths

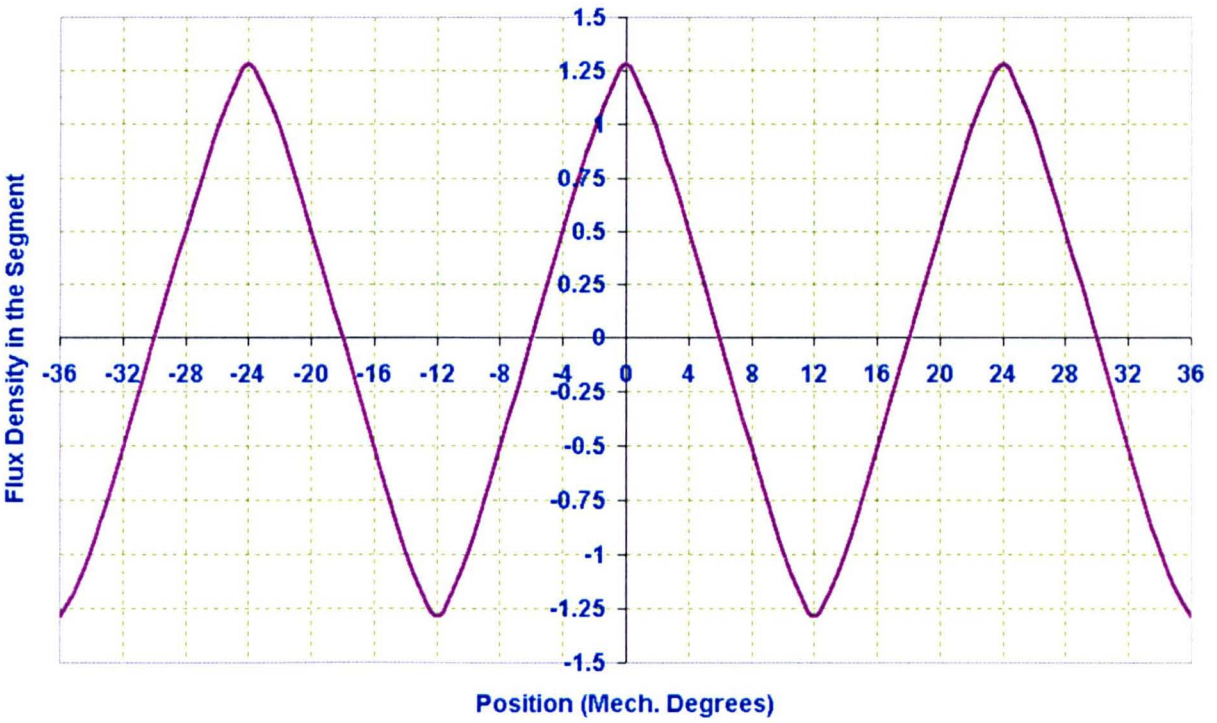

Fig. 9.31 The Flux Density in the Segment

9.8.6 Loss Calculations

The table below shows the calculated iron loss components for each part of the machine. Hysteresis loss in the stator continues to dominate the iron loss distribution. Table 9.3 compares the iron loss in different sections of the 12/10 segmented-rotor SRM.

	Yoke	Stator Teeth	Unwound Stator Teeth	Rotor Segments
Volume (m^3)	0.000660	0.000374	0.000187	0.000272
Anomalous Loss Density (W/kg)	0.91	0.91	0.895	3.29
Hysteresis loss Density (W/kg)	10.92	10.92	14.8	2.67
Eddy Current Loss Density (W/kg)	1.35	1.35	1.636	7.16
Total Loss (W)	69.11	36.3832	12	28.34

Table 9.3 Comparison of Machine Iron Losses in Different Sections of the 12/10 Segmented Rotor SRM

Total iron loss = 157.785Watts

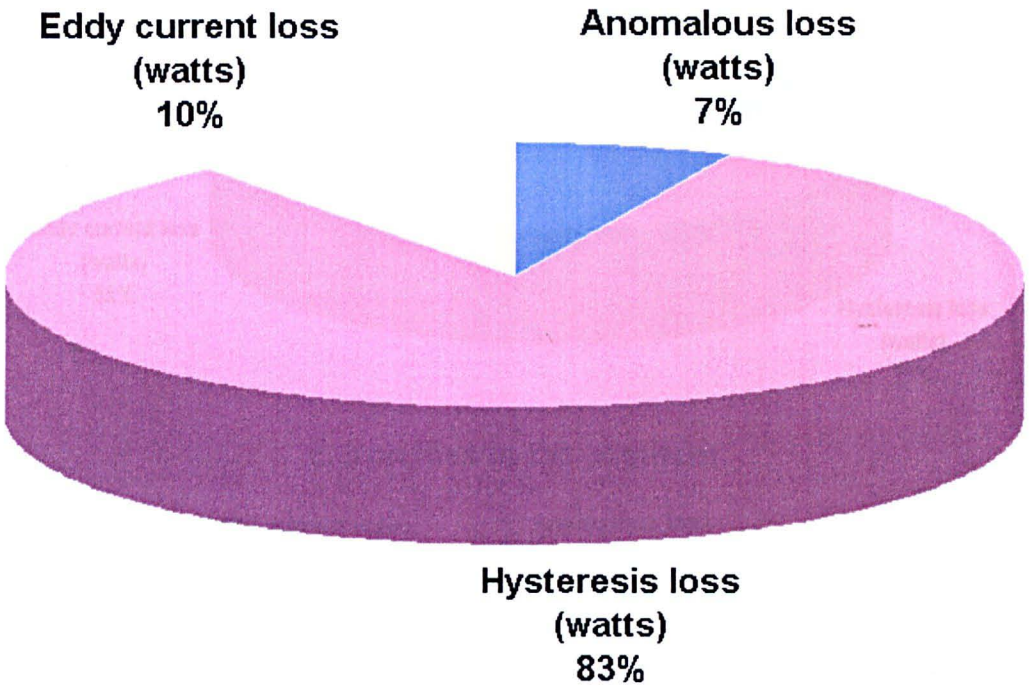

a. Iron loss in the main stator pole

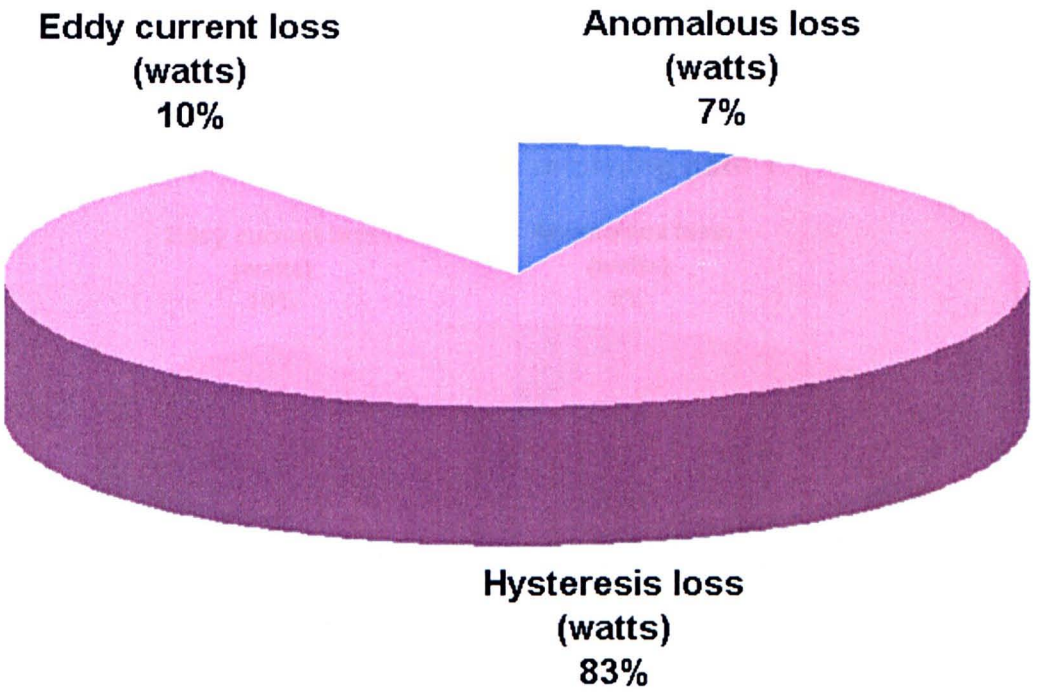

b. Iron loss in the yoke

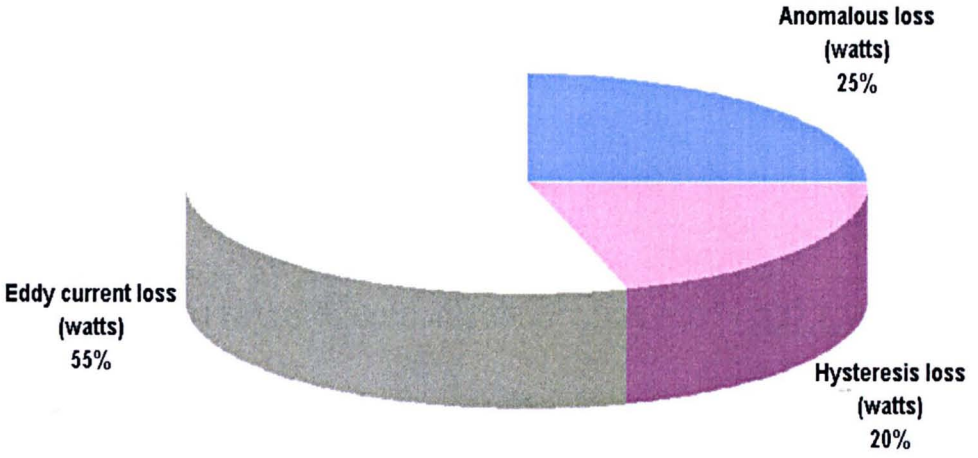

c. Iron loss in the segment

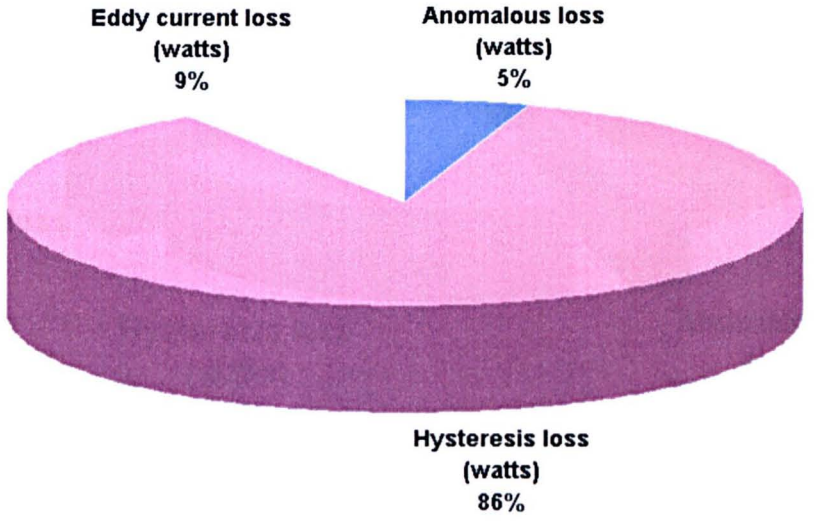

d. Iron loss in the returning path 1

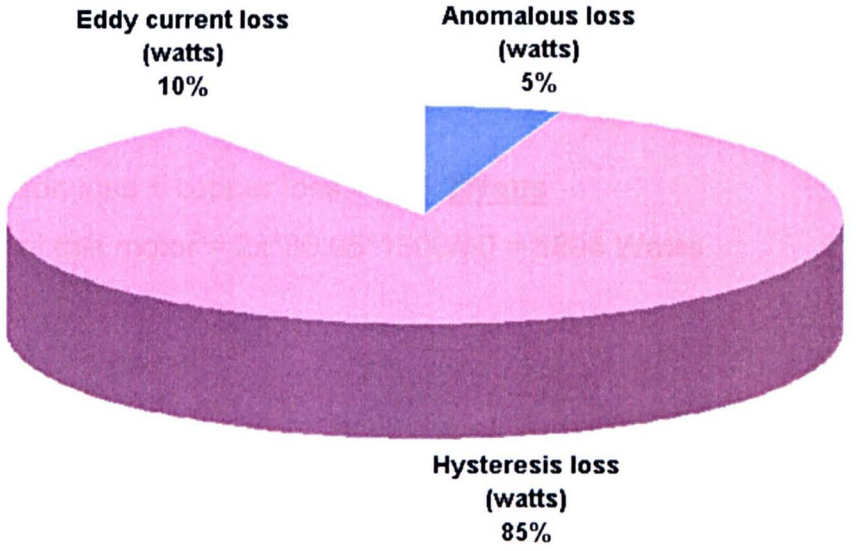

e. Iron loss in the returning path 2

Fig. 9.32 Distribution of Iron Loss

Fig. 9.32 shows the relative iron loss distribution in each section of the new 12/10 segmented-rotor SRM.

9.9 Estimation of the Copper Loss

Total Copper loss: $P = 3J^2 \rho V_{cu}$

$=3*(9.21143*10^6)^2*0.0178*10^{-6}*200*0.4266536*1.028*10^{-6}=$ 397.5 Watts

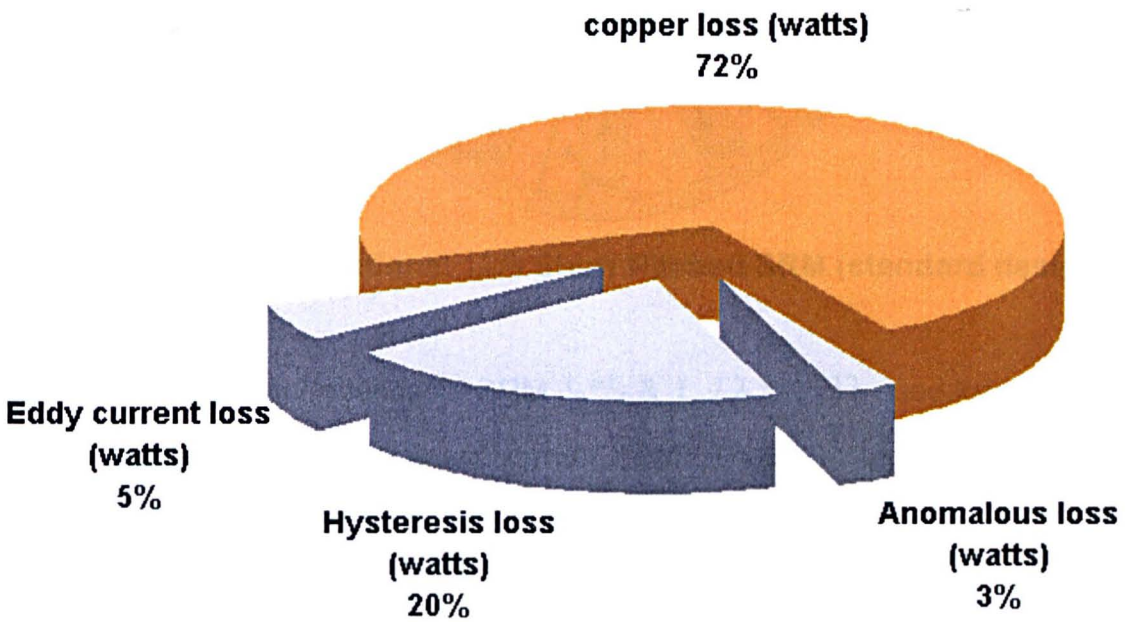

Fig. 9.33 Distribution of the Losses

Fig. 9.33 shows the relative distribution of the different loss in the 12/10 new segmented-rotor SRM.

Total losses =iron loss + copper loss = **555.2Watts**

Output power of this motor = $2\pi*36.95*1500/60$ = **5804 Watts**

9.10 Short Pitched 12/8 SRM

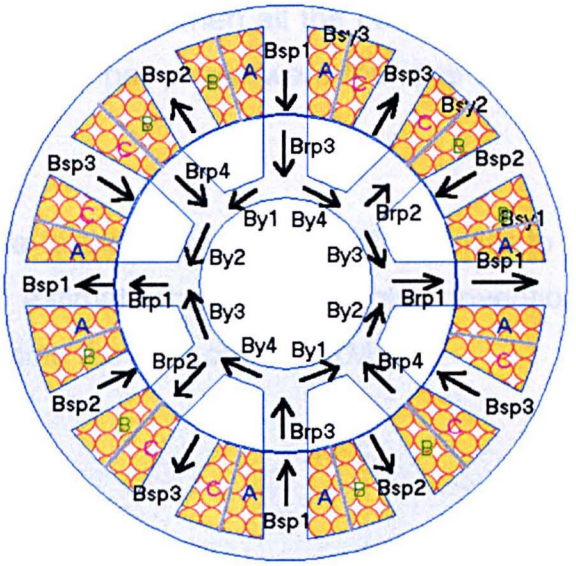

Fig. 9.34 Conventional 12/8 Short Pitched SRM (standard design)

Fig. 9.34 shows the conventional SRM $t_s = t_r$ & $t_s / \lambda = 0.33$ used for the comparison of its losses with the new segmented-rotor SRM. The dimensions of this machine are taken as the standard dimensions of the conventional SRM. The width of the yoke is half the width of the tooth in both the rotor and stator.

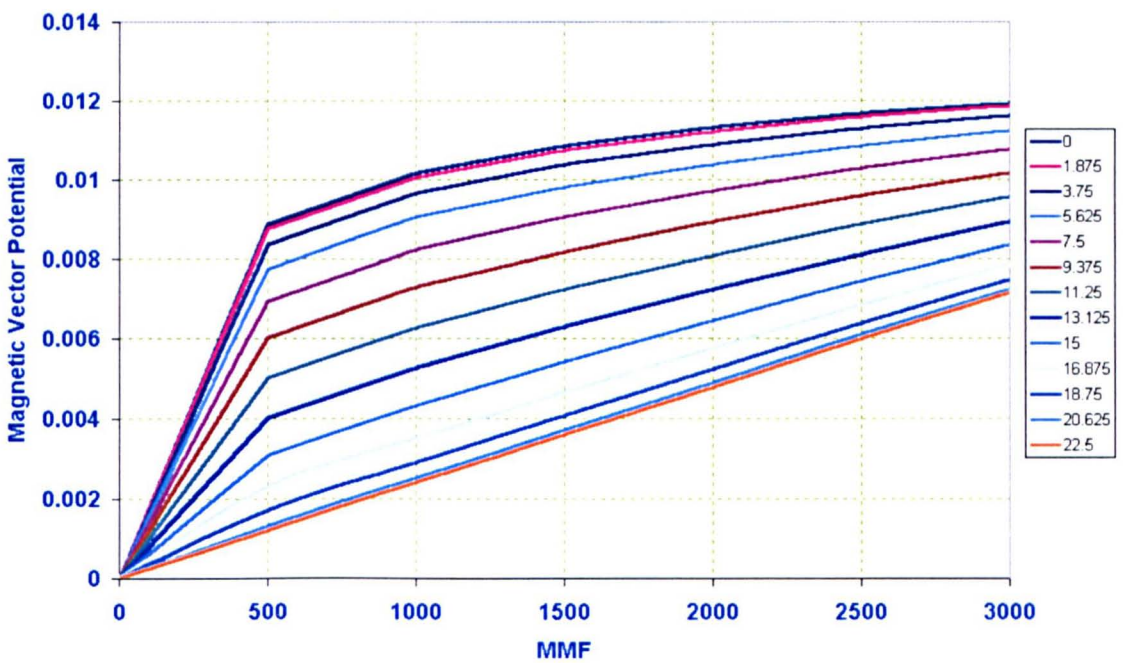

Fig. 9.35 Magnetic Vector Potential versus the MMF (Conventional SRM)

Fig. 9.35 shows the magnetic vector potential versus the MMF for one slot of the convention SRM (one slot mean when all the conductors fill the slot area). For this machine a total of 300 turns per phase were found to coincide with a base speed of 1500 rpm.

Figures are drawn here to the conventional SRM similar to the same figures of the previous two SRMs to estimate the losses in this conventional 12/8 SRM (see Fig. 9.36 to Fig. 9.43) but using the data of this SRM.

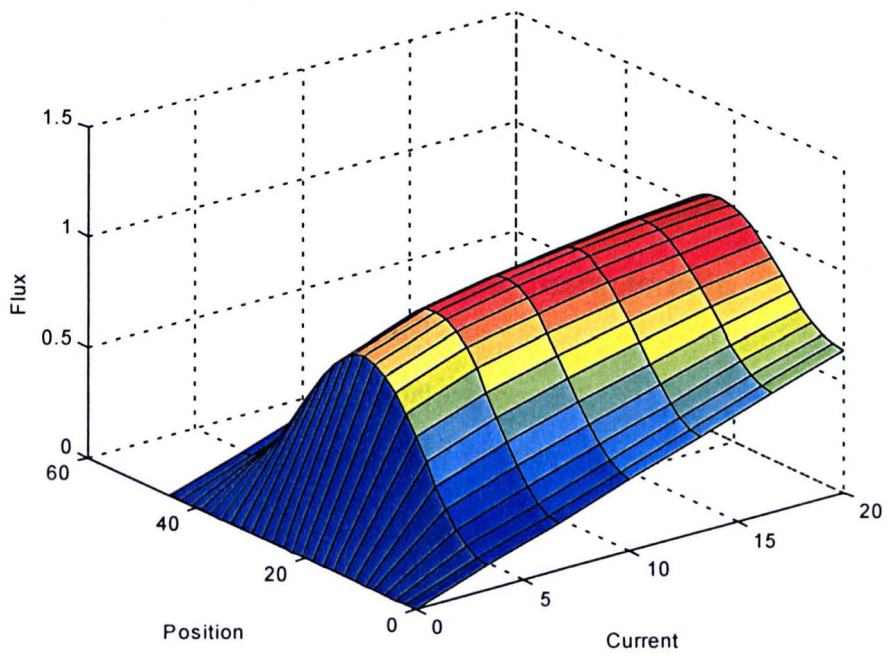

Fig. 9.36 Flux-Linkage Characteristic

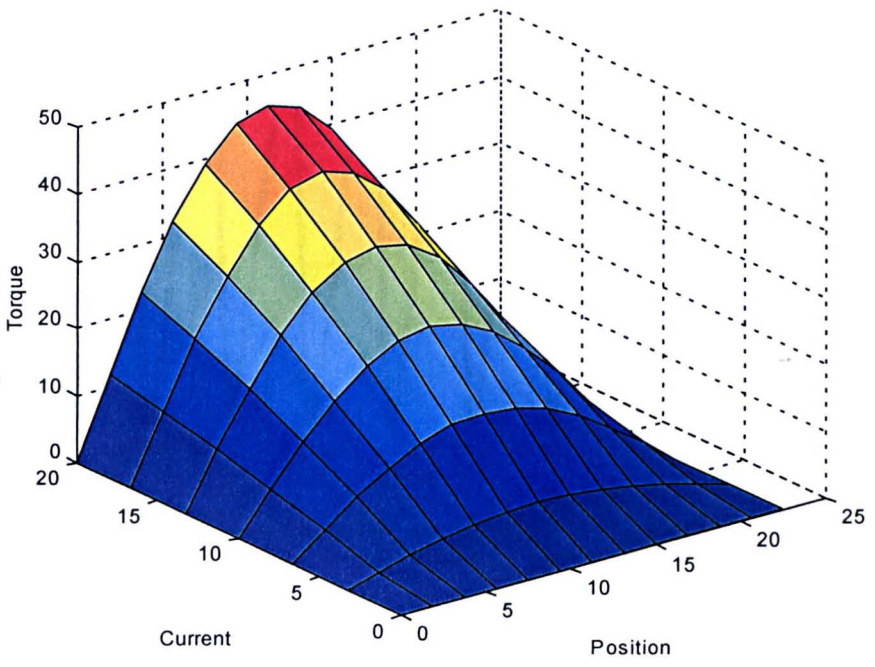

Fig. 9.37 Static Torque Characteristic

Area of one slot =430 mm^2 , Assuming fill factor=0.4.

There are 300 turns / phase and four coils / phase.

Area of one conductor = $\frac{0.4*430*0.5}{75}$ =1.1466 mm^2

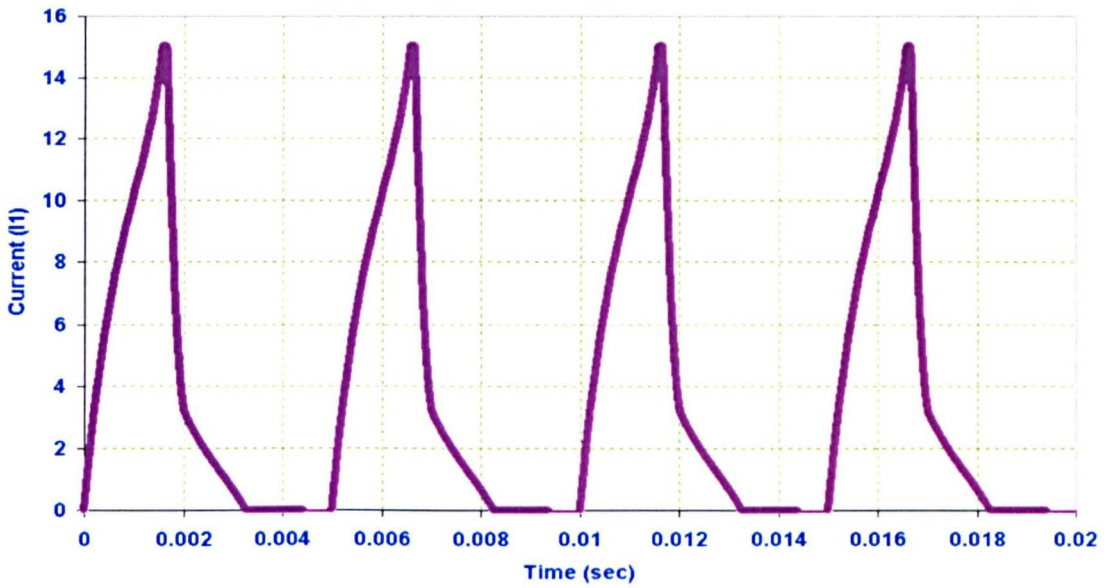

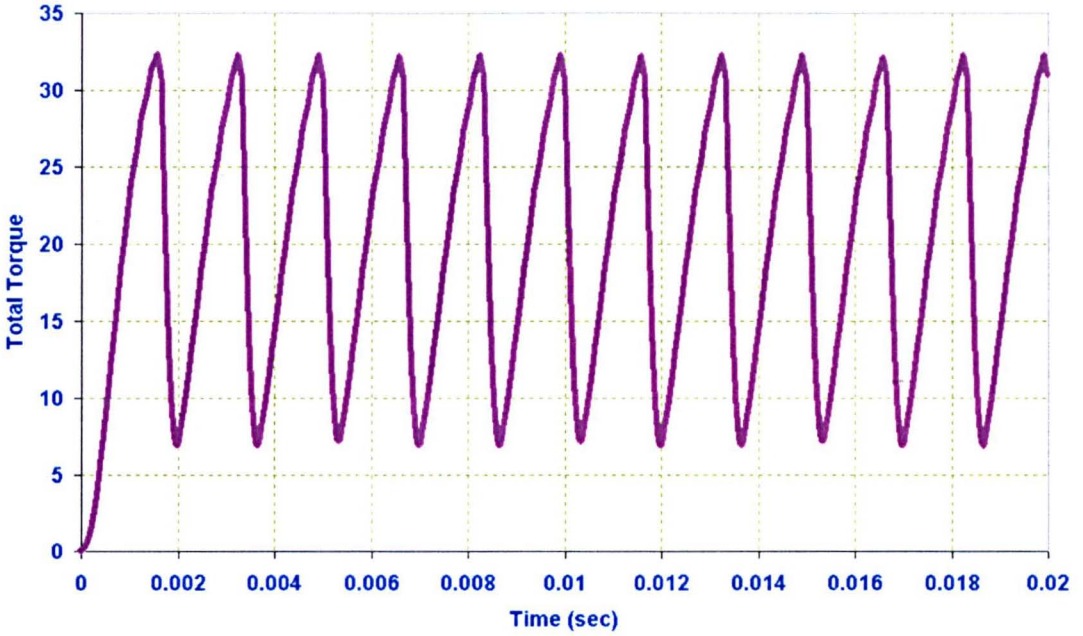

Fig. 9.38 Current and Torque Wave Forms

I_{rms} = 5.7Amp (on/off angles: 0/15 Mech. degrees)

$J_{rms} \frac{I_{rms}}{\text{Area of one conductor}} = \frac{5.7}{0.5733} \cong 10$ Amp/mm^2 and mean output torque is 20.0 Nm

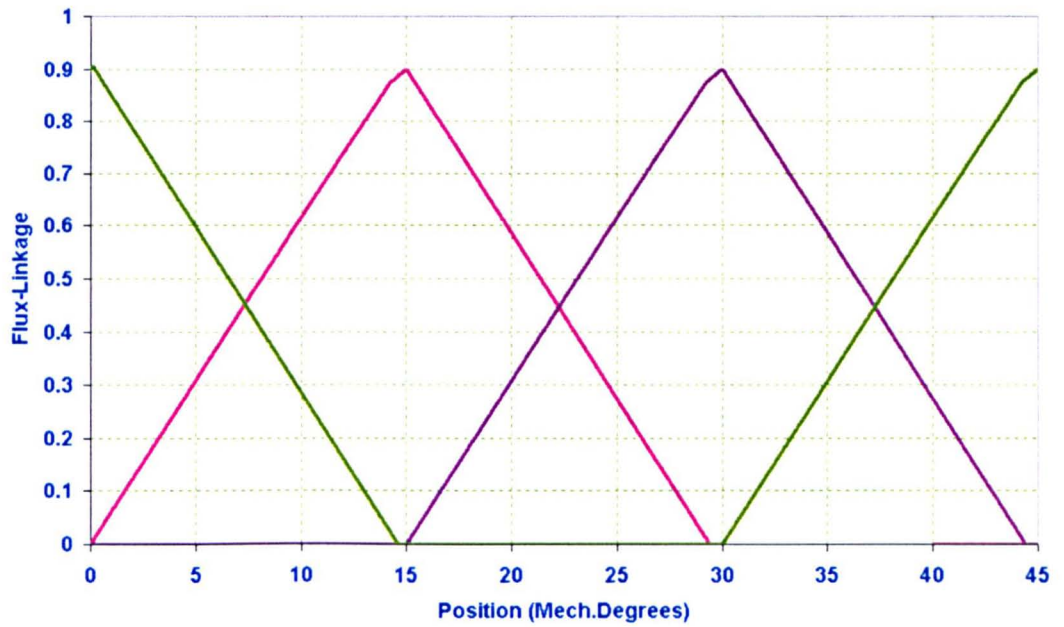

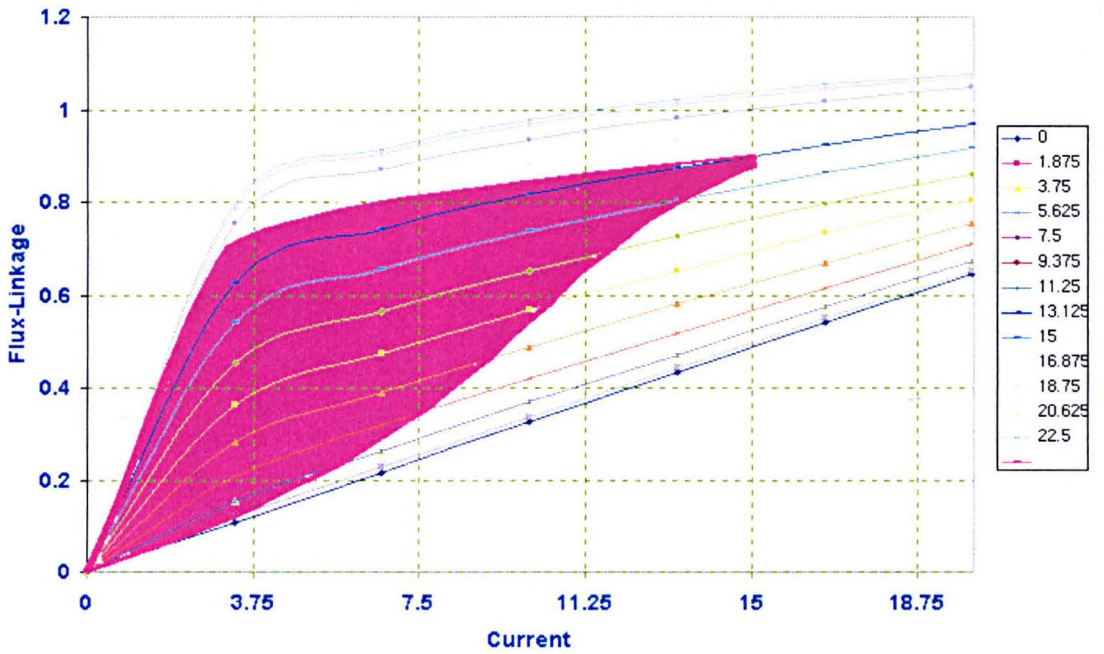

Fig. 9.39 Flux-Linkage Waveform and Flux-Linkage Trajectory

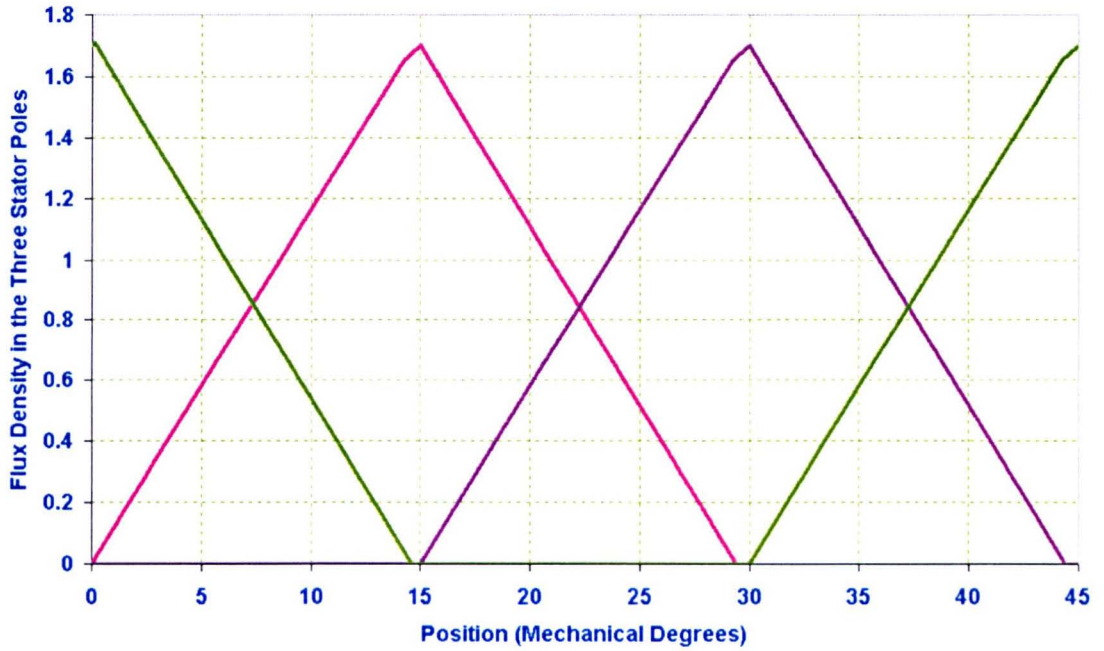

Fig. 9.40 Flux Density in the three Stator Poles

From Fig. 9.34 [229-235]:

$B_{sy1}=B_{sp2}+B_{sp1}-B_{sp3}$, $B_{sy2}=B_{sp1}-B_{sp2}-B_{sp3}$, $B_{sy3}=B_{sp1}+B_{sp3}-B_{sp2}$

$B_{sy1}=B'_{sy1}$, $B_{sy2}=B'_{sy2}$, $B_{sy3}=B'_{sy3}$

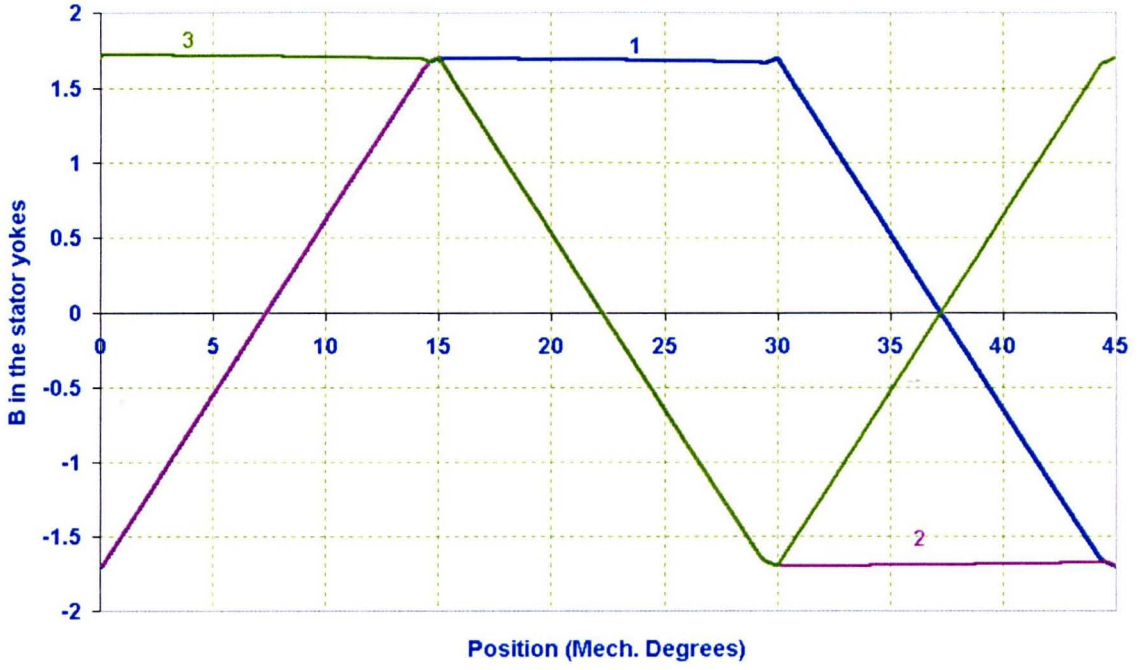

a

b

Fig. 9.41 Flux Density in Stator Yokes and Rotor Poles1&3

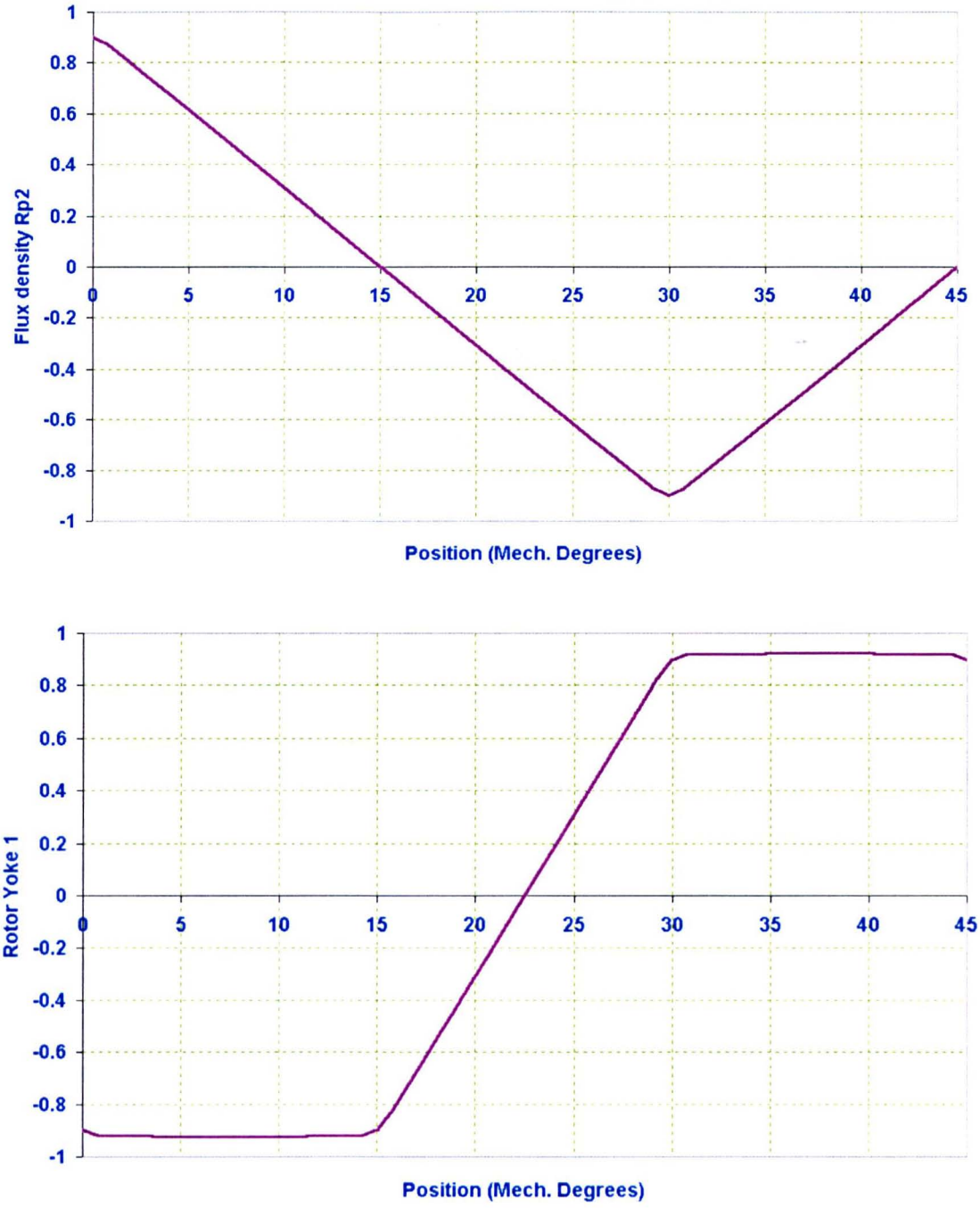

Fig. 9.42 Flux Density in Rotor Poles2&4 and Rotor Yoke 1

Fig. 9.43 Rotor Yoke 2

9.11 Estimation of Losses in the Conventional Short pitched 12/8 SRM

Table 9.4 compares the iron loss in the different parts of the conventional SRM.

	Yoke	Stator Teeth	Rotor Teeth	Rotor Core Back
Volume (m^3)	0.000400	0.000496	0.000233	0.0001438
Anomalous Loss Density (W/kg)	2.4482	0.8651	0.497	0.94
Hysteresis loss Density (W/kg)	10.927	10.672	3.21	3.4482
Eddy Current Loss Density (W/kg)	5.427	1.362	0.5688	1.5
Total Loss (W)	60	50.7691	6.74	7.9243

Table 9.4 Comparison of Machine Iron Losses in Different Sections of the 12/8 Conventional SRM

Total iron loss = 86.893+13.1786+25.3944=125.45Watts

9.11.1 Calculation of the Copper Losses

Total length of one turn=2*0.15+2*(1.5*0.01176)+2*0.0209=0.37708m

Copper loss for 3-phases

$P = 3J^2 \rho V_{cu}$ =3*(10*10^6)^2*0.0178*10^{-6}*300*0.37708*1.1466 *10^{-6}=692.64 Watts

Total losses = 818.09 Watts. Output Power=2π*1500*20/60=3142.857Watts

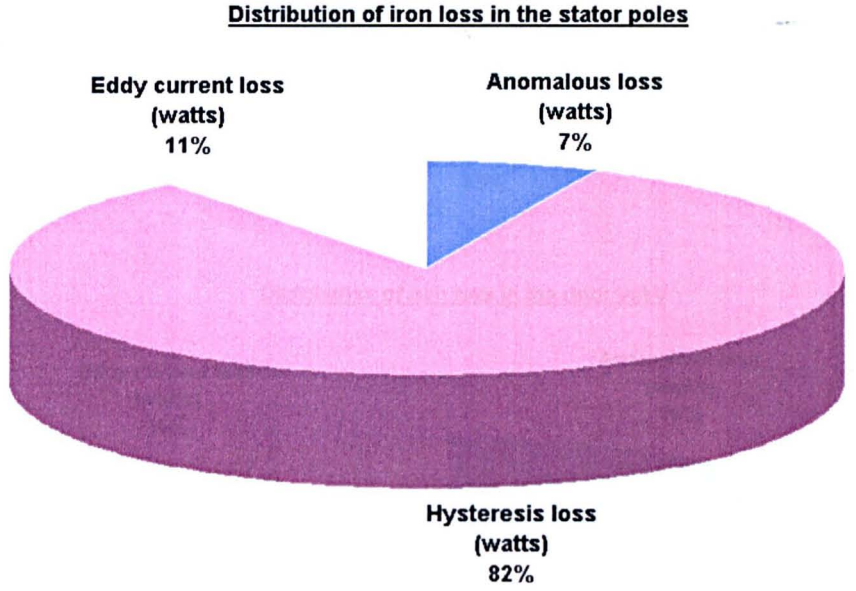

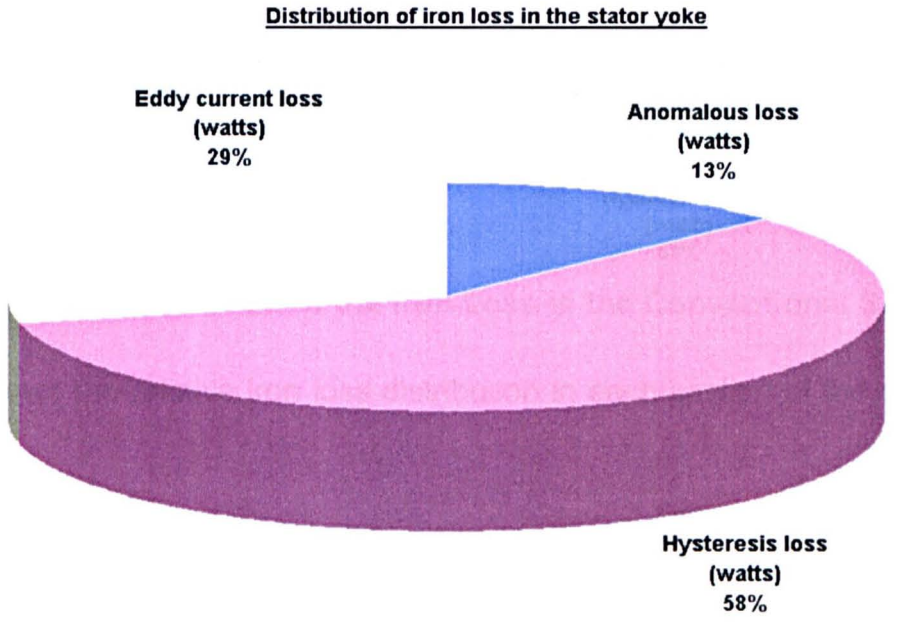

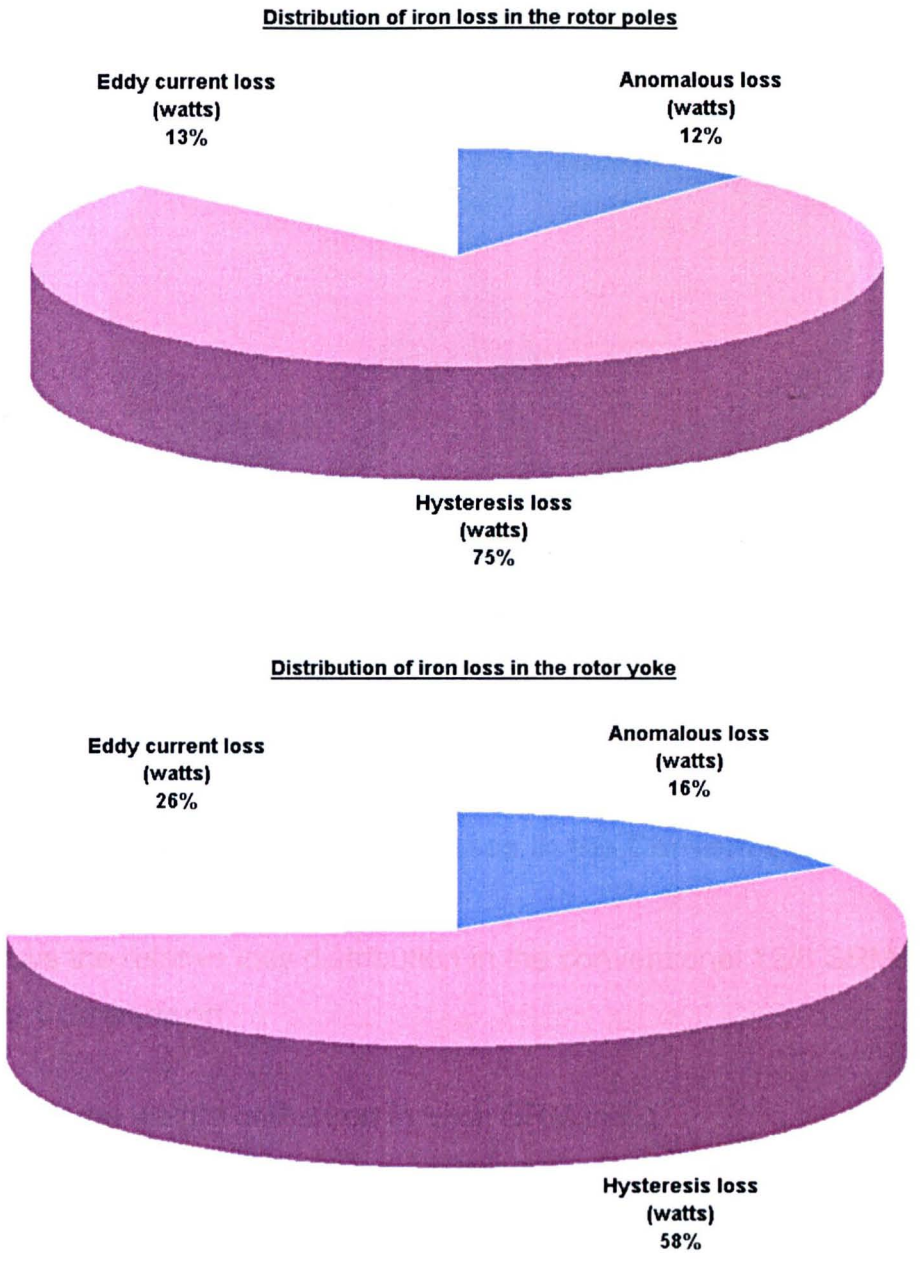

Fig. 9.44 Distribution of the Iron Loss in the Conventional SRM

Fig. 9.44 shows the relative iron loss distribution in each section of the conventional 12/8 SRM.

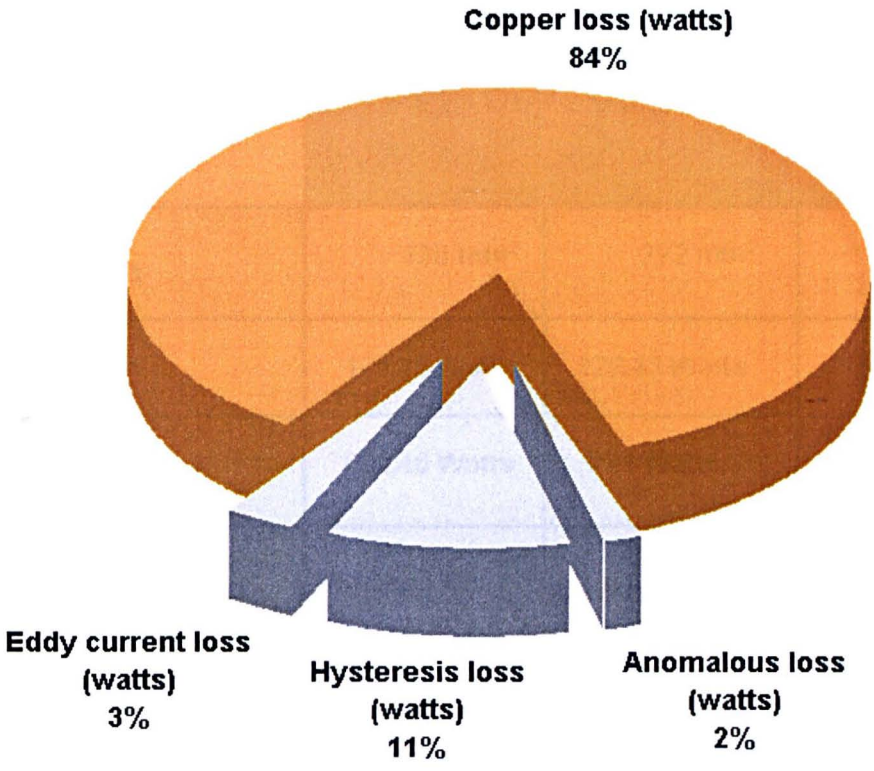

Fig. 9.45 Distribution of the Losses in the Conventional SRM

Fig. 9.45 shows the relative loss distribution in the conventional 12/8 SRM.

9.12 General Comparison

Table 9.5 shows the weight of the iron in each SRM in Kg

12/8 Segmented-Rotor SRM	12/10 Segmented-Rotor SRM	12/8 Toothed-Rotor SRM
10.686 Kg	11.549 Kg	10.11 Kg

Table 9.5 Weight of the Iron in Each SRM

	Conventional SRM	12/8 New SRM	12/10 New SRM
Slot Area	430 mm^2	272 mm^2	257 mm^2
iron Loss	125.45 Watts	122.43 Watts	157 Watts
Copper Loss	692.46 Watts	721 Watts	397.45 Watts
Total Loss	0.818 kW	0.844 kW	0.555 kW
Output Kw	3.14 kW	4.99 kW	5.804 kW

Table 9.6 General Comparison between the SRMs

Table 9.6 compares the losses in the new segmented-rotor SRMs with the conventional toothed-rotor SRM. The comparison shows the 12/10 SRM has lower end-winding copper loss than the 12/8 segmental machine since the conductors of each phase are closer to each other. It also has lower copper loss than the conventional SRM because the slot area is much smaller, giving a lower winding loss when the current density is fixed.

Iron loss in the two 12/8 machines is similar, but the 12/10 machine has approximately 25% greater loss, coinciding with the 25% increase in electrical frequency.

9.13 The Losses at Higher Speed

In this section the iron losses are compared for machines designed for operating at higher speed. This comparison will be done in a simple manner: as the machine runs faster the number of turns is proportionally reduced, so that the flux waveform variation with position remains effectively constant.

Table 9.4 shows the previous estimated losses in detail in each of the three SRMs at 1500 rpm.

	Anomalous	Hysteresis	Eddy Current	Copper
12/8 Segmented-Rotor SRM	7.586W	103.9W	10.9W	721.65W
12/10 Segmented-Rotor SRM	15.62W	113.677W	28.5W	397.46W
12/8 Toothed-Rotor SRM	13.178W	86.89W	25.394W	692.64W

Table 9.4: The Losses of the three SRMs at 1500 rpm

From the previous equations of the iron losses estimation: Increasing the frequency by factor X increases the anomalous losses by factor $(X)^{1.5,}$ the hysteresis loss by a factor X and the eddy current losses by a factor $(X)^2$. This results in the following overall variation in iron loss with speed.

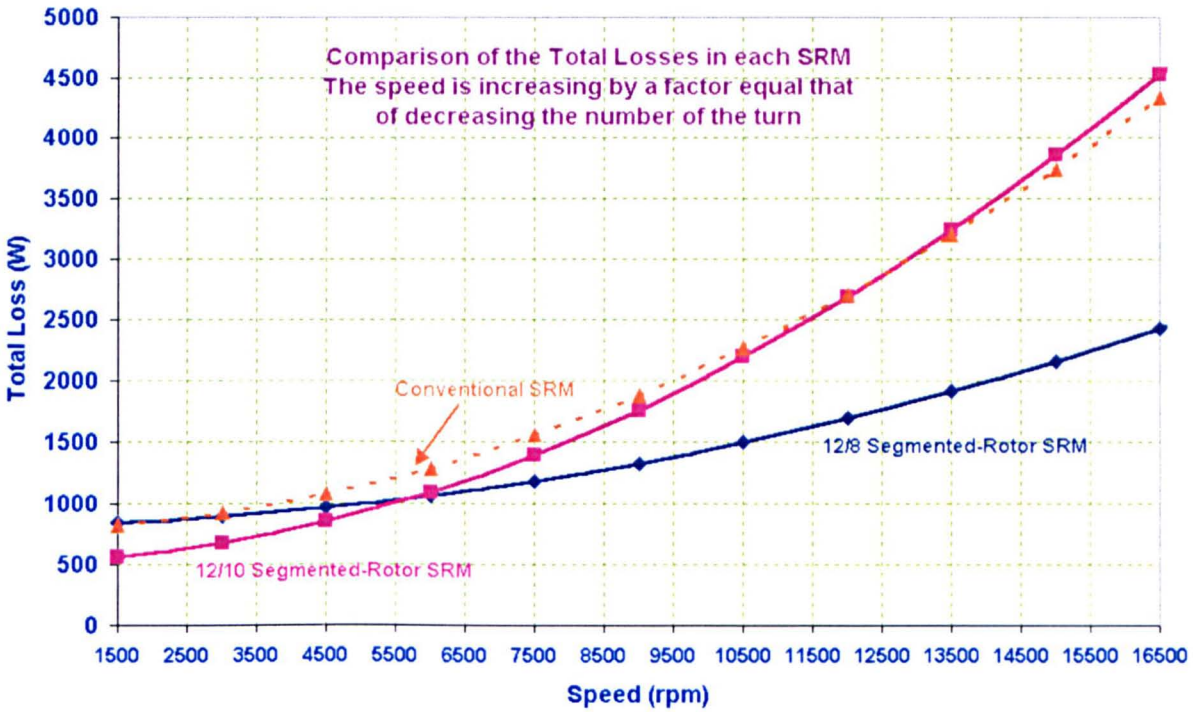

Fig. 9.46 Comparing the Losses at High Speeds

Fig. 9.46 shows the losses at high speed. The new 12/8 segmented-rotor SRM has only about 60% of the iron loss of the conventional 12/8 SRM, despite it having almost the same volume and excitation frequency. This can be understood from examination of the flux variations in each component.

In the 12/8 segmented-rotor SRM the peak rate of change of flux density occurs in the stator teeth during the period when two adjacent phases are both increasing their flux-linkage. This rate of change of flux density is double that of the core back, which only ever sees the flux of one phase. Fig 9.13 shows how this peak rate of change of flux density occurs for one third of a cycle. The eddy current loss is directly proportional to the square of this value multiplied by the duration over which it occurs.

In the conventional SRM the peak rate of change of flux density occurs in the stator core back, which sees the flux of all three phases. Fig. 9.41 shows how the same flux density variation occurs for two thirds of a cycle. Consequently it seems that the eddy current losses are effectively doubled.

9.14 Conclusion

The estimation of the iron loss has been introduced in this chapter for the new segmental SRMs and compared to an equivalent conventional SRM. The methods used split each machine into a few regions, evaluate the flux variation in those regions, and then determine the flux density variation, assuming an even flux density distribution. A modified iron loss formula for non-sinusoidal waveforms is used for each type of SRM, splitting the iron loss into hysteresis loss density, anomalous loss density and eddy current loss density.

At 1500 rpm the iron loss in all three machines is dominated by hysteresis loss. The 12/8 segmental machine has similar iron loss to a 12/8 conventional SRM at this speed, whilst the 12/10 segmental machine has 25% greater iron loss because a 25% higher electrical frequency is employed.

At higher speeds of 15,000 rpm or more the iron loss is dominated by eddy current loss and a different situation occurs in which the 12/8 segmental machine appears to have only 60% of the iron loss of a conventional 12/8 SRM. This is thought to be because the regions which have the greatest rate of change of magnetic flux density

variation are the teeth, which only have the high rate of change of flux density for one third of a cycle and only carry uni-directional flux. In the conventional SRM the core back has the greatest rate of change of flux density, with the flux varying from peak negative to positive values for two thirds of a cycle, thereby increasing the eddy current loss density.

10 Running Test of the Segmented-Rotor SRM

10.1 Introduction

This chapter tests the dynamic performance of the new segmented-rotor SRM. Two prototypes of the new segmented-rotor SRM are tested under different running conditions. The switching on or advance angle, the conduction angle and the speed were changed to study the effect on the torque (average and ripple) and the performance. The chapter tests the new SRMs using simulated results and uses some measured results for validation.

10.2 Simulation of the SRMs

A Matlab based package for simulating the equations of the SRM (which were introduced in chapter (1)) is used here to investigate the SRM with different operating conditions [62]. Both the predicted and measured Flux-Linkage characteristics of the SRM are used in the simulation, to inspect the degree of the accuracy of the simulation by the measured results [62].

10.3 Testing of the SRMs

The machines were each coupled to a three phase asymmetric half bridge inverter and subjected to an extensive series of running tests. The inverter employs IGBTs, fed from a d.c. link, switching at 20kHz, with rotor position measured using a twelve bit optical encoder. Rotor position and the phase currents are fed back into a DSP based PI controller, which implements the phase current control. The current demand for each phase is constant during its desired conduction period and zero for the rest of a cycle. The machine is coupled to a d.c. load machine, via a torque transducer, capable of measuring up to 100 Nm [62][122-124].

10.4 The 12/8 Fully Pitched Segmented-Rotor SRM

10.4.1 Torque / Speed Envelope

The simulation package was used to predict the torque/speed envelope of the drive. The converter voltage and the conduction angle were kept constant while the speed and the switch on angle were changed. A fixed current demand (current density J=10 Amp/mm^2) was employed, with a conduction angle of 180 electrical degrees, corresponding to 22.5 mechanical degrees. The family of characteristics for different switch on angles are shown in Fig. 10.1. Note that zero degrees corresponds to the unaligned position and a negative angle corresponds to phase advance before the unaligned position. The curves show how at low speeds, under current control, peak torque occurs from switching on at the unaligned position and off at the aligned position, but at higher speeds, when the machine moves into voltage control an increasingly large amount of phase advance is required.

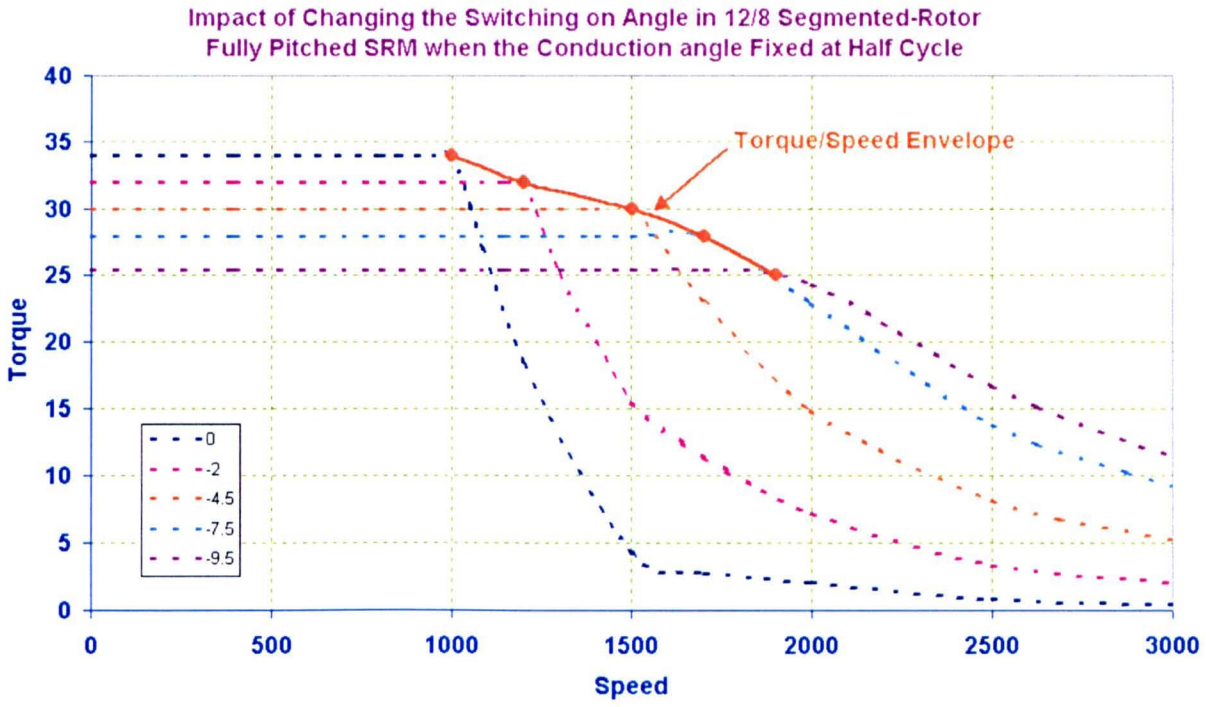

Fig. 10.1 Simulation Results of Torque/Speed Envelope

10.4.2 Comparing Simulated and Measured Results

A realistic control strategy for the SRM drive has to take into the consideration the mutual dependence between the motor parameters, the excitation and the limitations of the switching circuit. At low speed, the rate of increase of the current following the switching-on is high because the back-emf at low speed is small, and peak current has to be limited by chopping. But at high speed, the back-emf becomes dominant so current peaks before commutation. When the SRM is to be operated as a variable speed drive two different switching strategies are used. First, low speeds operation; in which the current level has to be limited by chopping (current control). The second at high speeds operation; in which both the switching on and conduction angles should be controlled properly to enable the torque to satisfy the load conditions and to be as smooth as possible [7].

In this section the dynamic test results are arranged according to the speed of the SRM:

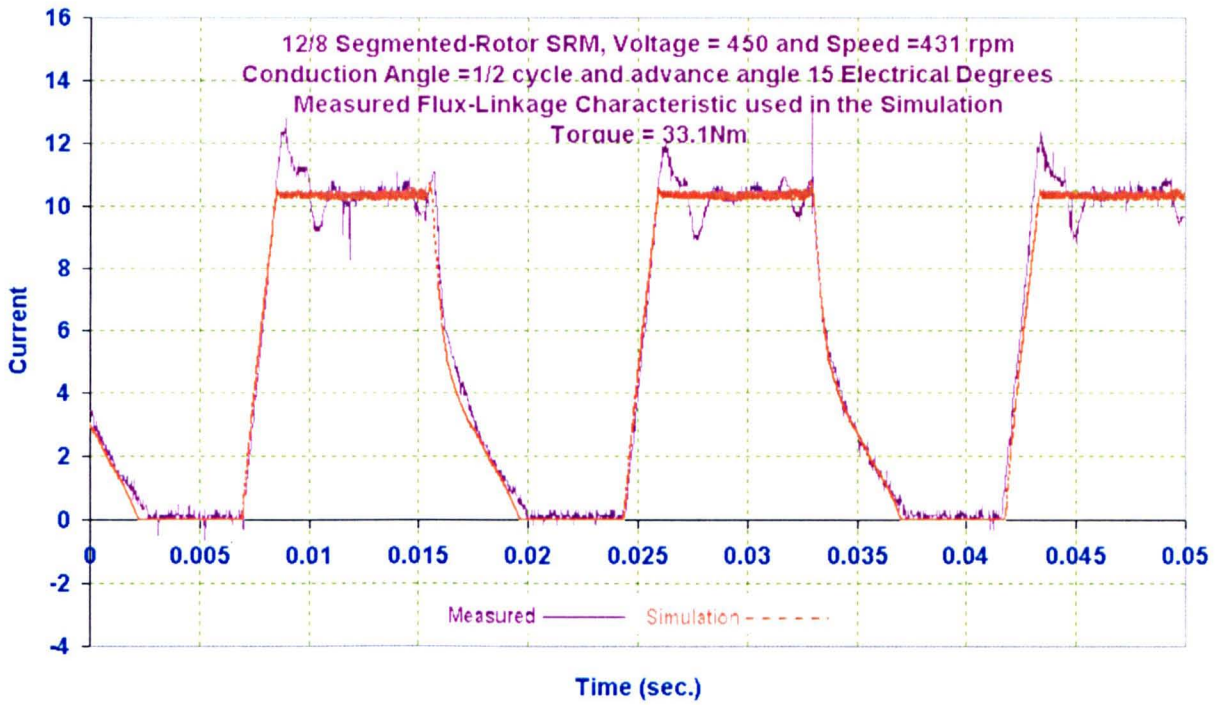

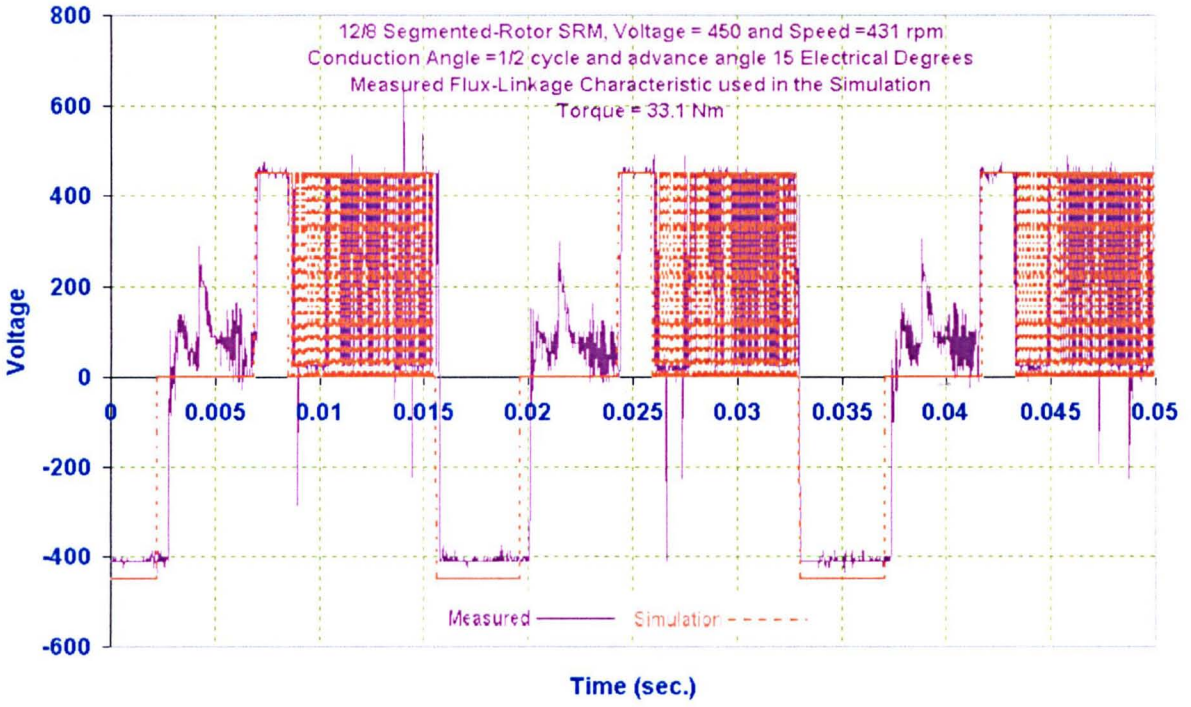

Fig. 10.2 12/8 Segmented-Rotor SRM Running at 431 rpm (conduction for half cycle)

Fig. 10.2 shows the current and the voltage of the machine when it runs at a low speed under current control. Applying positive voltage from the converter increases the current until it reaches the current demand. The current limiter limits the current to the required value. The running conditions of this test were set to give a large torque from the machine. The conduction angle is half the cycle and the advance angle is relatively high, both aspects combine to make the SRM deliver a large torque. The current is fixed due to the current limiter, and negative voltage is applied before the unaligned position to decrease the phase current to zero. The machine in this test delivers 33.1 Nm. The measured Flux-Linkage characteristic is used in the simulation and the simulated results can be seen to be very close to those measured. Note how during the off period the appearance of considerable voltage induced in an off phase. This may be due to capacitive coupling between phases.

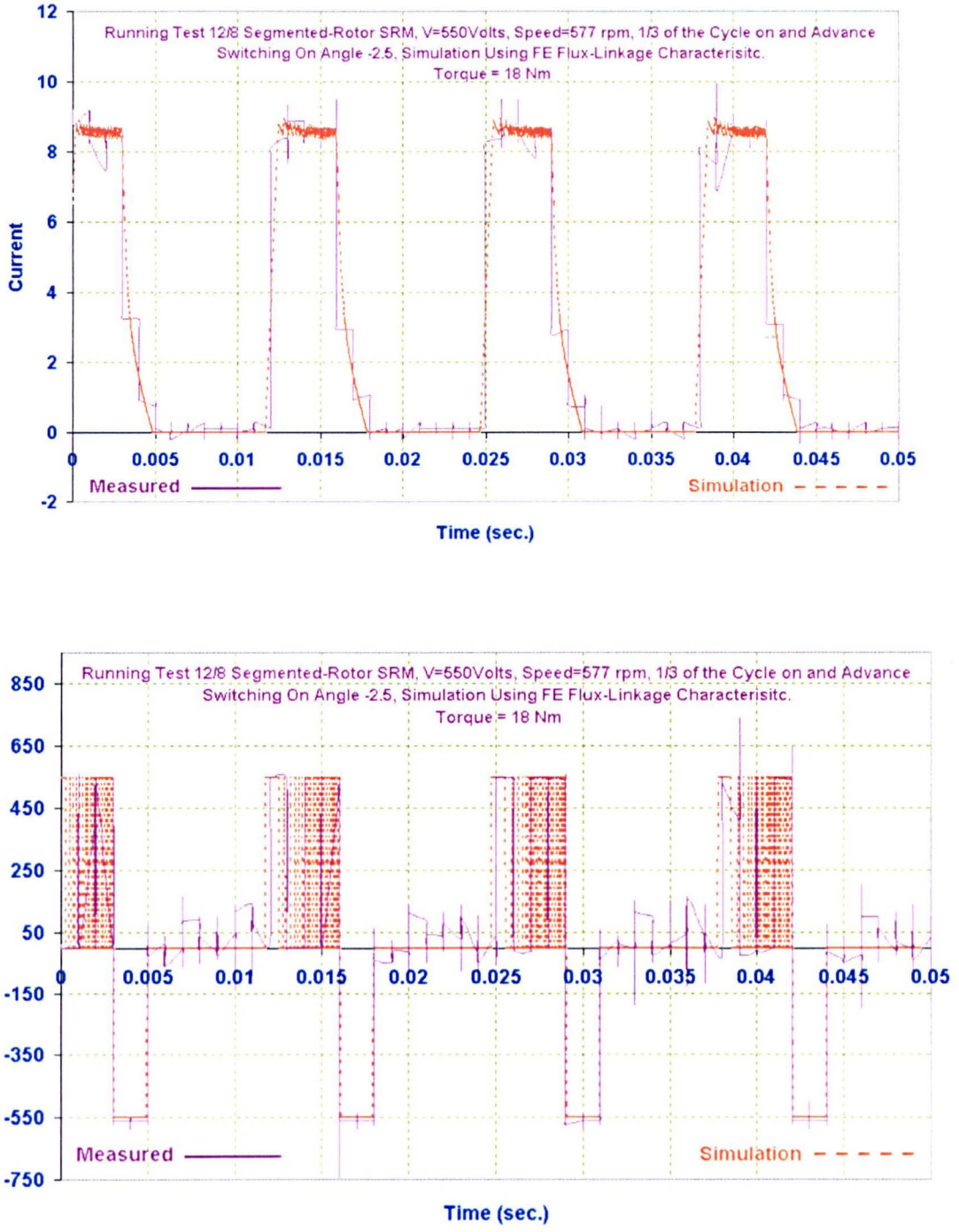

Fig. 10.3 12/8 Segmented-Rotor SRM Running at 577 rpm (conduction for third cycle)

The above test, Fig. 10.3, is similar to the previous one, but the conduction angle is reduced. The torque output is thus decreased. Note that the predicted Flux-Linkage characteristic, generated using 2D FE, is used in this test in a comparison with the measured results.

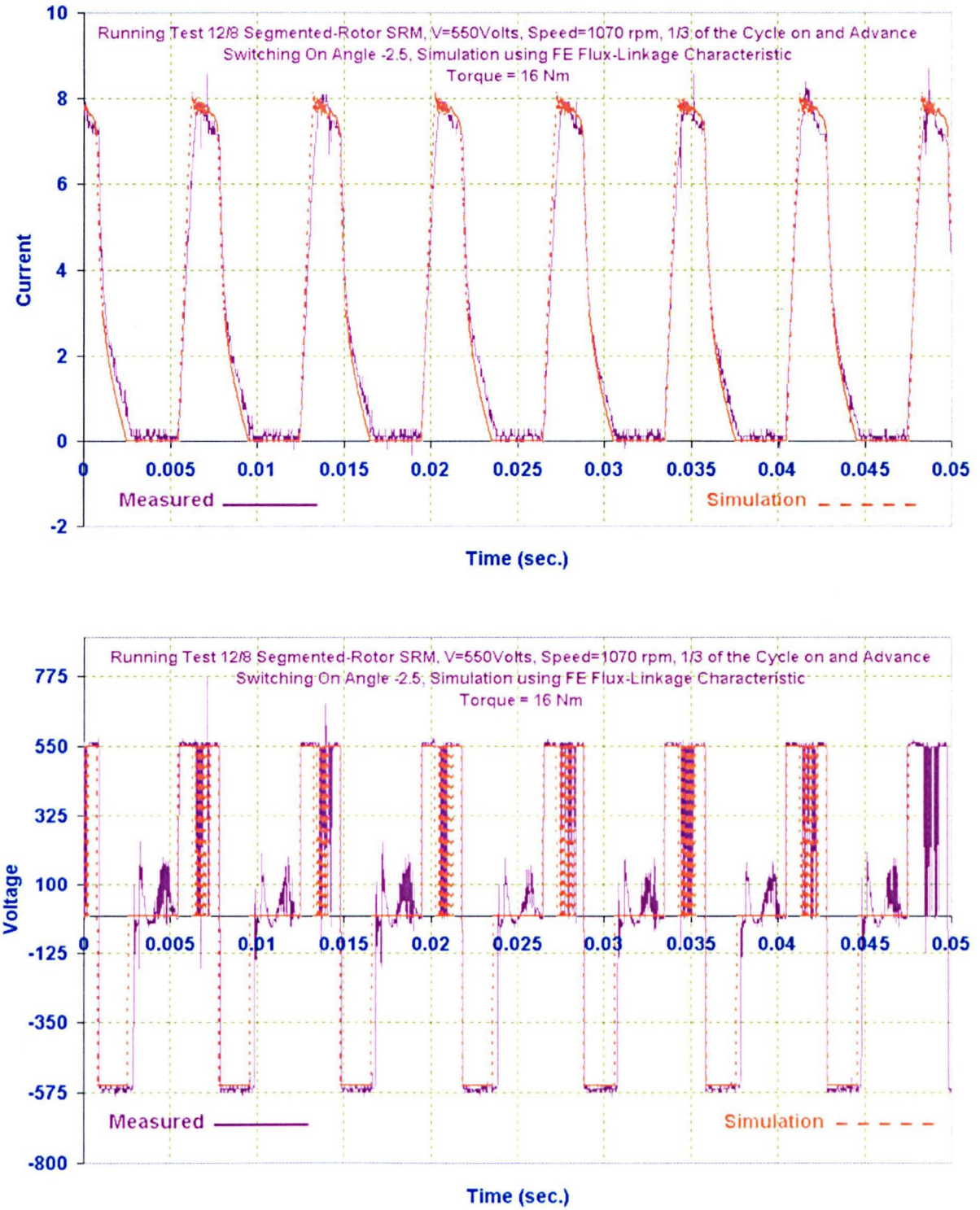

Fig. 10.4 12/8 Segmented-Rotor SRM Running at 1070 rpm (conduction for third cycle)

Fig. 10.4 shows the machine running at a medium speed, with a conduction angle of 1/3 of a cycle and 2.5 mechanical degrees of phase advance.

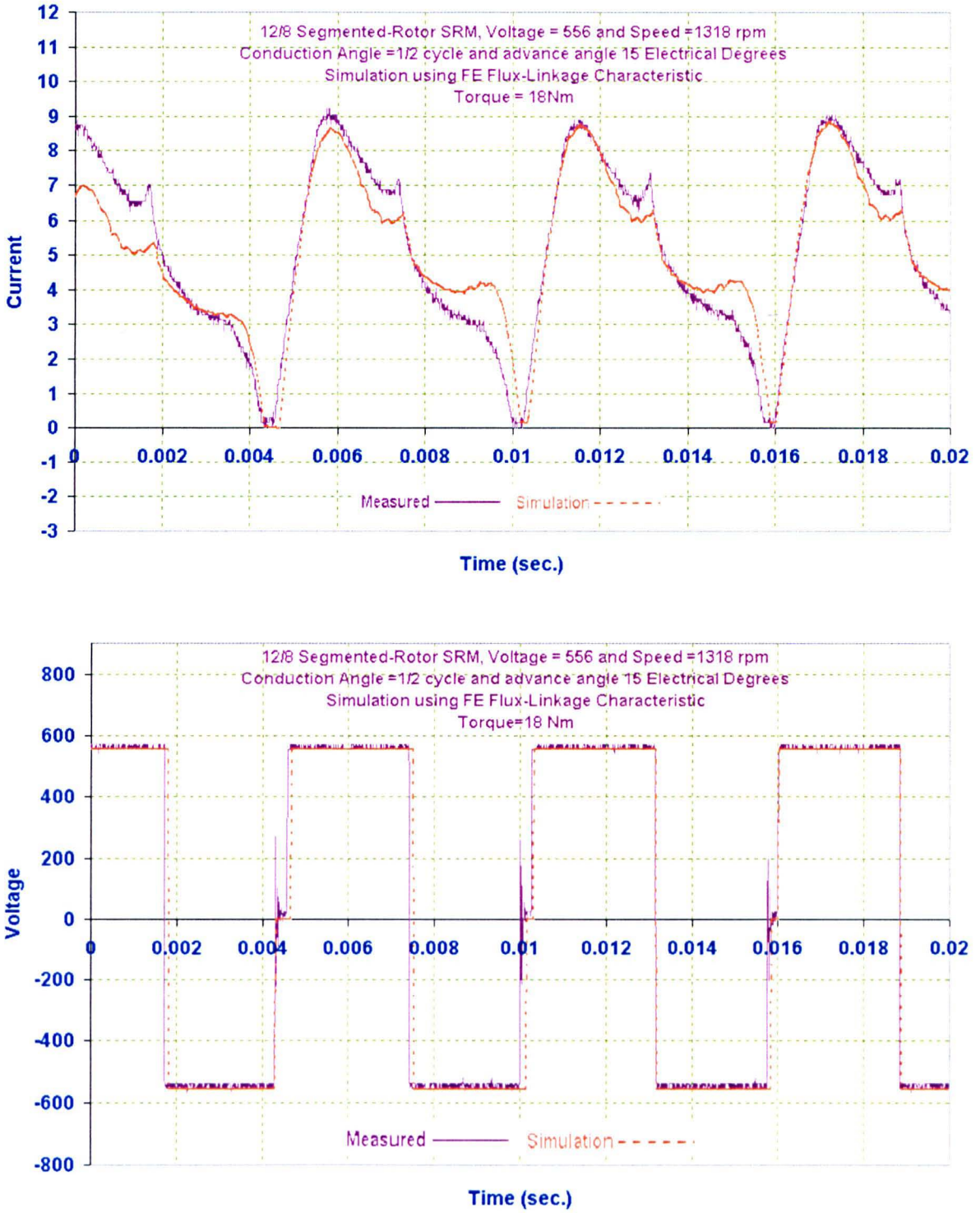

Fig. 10.5 12/8 Segmented-Rotor SRM Running at 1318 rpm (conduction for half cycle)

Fig. 10.5 shows dynamic performance of the SRM when running at high speed. The current demand never reaches the demanded value and so the drive operates in true voltage controlled mode throughout. Correlation between measured and simulated

results is very good; in addition to predicting the mean levels of current accurately the current waveshape is accurately simulated. Note that for this last test the SRM delivered 18 Nm.

10.5 Testing the 12/10 Short Pitched Segmental-Rotor SRM

10.5.1 Torque/Speed Envelope

Similarly to the 12/8 machine the simulation package was used to predict performance of the 12/10 machine, using a fixed current demand (J =10Amp/mm^2). The results are shown in Fig. 10.6, once more illustrating the requirement for phase advance in order to produce significant torque at high speed.

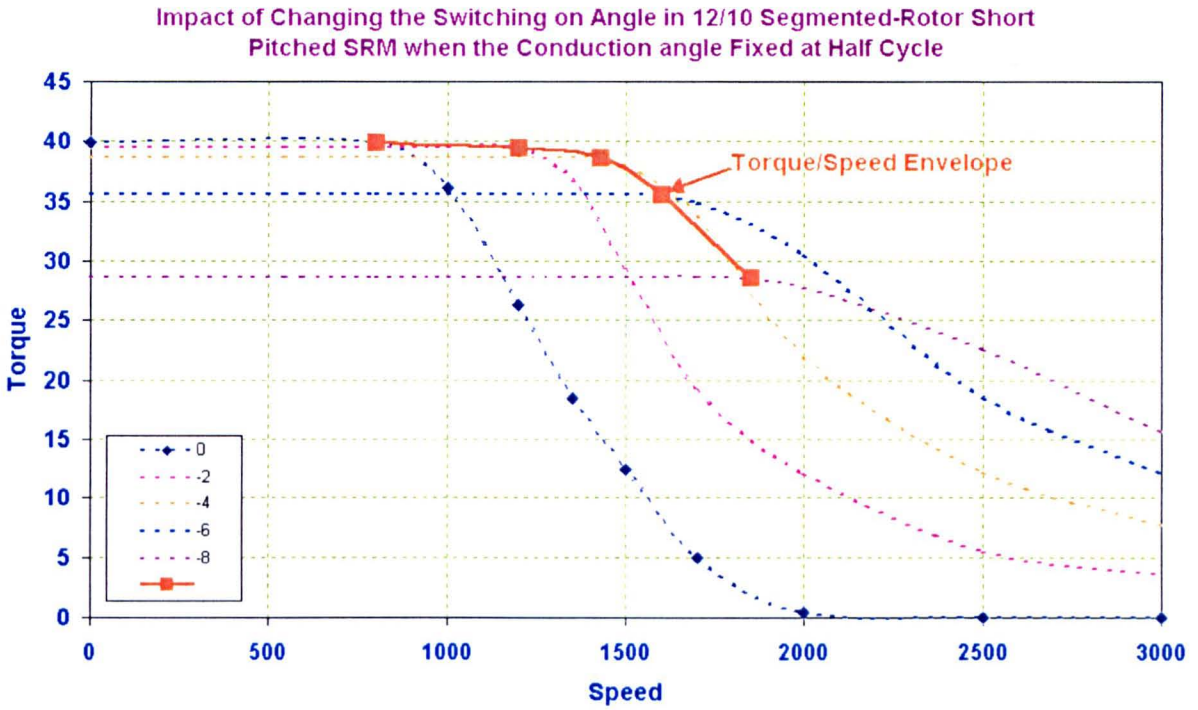

Fig. 10.6 Torque Speed Envelop

10.5.2 Predicted Torque Ripple

Fig. 10.7 shows simulated results of the instantaneous phase current and three phase torque for conduction angles equal to a third and a half cycle when operating at the same speed. It is clear from the figure that in all cases the torque ripple is high. Advancing the switching on angle increases the mean output torque, but it also

increases the torque ripple. However, increasing the conduction angle to 180 electrical degrees results in much lower levels of torque ripple than occur when the conduction angle is only 120 electrical degrees.

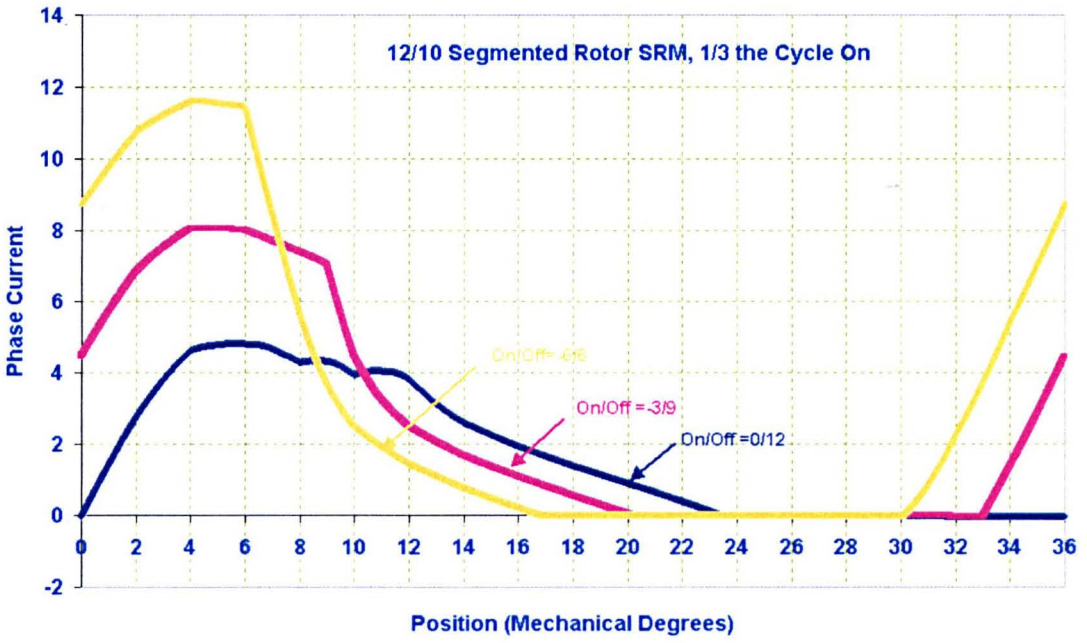

Fig. 10.7.a

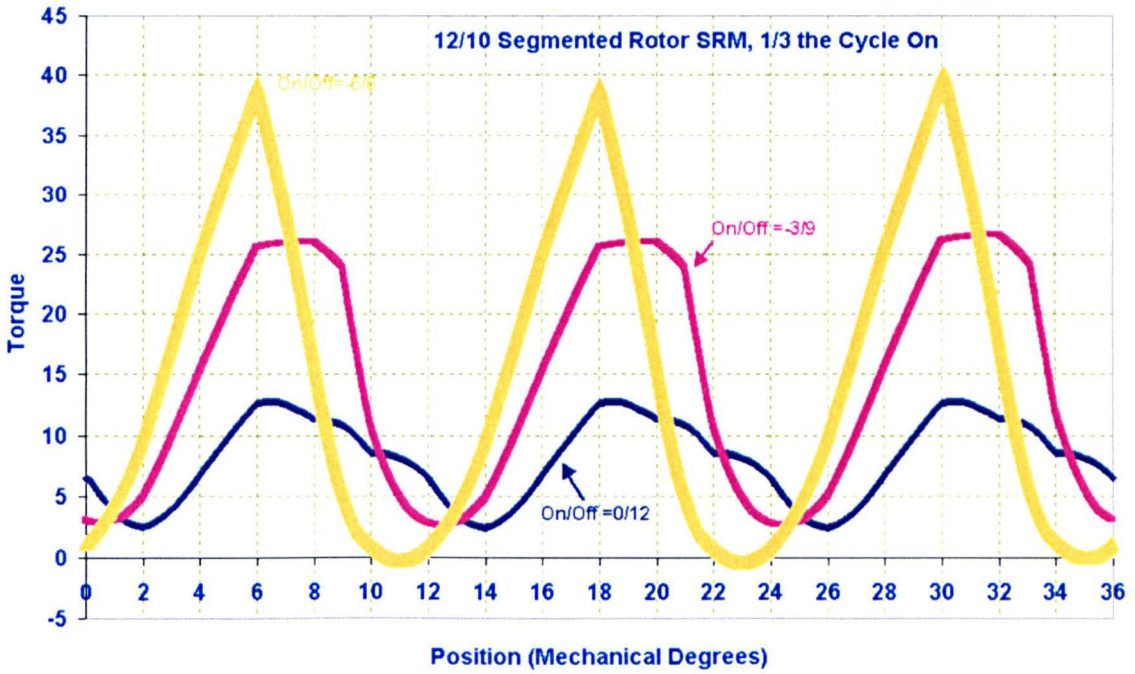

Fig. 10.7.b

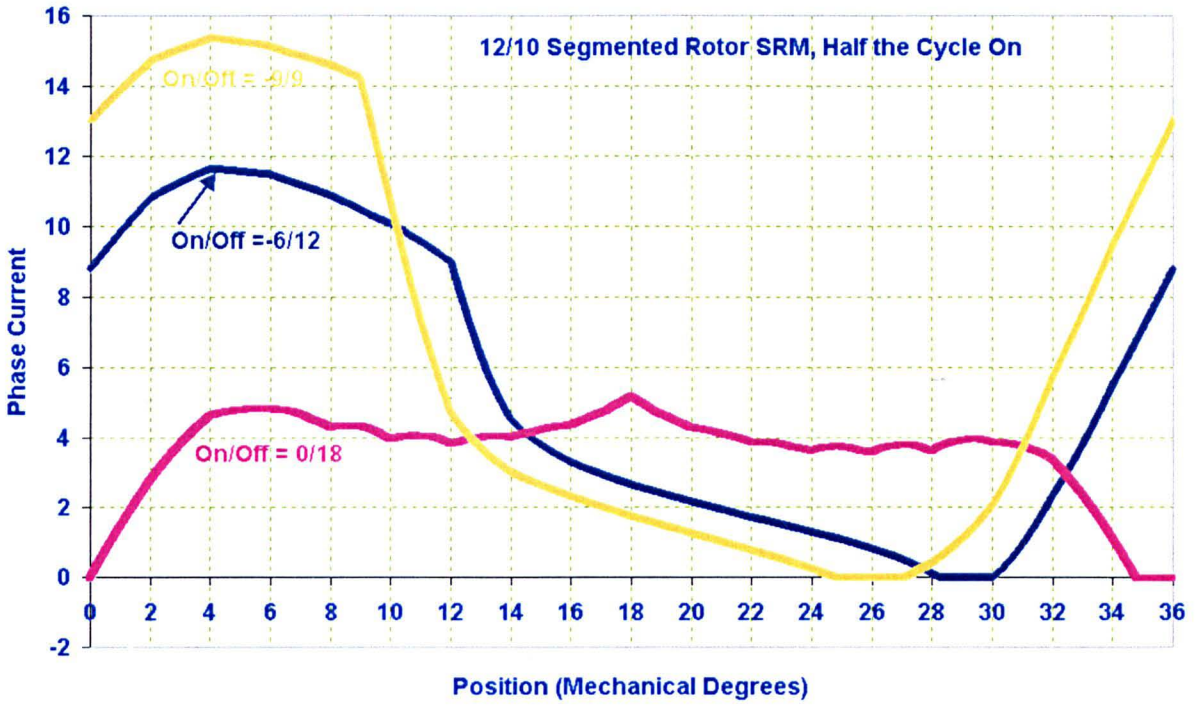

Fig. 10.7.c

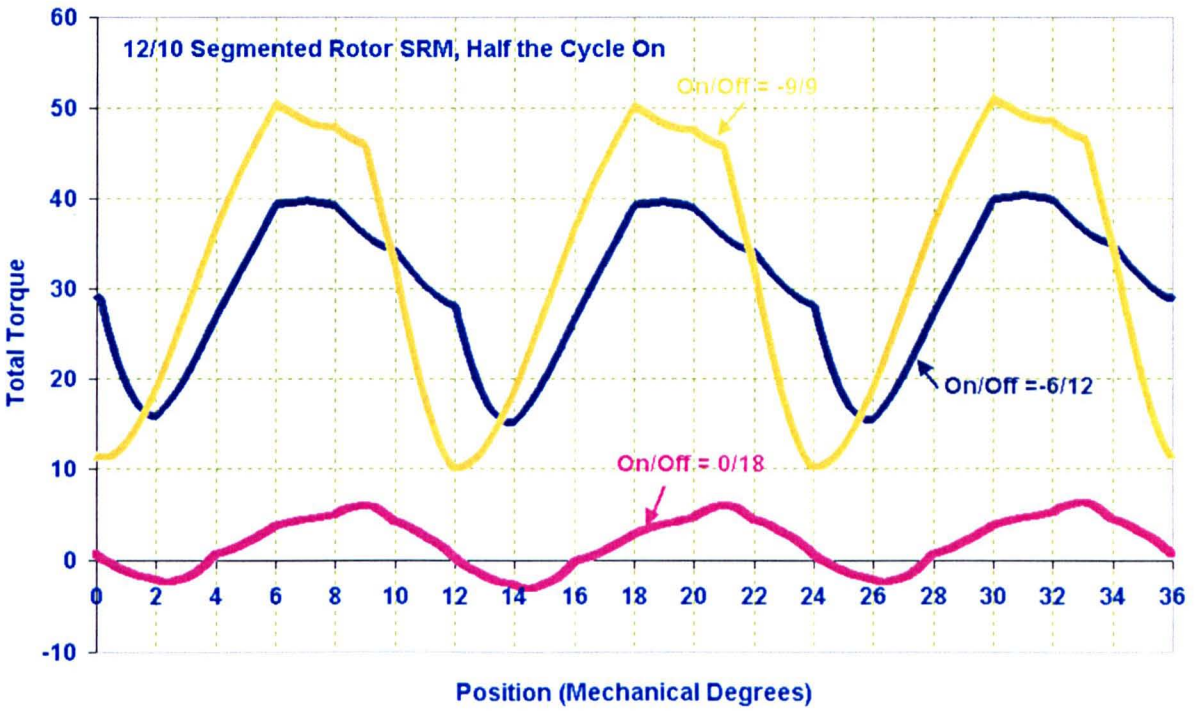

Fig. 10.7.d

Fig. 10.7 Studying the Torque (Average & Ripples) in the 12/10 Segmented-Rotor SRM

10.5.3 The Running Test

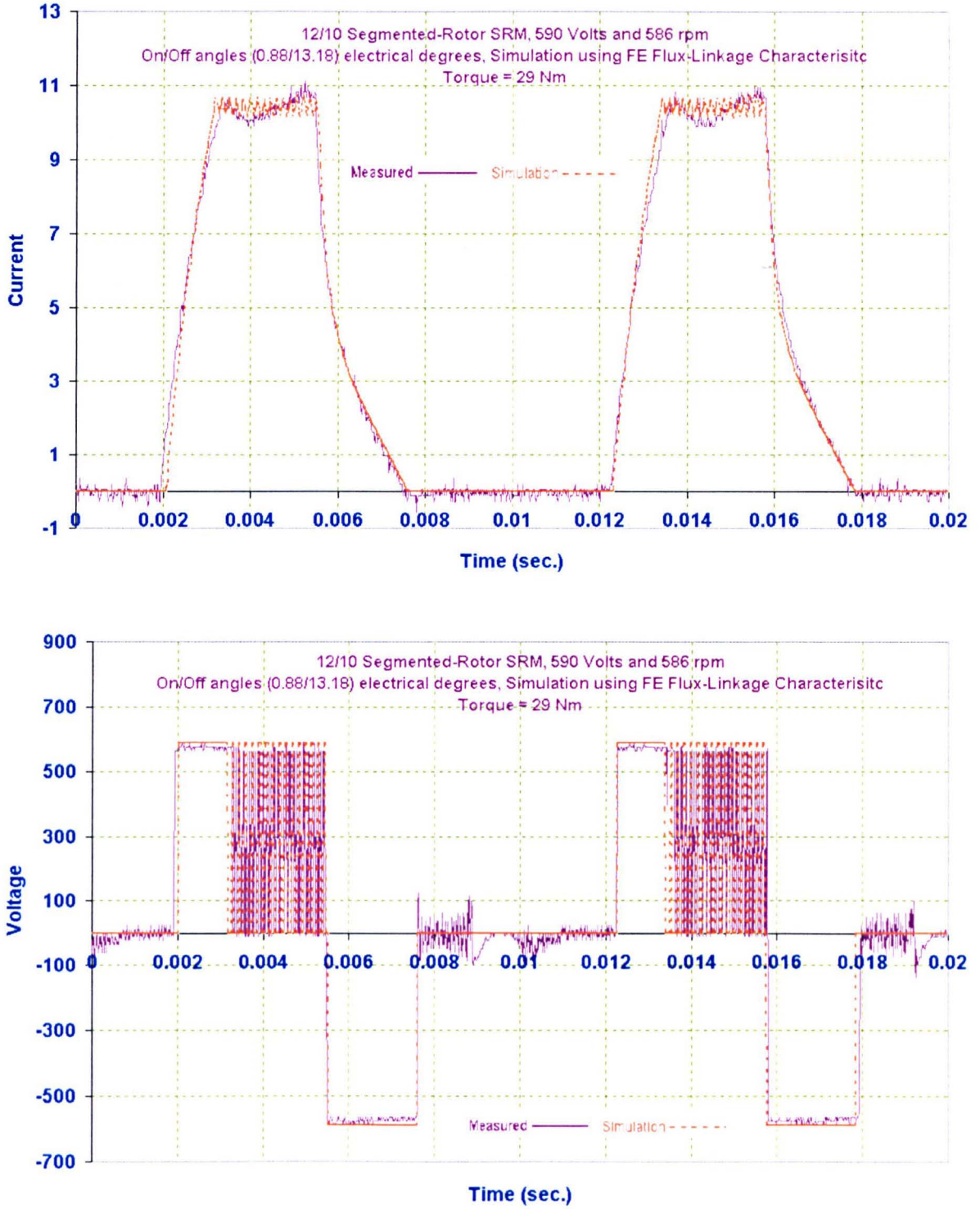

Fig. 10.8 12/10 Segmented-Rotor SRM Running at 586 rpm

Fig. 10.8 shows the test results of the 12/10 segmented-rotor SRM operating in what is essentially current controlled mode, and in this case delivering 29 Nm. As in the 12/8 machine the correlation between measured and simulated results is very good.

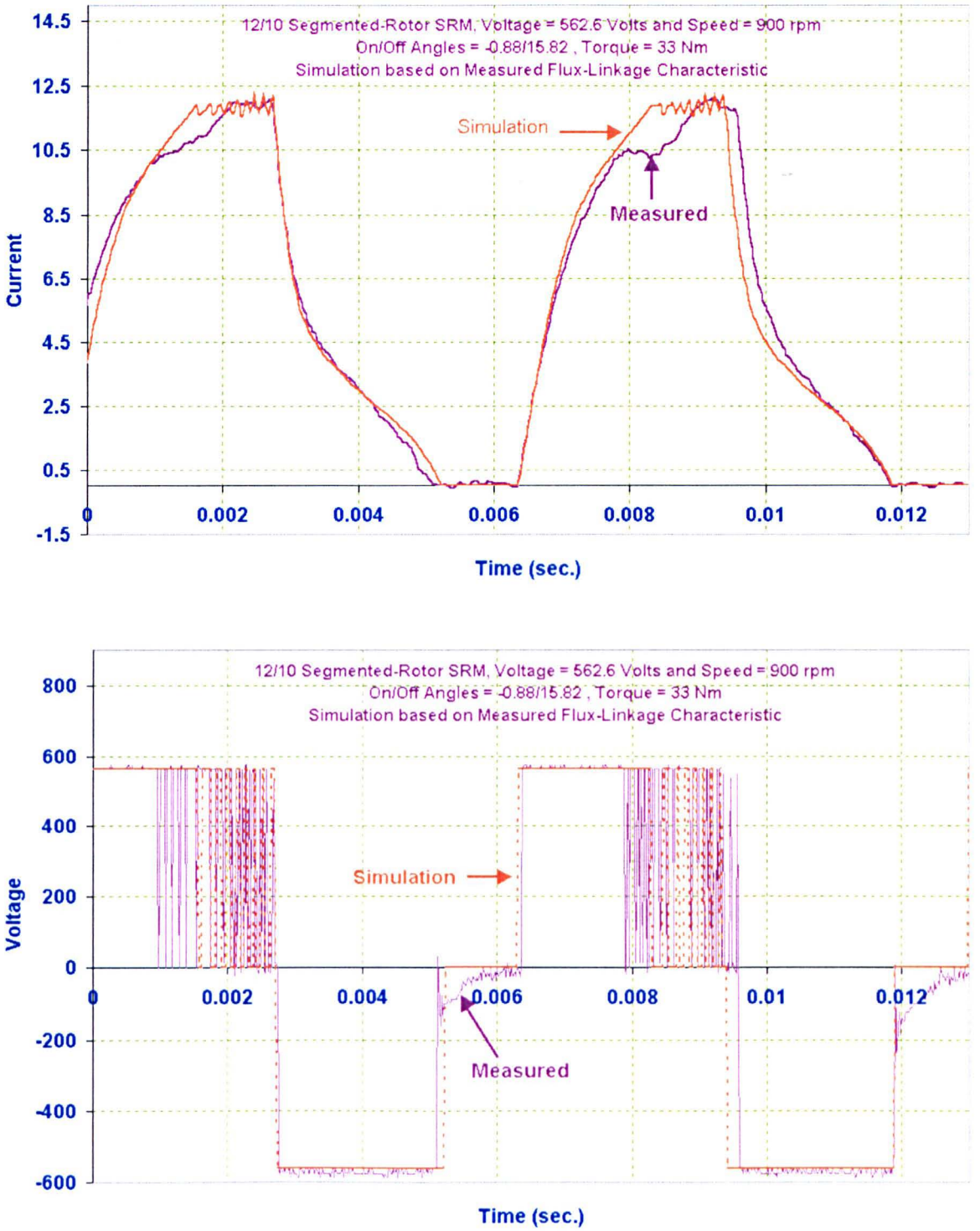

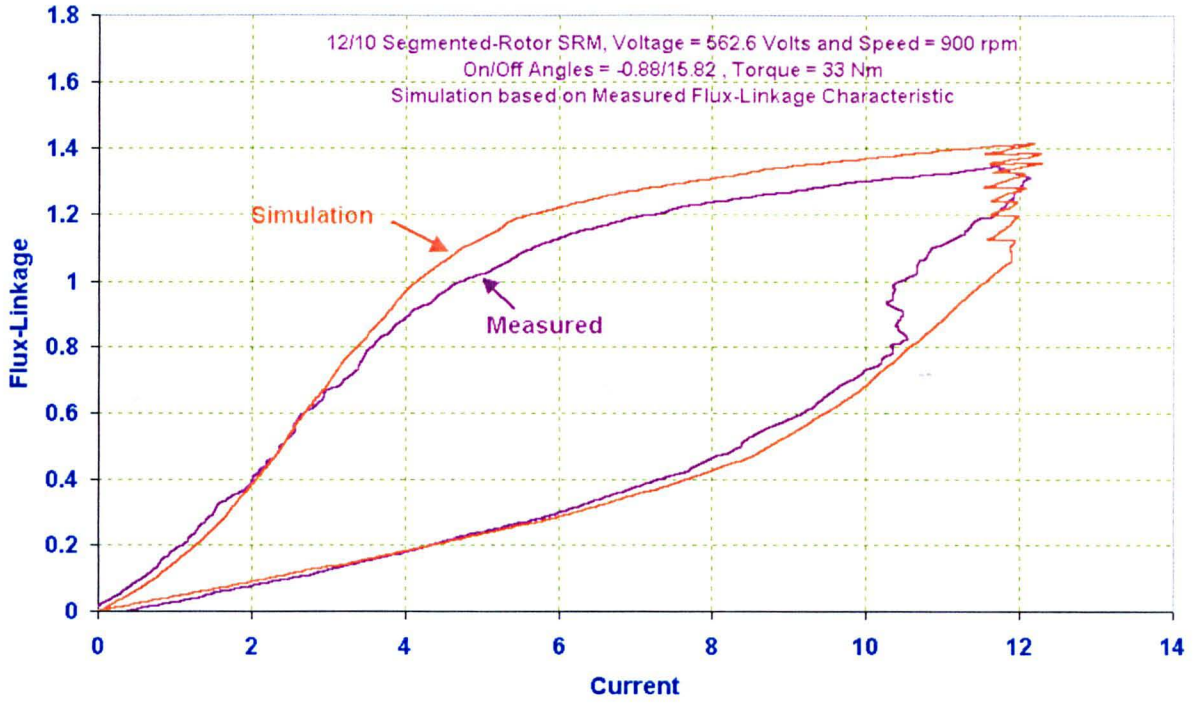

Fig. 10.9 12/10 Segmented-Rotor SRM Running at 900 rpm

In Fig. 10.9 the speed was increased, but the correlation remains good. Note, however, how the actual controller does not achieve the demanded value quite as quickly as the simulation predicts. This is almost certainly caused by a difficulty in ensuring that the proportional and integral gains in the current controller of both the simulation and actual controller are identical.

Fig. 10.10 and Fig. 10.11 show further examples of both simulated and measured results for the 12/10 machine operating under full voltage control, with a range of conduction angles. Once more the comparison between measured and simulated values is very good throughout.

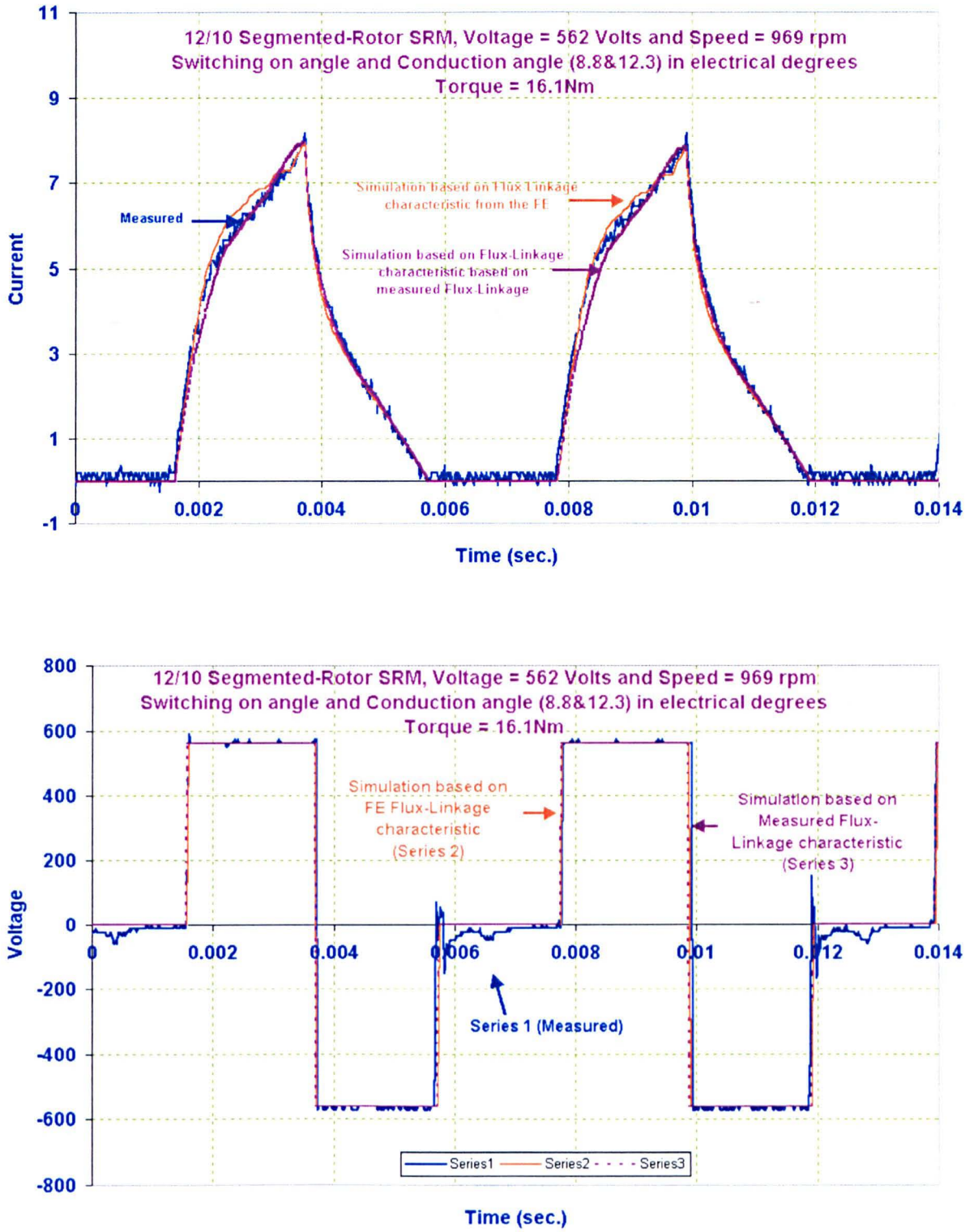

Fig. 10.10 12/10 Segmented-Rotor SRM Running under full Voltage Control. (Both the measured and the predicted Flux-Linkage characteristics used to see the degree of the accuracy)

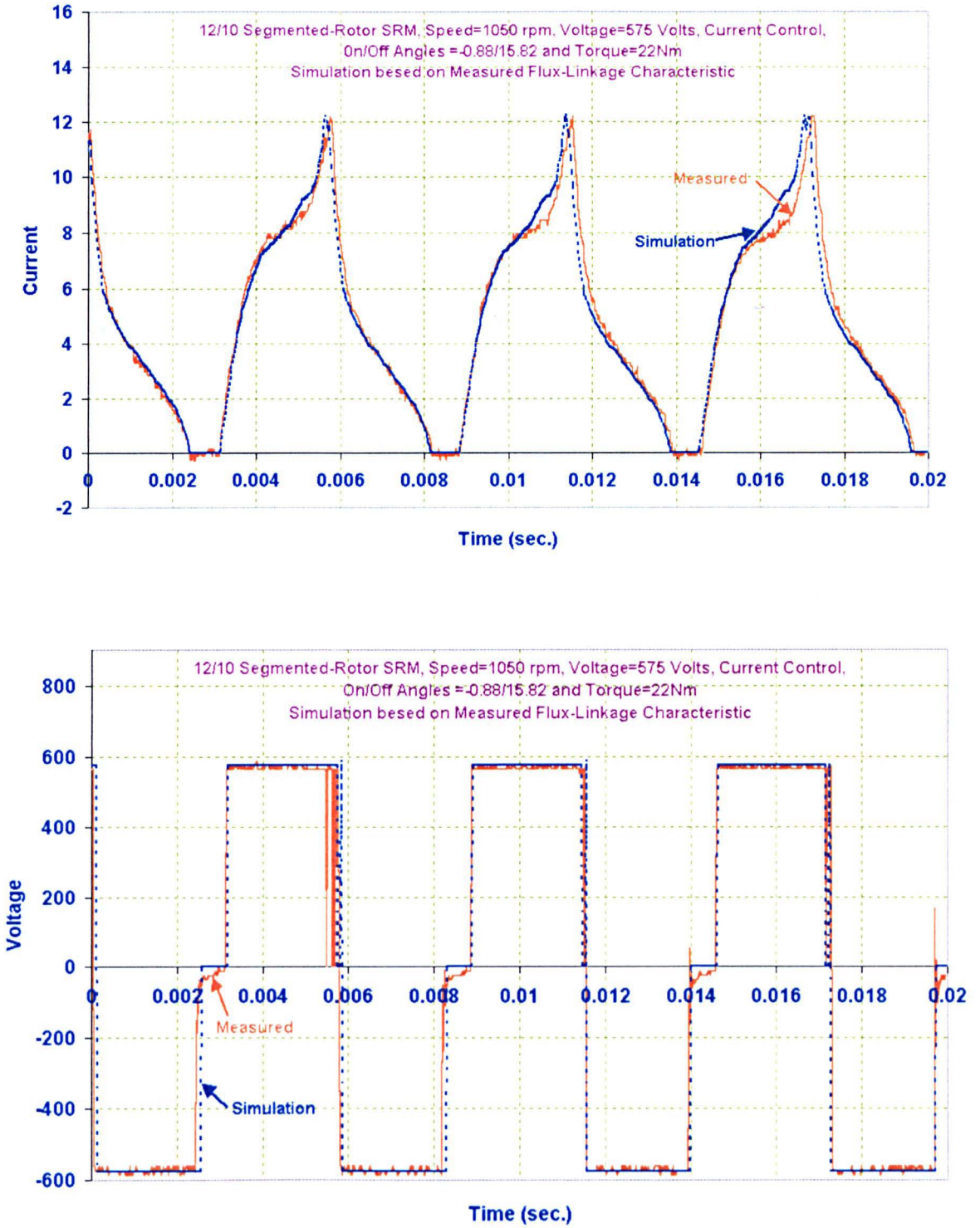

Fig. 10.11 12/10 Segmented-Rotor SRM Running with High Speed

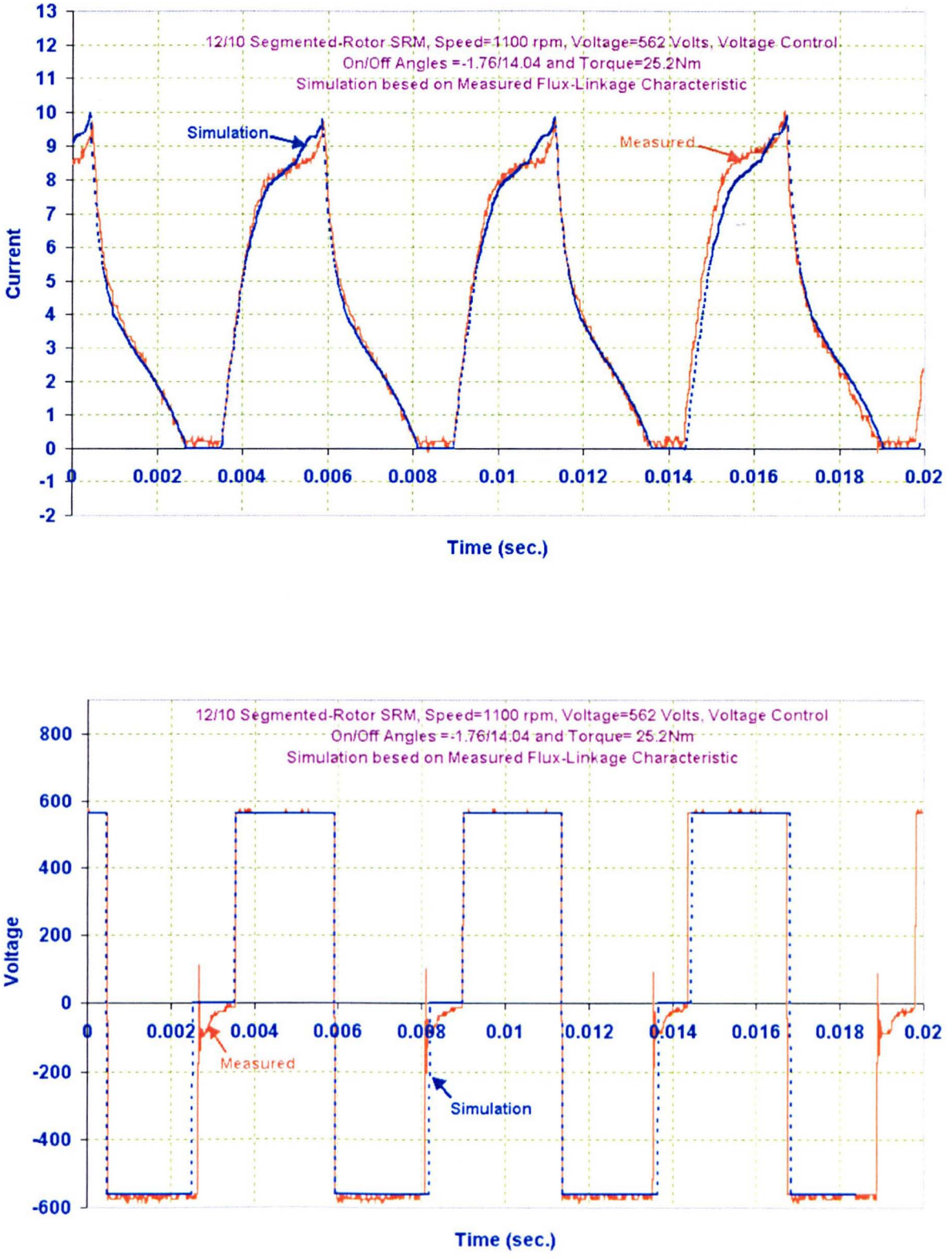

Fig. 10.12 Running Test of the 12/10 Segmented-Rotor SRM (High Speed)

10.6 Conclusion

This chapter has shown both machines operating successfully as rotating drives. Performance of the drives correlates closely with predictions made using a drive simulation package. This package was based around the flux-linkage/current characteristics of the machines. The results show that there are no unforeseen problems during dynamic operation. Any significant effects, such as major induced eddy currents, would affect the dynamic characteristics and result in a large discrepancy between measured and predicted waveforms.

The chapter brings together much of the previous work presented in the thesis. The running tests serve to validate previous work. This validation covers the previous simulated results, which is extremely important because it is not possible to build many prototypes of the segmented-rotor SRM. Now this simulation has been validated, it can be used for other designs of the segmented-rotor SRM. Different running results of both the two new SRMs were arranged according to the speed. In addition, how to increase the output by increasing either the conduction angle or the advance switching on angle has been described.

11 Conclusion

This thesis has introduced a novel design of SRM in which a toothed rotor is replaced with one containing a series of discrete segments. Each segment represents one rotor pole. In single phase machines the air-gap force density has been shown to exceed that of a conventional SRM when the active portion of the air-gap exceeds one half of a pole pitch. However, under such circumstances there may be insufficient room for the windings. In three phase machines the air-gap force density has been calculated as a function of electric loading and shown to be almost exactly double that of a conventional SRM. The principal reason for the increase in performance is due to better magnetic utilisation of the machine, which has double the active air-gap area of a conventional SRM.

Two different three phase machine topologies have been introduced, based around some design rules which were established. Both machine designs are based around the requirement to have only the windings of a single phase occupying any one slot.

In the first machine the conductors of each phase occupy every third slot and this leads to a multi-tooth or, in this case, a fully pitched winding. A machine of this type has been designed, built and tested. Torque has been measured as a function of both current and position, showing good agreement with predictions. Comparisons with other switched reluctance machines with the same outside diameter and core length has shown a 41% increase in torque per unit copper loss at thermal limit. This is primarily because each turn of the segmented-rotor SRM links almost double the flux of a conventional SRM. The increased end-winding length requires more copper and so the torque per unit copper mass is not increased.

The second design combines a segmental rotor with short pitched windings, placed around a single tooth. In order to maintain one phase winding per slot it has been necessary to place the winding round every other tooth. The concept enables a large increase in the flux linking each turn of the machine, thereby creating a large increase in torque density. The machine delivers over 40% more torque than a conventional SRM and equals the torque capability of the first segmental SRM design

with windings spanning three teeth, whilst using 29% less copper volume. In comparison to the earlier segmental design the windings are used more efficiently because of the shorter end-winding length, but the magnetic performance is reduced: these two effects approximately balance out to give equal torque capability. The design offers an advantage over segmental rotor SRMs, with windings spanning multiple teeth, due to the short length of the end-windings. This makes the concept particularly suitable for machines of a relatively short axial length and removes the limitation of the earlier multi tooth segmental designs. The concept has many of the attributes desired for a fault tolerant drive: the windings are magnetically, thermally and mechanically isolated from each other to a greater degree than in a conventional SRM. The machine may therefore be particularly suitable for such applications. However, the high torque density achieved suggests that its applications may be more widespread

Measured flux-linkage and torque characteristics in both machines are in line with those predicted using the finite element method. During operation as a drive, supplied with current from three asymmetric half bridges the machines continue to perform in line with predictions. Static torque at thermal limit is over 30 Nm in a machine of 150 mm outside diameter and 150 mm lamination stack length.

The mutual coupling between the phases was studied by testing the segmented-rotor SRMs with two modes of operation; one in which a fixed MMF is applied to one phase, whilst the other is excited with a varying current, and one when two phases are excited simultaneously with the same current. The mutual inductance between phases has bee. shown to be less than 4% of the self inductance, so that it never has a major impact. For some winding polarities the effect of mutual flux between phases has a beneficial effect, whilst for others it adds to saturation levels and detracts from torque production.

A modified formula of estimating the iron losses for non-sinusoidal waveforms has been used to estimate the iron losses in the segmented-rotor SRMs, along with those in a conventional toothed-rotor SRM. The segmental rotor SRMs have short flux paths and, unlike conventional SRMs, the magnetic flux in any one section of the

core back is only ever the flux of a single phase. Consequently the rate of change of flux is low and this helps reduce the core back iron loss. However, the stator teeth share the flux of more than one phase and, depending upon the orientation of magnetisation of the coils, this can lead to increased stator tooth loss.

The machine requires similar converter arrangements to that of a conventional SRM. The ratio of aligned and unaligned permeance is also similar, so there appears to be almost identical converter volt-ampere requirements.

The thesis finally advocates the new design of SRM as a replacement for conventional SRMs because of the excellent results shown.

Appendix1

Determination of Parameters in a Fully Pitched Segmental SRM 12/8

Choose all teeth to be same width

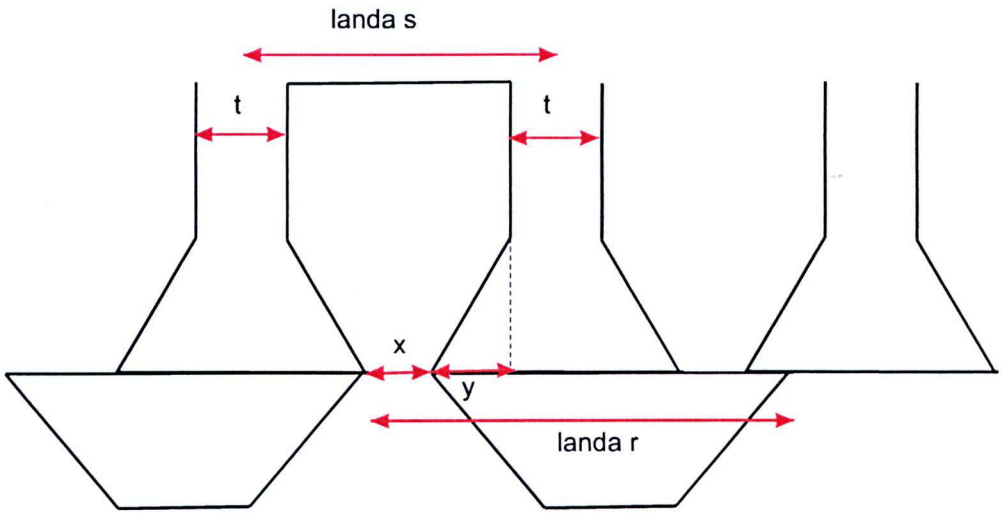

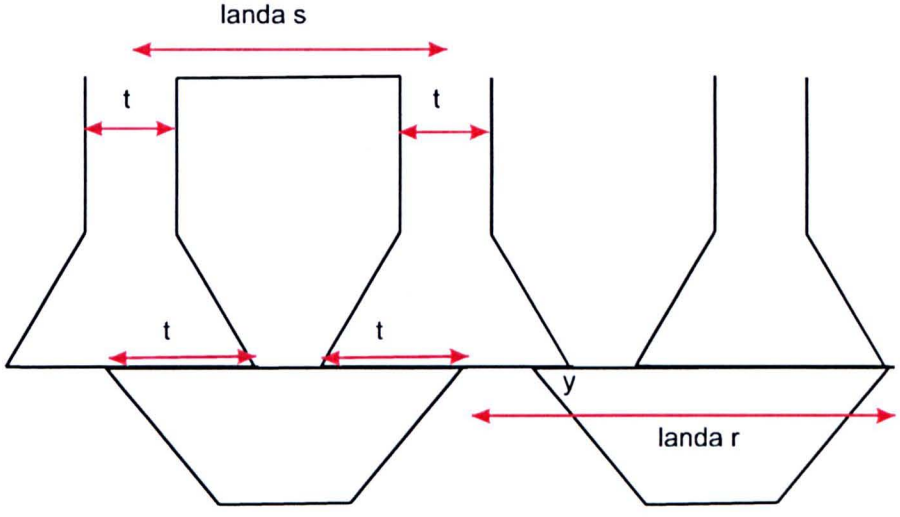

Make rotor and stator slot arcs equal, so stator and rotor leakage should be similar

Consider the above diagram

Equating values with the rotor pole arc

$$2t + 2x = \lambda_r \qquad (1)$$

From the arc of the stator pole

$$t + x + 2y = \lambda_s \qquad (2)$$

λ_s	30
λ_r	45

t (deg)	X	a	slot width
5.00	17.50	3.75	25.00
6.00	16.50	3.75	24.00
7.00	15.50	3.75	23.00
8.00	14.50	3.75	22.00
9.00	13.50	3.75	21.00
10.00	12.50	3.75	20.00
11.00	11.50	3.75	19.00
12.00	10.50	3.75	18.00
13.00	9.50	3.75	17.00
14.00	8.50	3.75	16.00
15.00	7.50	3.75	15.00
16.00	6.50	3.75	14.00
17.00	5.50	3.75	13.00
18.00	4.50	3.75	12.00
19.00	3.50	3.75	11.00
20.00	2.50	3.75	10.00

Appendix 2

Determination of Parameters in a Short Pitched Segmental SRM 12/10

Choose intermediate teeth to be one half width of main teeth

Make rotor and stator tooth tip arcs equal, so stator and rotor leakage should be similar

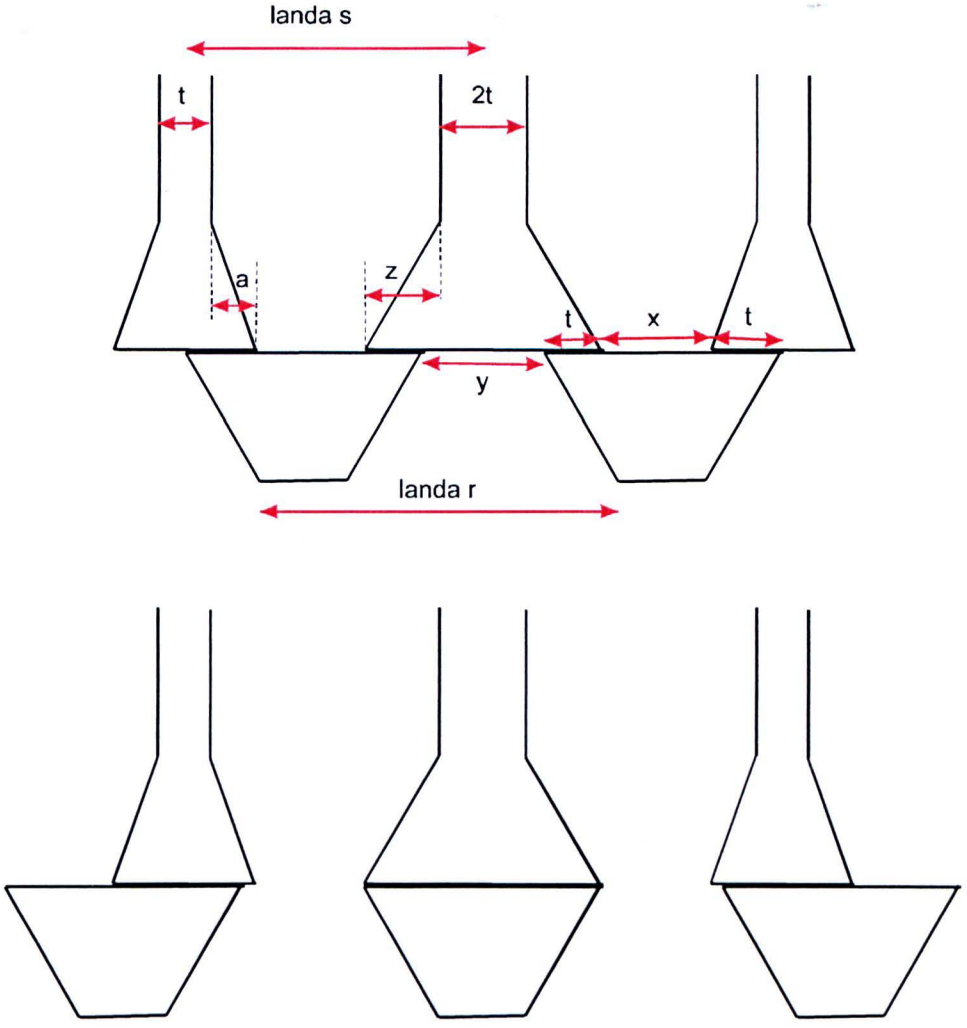

Consider the above diagram

In the unaligned position the rotor and stator pole tips are the same arc. Hence

$$2(t+z)+y=\lambda_r \qquad (1)$$

From the arc of the stator pole

$$t+z+x+a+\frac{t}{2}=\lambda_s$$

hence $z + x + a + \frac{3t}{2} = \lambda_s$ (2)

From the overlapping angle between rotor and stator in the aligned position

$\frac{y}{2} + t = t + z \quad hence \quad y = 2z$ (3)

sub (3) in (1) to get

$2t + 4z = \lambda_r$ (4)

Finally, in the aligned position, equate rotor and stator angles to determine x

$\lambda_r - y - 2t = x$ (5)

If λ_r and λ_s are known, then for any value of t it is possible to determine z from (4), then y from (3), x from (5) and a from (2)

λ_s	30
λ_r	36

t (deg)	Z	y	x	a	slot width
5.00	6.50	13.00	13.00	3.00	22.50
6.00	6.00	12.00	12.00	3.00	21.00
7.00	5.50	11.00	11.00	3.00	19.50
8.00	5.00	10.00	10.00	3.00	18.00
9.00	4.50	9.00	9.00	3.00	16.50
10.00	4.00	8.00	8.00	3.00	15.00
11.00	3.50	7.00	7.00	3.00	13.50
12.00	3.00	6.00	6.00	3.00	12.00
12.60	2.70	5.40	5.40	3.00	11.10
13.00	2.50	5.00	5.00	3.00	10.50
14.00	2.00	4.00	4.00	3.00	9.00
15.00	1.50	3.00	3.00	3.00	7.50

Appendix3

Winding of Fully Pitched Segmental SRM

Winding has been wound to give:

- 4 pole
- 3 phase
- Double Layer
- Fully Pitched (i.e. 1-4, spanning 3 teeth)
- 4 coils per phase, all connected in series
- 2 coils per slot
- wire diameter 1.00 mm equivalent.
- Class F.
- Both ends of each phase are brought out.

Number of turns per coil has been maximised, giving a final total of 75, corresponding to a slot fill factor of 0.455.

Thesis References

[1] P. Pillay, Y. Liu, W. Cai and T. Sebastian, 'Multiphase Operation of Switched Reluctance Motor Drives' IEEE IAS 1997.

[2] Omekanda, 'Method of Optimising Performance Parameters of a Switched Reluctance Motor' US patent 2002/0121876, Sep. 5, 2002.

[3] F. B. Morinigo, 'Switched Reluctance Motor Delivering Constant Torque from Three Phase Sinusoidal Voltages' US 2002/0125783, Sep. 12, 2002.

[4] A. Schumacher, 'Switched Reluctance Motor with Magnetic Position Sensor' UK Patent GB 2 365 531.

[5] J. Corda, and J. M. Stephenson, 'Analytical Estimation of the Minimum and Maximum Inductances of a Double Salient Motor' in Proc. Leeds Int. Conf. Stepping Motors and Systems, Leeds, U.K., Sept. 1979, Pages: 50-59.

[6] W. A. Pengov, 'Switched Reluctance Motor' US 6114789, Sep. 5, 2000.

[7] M. Moallem, 'Performance Characteristics of Switched Reluctance Motor Drive' Ph.D. Thesis Purdue University, US, 1989.

[8] M. R. Harris, J. W. Finch, J. A. Mallick, T. J. E. Miller, 'A Review of Integral-Horsepower Switched Reluctance Drive' IEEE Transactions on Industry Applications, Vol. IA-22, No. 4, July/ August 1986.

[9] J. F. Lindsay, R. Arumugan and R. Krishnan, 'Finite Element Analysis Characterisation of a Switched Reluctance Motor with Multi-tooth per stator pole' IEE Proceedings. Vol. 133, PT. B, No.6, November 1986.

[10] R. Krishnan, R. Arumugam and J. F. Lindsay, 'Design Procedure for Switched Reluctance Motors' IEEE Transaction on Industry Application, Vol. 24, No. 3, May/June 1988.

[11] A. R. Miles, 'Design of a 5MW, 9000V Switched Reluctance Motor' IEEE Transaction on Energy Conversion, Vol. 6, No. 3, September 1991.

[12] T. J. E. Miller, 'Optimal Design of Switched Reluctance Motors' IEEE Transactions on Industrial Electronics, Vol. 49, No. 1, February 2002.

[13] K. M. Richardson, C. Pollock and J. O. Flower, 'Design of a Switched Reluctance Sector Motor for an Integrated Motor/Propeller Unit' IEE Electrical Machines and Drives' 11-13 September 1995.

[14] A. Michaelides and C. Pollock, 'Design and performance of a high efficiency 5-phase switched reluctance motor' IEE conference of Electrical Machines and Drives 11-13 September 1995.

[15] A. Michaelides and C. Pollock, 'Modelling of a New Winding Arrangement to Improve Performance in the Switched Reluctance Motor', IEE Conference of Electric Machines and Drive, 1993.

[16] B. C. Mecrow, ' Fully Pitched-Winding Switched Reluctance and Stepping-Motor Arrangements' IEE proceedings-B, Vol.140, No. 1, January 1993.

[17] P. G. Barrass, 'High Performance Switched Reluctance Drives' Ph.D. Thesis University of Newcastle upon Tyne, September 1995.

[18] B. C. Mecrow, 'New Winding Configurations for Doubly Salient Reluctance Machines' IEEE Transactions on Industry Applications, Vol. 32, No. 6, November/December 1996.

[19] Tang et Al., 'Reluctance Machine with Fractional Pitch Winding and Drive Therefore' US Patent No.5889347.

[20] A. F. Anderson, 'Robert Davidson – Father of Electric Locomotive' Proc. of IEE Conf. on the History of Electrical Engineering, 1975.

[21] A. Matveev, T. Undeland, R. Nilssen, 'Design Optimisation Of Switched Reluctance Drives Using Artificial Neural Networks' EPE-PEMC 2002 Dubrovnik & Cavtat.

[22] S. Risse and G. Henneberger, 'Design and Optimisation of a Switched Reluctance Motor for Electric Vehicle Propulsion', ICEM 2000, Pages: 1526-1530.

[23] J. Reinert, R. Inderka, M. Menne, and R. W. De Doncker, 'Optimisation Performance in Switched Reluctance Motor' IEEE Industry Applications Magazine, July/August 2000.

[24] M. Sanada, S. Morimoto, Y. Takeda and N. Matsui, 'Novel Rotor Pole Design of Switched Reluctance Motors to Reduce the Acoustic Noise' IEEE Conf. IA 2000, Italy.

[25] P. O. Rasmussen, F. Blaabjerg, J. K. Pedersen, P. C. Kjaer, T. J. E. Miller, 'Acoustic Noise Simulation for Switched Reluctance Motors with Audible Output' Proceed. of EPE '99.

[26] Huh et al., 'Switched Reluctance Motor Having Noise And Vibration Reduced' US Patent 6040678, 24/6/98.

[27] B. Fahimi and M. Ehsani, 'Spatial Distribution of Acoustic Noise Caused by Radial Vibration in Switched reluctance Motors: Application to Design and Control' IEEE Conf. IA 2000, Italy.

[28] R. S. Wallace and D. G. Taylor, 'Three Phase Switched Reluctance Motor Design to Reduce Torque Ripple' International Conference on Electrical Machines ICEM'90, Pages: 782-787.

[29] J. R. Gyorki, 'Design Secrets of Switched Reluctance Motors', September 26, 1996 Journal Machine Design.

[30] S. Ayari, M. Besbes, M. Lecrivain and M. Gabsi, 'Effects of the Air Gap Eccentricity on the SRM Vibrations' IEEE IAS, 1999.

[31] A. Stassis and A. M. Michaelides, 'The design of low vibration doubly salient motors' Electric Machines and Power Systems 1999.

[32] J. Hong, K. Ha, J. Lee, 'Stator Pole and Yoke Design for Vibration Reduction of Switched Reluctance Motor' Magnetics, IEEE Transactions on, Volume: 38 Issue: 2 Part: 1, March 2002 Pages: 929-932.

[33] D. S. Schramm, 'Control Techniques to Reduce Torque Ripple of Switched Reluctance Motor Drives' Ph.D. Thesis, Heriot-Watt University, 1993.

[34] O. Diril and R. N. Tuncay, 'The Torque Ripple Minimisation of Switched Reluctance Motors by Torque Waveform Control' ICEM 2000, 28-30 August 2000 Espoo, Finland.

[35] K. M. Rahman, S. Gopalakrishnan, B. Fahimi, M. Rajarathnam, 'Optimised Torque Control of Switched Reluctance Motor at all Operating Regimes Using Neural Network' Industrial Applications, IEEE Transactions on, Volume: 37 Issue: 3, May-June Pages: 904-913.

[36] B. Fahimi, 'Control of vibration in switched reluctance motor drives', Ph.D. Thesis, 1999 Texas A&M University, US.

[37] I. Husain, 'Minimisation of Torque Ripple in SRM Drives' Industrial Electronics, IEEE Transactions on, Volume: 49 Issue:1 , Feb. 2002 Pages: 28-39.

[38] M. E. Zaiom, K. Dakhouche and M. Bounekhla, 'Design for Torque Ripple Reduction of a Three-Phase Switched-Reluctance Machine' IEEE Transactions on Magnetics, Vol. 38, No. 2, March 2002.

[39] T. Saitou, 'Reluctance Type Motor Apparatus and Driving Method Capable of Reducing Ripples in Motor Output Torque' US patent US 6232741, May 15, 2001.

[40] A. M. Omekanda, 'A New Technique for Multi-Dimensional Performance Optimisation Switched Reluctance Motors for Vehicle Propulsion' Industry Applications Conference, 2002, 37th IAS Annual Meeting, Conference of the, Volume: 1, 2002, pages 22-26.

[41] X. Wang, 'Modeling And Implementation of Controller for Switched Reluctance Motor with AC Small Signal Model' M.Sc. Thesis, October 2001, Virginia Polytechnic Institute and State University, US.

[42] T. J. Miller, 'Switched Reluctance Motors and Their Control' Clarendon Press, Oxford, 1993.

[43] M. R. Harris, V. Andjargholi, A. Hughes, P.J. Lawrenson, and B. Ertan, 'Limitations of Reluctance Torque in Doubly-Salient Structures' Proceeding of International Conference On Stepping Motors and Systems, University of Leeds, July 1974, pp. 158-168.

[44] C. Choi, S. Kim, Y. Kim and K. Park, 'A New Torque Control Method of a Switched Reluctance Motor Using Torque-Sharing Function' Magnetics, IEEE Transaction on, Volume: 38 Issue: 5 Part: 1, Sep. 2002, Pages 3288-3290.

[45] M. R. Harris, A. Hughes, and P. J. Lawrenson, 'Static Torque Production in Saturated Doubly-Salient Machines', Proc. IEE, 1975, 122, (10), pp. 1121-1127.

[46] M. R. Harris, V. Andjargholi, P. J. Lawrenson, A. Hughes, and B. Ertan, 'Unifying Approach to the Static Torque of Stepping-Motor Structures', Proc IEE, 1977, 124, (12), pp. 1215-1224.

[47] P. J. Lawrenson, J. M. Stephenson, P. T. Blenkinsop, J. Corda, and N. N. Fulton, 'Variable-Speed Switched Reluctance Motors', IEE Proc. B, 1980, 127, (4), pp. 253-265.

[48] B. S. Rahman and D. K. Lieu, 'Optimisation of Magnetic Pole Geometry for Field Harmonic Control in Electric Motors' Journal of Vibration and Acoustics, April 1994, Vol. 116/173.

[49] C. Neagoe, A. Foggia, R. Krishnan, 'Impact of Pole Tapering on the Electromagnetic Torque of the Switched Reluctance Motor', 1997 IEEE International Electric Machines and Drives Conference Record, WA1/2.1-3, Milwaukee, WI, USA, 18-21, May 1997.

[50] C. WU, and C. Pollock, 'Analysis and Reduction of Vibration and Acoustic Noise in the Switched Reluctance Drive,' IEEE Trans., 1995, IA-31, (1), Pages: 91 –98.

[51] M. Sanada, S. Morimoto, Y. Takeda, and N. Matsui, 'Novel Rotor Pole Design of Switched Reluctance Motors to Reduce the Acoustic Noise', IEEE Conference on Industry Applications, Rome, October 2000.

[52] P. Pillay and W. Cai, 'An Investigation into Vibration in Switched Reluctance Motors' IEEE Transactions on Industry Applications, Vol.35, No.3 May/June 1999.

[53] H. C. Lovatt, and J. M. Stephenson, 'Influence of Number of Poles Per Phase in Switched Reluctance Motors', IEE Proc. B, 1992, 137, (4), pp. 307-314.

[54] R. S. Wallace, and D. G. Taylor, 'Three Phase Switched Reluctance Motor Design to Reduce Torque Ripple', International Conference on Electrical Machines ICEM'90, Boston, pp. 782-787.

[55] A. R. Eastham, H. Yuan, G. E. Dawson, P. C. Choudhuhury, P.M. and Cusack, 'A Finite Element Evaluation of Pole Shaping in Switched Reluctance Motors', Electrosoft, 1990, 1, (1).

[56] F. Sahin, B. Ertan, and K. Leblebicioglu, ' Optimum Geometry for Torque Ripple Minimisation of Switched Reluctance Motors', International Conference on Electrical Machines ICEM' 96, Vigo, Spain, Vol.2, Pages: 110-115.

[57] E. Hoang, B. Multon, R. Vives Fos, and M.Geoffroy, 'Influence of Stator Yoke Thickness and Stator Teeth Shape upon Ripple and Average Torque of Switched Reluctance Motors' Speedam Conf., Taormina, Italy, June 8-10, 1994, pp. 145-149.

[58] J. W. Finch, M. R. Harris, A. Musoke, and H. M. B. Metwally, 'Variable Speed Drives Using Multi-Tooth per Pole Switched Reluctance Motors', 1984, Incr. Motion, Cont. Sys. Dev., Illinois, 13, Pages: 293-301.

[59] J. F. Lindsay, R. Arumugam and R. Krishnan, 'Finite Element Analysis Characterisation of a Switched Reluctance Motor with Multi-Tooth per Stator Pole', Proceeding IEE, Vol. 133, Pt. B, November 1986, pp. 347-353.

[60] J. T. Gierer, 'Switched Reluctance Motor Having Stator Inserts for Noise Reduction, Magnet Positioning, and Coil Retention' US 6232693, May 15, 2001.

[61] J. M. Stephenson, J. Corda, 'Computation of torque and current in Doubly Salient Reluctance Motors from Nonlinear Magnetisation Data' Proc. IEE, Vol. 126, No.5 Pages 393-396, May 1979.

[62] C. Weiner, 'High Performance Switched Reluctance Drives for Electric Vehicle Application' Ph.D. Thesis University of Newcastle upon Tyne, UK November, 2000.

[63] T. J. E. Millar, 'Optimal Design of Switched Reluctance Motors' Industrial Electronics, IEEE Transactions on, Volume: 49 Issue:1, Feb. 2002 Pages:15-27.

[64] S. Masashi, 'Switched Reluctance Motor' Japanese patent 10336979 30/5/97.

[65] L. XU, Y. Tang and L. Ye, 'Comparison Study of Rotor Structures of Doubly Excited Brushless Reluctance Machine by Finite Element Analysis' IEEE Transactions on Energy Conversion, Vol.9, No. 1, March 1994.

[66] P. L. Chapman, S. D. Sudhoff, 'Design and Precise Realisation of Optimised Current Waveforms Switched Reluctance Drive' Power Electronics, IEEE Transactions on, Volume: 17 Issue: 1, Jan. 2002 Pages: 76-83.

[67] L. A. Pattison, 'Modelling and Control of the Switched Reluctance Machine' M.Sc. Thesis Queen's University, Kingston, Ontario, Canada April 15, 1988.

[68] R. S. Wallace, 'Design and Control of Switched Reluctance Motors To Reduce Torque Ripple' Ph.D. Thesis, Georgia Institute of Technology, November, 1990.

[69] B. C. Mecrow, J.W. Finch, E.A. El-Kharashi and A.G. Jack, 'Switched Reluctance Motors with Segmental Rotors' IEE Proc.-Electr. Power Appl., Vol. 149, No. 4, July 2002.

[70] B. C. Mecrow, J. W. Finch, E. A. El-Kharashi and A. G. Jack, 'The Design of Switched Reluctance Motors with Segmental Rotors' ICEM 2002, 15th International Conference on Electrical Machines' Brugge, Belgium, August 25-28, 2002.

[71] M. R. Harris, V. Andjargholi, A. Hughes, P. J. Lawrenson, and B. Ertan, 'Limitations of Reluctance Torque in Doubly-Salient Structures' Proceeding of International Conference On Stepping Motors and Systems, University of Leeds, July 1974, pp. 158-168.

[72] S. Ayari, M. Besbes, M. Lecrivain and M. Gabsi, 'Effects of the Air-Gap Eccentricity on the SRM Vibrations' IEEE IAS 1999.

[73] Takashi Kosaka and Nobuyuki Matsui, 'Optimal Combination of Pole Configuration and Current Waveform of SRM for Torque Maximisation' IEEE IAS 98.

[74] J. P. Johnson, A. V. Rajarathnam, H. A. Toliyat, S. Gopalakrishnan and B. Fahimi, 'Torque Optimisation for a SRM using Winding Function theory with a Gap-Dividing Surface' IEEE IAS 1996.

[75] Gwan-Sik Kong et al, 'Predicting the Torque Characteristic of Switched

Reluctance Motor Non-Linear Inductances Profiles', IEEE Tencon, 1993, pp.580-584.

[76] T. Lipo, 'Lecture Notes on Winding Function Theory', University of Wisconsin, Madison, Wi. ,1995.

[77] D. S. Schramm et al, 'Torque Ripple Reduction of Switched Reluctance Motors by Phase Current Profiling' ,IEEE Power Electronics Specialists Conference, 1992, pp.857-860.

[78] T. J. E. Miller, Switched Reluctance Motor Drives-Reference book of Collected Papers, PCIM: Intertec Communications Inc, 1988.

[79] J. W. Finch, M. R. Harris, H. M. B. Metwally, and A. Musoke, "Switched Reluctance Motors with Multiple Teeth per Pole: Philosophy of Design", Proc. IEE Conference on Electrical Machines- Design and Application, 1985, (Sept.), London, Pages: 134-138.

[80] Li et al., 'Axial Flux Reluctance Machine with Two Stators Driving A Rotor' US Patent, US 5925965, Jul. 20, 1999.

[81] B. C. Mecrow , Patent No. 9 126 206.3, December 1991.

[82] B. C. Mecrow, ' New Winding Arrangements for Doubly Salient Reluctance Machines', IEEE IAS Conference Proceedings, Vol.1 pp249, 1992.

[83] B. C. Mecrow, A. C. Clothier, P. G. Barrass, 'High Performance Switched Reluctance Drives using Novel Windings', IEE Colloquium (Digest), N.152, 1996.

[84] T. Lipo , 'Variable Speed Machine with High Power Density' US Patent Number 5010267 22/12/1989.

[85] T. Lipo, 'Doubly AC-Excited Variable-Speed Reluctance Motor' WO 94/19864, 1/9/1994.

[86] T. Lipo, 'Variable Reluctance Motor With Full and Short Pitch Windings' US patent 5376851, Dec. 27, 1994.

[87] D. Qin, R. Qu, T. A. Lipo, 'A Novel Electric Machines Employing Torque Magnification and Flux Concentration Effects' IEEE-IAS Conf. Rec. Phoenix, AZ. October 1999. Vol. 1. pp. 132-139.

[88] L. Xu. T. A. Lipo and S. C. Rao, 'Analysis of a New Variable-Speed Singly Salient Reluctance Motor Utilizing Only Two Transistor Switches' IEEE Transactions on Industry Applications, Vol. 26, No. 2 March/April 1990.

[89] T. A. Lipo, L. Xu, 'A Novel Converter Fed Reluctance Motor with High Power Density' Symposium on Electrical Drives, Cagliari, Italy, Sept 15 -17, 1987, Pages

315-321.

[90] Hendershot, 'Polyphase Switched Reluctance Motor' US-Patent, US5111095, May 5, 1992.

[91] A. Michaelides and C. Pollock, 'Design and Performance of a High Efficiency 5-phase Switched Reluctance Motor' IEE Conference of Electrical Machines and Drives 11-13 September 1995.

[92] P. J. Lawrenson, S. Mem and S. K. Gupta, 'Developments in the Performance and Theory of Segmental-Rotor Reluctance Motors' Proc. IEE, Vol. 114, No. 5, May 1967.

[93] S. Chandrasekhara, 'Dynamic Performance of Reluctance Motors With Magnetically Anisotropic Rotors' IEEE Transactions on Power Apparatus and Systems, Vol. PAS-95, No. 4, July/August 1976.

[94] A. M. El-Antably, J. D. Edwards, G. Williams, P. Lindon and P. D. Luke, 'Steady State Performance Characteristics of Linear Reluctance Motors' IEEE Transactions on Magnetics, Vol.Mag-15, No. 6, November 1979.

[95] P. J. Lawrenson and S. K. Gupta, 'Fringe and Permeance Factors for Segmented Rotor Reluctance Machines' Proc. IEE, vol. 118, No. 5, May 1971.

[96] M. Ramamoory and P. J. Rao, 'Optimisation of Polyphase Segmented Rotor Reluctance Motor Design: A Nonlinear Programming Approach' IEEE Transaction on Power Apparatus and Systems, Vol.PAS-98, No.2 March/April 1979.

[97] G. E. Horst, 'Isolated Segmental Switched Reluctance Moror' EP Patent 0504093, 5/3/92.

[98] Wedman, L. Nikolaus, 'Segmented Magnet Dynamoelectric Machine with Series Connected Rotor Conductors' European Patent 0023073, 28/1/81.

[99] M. N. Anwar, I. Husain and A. V. Radum. 'A Comprehensive Design Methodology for Switched Reluctance Machines', IEEE Transactions on Industry Applications, Vol. 37, No. 6, November/December 2001.

[100] I. E. Chabu, S. I. Nabeta and J. R. Cardoso, 'Design Aspects of 4:2 Pole- 2 Phase Switched Reluctance Motors' 1999 IEEE IAS.63-65.

[101] D. A. Philips, 'Switched Reluctance Drives: New Aspects' IEEE Transactions on Power Electronics, Vol. 5, No. 4, October 1990.

[102] A. V. Radun, 'Design Considerations for the Switched Reluctance Motor' IEEE Transactions on Industry Applications, Vol. 31, No.5, September/October 1995.

[103] I. Bahn, Nerima, 'Reluctance-Type Motor' US5168190, US-Patent, 1/12/1992.

[104] I. Bahn, 'Three Phase Reluctance Type Motor' US 5214365 US-Patent 25/5/1993.

[105] A. B Lovins, B. Howe, 'Switched Reluctance Motor Systems Poised for Rapid Growth' November 8614.728, 1992 E source boulder.

[106] J. Faiz and J. W. Finch, 'Aspects of Design Optimisation for Switched Reluctance Motors' IEEE/PES 1993 Winter Meeting.

[107] P. C. Kjaer, P. Nielsen, L. Andersen, and F. Blaabjerg, 'A New Energy Optimisation Control Strategy for Switched Reluctance Motors' IEEE Transaction on Industry Applications, VoL.31, No. 5, September/October 1995.

[108] R. Arumugam et al, 'Sensitivity of Pole Arc/Pole Pitch Ratio on SRM Motor Performance' , IEEE-IAS Proc., Oct. 1988.

[109] Z. Zuncheng and Y. Shouyou, 'Determination of the Rectangular Teeth Geometry of the VR Motor' IEEE Transactions on Magnetics, Vol. Mag-21, No. 6, November 1985.

[110] S. S. Murthy, B. Singh and V. K. Sharme, 'Finite Element Analysis to Achieve Optimum Geometry of Switched Reluctance Motor' IEEE IAS 1998 414-418.

[111] A. G. Jack, J. W. Finch, and J. P. Wright, 'Adaptive Mesh Generation Applied to Switched-Reluctance Motor Design' IEEE Transaction On Industry Applications, Vol.28, No. 2, March/April 1992.

[112] A. G. Jack, 'Automation of the Design Process for Electrical Machines' International Conference on Electrical Machines and Power Electronics' Kusadasi-Turkey 27-29 May 1992, CEMP 92.

[113] Y. Liu, 'Improved Design of Switched Reluctance Motor Drives (flux linkage, output torque, split link converter), Ph.D. Thesis Clarkson University, 1999.

[114] T. J. E. Miller, A. Hutton, C. Cossar, and D. A. Staton, 'Design of a Synchronous Reluctance Motor Drive' IEEE transaction on Industry Applications, Vol.27, No. 4, July/August 1991.

[115] I. Hajdarevic and H. Koefler, 'A Closer View on Inductance in Switched Reluctance Motors' ICEM 2002, 15th International Conference on Electrical Machines' Brugge, Belgium, August 25-28, 2002.

[116] Fulton, N. Neilson, 'Operation of Switched Reluctance Machines' European Patent, EP 0959555, 24/11/1999.

[117] X. Feng, R. Belmans, D. Verdyck, W. Geysen and K. U. Leuven, 'Reluctance Motor with a Radially-Laminated Rotor using Anisotropic Material' IEE Electric Machines and Drives Conference 1993.

[118] Rao, 'Ac Synchronous Motor Having an Axially Laminated Rotor' US patent, US 4110646, 29/8/1978.

[119] Nashiki et al, 'Reluctance Motor' US-Patent, US 6121706, 19/09/2000.

[120] D. A. Staton, W. L. Soong and T. J. E. Miller, 'Unified Theory of Torque Production in Switched Reluctance and Synchronous Reluctance Motors' IEEE Transactions on Industry Applications, Vol. 31, No. 2, March/April 1995.

[121] N. N. Fulton and P. D. Webster, 'The Development and Application of 2-Phase Switched Reluctance Drives' EMD97 1-3 September 1997.

[122] B. C. Mecrow, UK Patent Application No. 0209794.7, 'Switched Reluctance Electrical Machine with Segmented Rotor', 30th April 2002.

[123] B. C. Mecrow, E. A. El-Kharashi, J. W. Finch and A. G. Jack, 'Segmental Rotor Switched Reluctance Motors with Single Tooth Windings' IEE Proc.-Electr. Power Appl., to be published.

[124] B. C. Mecrow, E. A. El-Kharashi, J. W. Finch and A. G. Jack, 'Performance Evaluation of Switched Reluctance Motors with Segmental Rotors' IEMDC (IEEE International Electric Machines and Drives conference) Madison WI, USA. pp. 568-574, June 1st-4th, 2003.

[125] Tasner, 'Switched Reluctance Electric Motor' International Patent Classification, WO 98/24167, 4 June 1998. (segmented stator SRM).

[126] P. Andrada, B. Blanque, E. Martinez, J. I. Perat, J. A. Sanchez, M. Torrent, 'Performance Comparison of Switched Reluctance Motors with 6/4 and 12/8 Magnetic Structures' ICEM 2002, 15th International Conference on Electrical Machines' Brugge, Belgium, August 25-28, 2002.

[127] H. Moghbelli and M. Rashid, 'Performance Review of AC Adjustable Variable Reluctance Drive' in Proceedings of the IECON' 90, pp. 895-901, 1990.

[128] Oku et al., 'Variable Reluctance Type AC Servo Motor' United states patent US 5148090, Sep. 15, 1992.

[129] T. S. Low, H. Lin and S. X. Chen, 'Analysis and Comparison of Switched Reluctance Motors With Different Physical Sizes Using A 2D Finite Element Method' IEEE Transactions on Magnetics, Vol. 31, No. 6, November 1995.

[130] M. Moallem and C. Ong, 'Predicting the Steady-State Performance of an Switched Reluctance Machine' IEEE Transactions on Industry Applications, VOL. 27, No 6, November/December 1991.

[131] N. Fulton, 'The Application of CAD to Switched Reluctance Drives' IEE Conference of Electric Machines and Drives 1987.

[132] M. N. Anwar and I. Husain, 'Design of a Switched Reluctance Machine for Wide-Speed Range Operation' ICEM, 28-30, August, 2000, Espoo, Finlad.

[133] A. V. Radun, C. A. Ferreira and E. Richter, 'Two-Channel Switched Reluctance Starter/Generator results',IEEE Transaction on Industry Applications, Vol. 34, no. 5, September/October 1998.

[134] A. M. Michaelides, 'The Design of Switched Reluctance Motors for Efficient Energy Conversion' Ph.D. Thesis University of Warwick, Sept. 1994.

[135] A. V. Radun, 'Design Considerations for the Switched Reluctance Motor' IEEE Transactions on Industry Applications, Vol. 31, No.5, September/October 1995.

[136] U. Bock, 'A Novel Approach of Modeling SR Motor Systems' ICEM 2002, 15th International Conference on Electrical Machines' Brugge, Belgium, August 25-28, 2002.

[137] L. Xu and E. Ruckstadter, 'Direct Modelling of Switched Reluctance Machine by Coupled Field-Circuit Method' IEEE Transactions on Energy Conversion, Vol. 10, No. 3, September 1995.

[138] B. Multon, S. Hassine and J-Y. Le Chenadec, 'Pole Arc Optimisation of Vernier Reluctance Motors Supplied with Square Wave Current, Elec. Machines Power Systems, Vol. 21, No.6 PP. 695-7-9, 1993.

[139] H. Lin, T. S. Low and S. X. Chen, 'Investigation on Magnetic Saturation in Switched Reluctance Motor Using 2D Hybrid Finite Element Method' IEEE Transaction on Magnetics, Vol. 32 No. 5, September 1996.

[140] H. Moghbelli, 'Analysis of the Switched Reluctance Motor Drive Using Finite Element Method (FEM) to Predict Steady Estate Performance', Ph.D. Thesis 1989, University of Missouri-Columbia.

[141] R. Arumugam, D. A. Lowther, R. Krishnan and J.F. Lindsay, 'Magnetic Field Analysis of Switched Reluctance Motor Using A Two Dimentional Finite Element Model' IEEE Transaction on Magnetics, Vol. Mag-21, No.5, September 1985.

[142] J. Luomi and H. Rouhianen, 'Adaptive Mesh Refinement for Magnetic Field Problems Involving Saturable Ferromagnetic parts' IEEE Transactions on Magnetics, Vol.24, No. 1, January 1988.

[143] W. Shuhong and Z. Guang, 'A Novel Fully Automatic Finite Element Mesh Generation for Arbitrary Multiply Connected Regions in Electric-Magnetic Field Analysis of Electrical Machines' Proceedings of the Third Chinese International Conference on Electrical Machines, August 29~31 1999, Xi'an, China Volume1.

[144] Kolomeitsev, 'Switched Reluctance Motor with Low Mutual Inductance Between Phases' US-Patent US5777416, Jul. 7, 1998.

[145] D. E. Cameron, J. H. Lang, and S. D. Umans, 'The Origin and Reduction of Acoustic Noise in Doubly Salient Variable-Reluctance Motors, 'IEEE Trans. Ind. Applicat., Vol. 28, No.6, PP. 1250-1255,1992.

[146] A. J. Ellison and C. J. Moore, 'Acoustic Noise and Vibration of Rotating Electric Machines', in IEE Proc., vol. 115, no. 11,pp. 1633-1640, 1968.

[147] C. Yongxiao, W. Jianhua and H. Jun, 'Analytical Calculation of Natural Frequencies of Stator of Switched Reluctance Motor' EMD97 1-3 September.

[148] E. S. Serafim, J. P. A. Bastos, N. Sadowski, 'Influence of the Geometric Variations on the Vibration and Acoustic Noise Behaviour of a SRM' ICEM 2002, 15th International Conference on Electrical Machines' Brugge, Belgium, August 25-28, 2002.

[149] A. Vagati, M. Pastorelli, G. Franceschini and C. Petrache, 'Design of Low Torque Ripple Synchronous Reluctance Motors' IEEE Industry Application Society, New Orleans, Louisiana 1997.

[150] R. S. Wallace and D. G. Taylor, 'Torque Ripple Reduction in Three Phase Switched Reluctance Motor' American Control Conference SAN Diego, May 1990 PP. 1526-1527.

[151] R. S. Wallace and D. G. Taylor, 'A Balanced Commutator for Switched Reluctance Motors to Reduce Torque Ripple' IEEE Transactions On Power electronics, Vol. 7, No. 4, October 1992.

[152] E. A. Fisher, E. Richter, 'Conical Rotor for Switched Reluctance Motor' US5233254, US-Patent, 3/8/1993.

[153] J. Y. Le chenadec, M. Geoffroy, B. Multon and J. C. Mouchoux, 'Torque Ripple Minimsation in Switched Reluctance Motors by Optimisation of Current wave-Forms

and of Tooth Shape with copper Losses and V.A. Silicon Contraints' ICEM'94, Paris, France, September 5-8, 1994, Vol. 3, pp. 559-564.

[154] T. Saitou, 'Reluctance Type Motor Apparatus and Driving Method Capable of Reducing Ripples in Motor Output Torque' US-Patent US 6232741 May15, 2001.

[155] L. Venkatesha, and V. Ramanarayanan, 'A Comparative Study of Pre-Computed Current Methods for Torque Ripple Minimisation in Switched Reluctance Motor', IEEE Conf. IA 2000 Italy.

[156] R. S. Wallace and G. G. Taylor, 'Low Torque Ripple Switched Reluctance Motors for Direct Drive Robotics' IEEE Trans. Robotics and Automation, Vol. 7, No. 6, pp.733-742, December 1991.

[157] K. Koibuchi, T. Ohno and K. SAWA, 'A Basic Study for Optimal Design of Switched Reluctance Motor by Finite Element Method' IEEE Transactions on Magnetics, Vol. 33, No. 2, March 1997.

[158] F. Sahin, H. B. Ertan and K. Leblebicioglu, 'Optimum Geometry For Torque Ripple Minimisation of Switched Reluctance Motors', ICEM' 96.

[159] F. Sahin, H. B. Ertan and K. Leblebicioglu, 'Optimum Geometry for Torque Ripple Minimisation of Switched Reluctance Motor' IEEE Transactions on Energy Conversion, Vol. 15, No. 1, March 2000.

[160] McCann, 'Low Torque Ripple Switched Reluctance Regulation System' US-Patent, US6002233, 14/12/1999.

[161] N. Inanc, A. Derdiyok, V. Ozbulur, N. Abut and F. Arslan, 'Torque Ripple Reduction of a Switched Reluctance Motor Including Mutual Inductances' ISIE'97 Guimaraes, Portugal.

[162] S. Y. Kim, S. KR, 'Method For Reducing Torque Ripple of Switched Reluctance Motor' US-Patent, US 2002/0109476, 15 Aug. 2002.

[163] M. Nashiki, Niwa-gun, 'Motor with Reduced Torque Ripple' US-Patent US 6285104, 4 Sep, 2001.

[164] E. Hoang, B. Multon, R. V. Fos and M. Geoffroy, 'Influence of Stator Yoke Thickness and Stator Teeth Shape upon Ripple and Average Torque of Switched Reluctance Motors' SPEEDAM Conf., Taormina, Italy, June 8-10, 1994, pp. 145-149.

[165] Kim, 'Method for Reducing Torque Ripple of Switched Reluctance Motor' US-Patent, US-0109476, 15/08/2002.

[166] B. C. Mecrow, 'Doubly Salient Reluctance Machines' US-Patent, US5545938, Aug. 13, 1996.

[167] J. V. Byrne, 'Tangential Forces in Overlapped Pole Geometries Incorporating Ideally Saturable Material' IEEE Transactions on Magnetics, Vol. Mag-8, No. 1, March 1972.

[168] Kliman, 'Composite Rotor Lamination For Use in Reluctance Hompolar, and Permanent Magnet Machines' US patent, US4916346, 10/4/1990.

[169] R. Mastromattei, 'Magnetically Enhanced Variable Reluctance Motors Systems' US patent no.4713570.

[170] M. Moallem, C. Ong and Lewis E. Unnewehr, 'Effect of Rotor Profiles on the Torque of a Switched-Reluctance Motor' IEEE Transactions on Industry Applications, Vol. 28, No. 2, March/April 1992.

[171] S. Naoyuki, H. Yukio, M. Hiroshi and Y. Shizuka, 'Rotor for Reluctance motor' Japanese Patent, no. 10150753 (2/6/98).

[172] McClelland, Michael Leo, 'A set of laminations for a switched reluctance machine' European Patent Application, EP 0961390, 1/12/1999.

[173] McClelland, 'Set of Laminations for a Switched Reluctance Machine' US Patent 6093993, 25/7/2000.

[174] Randall, S. Paul, 'A Winding for Switched Reluctance Machines' EP 1069668, 17/1/2001.

[175] Y. Li and Y. Tang, 'Switched Reluctance Motor Drives with Fractionally-Pitched Windings Design, IEEE IAS 1997, Pages 875-880.

[176] K. Yusuke, 'Motor Stator and Motor Frame' Japanese patent no. 10201146, 8/1/97.

[177] D. Lei, L. Diji and C. Zhiliang, 'A Novel Switched Reluctance Motor Propulsion System for Electric Vehicle' Proceedings of the Third Chinese International Conference on Electrical Machines, August 29~31 1999, Xi'an, China Volume1.

[178] D. J. Willliams, 'Fan Assembly Including A Segmented Stator Switched Reluctance Motor' US patent Sep. 26, 2002, US 2002/0135255.

[179] Kliman et al., 'Construction of Reluctance Motors' US patent US5053666 1/10/1991.

[180] K. Yasuyuki, 'Manufacturing Method of Stator or Rotor of Variable Reluctance Type Motor' Japanese Patent, JP10-2011 46, 3/10/1980.

[181] P. P. Acarnley, R Aggarwal, 'Inductance and Static Torque Measurement in Small Reluctance-Type Machines' Proc. UPEC, Nottingha, UK 1988.

[182] P. Andrada, E. Martinez, J. I. Perat, J. A. Sanchez, and M. Torrent, 'Experimental Determination of Magnetisation Curves of Switched Reluctance Motors' ICEM 2000, 28-30 August, Espoo, Finland.

[183] A. Ferrero, A. Raciti and C. Urzi,' An Indirect Test Method for Characterization of Variable Reluctance Motors' IEEE Transactions on Instrumentation and Measurement, Vol. 42, No. 6, December 1993.

[184] A. D. Cheok and N. Ertugrul, 'Computer-Based Automated Test Measurement System for Determining Magnetisation Characteristic of Switched Reluctance Motors' IEEE Transactions on Instrumentation and Measurement, Vol. 50, No.3 June 2001.

[185] Murthy, B. Singh, V. K. Sharma, 'A Frequency Response Method to Estimate Inductance Profile of Switched Reluctance Motor' Proc. IEEE Conf. PEDES'96, New Delhi, India, Jan 1996.

[186] V. Ramanarayanan, L. Venkatesha and D. Panda, 'Flux-linkage Characteristics of Switched Reluctance Motor' Proc. IEEE Conf. PEDES'96, New Delhi, India, Jan 1996.

[187] Kintz, Jr. et al. 'Rotor Assembly' US Patent US 4531071, 23/7/1985.

[188] McClelland, 'Rotor for a Reluctance Machine' US-Patent, US 5828153, 27/10/1998.

[189] Olson, 'Rotor for a Permanent Magnet Generator' US-Patent US4486678 4/12/1984.

[190] Horst, 'Switched Reluctance Motor Stator Assembly' US-Patent, US5770910, June 23, 1998.

[191] M. R. Harris, et al. 'Static Torque Production in Saturated Doubly-Salient Machines', Proc. IEE, Vol.122, No.10, October 1975. pp1121~1127.

[192] A. Ferrero and A. Raciti, 'A Digital Method for the Determination of the Magnetic Characteristic of Variable Reluctance Motors' IEEE Transaction on Instrumentation and Measurement, Vol. 39, No. 4, August 1990, Pages 604-608.

[193] M. Moallem, C. M. Ong, 'Predicting the Torque of a Switched Reluctance Machine From its Finite Element Field Solution' IEEE Transactions on Energy Conversion, Vol. 5, No. 4, December 1990.

[194] R. M. Davis, 'Variable Reluctance Rotor Structures- Their Influence on Torque Production', IEEE Transaction on Industrial Electronics, Vol.39, No. 2 April 1992.

[195] V. K. Sharma, S. S. Murthy and B. Singh, 'An Improved Method for the Determination of Saturation Characteristics of Switched Reluctance Motors' IEEE Transactions on Instrumentation and Measurement, Vol. 48, No. 5, October 1999.

[196] L. Shengjin, L. Gang and M. Ruiqing, 'Design and Test for 4KW Switched Reluctance Starter/Generator' Proceedings of the Third Chinese International Conference on Electrical Machines, August 29~31 1999, Xi'an, China Volume1.

[197] A. M. Michaelides, C. Pollock, 'Modelling and Design of Switched Reluctance Motors with Two Phases Simultaneously Excited" IEE Proc. Electric Power Appl. Vol. 143, No. 5, September 1996.

[198] A. V. Rajarathnam, K. M. Rahman and M. Ehsani, 'Improvement of Hysteresis Control in Switched Reluctance Motor Drives' IEEE IAS 1999.

[199] H. Bausch, A. Greif, B. Lange and R. Bautz, 'A 50KW/1500rpm Switched Reluctance Drive for an Electric Vehicle: Current Control And Performacne Characteristic' ICEM 2000, 28-30 August, Espoo, Finland.

[200] Li et al., 'Wide Pole Switched Reluctance Machine and Method of Its Control' US patent, US5936373, 10/8/1999.

[201] L. Chuang, Z. Xuezhong, 'PWM Control for the Switched Reluctance Generator' Proceedings of the Third Chinese International Conference on Electrical Machines, August 29~31 1999, Xi'an, China Volume1.

[202] Doyle, 'Switched Reluctance Motor Drive Control System', US-Patent US5825153, 20/10/1998.

[203] McCann, 'Switched Reluctance Motor Controller' US patent 17/11/1998, US5838133.

[204] P. Wach, K. Tomczewski, 'Control Characteristic of Switched Reluctance Motors' ICEM 2002, 15th International Conference on Electrical Machines' Brugge, Belgium, August 25-28, 2002.

[205] M. Torrent, P. Andrada, B. Blanque, J. I. Perat, 'Simulation of Switched Reluctance Motor (SRM) Using Non-Linear Models' ICEM 2002, 15th International Conference on Electrical Machines' Brugge, Belgium, August 25-28, 2002.

[206] E. J. Rucksadter and R. J. Kee, 'Modelling and Steady State Simulation of a Switched Reluctance Motor Drive' IECEC paper No. AP-390 ASME, 1995, 249-254.

[207] B. C. Mecrow, C. Weiner and C. Clothier, 'The Modeling of Switched Reluctance Machines With Magnetically Coupled Windings' IEEE Transactions on Industry Applications, Vol. 37, No. 6, November/December 2001.

[208] D. Miljavec, P. Jereb and M. Popovic, 'Pulsating Losses in Synchronous Reluctance Motor' Electrical Machines and Drives, 11-13 September 1995 Conference Publication, No. 412, IEE, 1995.

[209] S. D. Calverley, G. W. Jewell and R. J. Saunders, 'Aerodynamic Losses in Switched Reluctance Machines' IEE Proc.-Elec. Power Appl. Vol. 147, No.6 November 2000.

[210] Y. Tang, 'Characterisation, Numerical Analysis, and Design of Switched Reluctance Motors' IEEE Transactions on Industry Applications, Vol. 33, No. 6, November/December 1997.

[211] S. P. Liou and J. Ye, 'Flux Distribution and Core Losses of Switched Reluctance Motors' CCECE'96.

[212] D. A. Philips and L. R. Dupre, 'A Method for Calculating Switched Reluctance Motor Core Losses', International Conference on Electrical Machines and Power Electronics (ACEMP), Kuzadon, Turkey, May 1992.

[213] J. Boivie, 'Iron loss Model and Measurements of the Losses in a Switched Reluctance Motor' IEE Conference of Electric Machines and Drives 1993.

[214] P. Materu and R. Krishnan, 'Estimation of Switched Reluctance Motor Losses' IEEE-IAS Proceedings, Pittsburgh, PA, October 1988.

[215] P. N. Materu, 'Estimation of Switched Reluctance Motor Losses' IEEE Transaction on Industry Applications, Vol.28, No.3, May/June 1992.

[216] F. Leonardi, T. Matsuo and T. A. Lipo, 'Iron Loss Calculation for Synchronous Reluctance Motor' in Proc. IEEE IAS Annual Meeting, 1989, 307-312.

[217] Z. Cheng, N. Takahashi, S. Gao and Q. Hu, 'Hysteresis Loss Analysis in Steel Based on W_h-B_m Curve' Proceedings of the Third Chinese International Conference on Electrical Machines' August 29~31, 1999, Xi'an, China. Volume1.

[218] L. Dupre, M. De Wulf, D. Makaveev, V. Permiakov, A. Pulnikov, J. Melkebeek, 'Evaluation of Electromagnetic Losses in Electrical Machines' ICEM 2002, 15th International Conference on Electrical Machines' Brugge, Belgium, August 25-28, 2002.

[219] Hendershot, 'Polyphase Electronically Commutated Reluctance Motor' US-Patent, US4883999, Nov. 28,1989

[220] Hancock et al., 'Method of Making an Electronically Commutated Reluctance Motor' US-Patent, US4995159, Feb. 26, 1991.

[221] K. Venkatachalam, 'Accurate Prediction of Ferrite Core Loss with Nonsinusoidal Waveforms Using Only Steinmetz Parameters' COMPEL 2002:8Th IEEE Workshop on Computers in Power Electronics.

[222] M. Albach, T. Durbaum, and A. Brockmeyer, " Calculating Core Losses in Transformers for Arbitrary Magnetizing Currents; a Comparison for Different Approaches", in PESC 96 Record, 27th Annual IEEE Power Electronics Specialists Conference, June 1996, vol.2, pp. 1463-8.

[223] W. K. Mo, D. K. W. Cheng and Y. S. Lee, "Simple Approximations of the DC Flux Influence on the Core Loss Power Electronic Ferrites and their use in Design of Magnetic Components", IEEE Transactions on Industrial Electronics, Vol. 44, No.6, pp. 788-99, 1997.

[224] J. Boivie, 'Losses in a Small Switched Reluctance Machine' Royal Institute of Technology, Stockholm, May 1995.

[225] J. Boivie, 'Iron Loss Model and Measurements of the Losses in a Switched Reluctance Motor' IEE 6th International Conference on Electrical Machines and Drives, Conference Publications No376, Oxford, September 1993, pp. 219-222.

[226] Dartmouth Magnetic Component Web Site, http://engineering.dartmouth.edu/.

[227] J. Gyselinck, L. Dupre, L. Vandevelde, J. Melkebeek, 'Calculation of Iron Losses in Electrical Machines using the Preisach Model' Proceedings of the Third International Workshop on Electric and Magnetic Fields (EMF'96), Liege, Belgium, 6-9 May 1996, PP. 423-428.

[228] M. Tohumcu, and H. B. Ertan, 'Prediction of Performance of Switched Reluctance Motor for Design Purposes' ICEM 88.

[229] C. Pollock and A. Michaelides, 'Switched Reluctance Drive: A Comparative Evaluation' Power Engineering Journal 1995.

[230] Sakuma Masashi, 'Switched Reluctance Motor' Japanese Patent no 11332189 30/11/99.

[231] N. M. Abe and J. R. Cardoso, 'A Virtual Lab for Electric Motors and Drives' IEEE Transactions on Magnetics, Vol.35 No 3, May 1999.

[232] G. E. Horst, 'Redundant Switched Reluctance Motor' US Patent 5386162, 6/4/1993.

[233] M. J. Nooton, P. Baachi and I. Takeshi, 'Switched Reluctance Motor' Japanees Patent No. 8182277.

[234] I. Bahn, Nerima, 'Reluctance-Type Motor' US5168190, US-Patent, 1/12/1992.

[235] R. Krishnan, 'Switched Reluctance Motor Drives: Modeling, Simulation, Analysis, Design and Applications' Boca Raton, FL London : CRC Press, c2001.

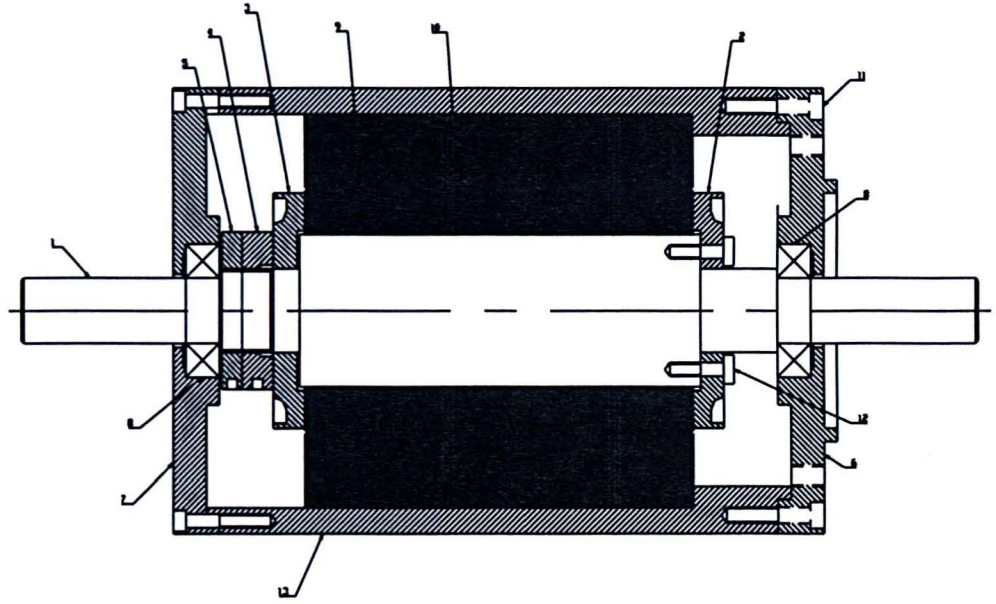

1 - Rotor Shaft
2 - Rotor End Plate
3 - Lamination Clamp
4 - Lamination Clamp Nut
5 - Lamination Clamp Lock Nut
6 - Flange End Cap
7 - End Cap
8 - (R16) Bearing
9 - Stator Lamination
10 - Rotor Lamination
11 - M6x35 Cap Screw
12 - M5x20 Cap Screw

ISSUE	DATE	INITIALS	ISSUE	DATE	INITIALS
1.00	07/06/2001				

DRAWN
DATE 07/06/2001
APPROVED -
SCALE 1:2

University of Newcastle
Department of Electrical & Electronic Engineering

TITLE SRM Machine

PART No. -
DRG. No. 1
SHT 1 of 11
ISSUE 1.00

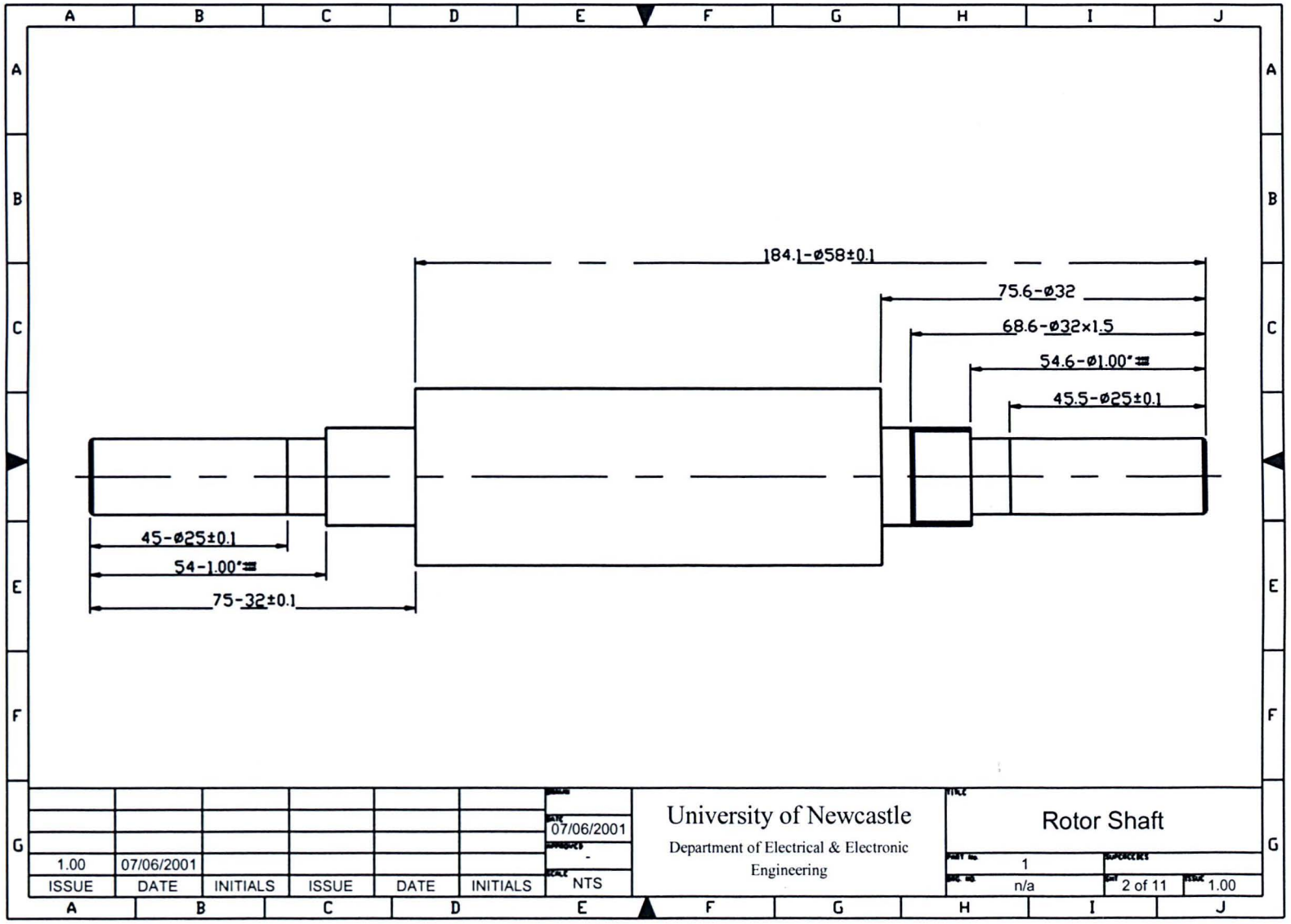
184.1-ø58±0.1
75.6-ø32
68.6-ø32×1.5
54.6-ø1.00"
45.5-ø25±0.1
45-ø25±0.1
54-1.00"
75-32±0.1
1.00
07/06/2001
ISSUE
DATE
INITIALS
ISSUE
DATE
INITIALS
07/06/2001
-
NTS
University of Newcastle
Department of Electrical & Electronic Engineering
Rotor Shaft
1
n/a
2 of 11
1.00

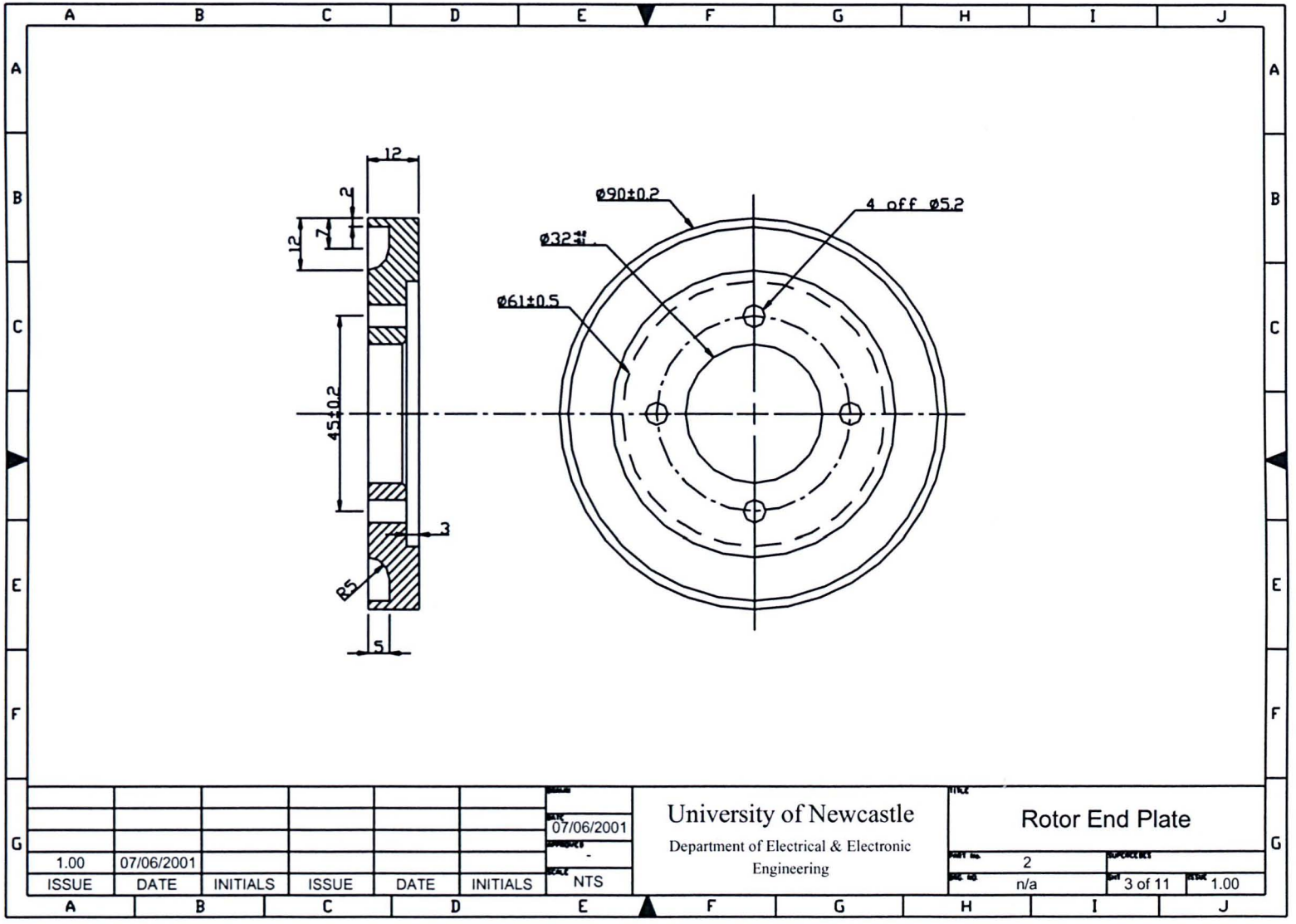
12
2
12
7
45±0.2
3
R5
5
Ø90±0.2
Ø32±
Ø61±0.5
4 off Ø5.2
1.00
07/06/2001
ISSUE
DATE
INITIALS
ISSUE
DATE
INITIALS
07/06/2001
NTS
University of Newcastle
Department of Electrical & Electronic Engineering
Rotor End Plate
2
n/a
3 of 11
1.00

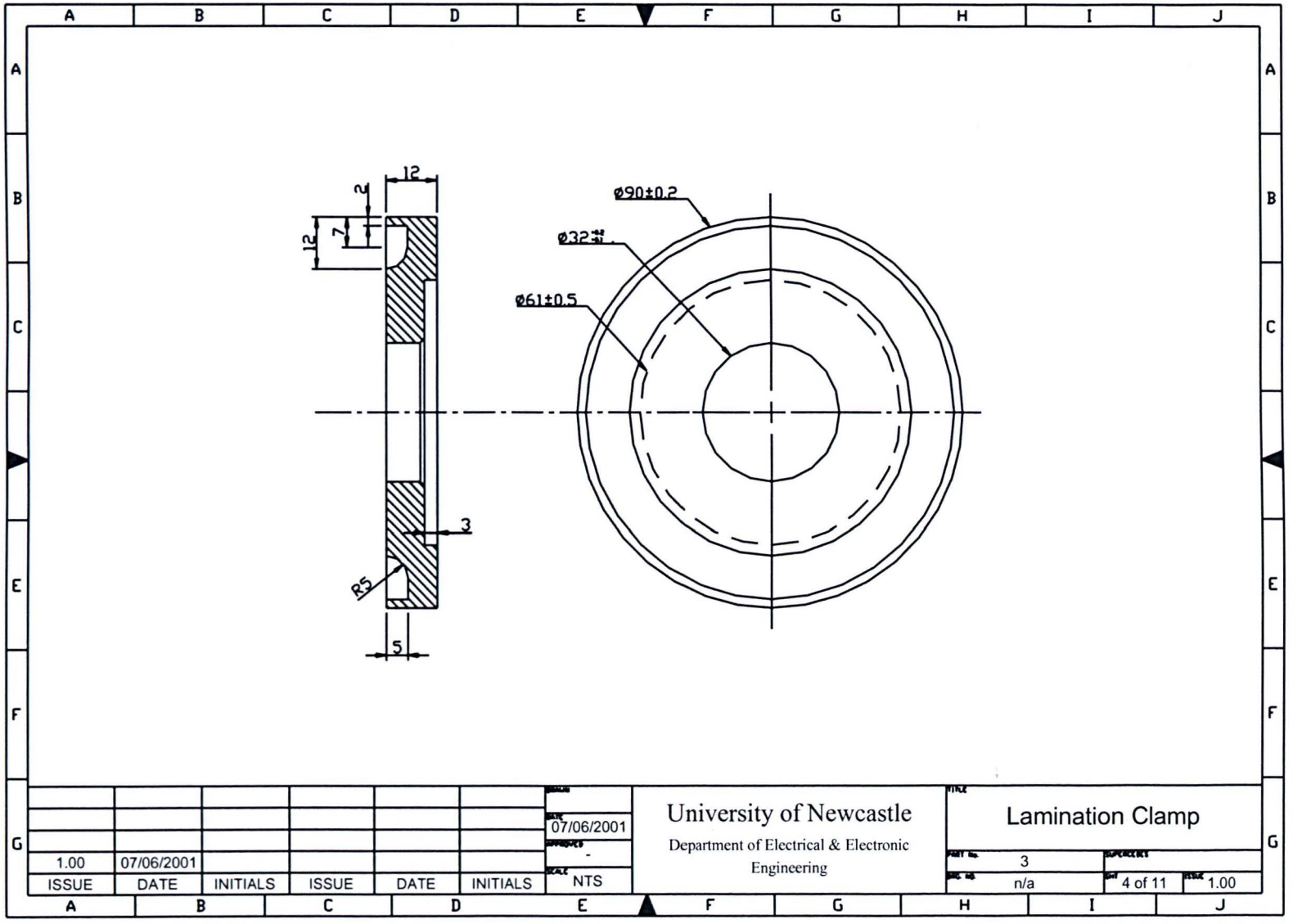
12
2
12
7
ø90±0.2
ø32±
ø61±0.5
3
R5
5
University of Newcastle
Department of Electrical & Electronic Engineering
Lamination Clamp
07/06/2001
NTS
3
n/a
4 of 11
1.00
1.00
07/06/2001
ISSUE
DATE
INITIALS
ISSUE
DATE
INITIALS

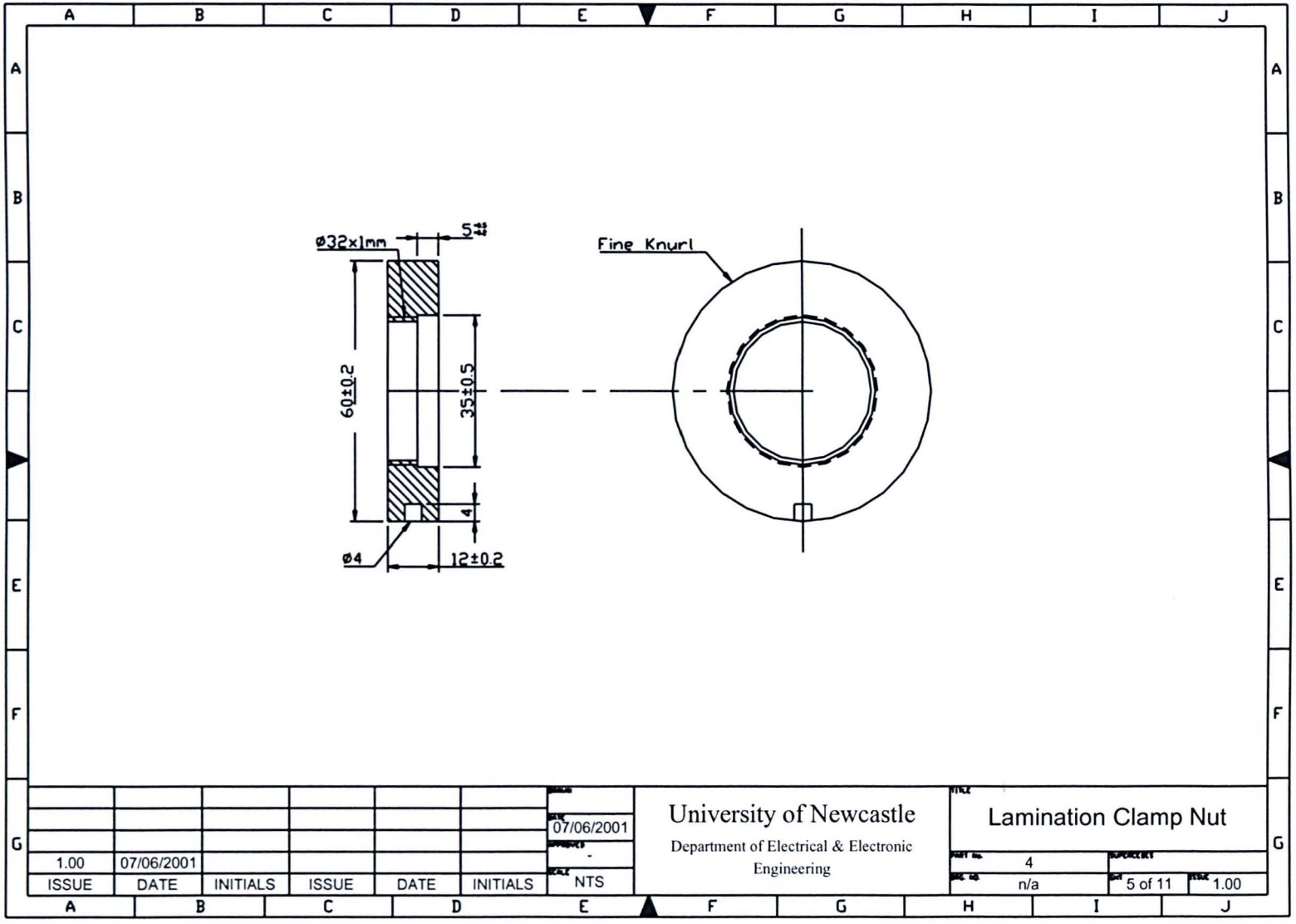

						07/06/2001	University of Newcastle Department of Electrical & Electronic Engineering
1.00	07/06/2001					-	
ISSUE	DATE	INITIALS	ISSUE	DATE	INITIALS	NTS	

Lamination Clamp Nut

4			
n/a	5 of 11	1.00	

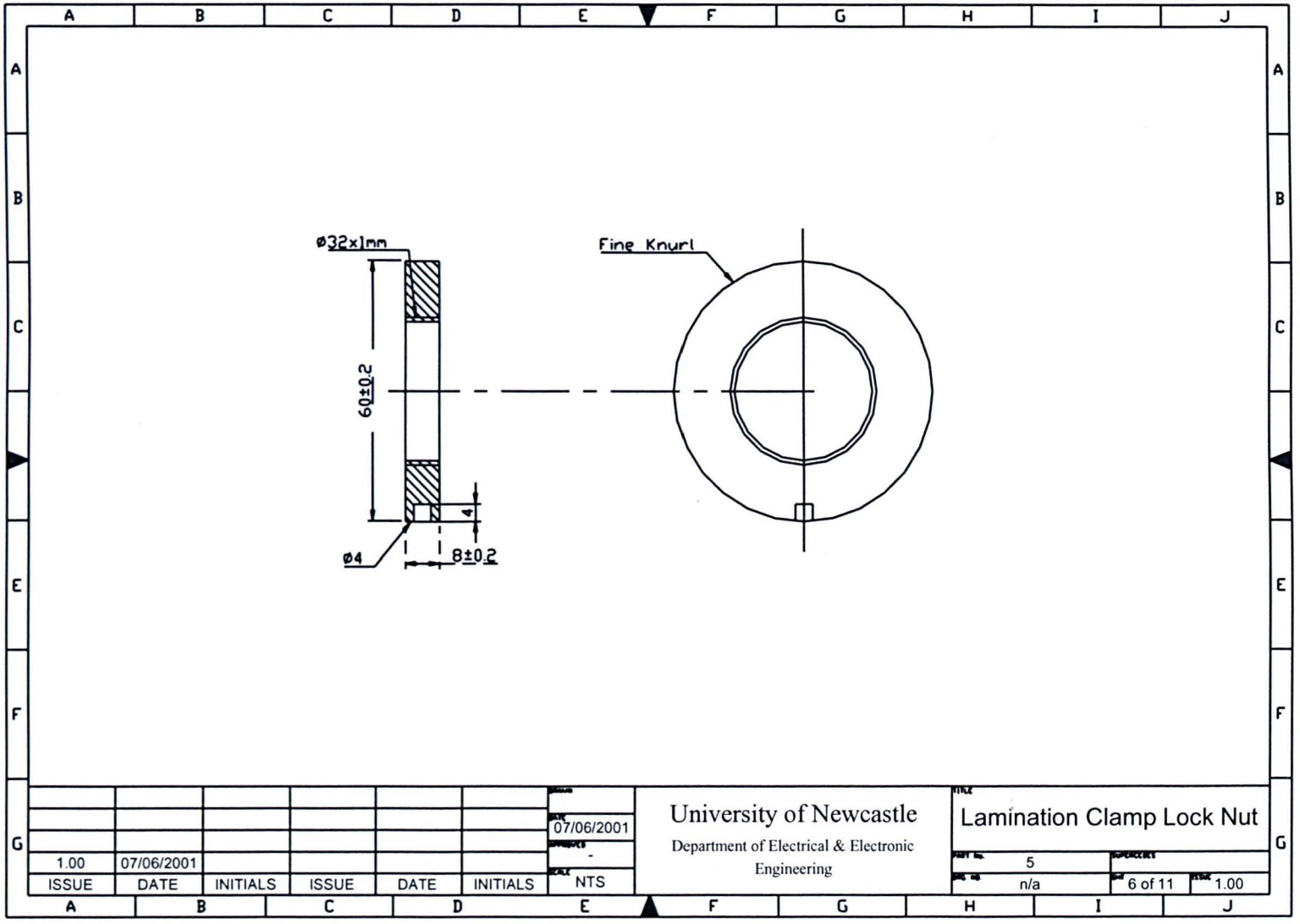

							07/06/2001	University of Newcastle Department of Electrical & Electronic Engineering
1.00	07/06/2001						-	
ISSUE	DATE	INITIALS	ISSUE	DATE	INITIALS		NTS	

Lamination Clamp Lock Nut		
5		
n/a	6 of 11	1.00

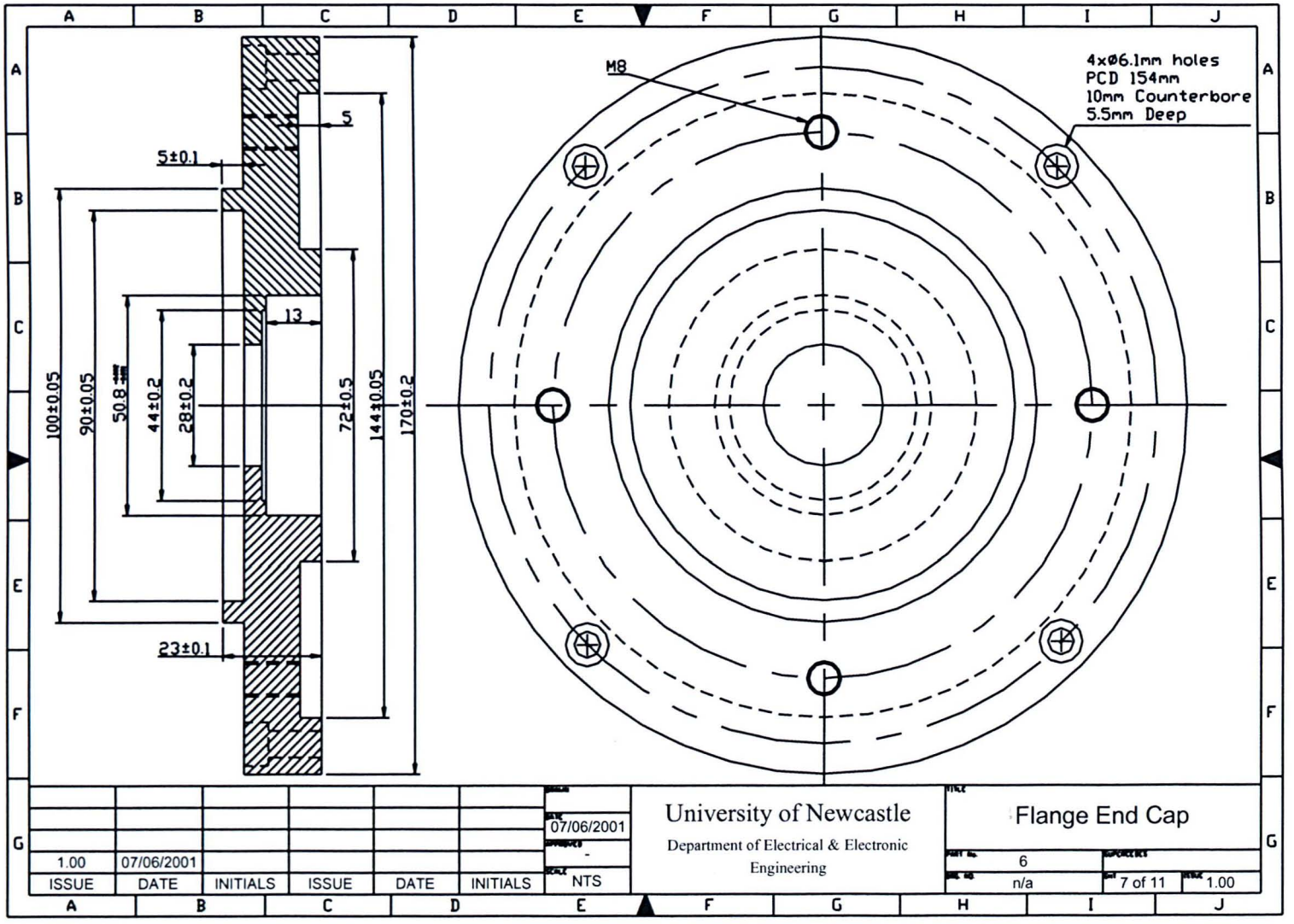
M8
4x⌀6.1mm holes
PCD 154mm
10mm Counterbore
5.5mm Deep
5
5±0.1
13
23±0.1
100±0.05
90±0.05
50.8
44±0.2
28±0.2
72±0.5
144±0.05
170±0.2
University of Newcastle
Department of Electrical & Electronic Engineering
Flange End Cap
07/06/2001
NTS
6
n/a
7 of 11
1.00
1.00 07/06/2001
ISSUE DATE INITIALS ISSUE DATE INITIALS

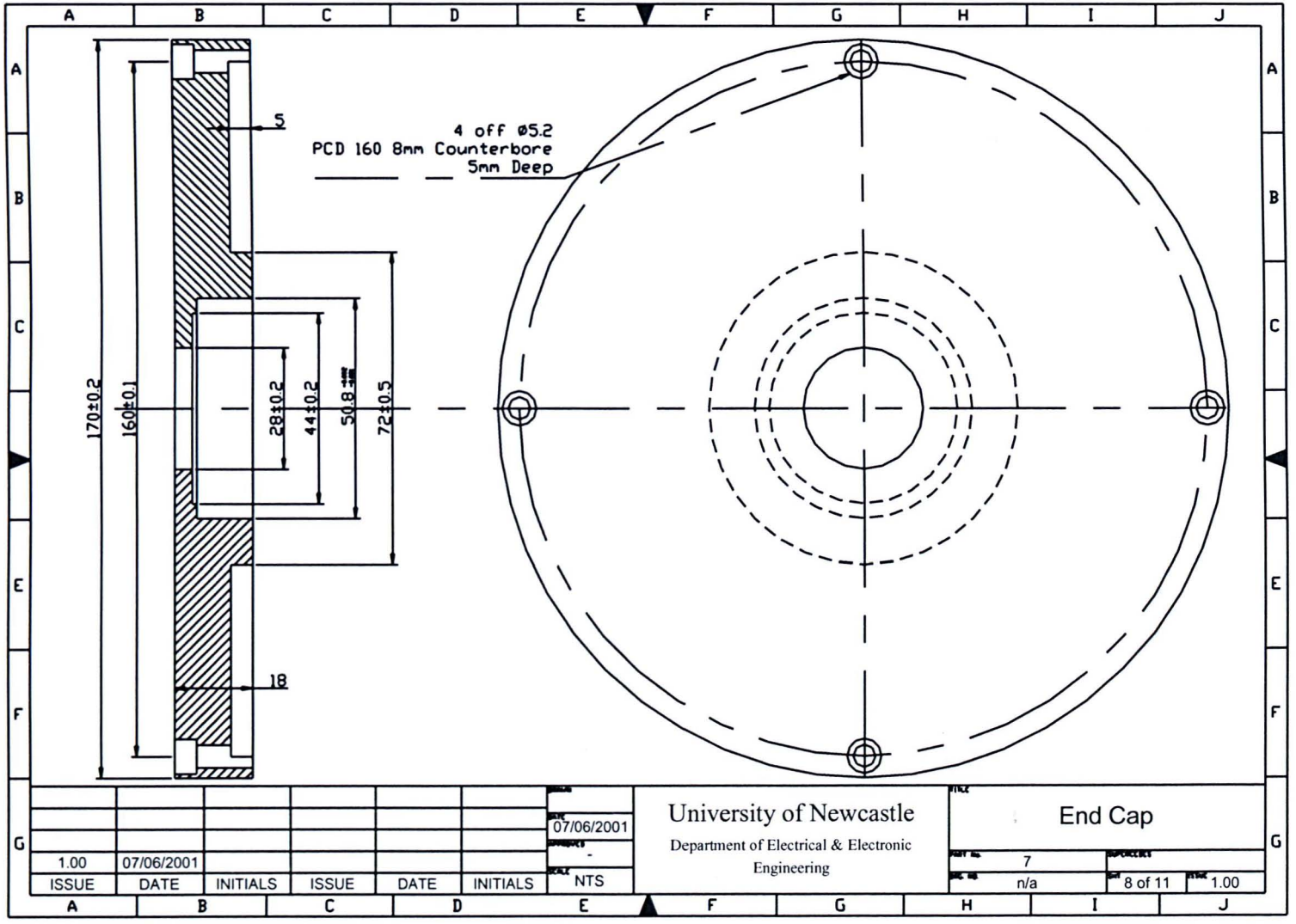
4 off Ø5.2
PCD 160 8mm Counterbore
5mm Deep
5
18
170±0.2
160±0.1
28±0.2
44±0.2
50.8±0.2
72±0.5
07/06/2001
University of Newcastle
Department of Electrical & Electronic Engineering
End Cap
7
n/a
8 of 11
1.00
NTS
1.00
07/06/2001
ISSUE
DATE
INITIALS

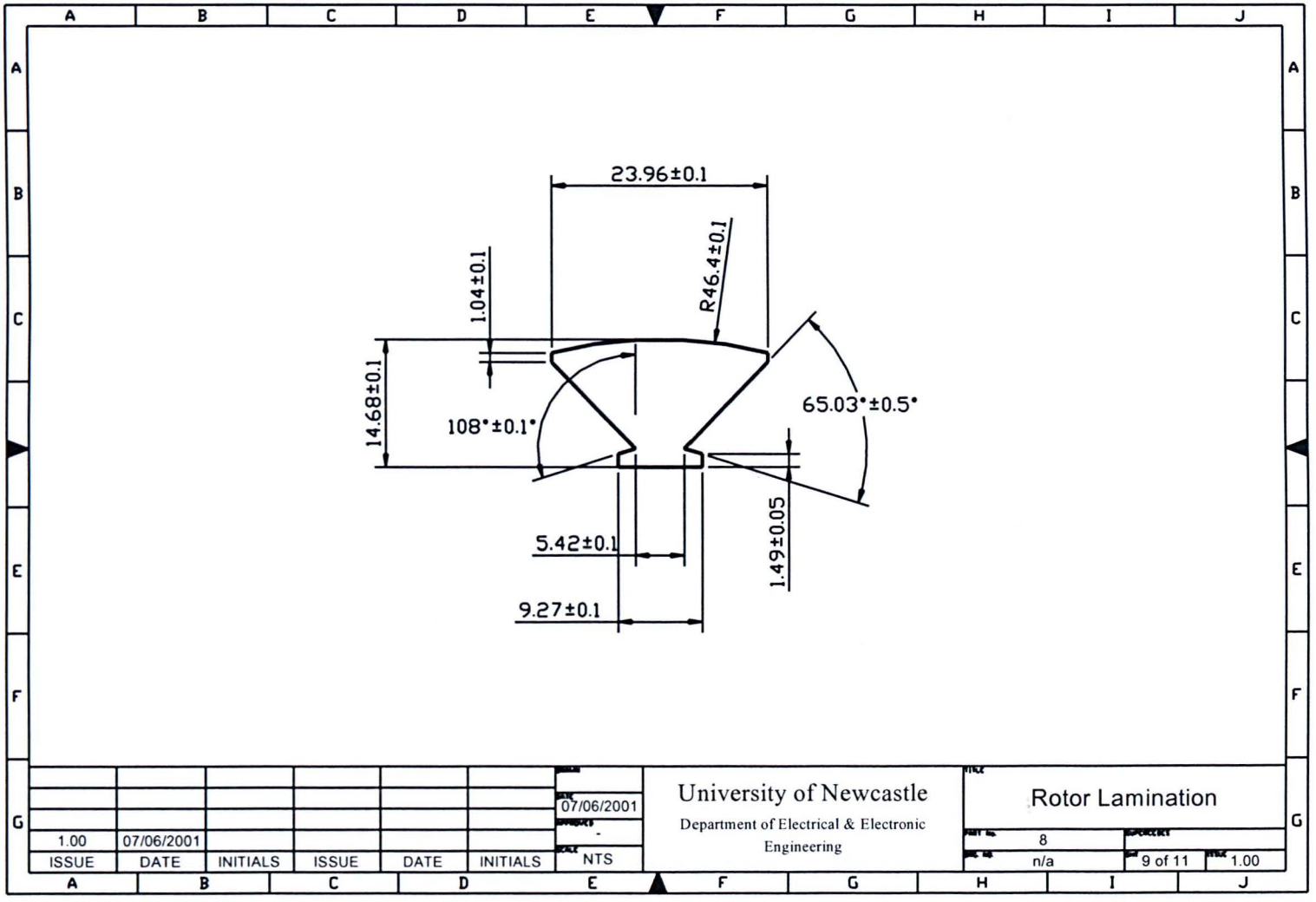
23.96±0.1
R46.4±0.1
1.04±0.1
14.68±0.1
108°±0.1°
65.03°±0.5°
5.42±0.1
9.27±0.1
1.49±0.05
07/06/2001
NTS
University of Newcastle
Department of Electrical & Electronic Engineering
Rotor Lamination
8
n/a
9 of 11
1.00
1.00 07/06/2001
ISSUE DATE INITIALS ISSUE DATE INITIALS

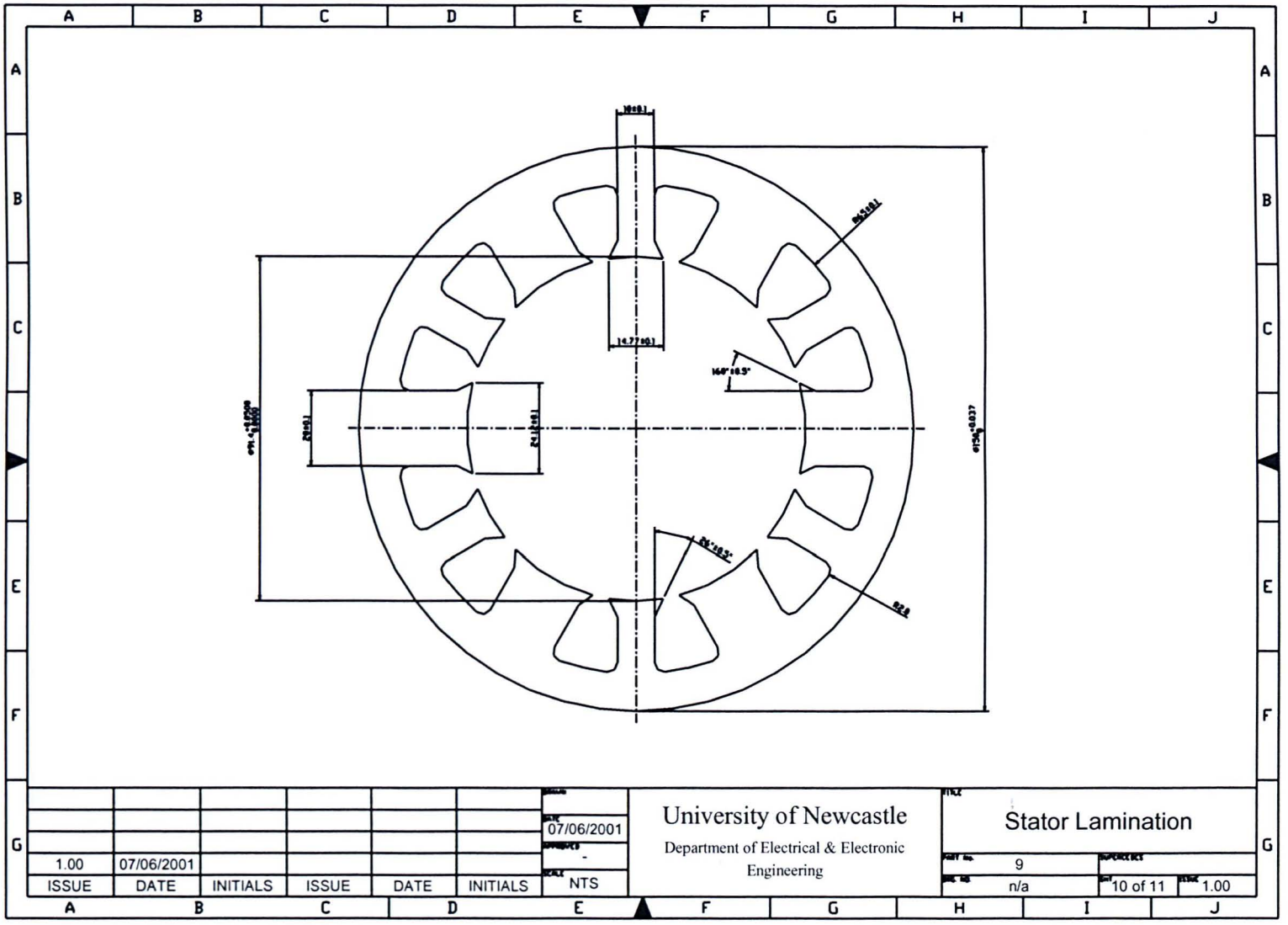

						07/06/2001	University of Newcastle	Stator Lamination
						-	Department of Electrical & Electronic Engineering	
1.00	07/06/2001					NTS		9 / n/a / 10 of 11 / 1.00
ISSUE	DATE	INITIALS	ISSUE	DATE	INITIALS			

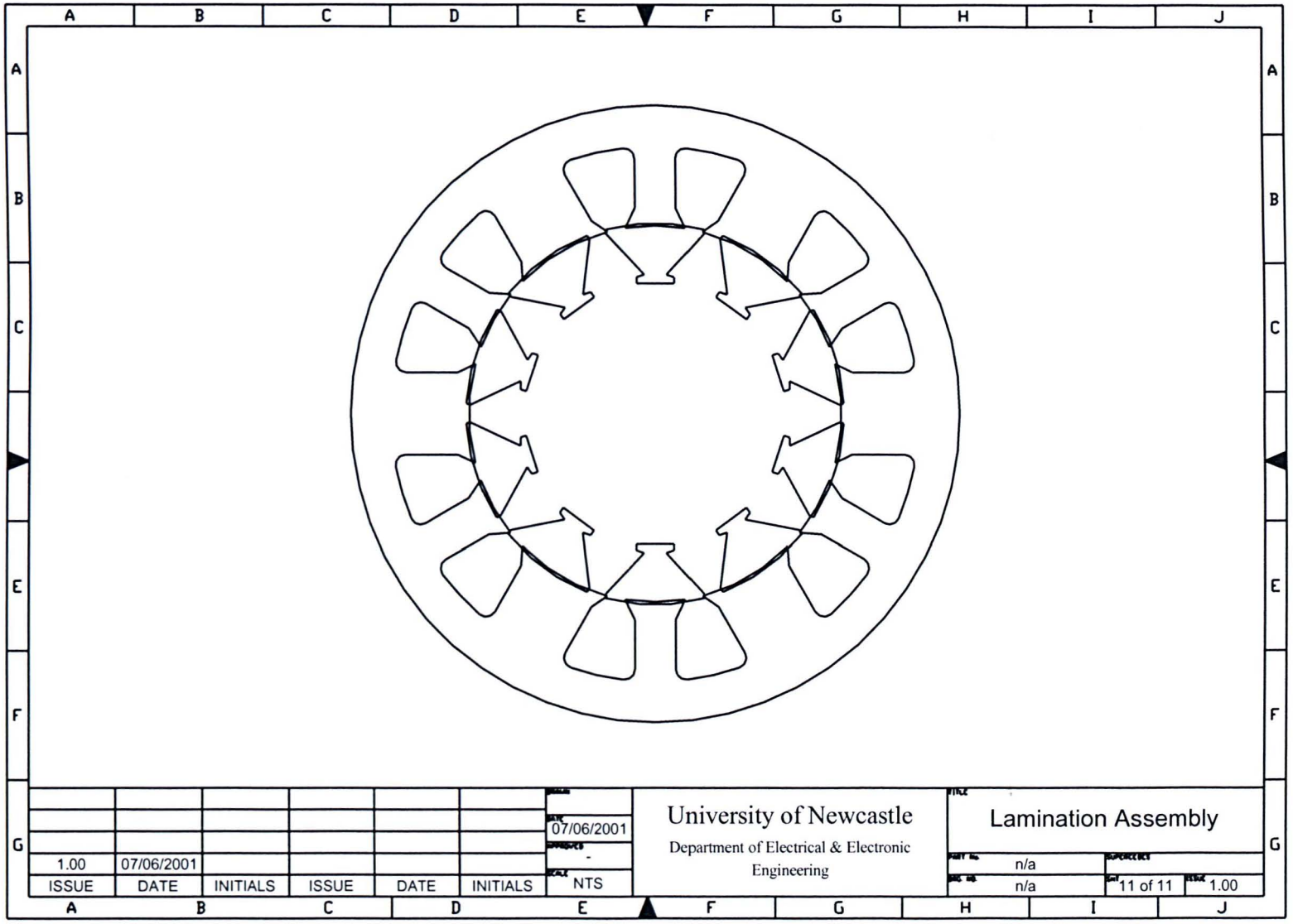
A B C D E F G H I J
A B C E F G
1.00 07/06/2001
ISSUE DATE INITIALS ISSUE DATE INITIALS
07/06/2001
-
NTS
University of Newcastle
Department of Electrical & Electronic Engineering
Lamination Assembly
n/a
n/a
11 of 11
1.00